STABILITY STUDIES ON SOME SUBSTITUTED AMINOBENZOIC ACIDS

Thesis submitted in fulfilment of the
requirements for the degree of

DOCTOR OF PHILOSOPHY
of
RHODES UNIVERSITY

by

MOSES KIPNGENO ROTICH

JUNE 2002

ABSTRACT

The thermal behaviour in the solid state of various substituted aminobenzoic acids (3-aminobenzoic acid (3-ABA), 4-aminobenzoic acid (4-ABA), 3-aminosalicylic acid (3-ASA), 4-aminosalicylic acid (4-ASA), and 5-aminosalicylic acid (5-ASA), as well as the "parent" benzoic acid (BA) and salicylic acid (SA) as reference substances, and possible decomposition products: 2-aminophenol (2-AP), 3-aminophenol (3-AP) and 4-aminophenol (4-AP), has been examined.

The various sets of isomers studied showed considerable and interesting differences. Most sublimed well before melting, generally with an increasing rate of mass loss beyond their very different melting points. The existence of ranges of isomers allows for the comparison of their behaviour, including such aspects as melting, vaporisation, and the influence of products on the course of decomposition of initially-solid reactants. The differences in behaviour of 4-ASA and 5-ASA were the most remarkable, with 5-ASA being far more stable and apparently not decarboxylating readily, while 4-ASA sublimed at temperatures below the melting point, becoming less stable and decarboxylating in the liquid form. There is also a marked difference in the thermal behaviour of 3-ASA, as compared with 4-ASA and 5-ASA. It decarboxylated at higher temperatures (260°C) than 4-ASA (150°C). The addition of the possible decomposition products to these compounds showed faster decomposition for 4-ASA mixed with 3-AP. The sodium salts of 3-ASA and 4-ASA decarboxylate while that of 5-ASA did not.

Binary mixtures of the substances listed above with beta-cyclodextrin (BCD), hydroxypropyl-beta-cyclodextrin (HPBCD) and gamma-cyclodextrin (GCD) were prepared (by simple physical mixing or by kneading with a solvent) and were then examined for possible interactions using DSC, TG-FTIR, HSM, XRD and NMR. Generally, kneaded mixtures showed greater changes in thermal behaviour from that of the individual components than the physical mixtures, but changes in the physical mixtures were also significant. Comparison of the effects of the different CDs on the thermal behaviour of individual ASA isomers showed that HPBCD has the greatest interaction with 3-ASA and 5-ASA, followed by GCD, while BCD generally showed the least interactions. For 4-ASA, the effect of GCD is more marked than for 3-ASA and 5-ASA. GCD has the largest molecular cavity.

ACKNOWLEDGEMENTS

First and foremost I would like to acknowledge my supervisor Prof.M.E.Brown for his supervision in this project. More so for being my constant source of support (for almost everything) to all my problems. Also my co-supervisor Prof. B.D Glass for her constant encouragement and support.

The technical team of Chemistry Department also deserve my thanks for they did a lot for me especially at the early stages of this project. They are Aubrey Sonemann, Johan Fourie, Johann Buys and Don Dondashe.

My fellow students Edith, Emmanuel, Jeff, Medina and Kevin for all that they did for me in the course of this research.

My friends Melane, Vuyelwa, Kimutai, Kevo, Goddy, Izzo, Ndungu, Tarus, Kimemia, Matanga, Oscar, Radul, Zukie and Matsiliza for their constant encouragement and company in most aspects of life in Grahamstown.

Thanks to Mr Alister Munthali and Vusumsi Pakade for helping in proof reading the script.

Rhodes University for their financial support throughout my entire time at Rhodes.

The National Research Foundation for their support.

My Kenyan friends at Rhodes for their company and support.

Egerton University management and staff for the assistance they offered towards this study.

My friends in Nairobi for their support and constant encouragement.

My relatives and people of Kiptere for making my coming to South Africa for this study possible.

My Family members: My dear wife Eunice Rotich, and My dear children: Caroline Chelangat, Calvin Kiprono (Kiprop), Mercyline Chepkemoi and Carlson Kipngetich and my dear parents.

Dedicated to my all my family members and especially my children Caroline Chelangat, Calvin Kiprono (Kiprop), Mercyline Chepkemoi, Carlson Kipngetich and My dear Wife Eunice Chebett Rotich. Also dedicated to my uncle Mr Shadrack Timdo and his entire family.

TABLE OF CONTENTS

LIST OF ABBREVIATIONS

2-AP - 2-aminophenol

3-ABA - 3-aminobenzoic acid

3-AP - 3-aminophenol

3-ASA - 3-aminosalicylic acid

4-ABA - 4-aminobenzoic acid

4-AP - 4-aminophenol

4-ASA - 4-aminosalicylic acid

5-ASA - 5-aminosalicylic acid

ASA - Aminosalicylic acid

BA - benzoic acid

BCD - beta-cyclodextrin

CD - cyclodextrin

Decarb.- decarboxylation

DSC - Differential scanning calorimetry

DTA - Differential thermal analysis

DTG - Derivative thermogravimetry

E - activation energy

EGA - Evolved gas analysis

FTIR - Fourier transform infrared

g - gas

GCD - gamma-cyclodextrin

GSR - Gram-Schmidt reconstruction

HPBCD - hydroxypropyl- beta-cyclodextrin

HSM - Hot-stage microscopy

ICTA - International confederation for Thermal Analysis

ICTAC - International confederation of Thermal Analysis and Calorimetry

IR - Infrared

KM (or k) - kneaded mixture

Liq.(l) - liquid

NATAS - North American Thermal Analysis Society

NMR - Nuclear magnetic resonance

op - open pan

PM (or p) - physical mixture

pp - sealed pressure pan

s - solid

SA - salicylic acid

Sublim.- sublimation

Temp. - Temperature

TG- FTIR - TG interface with Fourier transform infrared

TG - Thermogravimetry

UV - Ultraviolet

Vap. - Vaporisation

XRPD - X-ray powder diffraction

LIST OF FIGURES **PAGE**

LIST OF TABLES **PAGE**

1. INTRODUCTION

1.1 Drug stability

The stability of drugs, in their various dosage forms, is of great importance in the pharmaceutical industry. When drugs are unstable, the degradants formed may cause side effects when the drug is administered. Degradation may be due to the presence of moisture, temperature conditions during manufacture and storage, exposure to light, or any combination of these factors. The stability of solid dosage forms is important because clinical trials are often done in the solid dosage form. Other stress conditions that may accelerate degradation include pH, packaging, and manufacturing processes such as milling, drying and compression during tableting. Instability of the molecule in the dosage form also indicates lack of control of the manufacturing process and loss of potency of the drug.

The decompositions of crystalline solids to form solid + gaseous products have been widely investigated [1]. Decompositions of organic solids, including most pharmaceuticals, are often preceded or accompanied by melting [1-3]. The decomposition modes of pure solids can be to form mixtures of solid products, solid + liquid products, mixtures of liquids, solid + gas, liquid + gas products, or entirely gaseous products. Crystal structure in general, and the existence of polymorphic forms in particular, are extremely important parameters in determining the thermal behaviour of solids. Drugs in solid dosage forms, sometimes degrade via solid-solid reactions. These solid-solid reactions require several contributory diffusion steps, such as surface migration of one or both reactants, and penetration of one reactant into the grains, channels and crystal lattice of the other reactant.

Most crystals contain various structural imperfections. The number of these can be increased during mechanical treatment, such as milling during production. Decomposition is often initiated at imperfections and the decomposition process may result in the formation of more or larger imperfections.

The stabilities of pharmaceutical compounds on exposure to heat, moisture and light are often examined by accelerated testing under conditions considerably harsher than those to which the compounds are expected to be exposed in practice. Results are then extrapolated (with due care) to the more realistic conditions of storage and use [4].

Accelerated degradation studies on pharmaceuticals are based upon extrapolation of the Arrhenius equation for the temperature dependence of the rate constant, k = A exp(-E/RT), where the Arrhenius parameters, E, the activation energy and A, the frequency or pre-exponential factor, are characteristic of the process considered. Extrapolation of the Arrhenius equation is invalid if the degradation mechanism changes with temperature or extent of reaction, or if the degradation mechanism is complex with contributing steps that have different Arrhenius parameters [5].

1.2 Drug/ excipient mixtures

Excipients are the "the additives use to convert pharmacologically active compounds into dosage forms suitable for administration to patients" [6]. Excipients should not interact with, or promote other side reactions of the compounds and should not be hygroscopic. Some excipients promote the activity of the active ingredient (synergistic effect), or increase the solubility and

bioavailability of the drug (see cyclodextrins later). Some act as emulsifying or plasticizing agents. Their presence may affect the stability of the active ingredient in the formulation. The addition of excipients should not change the pH of the environment unless this is desired [7]. Common excipients used are calcium carbonate, sodium hydrogen carbonate, aluminium hydroxide, calcium sulphate, and starch-based compounds, namely, lactose, sorbitol, mannitol, cellulose and amylose.

1.3 Drug packaging

Formulations should be as dry as possible before packaging in order to prevent degradation on storage. Retention of water may cause the drug to undergo hydrolysis and loss of potency. The packaging material should also be hermetic (i.e. should not allow water or oxygen to enter). Where necessary, the packaging should shield the formulation from light. Colour changes during storage of compounds are often a sign of decomposition, although this may not necessarily mean that the compound is toxic.

1.4 Pharmaceutical uses of substituted aminobenzoic acids

4-aminosalicylic acid and its salts of K, Na and Ca have been used in various combinations for the treatment of tuberculosis. Other drugs which have been used with these compounds include streptomycin and isoniazid. 4-ASA exists as practically odourless, white or yellowish-white crystals. It darkens on exposure to light, heat or air. It undergoes decarboxylation in both the solid state and in aqueous solution to form 3-aminophenol. 4-ASA should be administered in its pure state, that is free of the decomposition product, 3-AP, which is associated

with a series of toxicity symptoms, for example, hard hemolytic anaemia connected with bruising [8, 9]. The technical grade of 4-ASA is a pale cream microcrystalline powder of 97 - 99% purity with a melting point of 139 - 141 °C. The pure substance is a white crystalline powder that melts at 150 - 151 °C.

4-ASA is slightly soluble in water(≈0.1%) but more soluble in ethanol, methanol and isopropyl ethanol. It has a synergistic effect (increases the activity of the drug) on the activity of streptomycin or dihydrostreptomycin in the treatment of tuberculosis (TB) [8]. It also helps in the prevention of the development of bacterial resistance to these drugs. Severe gastrointestinal (GIT) irritation accompanies the use of 4-ASA and its sodium salts. This effect can be overcome by the use of capsules, granules, use of coated tablets, or the prescription of antacids to be taken concurrently [9]. The sodium salt dihydrate, 4-ASA-$Na.2H_2O$, occurs as a yellowish-white odourless powder. The salt is soluble in ethanol and very soluble in water (pH =7.25). The pH range of its maximum stability is 7.0 - 7.5. Freshly prepared solutions are nearly colourless, but they develop an amber and, eventually, a dark brown to black colour on standing, due to decarboxylation. The potassium and calcium salts behave similarly. The formation of these salts increases the stability of the acids and is useful for drug storage.

Decarboxylation has been found to be topochemical and autocatalytic with an induction period followed by a rapid acceleratory period [7, 8]. The reaction has been reported to be accelerated by water and to be independent of the carbon dioxide pressure. Sunlight can also induce decarboxylation. The formation of an arenium ion has been used to explain the decarboxylation of 4-ASA in solution. The rate of reaction is zero-order, that is, independent of the 4-ASA concentration.

The first step is the dissociation of the carboxylic acid proton, followed by the electrophilic protonation of the aromatic ring, and loss of carbon dioxide (Figure 1.1) [10]. The proton for electrophilic protonation, therefore, comes from the dissociation of ArCOOH or ArOH. Decomposition in the solid-state is thought to occur by the same mechanism and to propagate through the crystal by addition of carboxylate from either ArCOOH or $ArCOO^-$.

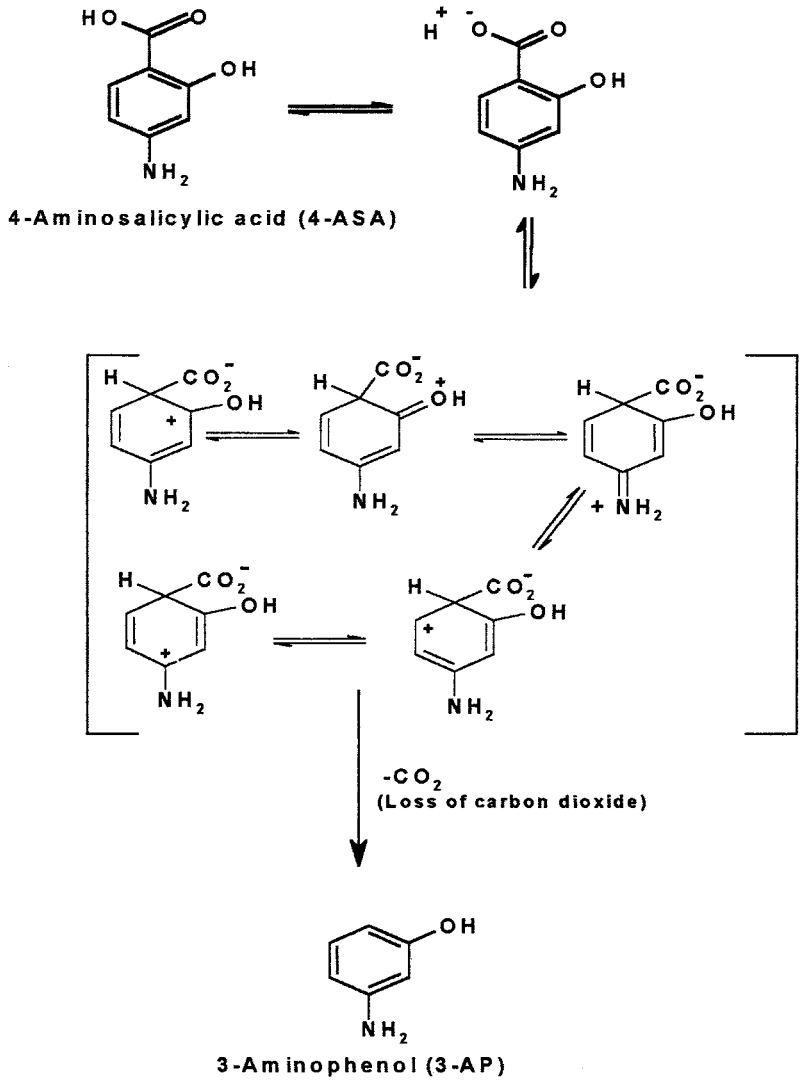

Figure 1.1: Decarboxylation of 4-ASA [10].

Sodium-4-ASA salt, which has similar applications to pure 4-ASA, has been reported [10] to be stable at temperatures below 100°C, but to decompose at higher temperatures. The decomposition of the salt rules out the proposal that the carboxylic proton is responsible for the decomposition of 4-ASA.

Morsi and Williams [11] used emission spectroscopy to study the decomposition of 4-ASA and, in particular, the source of protons for electrophilic substitution. They suggest the existence of the structures shown in Figure 1.2 as transition states.

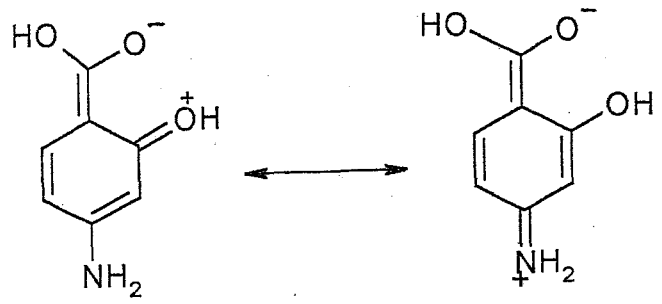

Figure 1.2: Resonance structures of 4-aminosalicylic acid [11].

5-ASA has been used for a long time in commercial formulations for the treatment of chronic inflammatory bowel diseases. The compound decarboxylates to form 4-AP and also tends to undergo auto-oxidation. These reactions lead to problems in pharmaceutical formulations. Cendrowska and co-workers [12] suggested that the degradation of 5-ASA could be observed by colour changes. 4-AP is known to auto-oxidise rapidly in aqueous media to give strongly coloured derivatives. Figure 1.3 shows the degradants formed in thermal studies of 5-ASA and its formulations. Jensen and co-workers [12a] have reported HPLC studies done to

determine the major degradation products of 5-ASA, and pharmaceutical formulations containing 5-ASA as active ingredient, in buffered solution at pH 7.0. Polymeric products formed by oxidative self-coupling of 5-ASA moieties were reported. Some of the identified products have been found in 5-ASA-containing formulations on exposure to heat or light during storage (Figure 1.3).

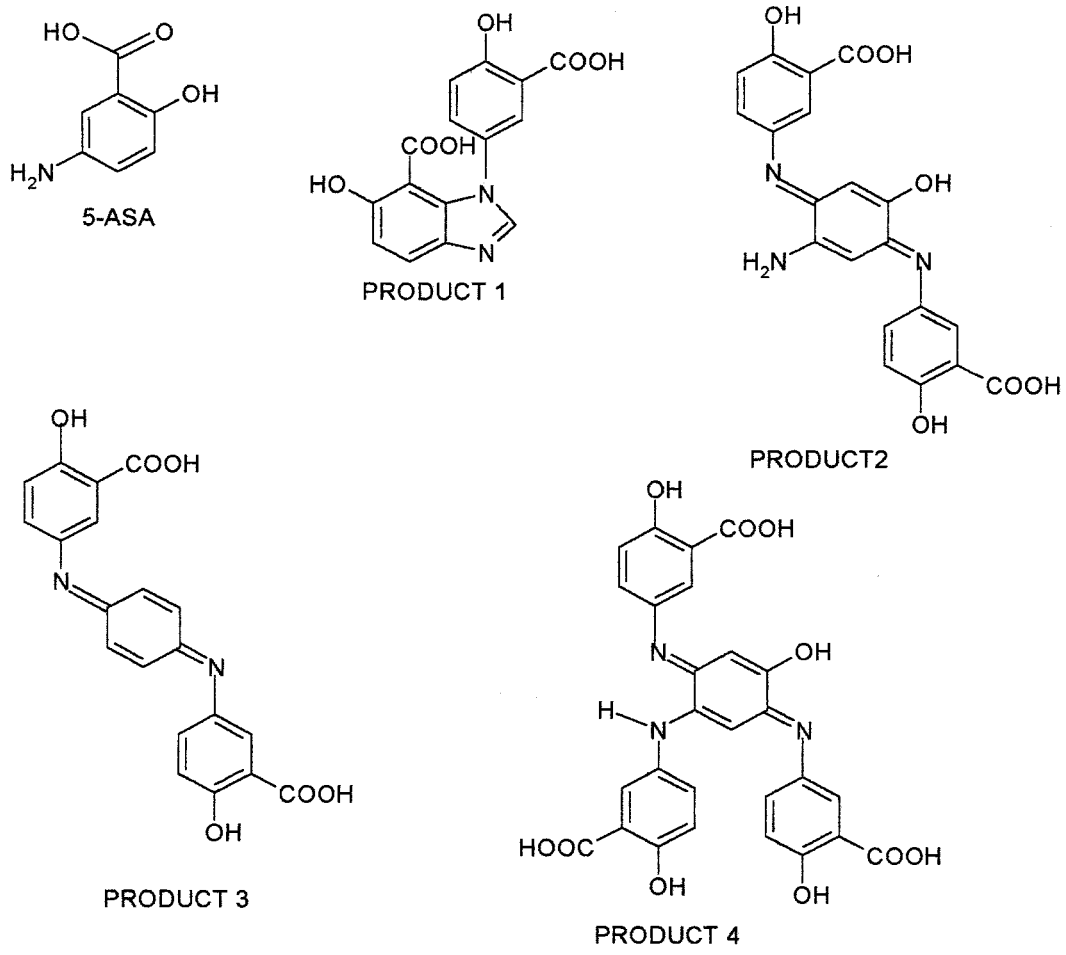

Figure 1.3: The structures of 5-ASA and its degradation products [12].

Benzoic acid and its simple derivatives are widely distributed in nature. They are used as preservatives in medicines, food, cosmetics, and for many other purposes. Benzoic acid was one of the first organic substances used for calibration and

reference purposes in calorimetry [13]. It has also been used as a model compound to study the process of sublimation and evaporation of organic compounds [14]. The thermal decompositions of benzoic acid and its derivatives containing OH, NH_2, COOH, and SO_3H functional groups as substituents in the ortho, meta, and para positions, together with sulphanilic acid, have been investigated [15] using DTA, TG and DTG in air. Wright *et al.* [16], have studied evaporation of the ortho-, meta- and para- derivatives of hydroxybenzoic acids. They reported activation energy values for the ortho-, meta- and para- derivatives as 64.8, 78.2 and 119.1 kJ mol^{-1}, respectively. Both sublimation and evaporation are affected by factors such as vapour pressure, molecular mass, temperature and the area of the surface exposed. Sublimation of benzoic acid was found to take place at temperatures between 80°C and 118°C and evaporation above 122°C. The average enthalpies of sublimation and evaporation were found to be 91.1± 1.4 and 66.1±2.0 kJ mol^{-1}, respectively [14]. The enthalpy of vaporisation for benzoic acid was reported to be 69.2 ± 0.2 kJ mol^{-1} [13].

4-aminobenzoic acid (4-ABA) is an antioxidant which has been used to protect skin from sunburn and hence prevent the possibility of skin cancer. The protection is due to its ability to absorb ultraviolet-B radiation (UVB). This compound is also important as a co-enzyme in the breakdown and utilization of protein and assists in the formation of red blood cells. A deficiency of 4-ABA may lead to depression, fatigue, gastrointestinal disorders, graying of hair, irritability, nervousness and patchy areas of white skin [17].

1.5 Crystal Structures

Variations in the thermal stabilities of solid compounds can sometime be related to differences in their crystal structures. In the crystalline state, atoms, molecules or ions are packed together so as to make the most energetically economical use of space. Many organic compounds have molecules that are irregular in shape but which, nevertheless, achieve a very efficient space-filling arrangement. Benzene has a planar hexagonal molecule, which packs easily, with weak intermolecular bonds, and, hence, benzene has a low melting point. The presence of moieties in a benzene-ring modifies the way in which space can be filled by packing of the compounds and this in turn affects the melting points and general stability of the compounds [18].

Holler [19] has studied the relationship between the melting points of the disubstituted isomers of benzene and their chemical constitution. The compounds were divided into two-groups containing either meta or ortho-para orienting substituents. When the disubstituted benzene contains one meta orientating (COOH) and one ortho-para orienting group ($-NH_2$), the order of the melting points is para > meta > ortho. The aminobenzoic acids are such an example and 4-aminobenzoic acid, 3-aminobenzoic acid and 2-aminobenzoic acid, have melting points of 187 - 188°C, 173 - 174°C and 144 - 145°C, respectively. If both substituents are ortho-para orienting groups, the melting points of the isomers are in the order: para > ortho > meta. Two such groups are -OH and $-NH_2$, and 2-aminophenol, 3-aminophenol and 4-aminophenol have melting points 173°C, 122°C and 184 - 186°C, respectively.

The crystal structure of benzoic acid (BA) (Figure 1.4) has planes containing centrosymmetrical dimers, with hydrogen bonding between the adjacent carboxyl groups. The benzene ring is accurately planar, but the carboxyl carbon atom and one of the oxygen atoms are found to deviate significantly from the plane. Longer H-bonds exist between pairs of dimers [20].

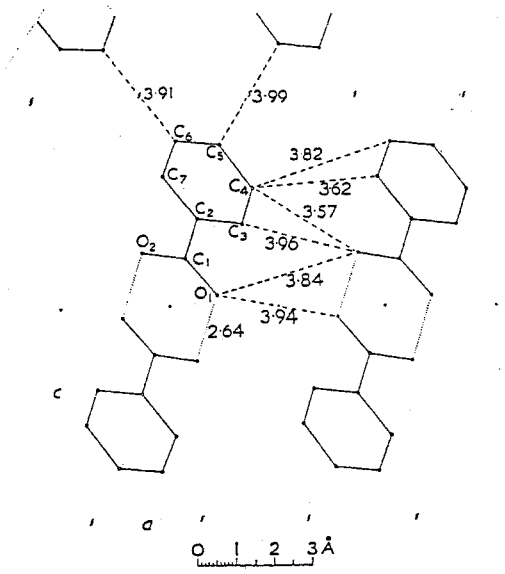

Figure 1.4: The crystal structure of benzoic acid [20].

The crystal structure of salicylic acid (SA) [21] shows that the benzene rings are distorted from hexagonal symmetry. Resonance structures (Figure 1.5) [21, 22] contribute to the overall molecular state of crystal of salicylic acid. Figure 1.6 shows the hydrogen bonding in the molecular structure of salicylic acid as a dimer [21].

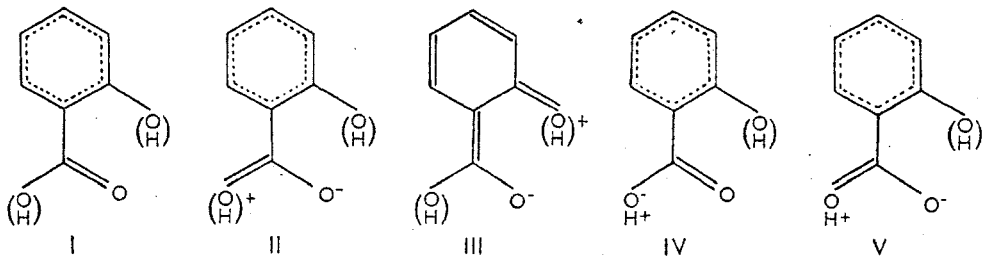

Figure 1.5: Resonance structures of salicylic acid (SA). The symbol in bracket with a positive sign indicates that the transfer of electrons may be from either atom [21].

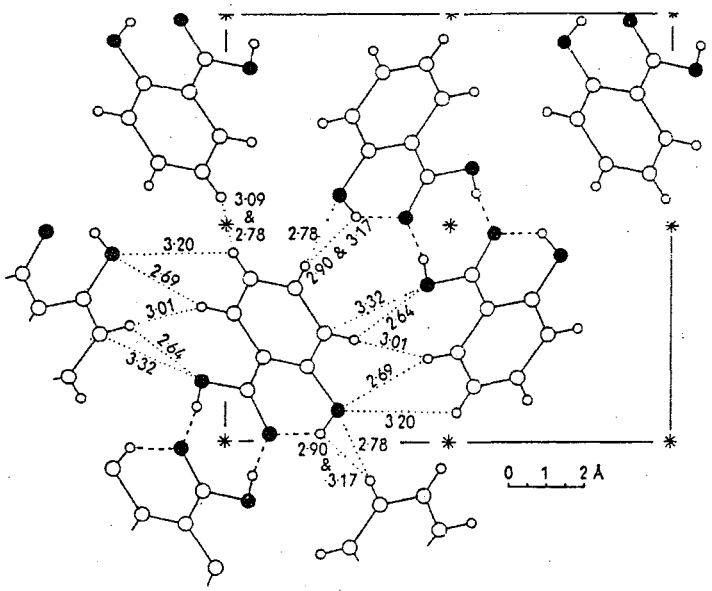

Figure 1.6: The crystal structure of salicylic acid (SA) [21].

The crystal structure of 4-ABA (Figure 1.7) is built up of dimers formed through hydrogen bonding of the OH from one carboxyl group with the carboxyl oxygen of a neighbouring molecule (O-H···O). This arrangement results in a close proximity between the $-NH_2$ group of one dimer and the carboxyl group of the neighbouring pair (N-H···O) [23, 24].

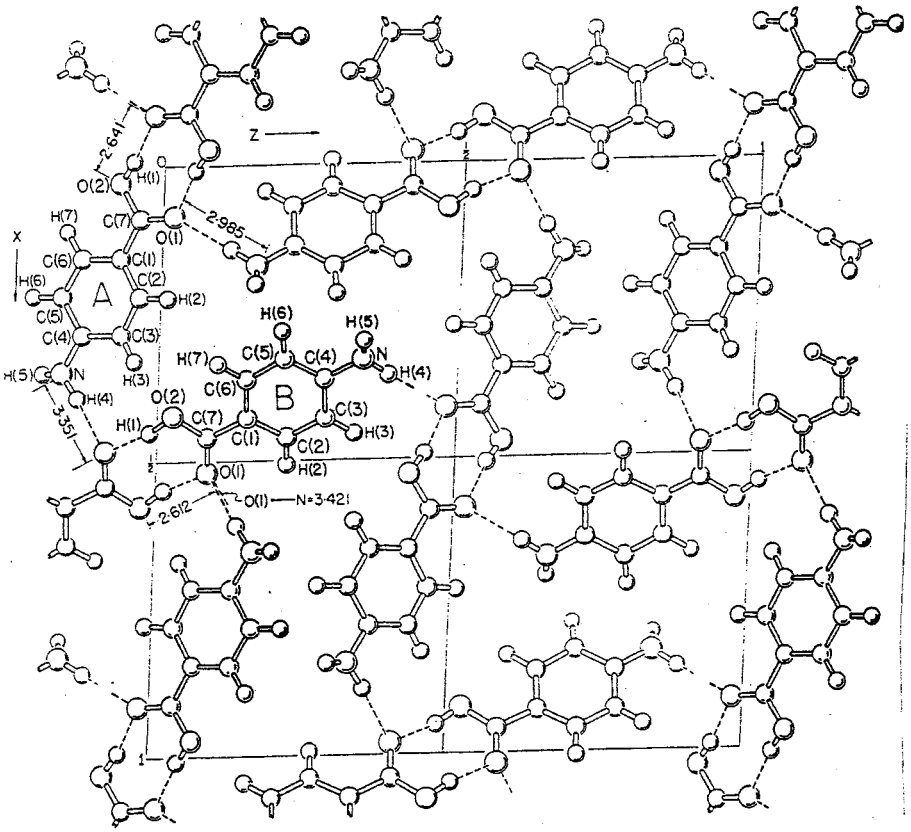

Figure 1.7: The crystal structure of 4-aminobenzoic acid (4-ABA) [23].

The crystal structures of other aminobenzoic acids (2-ABA and 3-ABA) were not found in available search materials.

The crystal structure of 4-ASA (Figure 1.8) shows an arrangement of dimers, formed through hydrogen bonding between the carboxyl groups. There exist also relatively strong intra-molecular hydrogen bonds between the hydroxyl group in 2-position and the carboxyl groups [23, 25]. The resonance structures given in

Figure 1.8, contribute significantly (40%) to the overall molecular structure of 4-ASA.

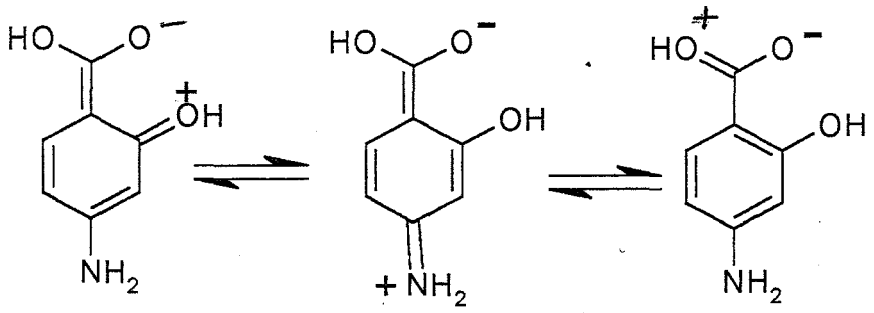

Figure 1.8: Resonance structures of 4-ASA [10, 25].

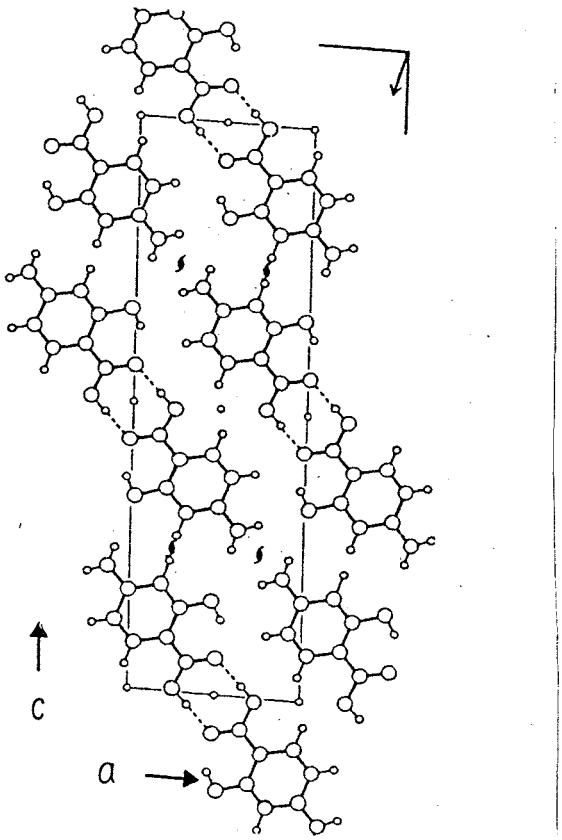

Figure 1. 9: The crystal structure of 4-aminosalicylic acid (4-ASA) [23].

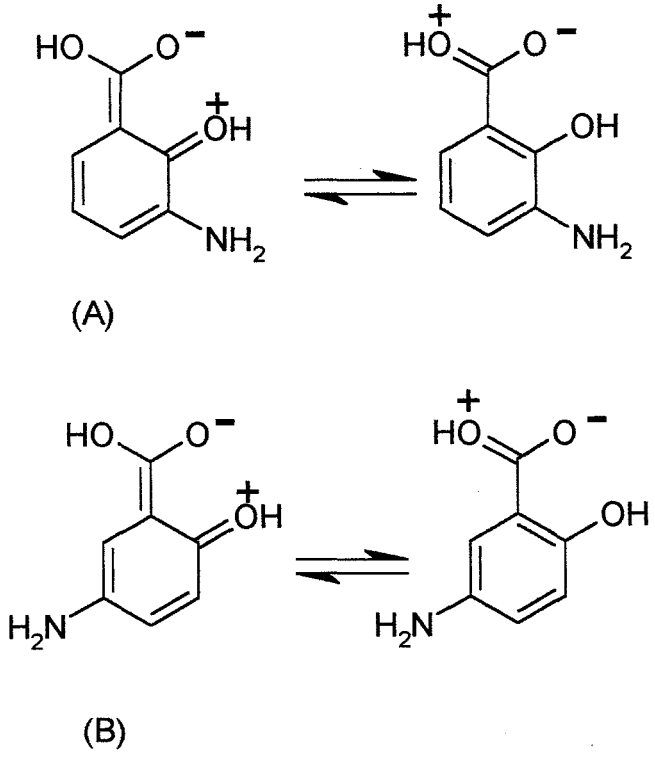

Figure 1.10: Resonance structures of (A) 3-ASA and (B) 5-ASA

The crystal structures for 3-ASA and 5-ASA were not available in the Cambridge Crystal Structure Database [26]. The work done by Gujrathi and Jose [27] on 3-ASA, 4-ASA, and 5-ASA revealed marked differences in the molecular structures of 3-ASA and 5-ASA compared to that of 4-ASA. The results show that molecules of 3-ASA and 5-ASA contain dipolar species (COO^- and NH_3^+), while 4-ASA contains neutral species (COOH and NH_2).

3-ASA and 5-ASA do not make use of $-NH_2$ to form resonance structures. They make use of only-OH to form the resonance structures given in Figure 1.10.

1.6 Cyclodextrins

1.6.1 Structural features

Cyclodextrins (CDs) are cyclic oligosaccharides consisting of six or more glucopyranose units ($C_6H_{10}O_5$, molar mass = 162 g/mol). They are mainly obtained from starch. The naming of the CDs is based on the number of the glucopyranose units and alpha, beta and gamma correspond to 6, 7 and 8 units, respectively. (Alpha, beta, and gamma are abbreviated in this work as A, B and G, respectively, so, for example, beta-cyclodextrin is abbreviated to BCD). The CDs have chair conformations of alpha-1,4-linked D-glucose units. Cyclodextrins having fewer than 6 units do not exist because of high steric hindrance. The secondary hydroxyl groups situated at the carbon-2 and carbon-3 atoms are located at one side of a torus, while the primary hydroxyl groups at the carbon-6 atom are located on the other side. This gives a truncated cone-shaped structure with the wider side having the secondary OH groups and the narrower side having the primary OH groups (Figure 1.11). The OH groups make the exterior hydrophilic, while the cavity is hydrophobic. The cavity is also lined with hydrogen atoms on C-3 and C-5 and this results in the hydrophobic nature of the cavity [28, 29, 30, 31, 32].

The cavity (with diameter 1.0 nm for GCD, 0.8 nm for BCD and 0.6 nm for ACD) is available for the formation of host-guest inclusion complexes. In the solid state, the guest may fit into the cavity or be accommodated in voids between host molecules. In the CDs as prepared, there is generally water present (Figure 1.12). The water present in the cavity is also a driving force during the process of inclusion. Large-cavity cyclodextrins, made of more than 8 units,

generally do not form inclusion compounds because the cavity may accommodate so many water molecules that their properties resemble water molecules in the bulk of the solvent. This enhances the retention of the water in the cavity [33].

1.6.2 Uses of cyclodextrins

Cyclodextrins have attracted much interest in pharmacy and in the food, flavour, cosmetic and chemical industries, in spite of their relatively high cost. By inclusion, CDs can convert liquid compounds (e.g. vegetable oils) into more manageable solid products and can mask unpleasant odours or tastes of compounds. Inclusion may also stabilise the guest compound to hydrolysis, photolysis and auto-oxidation. Improvement in thermal stability may also result from the decreased volatility of the guest compound [32, 34].

The development of drugs has often been hampered because of their low aqueous solubility and poor bioavailability on administration. These properties may often be improved by use of cyclodextrins in their formulation [28, 34].

Most of the more common CDs do not have very high aqueous solubilities themselves (e.g. BCD : 1.85 g/100 ml H_2O at 25 °C), but these may still be better than the aqueous solubilities of the pure guest compounds, so that inclusion can increase the solubility and, hence, the bioavailability of low solubility drugs. The included drug may be more compatible with other excipients than it would have been in the absence of the CD. Selected reactions between guest molecules may be promoted in a catalytic manner within a host cavity, depending on the nature and size of the cavity and the sizes of the guest molecules [29].

Natural CDs are limited in their pharmaceutical applications because of their low solubility, especially BCD. Wider application of CDs is achieved by modification of their structures by incorporating various functional groups (e.g. methyl-, ethyl-, and hydroxypropyl-) in natural CDs. The molecular mass can be controlled by the degree of substitution. The use of the hydroxypropyl-group in the modification of the structure of BCD increases the solubility to above 50 g/ 100 ml H_2O at room temperature [35]. The formation of these derivatives produces several isomers of different degrees of substitution. The hydroxypropyl-group randomly substitutes the OH groups of BCD and gives compounds which are highly amorphous. This is an important physico-chemical property of chemically modified CDs and can have beneficial effects on the aqueous solubility and the toxicity. Modification is also useful in the optimisation of other properties such as surface tension, viscosity, storage and tableting conditions. Chemical modification can also change the phase solubility characteristics of any complexes formed, for example, precipitation may be avoided by the solubilization resulting from addition of more CD. HPBCD is the most likely candidate of all modified CDs to be used as an excipient in drug formulations [28].

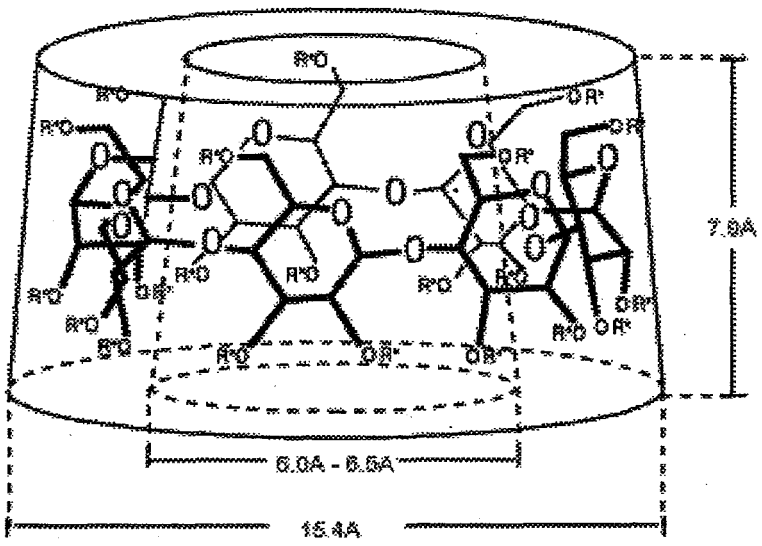

Figure 1.11: Truncated-cone shape of cyclodextrins [28].

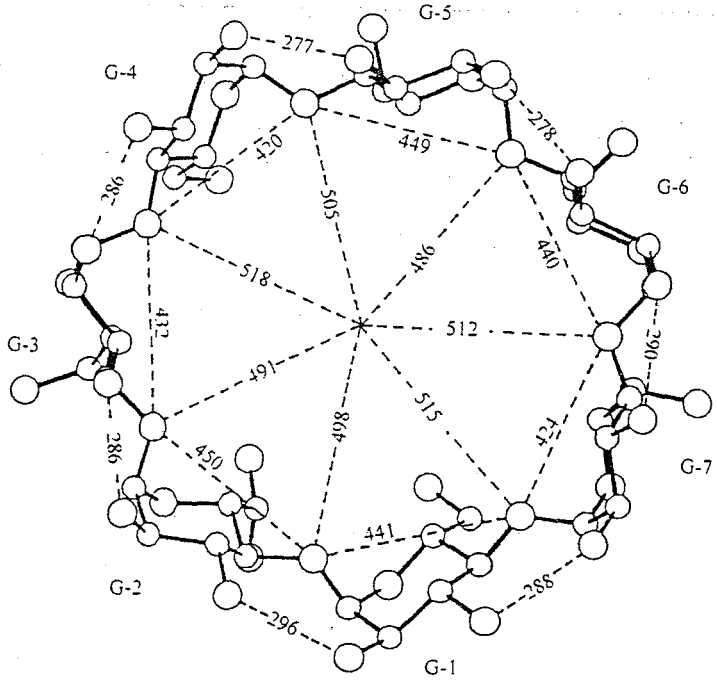

Figure 1.12: The structure of BCD in the dodecahydrate form (bonds lengths in picometers) [29].

Table 1.1: Some properties of natural and modified cyclodextrins [36, 37]

Property	ACD	BCD	GCD	HPBCD
Molar mass (g/mol)	972	1135	1297	1414
Units of Glucose	6	7	8	7
Internal cavity diameter (nm)	0.5	0.6	0.8	-
Solubility in water (g/100mL@25°C)	14.2	1.85	23.2	>50
Melting range (°C)	255-260	255-265	240-245	
Molecules of water of crystallisation*	10.2	13-15	8-18	
Water molecules in the cavity	6	11	17	

**This varies from sample to sample and with storage conditions*

The difference in cavity sizes (Table 1.1) results in different degrees of inclusion between CDs and various guest compounds. BCD has the lowest solubility at room temperature, while GCD has the highest among the natural CDs.

1.6.3 Complex formation by inclusion

As mentioned earlier, cyclodextrins have water in their hydrophobic cavities. These water molecules are energetically unstable and can be replaced easily by hydrophobic compounds (guest molecules). Inclusion is viewed as the replacement of water from the cavity by a less-polar guest compound to form a host/guest complex. The formation of inclusion complexes has been reported to be faster in solution than in the solid state [31]. In aqueous solutions, the guest molecule is in a hostile environment before inclusion takes place (Figure 1.13). The nature of the complex formed depends on the size of the cavity of the CD and the size and chemical nature of the guest molecule. The guest molecule may fit partially or completely into the cavity of the CD. For the molecule to be included, it must overcome any steric hindrance of its substituents at the cavity entrance. There will be an optimum size, geometry and functionality of a guest molecule for efficient accommodation in a given cavity. The formation of complexes will

usually be in stoichiometric guest : host molar ratios of 1:1, 1:2, 2:1 and so on. The inclusion can take place through the narrow (primary OH) or wide (secondary OH) section of the truncated cone-shaped cyclodextrin cavity. The process of inclusion is an equilibrium reaction and the time taken to attain a stable equilibrium depends on the nature of both the CD and the guest compound. Energetically favourable events are the displacement of water from the hydrophobic CD cavity, removal of the hydrophobic guest from the aqueous environment and interactions of the guest molecule(s) within the CD cavity [28, 33].

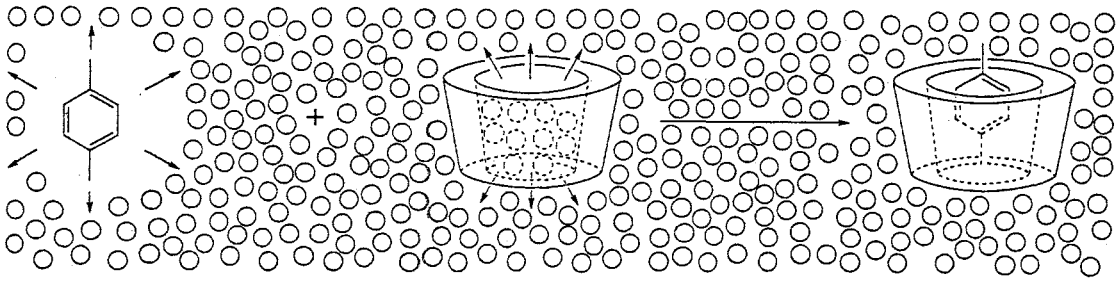

Figure 1.13: Representation of the inclusion of a guest molecule into the cyclodextrin cavity in a water environment [33].

The occurrence of inclusion can be indicated by methods of thermal analysis and confirmed by use of IR, NMR, UV and XRPD. IR spectra are often difficult to interpret because absorption by the CD molecules masks most of the bands due to inclusion complexes. However, the bands associated with carbonyl groups have been used for inclusion studies. Proton NMR spectra are useful because functional groups that are inserted into the cavity will have their coupling constants shifted and this can be clearly shown in the NMR spectra . The effect of

of inclusion can also be seen from the shielding of the host C-3-H and C-5-H hydrogen atoms in the interior of the cavity. For solid formulations, solid-state NMR is needed. X-ray powder diffraction patterns can reveal changes in the crystalline packing. Inclusion may result in an amorphous structure that gives characteristically poor XRPD patterns. Pure HPBCD is, however, an amorphous solid (see Table 1.1) to start with, so interpretation is not straightforward.

Kneading of physical mixtures of the drug and a cyclodextrin in the presence of small amount of a suitable solvent is often cited as a means of increasing the inclusion of the drug in the CD cavity. The possibility of the kneading process causing changes in crystallinity that are not related to inclusion has to be kept in mind.

To summarise, drug-CD complexation is not a simple process and requires time for equilibrium to be achieved especially in the liquid state. In the solid state, inclusion, if it occurs, is far more complicated and less-reproducible results are obtained. A variety of thermal and non-thermal methods should be used to determine the extent of complexation (if any) and the mechanism of complex formation.

1.7 Background to the relevant experimental techniques

1.7.1 Introduction

The methods used for studying the stability of pharmaceutical and other compounds may be divided into thermal and non-thermal methods. The thermal methods include differential scanning calorimetry (DSC), thermogravimetry (TG), thermogravimetry interfaced with Fourier transform infrared spectroscopy

(TG-FTIR), which is one of the major techniques of evolved gas analysis (EGA), and hot-stage microscopy (HSM). The non-thermal methods include X-ray powder diffraction (XRPD), Fourier transform infrared spectroscopy (FTIR) and nuclear magnetic resonance spectroscopy (NMR).

1.7.2. Differential scanning calorimetry (DSC)

DSC instruments exist in two types: power-compensated DSC and heat-flux DSC. Power-compensated DSC uses individual furnaces for heating the sample and the reference. The temperature difference between the sample and reference during the heating programme, is monitored and the instrument is designed to maintain a minimum temperature difference throughout the run by either adding or removing energy as required. The difference in the power supplied to the sample and to the reference is recorded against time or temperature. For heat-flux DSC, heat flows to both sample and reference material via an electrically heated constantan thermoelectric disk and the heat flow is proportional to the difference in temperature of the sample and the reference thermocouple junctions [38].

Van Dooren [39] considered the most important factors influencing DSC curves to be:- (1) the adjustment of the apparatus, such as the calorimetric sensitivity and the heating rate, (2) the sample's nature and mass, particle size, packing porosity and pretreatment, (3) the nature, mass and pretreatment of the reference material and (4) the atmosphere, if oxidising or inert gas, its thermal conductivity, and if flowing or static. Rapid heating gives large sharp endotherms or exotherms but small details may be lost. At lower heating rates, the temperature difference between sample and the reference is too small and some transitions may not appear on the curves. Low rates of heating are usually

recommended for most pharmaceutical analyses.

1.7.3 Thermogravimetry (TG)

Thermogravimetry (TG) provides quantitative information on mass changes but not on the nature of the reactions involved, hence the great advantage of the use of TG-FTIR (see later). Plotting the rate of mass-loss as a function of time or temperature (derivative thermogravimetry, DTG) is commonly used to detect subtle effects and for estimation of kinetic parameters. The mass-loss steps in a TG curve, which are associated with a series of reactions, are often more obvious and identifiable from DTG curves. It is also easier to compare the shapes of DTG curves with those obtained using other differential analysis methods like DTA, DSC, or evolved gas analysis (EGA).

1.7.4 TG interfaced with FTIR (TG-FTIR)

Thermogravimetry interfaced with Fourier transform infrared spectroscopy (TG-FTIR) provides simultaneous information about the loss of mass of a sample and the nature of any gaseous products formed. The technique is one of the many methods of evolved gas analysis (EGA). The TG system is connected to a gas cell in the FTIR instrument via a heated interface. Figure 1.14 shows an FTIR gas cell and Figure 1.15 shows the neighbourhood of TG furnace where heating of the sample takes place and gases are transferred to the FTIR gas cell.

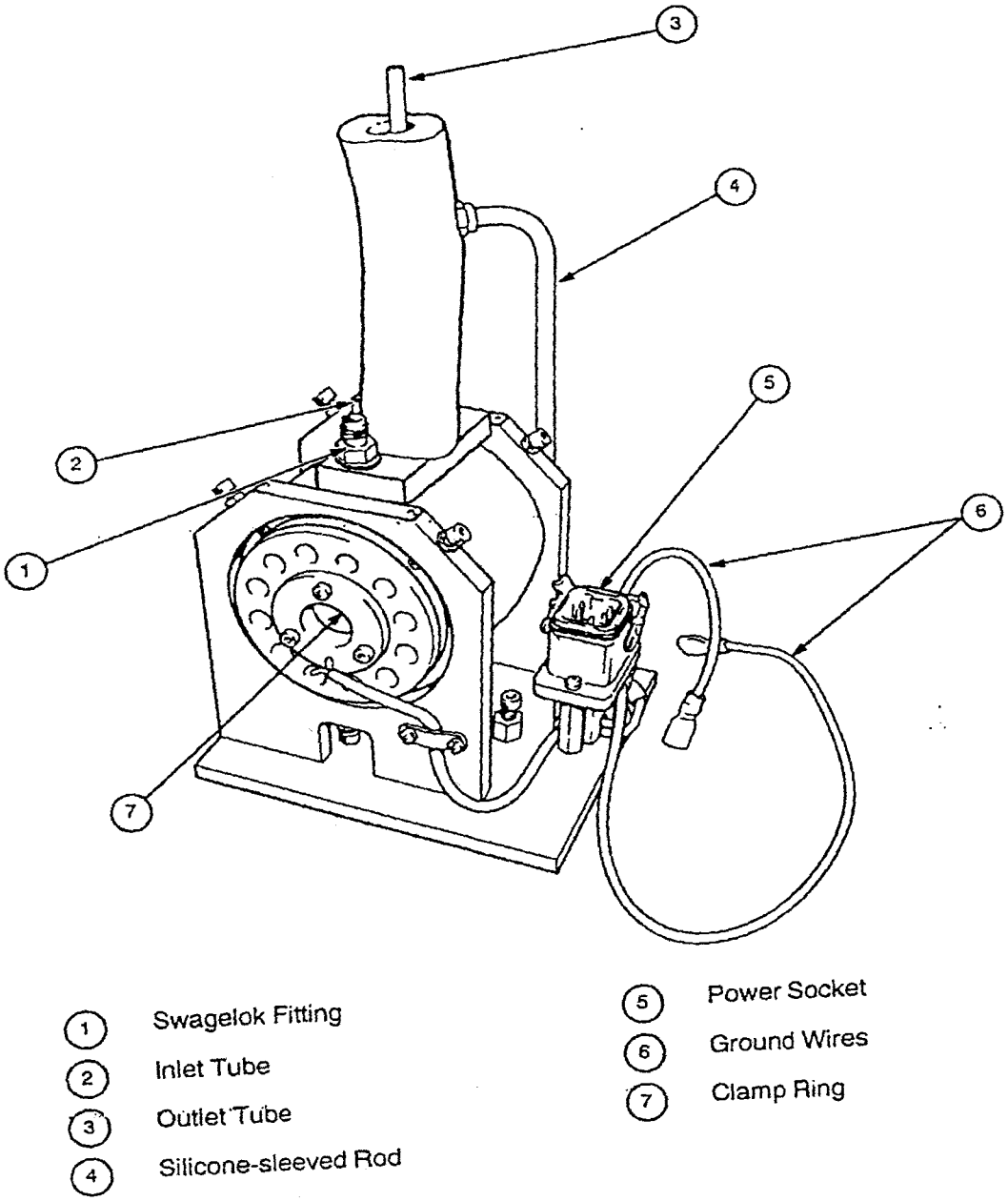

Figure 1.14: An FTIR gas cell [40].

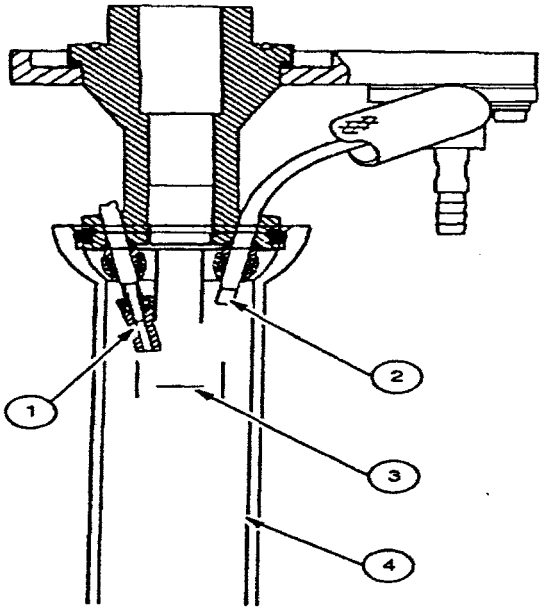

1 Ceramic Nozzle
2 Purge Outlet
3 Furnace
4 Furnace Tube

Figure 1.15: The neighbourhood of the TG furnace of the Perkin-Elmer Series 7 TG instrument where the gas is transferred to the FTIR gas cell [40].

The TG purge gas, which should be transparent to IR, acts as a carrier of the volatile products to a heated gas cell. The absorbances of the various decomposition products are recorded during the programmed heating of the sample in the TG. Gases such as water vapour, ammonia, and the oxides of carbon, sulphur, and nitrogen are easily identified by FTIR, even if produced simultaneously, because they have characteristic absorbances. The times at which the gaseous products are released from the decomposing compound are also recorded and can be related to the temperatures through the heating rate. Thus the nature of the decomposition can be determined far more easily and

accurately than when only TG is used. The results of TG-FTIR experiments are thus monitored by mass changes with time or temperature (TG and DTG curves), and simultaneous Gram-Schmidt reconstruction (GSR) curves (total IR absorbance) [41, 42]. In ideal cases, the DTG and GSR curves should be very similar. Typical curves, showing absorbances, wavelength ranges and scan times, are illustrated in Figures 1.16, 1.17, 1.18 and 1.19 from a study of the decomposition of calcium oxalate (CaC_2O_4) [40]. Figure 1.16 shows the TG curve, the temperature profile and the Gram-Schmidt curve. The stages of the mass-losses correspond to the peaks in the GSR curve. Calcium oxalate, on heating, produces both carbon monoxide and carbon dioxide gas. The individual GSR curves for each gas are printed separately so that differences in production are clearly indicated (Figures 1.18 and 1.19). Figure 1.18 indicates that carbon monoxide was produced during the second mass-loss only. Some carbon dioxide was produced during the second mass-loss and was the only gas evolved during the last (third) mass-loss (Figure 1.19). The formation of carbon dioxide (during the second mass- loss) is due to some oxidation of carbon monoxide. A stacked plot (Figure 1.17) showing, in three-dimensions, the evolution of gases at their characteristic absorbances does not differentiate between the two gases.

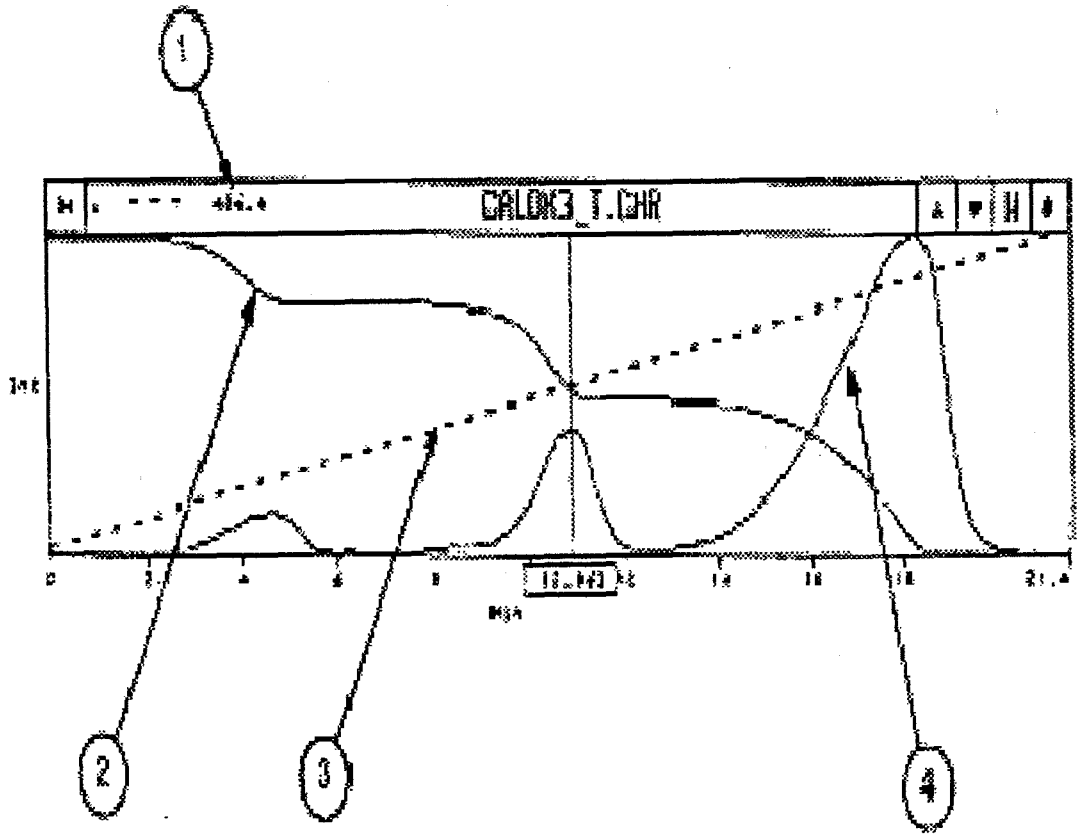

Figure1.16: TG-FTIR results for the decomposition of calcium oxalate (2) Mass-loss curve, (3) Temperature profile and (4) Gram-Schmidt curve [40].

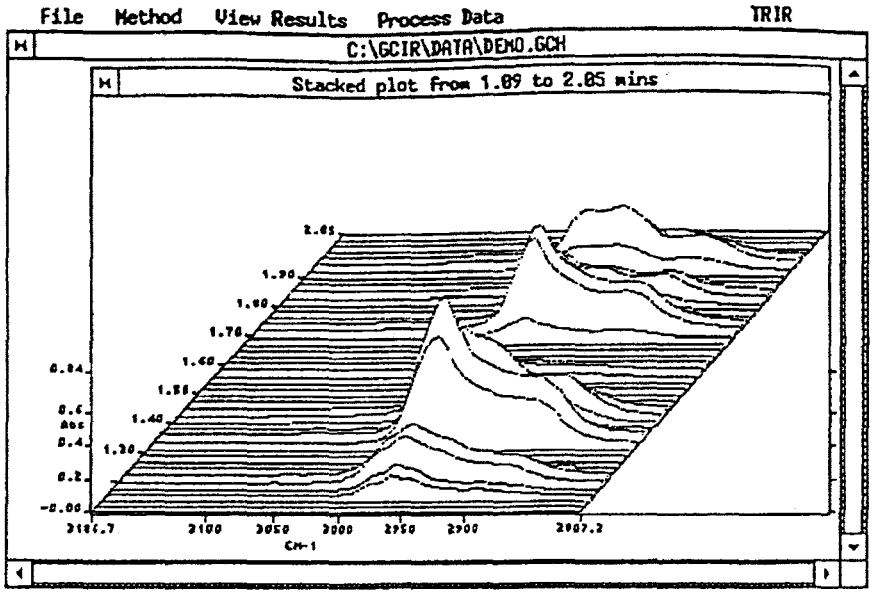

Figure 1.17: Three-dimensional plots of the IR absorbances of the gases evolved in a TG-FTIR analysis of calcium oxalate [40].

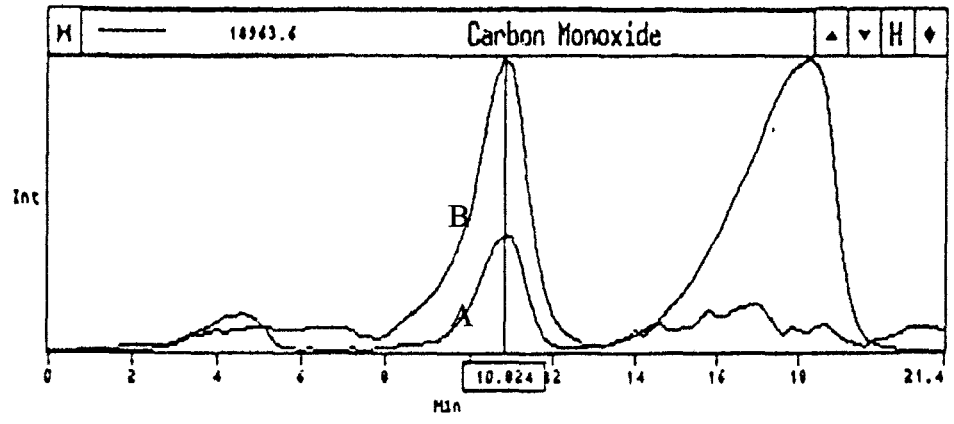

Figure1.18: The overall Gram-Schmidt curve (A) and the profile for the formation of carbon monoxide (B) during the decomposition of calcium oxalate [40].

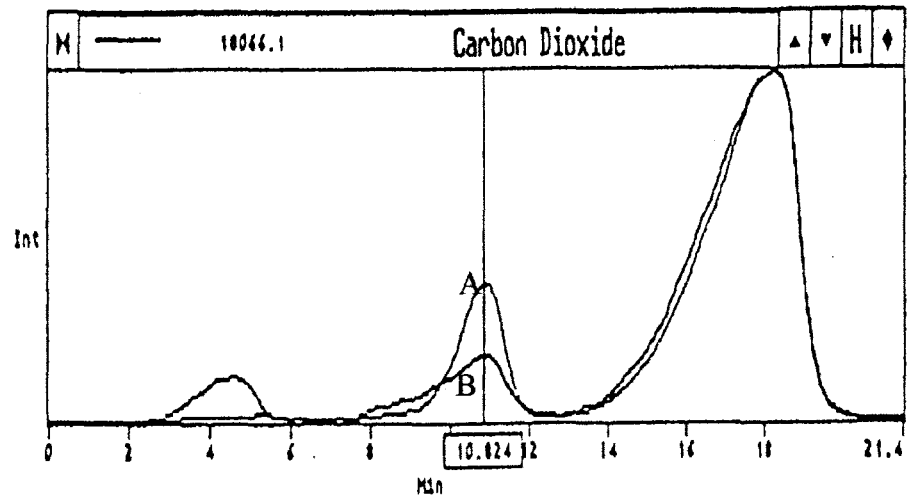

Figure 1.19: The overall Gram-Schmidt curve (A) and the profile for the formation of carbon dioxide (B) during the decomposition of calcium oxalate [40].

1.7.5 Hot-stage microscopy (HSM)

Hot-stage microscopy is used for studying morphological and other physical changes of crystals [38]. Some instruments provide for video recording of the changes. Changes that can be observed by hot-stage microscopy include loss of solvent of crystallization, sublimation, melting and re-solidification, phase transitions (polymorphic transformations), decomposition and solid-solid reactions. Drug-excipient interactions have also been studied. Observation of the melt-zone at the boundary interface can provide information on compatibilities or incompatibilities of the mixtures [43].

Observation of sublimation is important in interpreting TG results. The formation of and growth of nuclei of solid product during thermal decomposition

can sometimes be observed. Dehydration is also readily monitored by hot-stage microscopy [38].

1.7.6 Nuclear magnetic resonance spectroscopy (NMR)

Nuclear magnetic resonance spectroscopy (NMR) has been used, for example, to study the inclusion of para-hydroxybenzoic acid in BCD [33, 44]. The formation of complexes disturbs the orientation of the hydrogen atoms in the guest molecule and in the CDs. The hydrogen atoms in the cavity are C-3-H and C-5-H and are shielded by the included molecule, while the hydrogen atoms on the outer surface, C-2-H, C-4-H and C-6-H, are practically unaffected. Such observations can show the occurrence of inclusion, but not the kind of functional group which is important in the inclusion.

1.8 Estimation of thermodynamic properties

Experimentally determined values for all of the relevant thermodynamic properties, such as enthalpies of formation in the solid, liquid and gaseous phases, enthalpies of melting, vaporization and sublimation, and the enthalpies of the decarboxylation reactions of the appropriate (solid) acids are not usually available from the literature, but values can be estimated from tables of group contributions, according to the methods given by Domalski and Hearing [45]. These methods have been applied in this study (see Section 3.1) and compared, where possible, with experimental data. The most uncertain parts of such estimations are probably the allowances suggested for different isomers.

1.9 Estimation of kinetic parameters

The rate equations that have found application in solid-state kinetic analyses [46, 47] may be generalised in their derivative forms as: $d\alpha/dt = k\ f(\alpha)$ and the corresponding integrated forms as: $g(\alpha) = kt + c$, where α is the fractional extent of reaction and k is the rate constant. These expressions are grouped according to the shape of the isothermal α-time curves as acceleratory, sigmoid or deceleratory [46, 47]. The temperature dependence of the rate constant, k, is assumed to be described by the Arrhenius equation:

$$k = A \exp(-E/RT),$$

where E = the activation energy, A = the pre-exponential factor, R = the gas constant and T = the temperature in Kelvin.

As a consequence of the bonding in and, hence, the crystal structures of organic solids, melting or sublimation may often be expected to precede or accompany thermal decomposition. Galwey [1, 47] has discussed the possible role of melting in thermal reactions of initially solid reactants. The possibility of melting is not always considered in the interpretation of kinetic data and the formulation of reaction mechanisms. Formation of a liquid phase may result in increased rates of isothermal decomposition and produce sigmoid α - time curves.

Carstensen [1] has done much to promote consideration of the Bawn model [48] which applies to the situation where reactant A is soluble in product B with solubility, **s.** When the extent of decomposition is α, the fraction of A in the

liquid phase is α s, and in the solid phase is (**1** - α - α s). If the rate coefficients for reactions in the solid and in the liquid phases are $\mathbf{k_s}$ and $\mathbf{k_l}$, respectively, then:

$$d\alpha/dt = k_s (1 - \alpha - \alpha s) + k_l \alpha s = k_s + K \alpha \qquad (1)$$

where $K = k_l s - k_s s - k_s$, and:

$$\alpha = (k_s / K) [\exp (Kt) - 1] \qquad (2)$$

The expected ratio k_l / k_s can be estimated [1], as follows. Using:

$$k_s = A_s \exp (-E_s/RT) \quad \text{and} \quad k_l = A_l \exp (-E_l/RT)$$

and assuming that the difference $E_s - E_l$ is equal to the molar enthalpy of melting, then if $A_s \approx A_l$:

$$k_l / k_s \approx \exp (\Delta H_{melting}/RT)$$

For a typical value of $\Delta H_{melting} \approx 20$ kJ mol^{-1} and T = 400 K, $k_l / k_s \approx 410$.
The alpha-time curves for the Bawn model are sigmoidal, being acceleratory according to equation (2), up to the liquefaction point, where $\alpha = \alpha^* = 1/(1 + s)$ at $t = t^*$, and deceleratory beyond according to:

$$(1 - \alpha)/(1 - \alpha^*) = \exp [- k_l(t - t^*)] \qquad (3)$$

The Bawn model [48], however, does not usually appear in the familiar set of rate equations, because it is not strictly applicable to decompositions occurring

entirely in the solid state [49].

1.10 Evaporation and sublimation

Evaporation refers to the conversion of a liquid to a gas and sublimation to the conversion from solid to gaseous form without the intervention of a liquid phase. Sublimation and evaporation are zero-order rate processes, with the isothermal rate of mass-loss being constant for a constant surface area [50, 51].

$d\alpha/dt = k$ at constant temperature,

(α = extent of sublimation or evaporation and k is the rate coefficient).

In a TG experiment at a constant heating rate, β:

$$d\alpha/dt = d\alpha/dT.dT/dt = \beta d\alpha/dT$$

so

$$d\alpha/dT = k/\beta$$

Using the Arrhenius equation:

$$d\alpha/dT = (A/\beta)\exp(-E/RT)$$

k may be estimated from the slope of the TG curve (or from the DTG curve). An Arrhenius plot of ln k against the reciprocal of T should then be linear with slope equal to -E /R and intercept ln A.

The value of E, obtained under these conditions is almost equal to the enthalpy

of evaporation [52]. The values may be compared with those calculated using the methods given by Domalski and Hearing [45].

1.11 Some relevant stability studies in the solid state

There have been several studies of decompositions of various substituted aminobenzoic acids in the solid state [9, 11, 17, 23, 53-58] and even more studies in solution [59-64]. In addition to their pharmaceutical uses (see also Section 1.4) [9, 17], such reactants are of interest because the existence of ranges of isomers allows for comparison of behaviour. They also provide promising systems for the study of the participation of melting, vaporisation, and the influence of products, on the course of decomposition of an initially-solid reactant. Carstensen and Musa [55] have reported on the decompositions of benzoic acid derivatives in the solid state:

$$p\text{-}XC_6H_4COOH\ (s) \longrightarrow XC_6H_5\ (l) + CO_2\ (g).$$

Mention is made that thermal analysis methods were not used in the study because of sublimation problems. Kornblum and Sciarrone [54] have studied the solid state decarboxylation of 4-aminosalicylic acid (4-ASA) and Pothisiri and Carstensen [23] studied the decompositions of several p-substituted salicylic acids. Wesolowski [9] studied the kinetics and mechanism of decarboxylation of 4-ASA and its sodium and calcium salts in the solid state and in solution. A range of values for the melting point of 4-ASA has been reported (139 - 151°C). Discrepancies arise because melting is accompanied by decarboxylation, reported [9] to begin at about 110°C and to continue up to 150°C, and to be accelerated by water and the product, 3-aminophenol (3-AP).

DSC measurements [65] in an open pan are often distorted by mass losses due to sublimation, or release of water during chemical reaction. Although these conditions can often be avoided by the use of sealed pressure pans, Riesen *et al.* [65] showed that simultaneous DSC and TG measurements can be used to correct the measured enthalpy changes for actual sample mass.

1.12 The thermal behaviour of cyclodextrins

Kohata *et al.* [66] studied the thermal decomposition of ACD, BCD, GCD and modified BCD. Thermal analyses were done in helium at 10 K min^{-1}. The natural CDs lost most of their water at temperatures below 100°C (see Figure 1.20). The strongly bonded water in ACD and GCD was liberated between 260°C and 270°C, followed by decomposition. The mass losses of the CDs at 550°C were found to be: 98% for ACD, 88% for BCD and 98% for GCD (Figure 1.21).

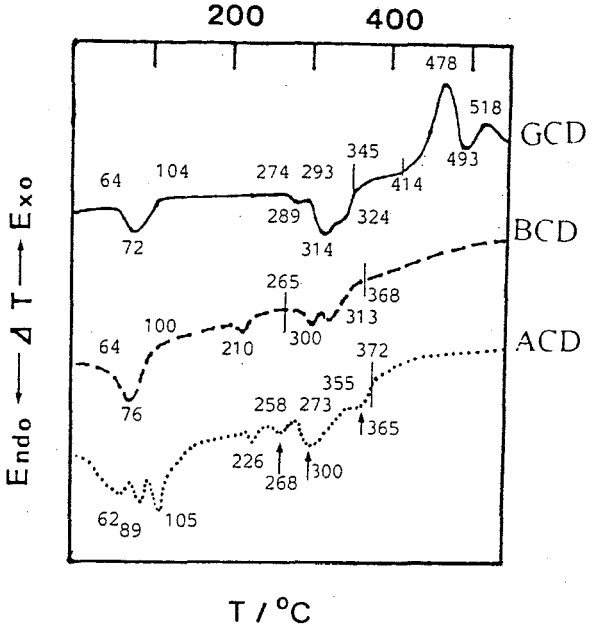

Figure 1.20: DSC curves for ACD, BCD, and GCD (heated in helium at 10 K min^{-1}) [66].

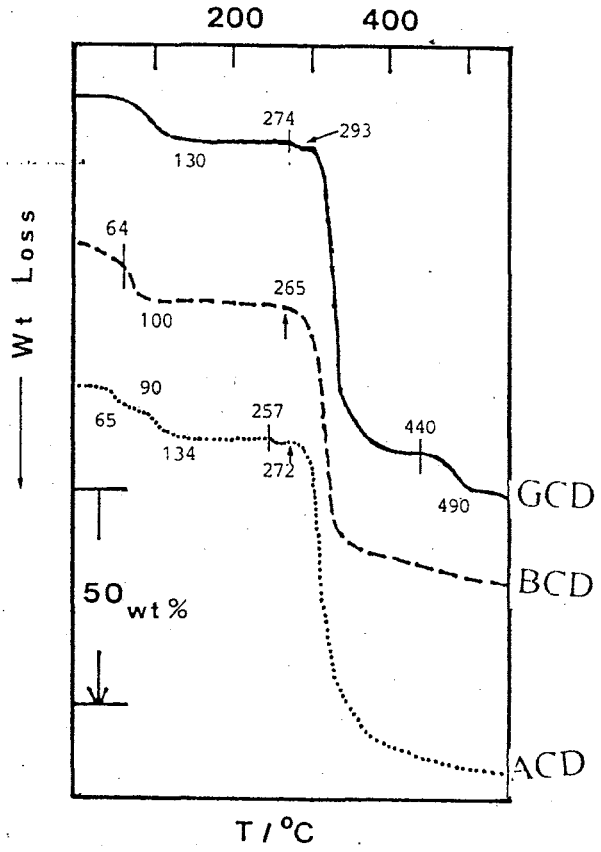

Figure 1.21: TG curves for ACD, BCD, and GCD (heated in helium at 10 K min^{-1}) [66].

BCD, on heating at 5 K min^{-1} in air [67], loses water (about 14%) up to 100°C. There is an endotherm at about 220°C associated with a reversible transition. Thermal decomposition (and oxidation in air) starts at 250°C. Melting occurs near 300°C. Ignition occurs in air above 300°C. TG, DSC, DTG and EGA curves are given in Figure 1.22.

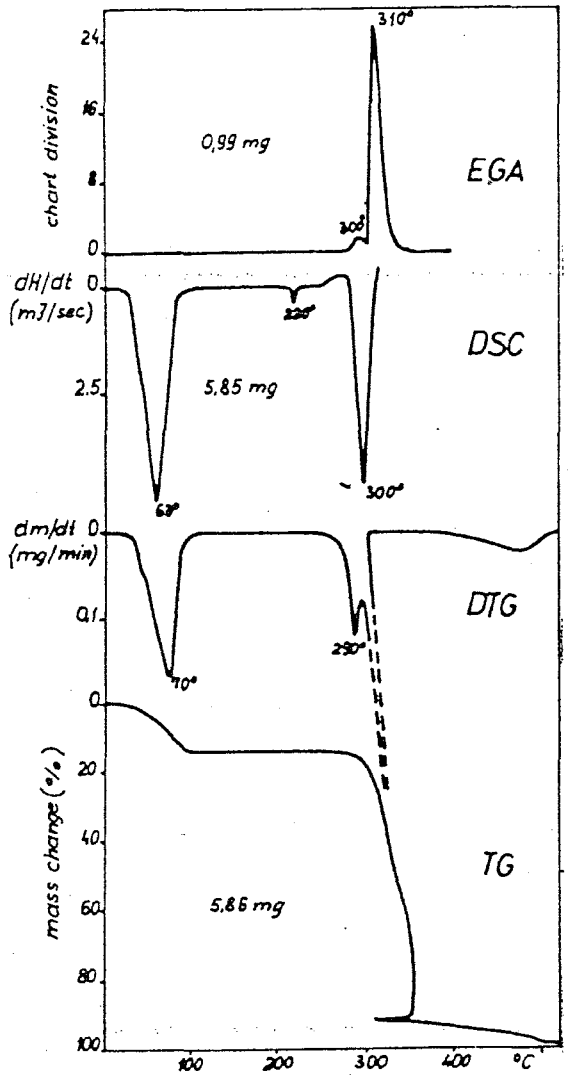

Figure 1.22: TG, DSC, DTG and EGA curves of BCD (heated in flowing nitrogen at 8 K min^{-1}) [67].

BCD was reported by Giordano *et al.* [37] to lose water from ambient temperature up to 120°C depending on the type of pan used (open, perforated or sealed lids) and to degrade (accompanied by oxidation in air) above 250°C. Between 120°C and 280°C the TG curve (Figure 1.23) shows no mass loss, while in the DSC curve (same figure) small endo or exo effects appear between 210°C and 240°C. These have been attributed [37] to a reversible

transformation of BCD. Assuming that the mass loss between about 45°C and 95°C (12.77%) is due to loss of water, then this sample of BCD contained 9 moles of water per BCD unit.

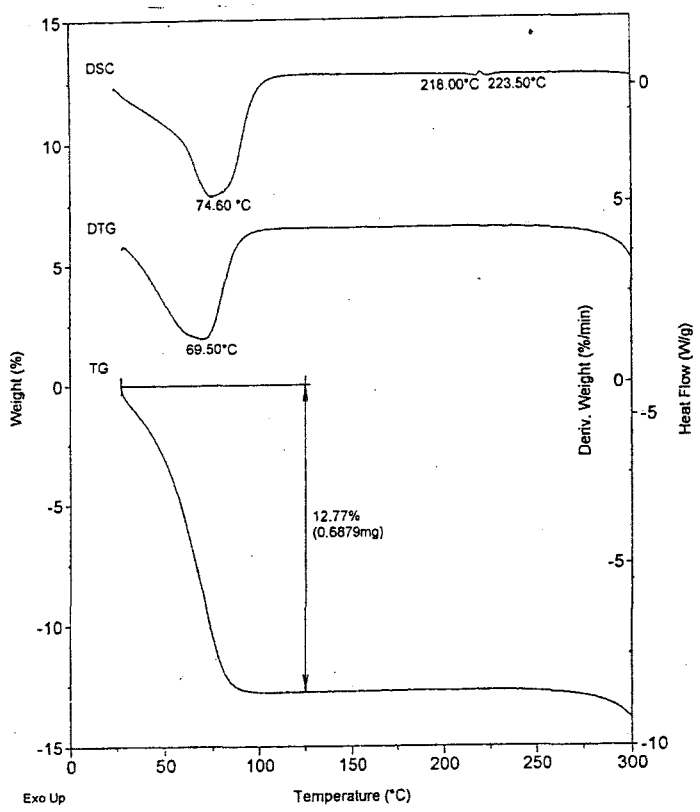

Figure 1.23: DSC ,TG and DTG curves for BCD (heated in flowing nitrogen at 10 K min^{-1}) [37].

Marini *et al.*[68] examined the thermodynamics of dehydration of BCD in dry nitrogen. The water in BCD exists in a variety of configurations and hydration/dehydration is a reversible process. The enthalpy of dehydration was 23.5 kJ / mol H_2O. Values as high as n = 12.6, for the number of moles of water per mole of CD, have been reported. Dehydration and the structural transition at 220°C are not unrelated.

Berbenni *et al.* [69] used TG, including high-resolution and constant rate TG, to study the stages of dehydration of ACD.$6H_2O$. Stage 1 is the release of adsorbed surface water. Stages 2 and 3 are removal of water from interstitial positions. Stage 4 corresponds to the removal of water from the ACD cavity (Figure 1.24).

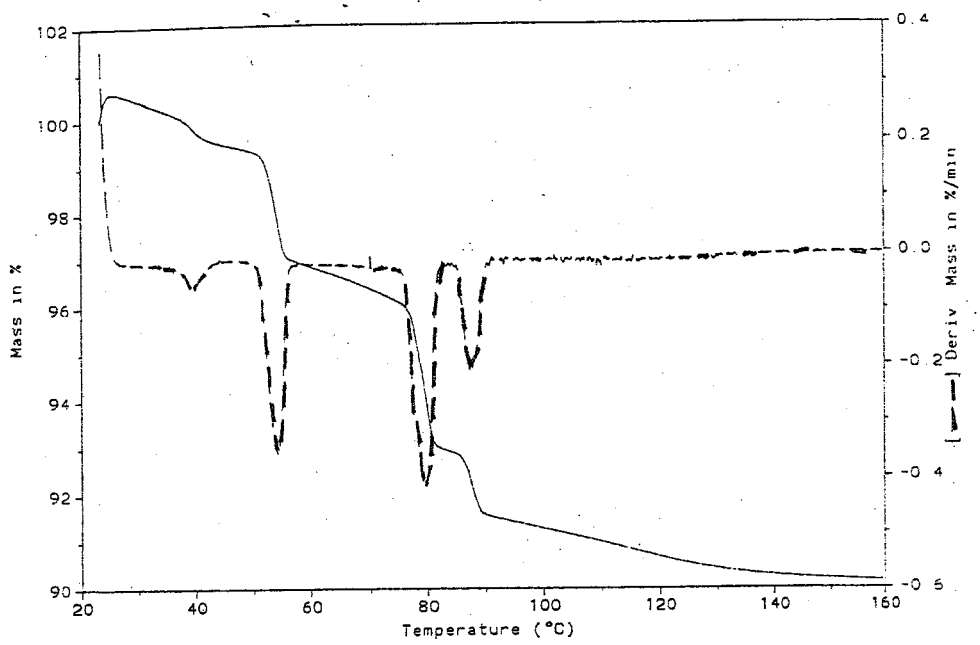

Figure 1.24: TG and DTG curves of ACD (heated at of 0.5 °C min^{-1} in flowing nitrogen) [69].

Giordano *et al.*[37] examined the literature concerning the thermal properties of natural and modified cyclodextrins and their inclusion compounds. They mentioned that cyclodextrins are marketed as hydrates with differing water contents, depending on the relative humidity, procedure of preparation and storage conditions. The general thermal behaviour is similar for all of the natural cyclodextrins, with differences only in water content (due to the variation in their cavity sizes), onset temperatures of thermal degradation and mass-loss values at given temperatures. Figure 1.25 gives the thermal behaviour (DSC and TG) of

GCD. They further reported that GCD loses 7 moles of water per mole of GCD at temperatures below 130 °C and a further one mole at about 275 °C.

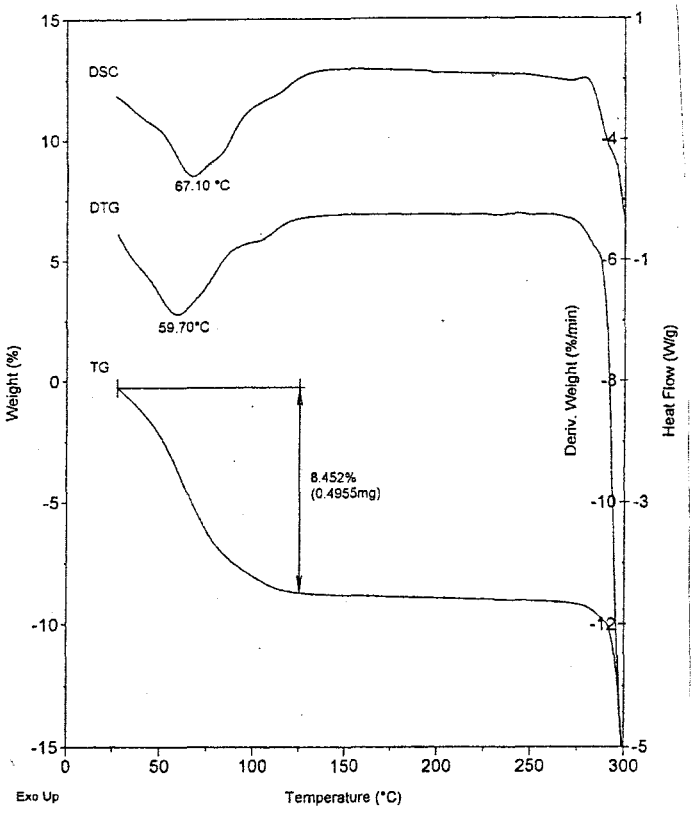

Figure 1.25: DSC, DTG and TG curves for GCD (heated in flowing nitrogen at 10 K min^{-1}) [37].

1.13 Thermal behaviour of drug/cyclodextrin mixtures

Novak *et al.* [31] compared the complexation behaviour of different CDs (alpha-, beta-, gamma-, dimethyl-beta-, and randomly methylated beta-) with tolperisone.hydrochloride ($C_{16}H_{23}NO.HCl$). The last two CDs did not give pronounced host-guest interactions. A DSC curve for BCD is given in their Figure 2 (Figure 1.26). No ΔH value was quoted for the first endotherm. IR spectroscopy was also used to study the inclusion of tolperisone.HCl with BCD.

The bands at 2533, 2580 and 2635 cm^{-1} were assigned to the N-H group, with strong intramolecular hydrogen bonds, and the band at 1677 cm^{-1} was assigned to the aromatic carbonyl group. The significant decrease of the N-H absorptions between 2500-2700 cm^{-1} shows that intramolecular hydrogen bonding is decreased in the kneaded mixture (Figure 1.27). This could be due to the formation of a complex with the cyclodextrin.

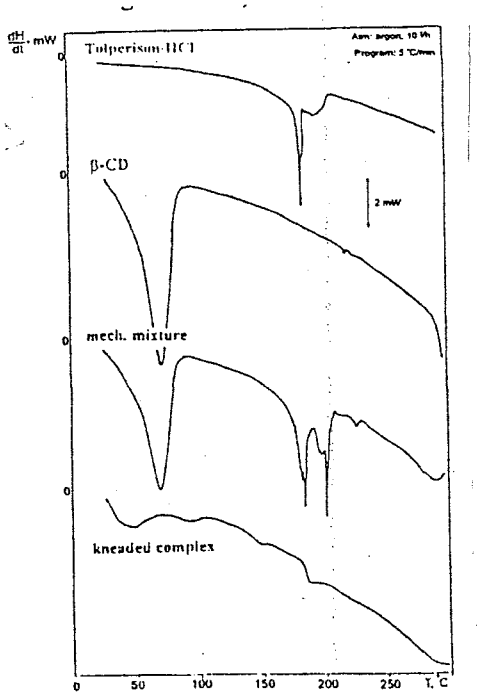

Figure 1.26: DSC curves of mixtures of tolperisone-HCl with BCD (heated in argon at 5 K min^{-1}) [31].

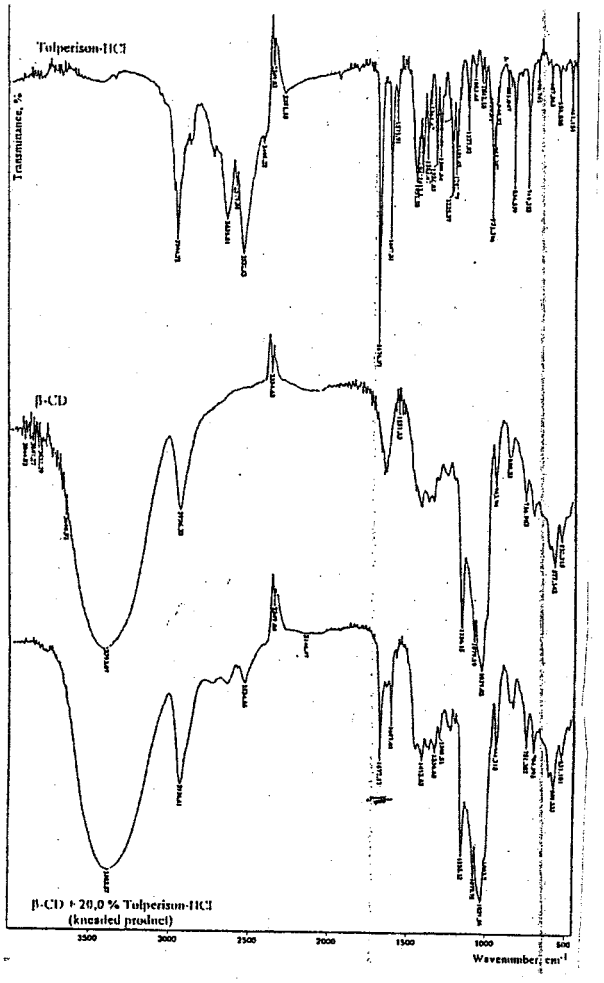

Figure 1.27: IR spectra of a mixture of 20 % tolperisone-HCl with BCD [31].

Fodor *et al.* [30] examined mixtures of mandelic acid ($C_6H_5CH(OH)COOH$) with alpha-, beta-, and gamma-CDs, prepared using kneading and grinding techniques. BCD gave the most stable complex. Their DSC curves are given in Figure 1.28. X-ray powder diffraction patterns for mixtures of mandelic acid with BCD showed clearly that interactions between mandelic acid and BCD occurred when

mixtures were ground for several hours. The XRPD patterns shown in Figure 1.29 became more diffuse after long periods of grinding.

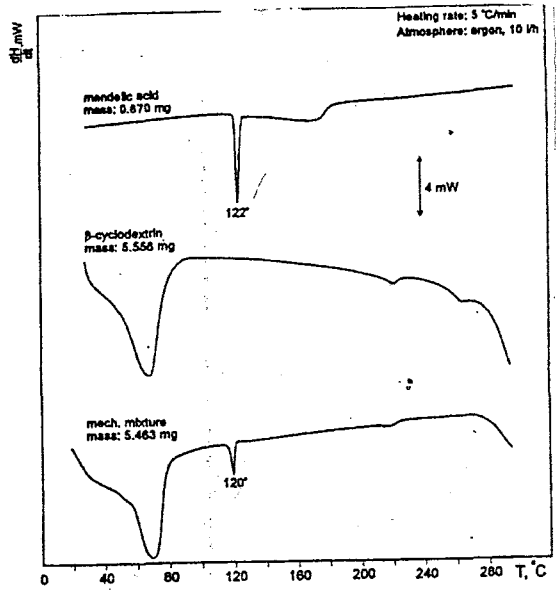

Figure 1.28: DSC curves of pure mandelic acid, BCD and their mechanical mixture (heated in flowing argon at 5 K min^{-1}) [30].

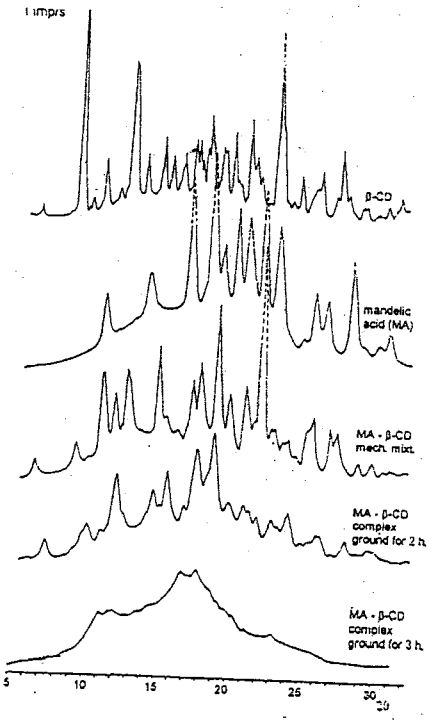

Figure 1.29: X-ray powder diffraction patterns of a mixture of 11% mandelic acid with BCD (prepared by dry grinding) [30].

In further studies, Novak *et al.* [70] examined cyclodextrin complexes with mandelic acid (both optically active and racemic) prepared by lyophilisation. DSC, TG and EGD were complemented by FTIR, SEM and dissolution-rate determinations. Formation of complexes between the guest compounds and the CDs was proven by thermoanalytical methods and FTIR.

Complexation of benzaldehyde (C_6H_5CHO) with BCD was studied by thermal analysis and X-ray powder diffraction [71]. The studies showed that the decomposition of the complex occurred in three stages: dehydration between 70°C and 120°C, dissociation of the dehydrated complex between 235°C and 270°C, and decomposition of BCD above 280°C (see Figure 1.30). XRPD studies were done to confirm the inclusion process and a clear difference between the pattern of the complex and that of BCD suggests the occurrence of inclusion (Figure 1.31).

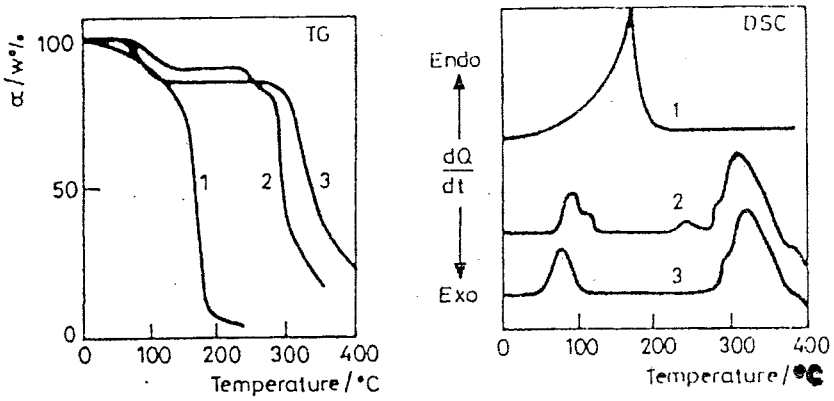

Figure 1.30: TG and DSC curves for (1) benzaldehyde. (2) the complex and (3) BCD (heated in static air at 5 K min^{-1}) [71].

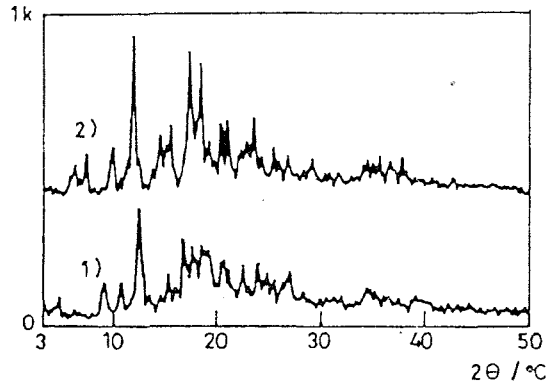

Figure 1.31: XRPD patterns of (1) BCD and (2) the complex of 8.8% benzaldehyde with BCD [71].

Cohen and Lach [72] investigated the interaction of hydroxybenzoic acids (C_6H_4(OH) COOH) and the esters of p-hydroxybenzoic acid with ACD and BCD in water. For each member of these series, the increase in solubility was found to be proportional to the total concentration of the CD present in solution. This indicated the formation of 1:1 complexes. Values of the formation constants, K_f, were calculated. The size of the guest molecule and the size of the cavity of the CD influenced the strength of inclusion. The same researchers [72] investigated the interaction of ACD and BCD in aqueous solution with some drugs, including 4-ASA and 4-ABA. All the drugs investigated interacted with the CDs. The lower the solubility of the drug in water, or the smaller the molecule, the greater the value of K_f and hence the stronger the interaction. Similar work on aminobenzoic acids and mono-halogenated benzoic acids gave K_f values that

decreased in the order Cl > Br and also in the order m- > p- > o-. K_f values for the same guest molecule were greater with BCD than with ACD [32].

Zerrouk *et al.*[73] have investigated the inclusion of 5-ASA in ACD and BCD. The mixtures were prepared using the kneading method. The results showed that 5-ASA did not include in ACD, and that the stability of inclusion with BCD was very low in solution. The study was done using DSC, thermomicroscopy, XRPD, SEM and MS.

Yilmaz *et al.* [74] reported on the thermal decomposition of inclusion complexes of ferrocene ($C_{10}H_{10}Fe$) and its derivatives with BCD, studied using DTA and TG. Three stages of decomposition were found and attributed to dehydration of the BCD cavity in the complex, liberation of the guest compound from the complex, and decomposition of the BCD. Sometimes dehydration and liberation of the compound occurred over the same temperature range and this caused difficulty in distinguishing between the two processes. The sample complexes were prepared by co-precipitation and physical mixtures were also examined for comparison. Most of the complexes of ferrocene and its derivatives had 1:1 mole ratios, except for BCD- benzoylferrocene ($C_6H_5CO.C_{10}H_9Fe$), which formed a 1 drug : 2 BCD mole ratio complex as shown by X-ray powder diffraction. A physical mixture of BCD and benzoylferrocene showed dehydration of BCD, a transition at 223 °C and other endotherms characteristic of benzoylferrocene, thus indicating no formation of a complex.

Zornoza *et al.* [75] studied the complexation of glisentide (o-$CH_3(C_6H_4)CONHCH_2CH_2C_6H_4SO_2NHCONHC_5H_8$), a poorly water-soluble drug, with three CDs (ACD, BCD and GCD) using DSC, NMR, XRPD and IR.

Mixtures were prepared by co-precipitation and by kneading. The IR results were difficult to interpret. The structure of the complex in solution form was elucidated by use of NMR spectroscopy. X-ray powder diffraction patterns of both types of mixtures showed that the co-precipitated systems were almost amorphous (indicative of inclusion), while the patterns for the kneaded and physical mixtures were similar to each other. The DSC curves for the co-precipitated complexes showed no endotherms at 160°C (the melting point of glisentide). In the kneaded mixtures the melting endotherms were only slightly decreased. The co-precipitation method was thus better than the kneading method for inclusion complexation.

Li *et al.* [76] examined the stability of the 1:1 mole ratio inclusion complex of BCD with cinnamic aldehyde (C_9H_8O) by means of TG and DSC. From TG, the first stage of mass-loss at 50°C to 120°C was due to the dehydration of the water in the CD cavity. Dissociation of the BCD-cinnamic aldehyde complex proceeds between 200°C and 260°C and then decomposition of BCD occurs above 280°C. The activation energy (E) and pre-exponential factor (A) for dissociation of the complex were found to be 160 kJ mol^{-1} and 5.8 x 10^{14} min^{-1}, respectively. The BCD-cinnamic aldehyde complex has been used in industry as a flavorant in the making of sweets.

The inclusion complexes of capric acid ($CH_3(CH_2)_8COOH$) and caprilic acid ($CH_3(CH_2)_6COOH$) with BCD and GCD were studied in the solid state using DSC, TG and FTIR [77]. The maximum mole ratio for complex formation was found to be 1:1 for caprilic (C_{10}) acid and BCD and 1:1.5 for capric (C_8) acid and BCD. For the same acids with GCD, these proportions were increased to 1:1.5 (C_{10}) and 1:2 (C_8). DSC was used to monitor the inclusion of the acid by

observation of the endotherms for BCD, the pure compounds and the complexes formed. Observation of the melting endotherm for the acids in the samples of the mixtures showed that the compound was not totally included. The use of TG showed clearly the behaviour of the acids in the complexes [78]. The stages of mass losses in the TG and DTG curves were due to (1) dehydration of the CDs, (2) the volatilisation of the acids and (3) the decomposition of the CDs. FTIR results showed that the absorption peak at 1712 cm^{-1} (C=O) and a characteristic cyclodextrin band at 1640 cm^{-1} decreased in their intensities when the inclusion complexes were formed and results were in agreement with the results from thermal analysis. The band at about 1640 cm^{-1} is due to the presence of moisture in the CDs [79].

Moyano *et al.* [80] studied mixtures of gliclazide (a drug used for the control of blood glucose level in diabetic patients) $\{C_{15}H_{21}N_3O_3S\}$ with BCD prepared by the following methods: kneading, co-precipitation, spray-drying, neutralisation and co-grinding. The mixtures were examined using DSC, TG and FTIR. A shift of the carbonyl band to higher wavenumbers was assumed to indicate that inclusion had taken place.

The interaction between the sunscreen agent, butyl-methoxydibenzoylmethane (BM-DBM) $\{(CH_3)_3CC_6H_4COCH_2COC_6H_4OCH_3\}$ and HPBCD was studied by DSC and XRPD [81]. DSC curves revealed some interaction between BM-DBM and HPBCD in the solid state. The DSC curves for BM-DBM crystals Figure 1.32 shows an endotherm at about 80°C (ΔH= 59.0 J/g). Two endotherms, corresponding to melting of BM-DBM and dehydration of HPBCD, were evident for the physical mixture. The disappearance of the endotherms in the kneaded mixture (using water-ethanol as a kneading agent) suggested complete inclusion.

X-ray powder diffraction studies revealed the crystalline nature of BM-DBM and the amorphous nature of HPBCD. XRPD patterns (Figure 1.33) showed superimposition of the BM-DBM and HPBCD patterns in the physical mixture. The XRPD pattern for the kneaded mixture showed no signals for BM-DBM, demonstrating complete amorphousness. The guest molecule was thus assumed to be included in the cavity of the CD.

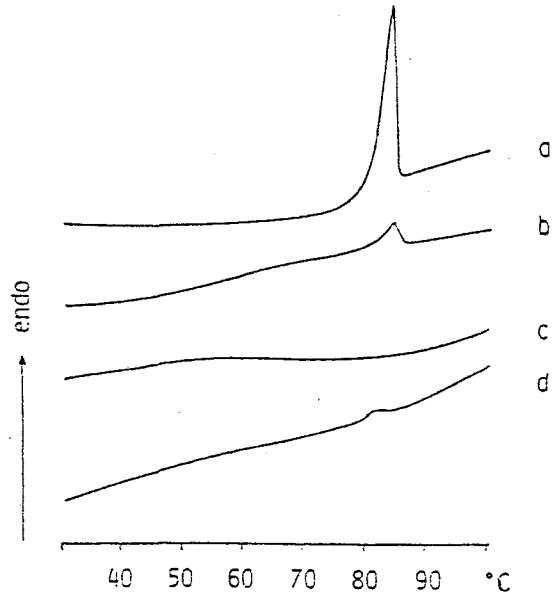

Figure 1.32: DSC curves of (a) butyl-methoxydibenzoylmethane (BM-DBM), (b) a physical mixture of BM-DBM with HPBCD, (c) a kneaded mixture of BM-DBM and HPBCD (water-ethanol agent) and (d) kneaded mixture of BM-DBM and HPBCD (ethanol agent) (heated in nitrogen in crimped aluminium pans at 5 K min^{-1}) [81].

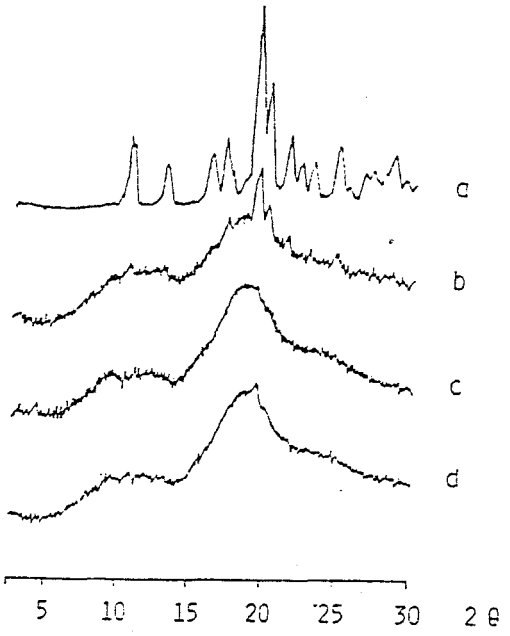

Figure 1.33: XRPD of (a) pure BM-DBM, (b) a physical mixture of BM-DBM and HPBCD, (c) a kneaded mixture of BM-DBM and HPBCD (water-ethanol agent) and (d) kneaded mixture of BM-DBM and HPBCD (ethanol agent) (mixtures of 1:2 molar ratio BM-DBM to HPBCD) [81].

1.14 Molecular modelling of cyclodextrins and their inclusion complexes

Lipkowitz [82] has provided an excellent review of the application of computational chemistry to the study of cyclodextrins. This review clearly shows the specialised expertise and experience required to tackle the molecular modelling of such complex molecules and the increased difficulties of modelling host–guest interactions.

The same special issue of Chemical Reviews [82] contains reviews of NMR studies of CDs, solid-state structures, thermochemical studies and reactions in CD environments.

The Lipkowitz review [82] also summarises the great deal of information currently available on CDs and their molecular interactions. In general, cyclodextrins are remarkably flexible and the symmetric structures illustrated in the literature are time-averaged structures. There is evidence that the host CD can adopt a structure which best accommodates a guest, for example elliptical structures to accommodate benzene derivatives, so that, in host-guest complexes, the CD structure may be far removed from its most–stable, low–energy conformation.

Full alkylation of CDs with methyl groups [83] leads to: (1) an increase in the cavity opening and the internal diameter; (2) the increase in the diameter on the secondary side being greater than on the primary side, and (3) the cavity opening on the primary rim being larger than the internal diameter of the O_4 glycosidic oxygens.

Comparisons of the dynamic behaviour of ACD in the solid state and in aqueous solution [84] showed that the mobility of the ACD molecule in solution is about twice that in the solid state. The positions of the O_6 atoms and the hydroxyl hydrogens are very different in the two states.

Lipkowitz [82] identifies the types of interaction involved in host-guest complexation as: (1) non–bonded (van der Waals attractive forces, steric repulsive forces and electrostatic forces); (2) hydrogen–bonding; (3) relief of conformational strain energy of the CD host on formation of a more stable host-guest structure; (4) hydrophobic forces involved in the exclusion of non-polar solutes from aqueous solution; and (5) the special 'high energy' nature of the water in the CD cavity.

Scheme 1 (Figure 1.34) [82, 85] shows the overall change in Gibbs energy for complexation as the sum of:

[1] $(CD.nH_2O) \rightarrow CD + nH_2O(g)$

[2] $H_2O(g) \rightarrow H_2O(l)$

[3] $G(aq) \rightarrow G(g)$ (G = non-polar guest)

[4] $CD + G(g) \rightarrow (CD.G)$

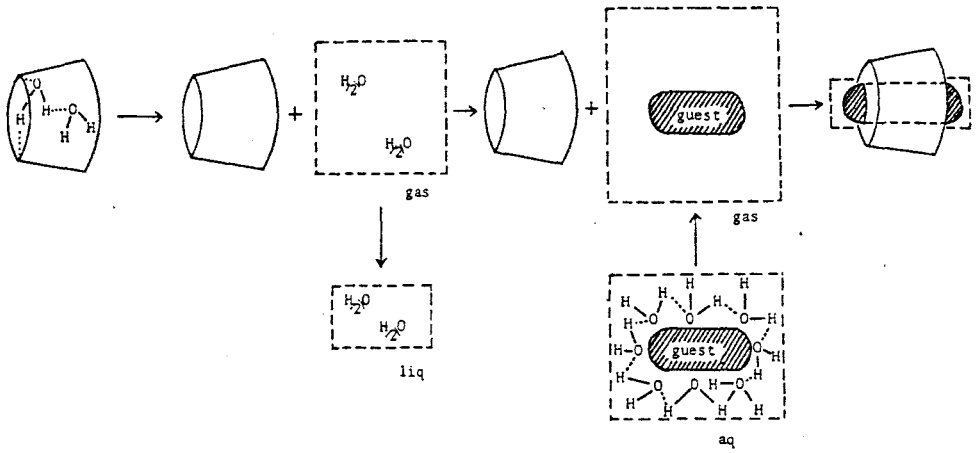

Figure 1.34: Schematic representation of the thermodynamic process of inclusion of an organic guest molecule by ACD in water solution [82, 85].

Van der Waals interaction, hydrogen bonding, and hydrophobic interaction were proposed as driving forces for the formation of inclusion complexes [86]. Kitagawa *et al.*[86] used molecular mechanics to calculate the various orientations of the various guest molecules in the CD cavity in complexes.

Helden *et al.*[87] showed, by molecular modelling, that the ACD molecules are distorted by the guest compounds. This distortion is correlated with the van der Waals volumes of guest molecules.

Lipkowitz [82] discusses the "docking problem" in the modelling of the host-guest interaction. Choice of the initial orientation of the guest can pre-determine

the outcome of the energy minimization. Some computational strategies are discussed [82]. Entrena and Jaime [88] reported the use of Allingers MM3 force fields for inclusion and optimisation of complex structures. The MM3 program was modified to handle the full-matrix of the Newton-Raphson minimizer with molecules containing up to 210 atoms.

Salvatierra *et al.* [89] studied the inclusion of benzoic acid in BCD by comparing experimental data obtained by NMR techniques and computational data from molecular mechanics calculations. The orientations of BA in the BCD cavity are shown in Figure 1.35. The agreement between the experimental and computational structures is good.

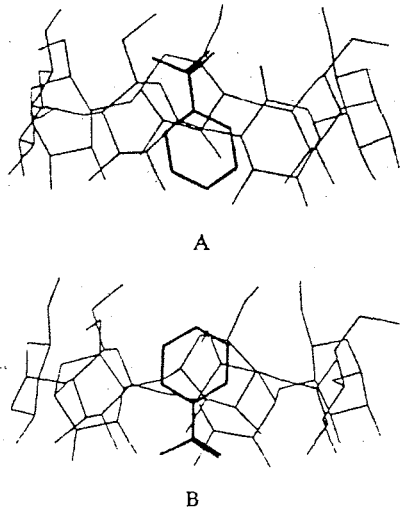

Figure 1.35: Structures of the energy minima obtained by MM2 calculations for the BCD/benzoic acid inclusion complex in two orientations [89].

Fathallah *et al.* [90] further reported the use of MM2 calculations to study inclusion processes and to calculate the minimum energy for possible complexes between benzene with various alkyl substituents and GCD/BCD. Despite the exclusion of water in the CD cavity, the computational model values and the experimental values are in agreement. Figure 1.36 shows the plots of ΔE versus

the Z-coordinates of the models for the complexes with different orientations, where (a) makes use of the wider rim (secondary hydroxyls) and (b) the narrower rim (primary hydroxyls). The complexes A and B result from different approaches of the substituent group in the benzene ring to the CD cavity. The CD molecule was oriented so as to keep the glycosidic oxygens in the XY plane, with the narrow rim in the upper region of the Z-axis. The centre of the CD was used as the reference position. The guest molecule was also oriented in the Z-axis and initially considered when far from the host molecule. The distance between the centre of the CD and the reference atom in the guest molecule gives the Z-coordinates.

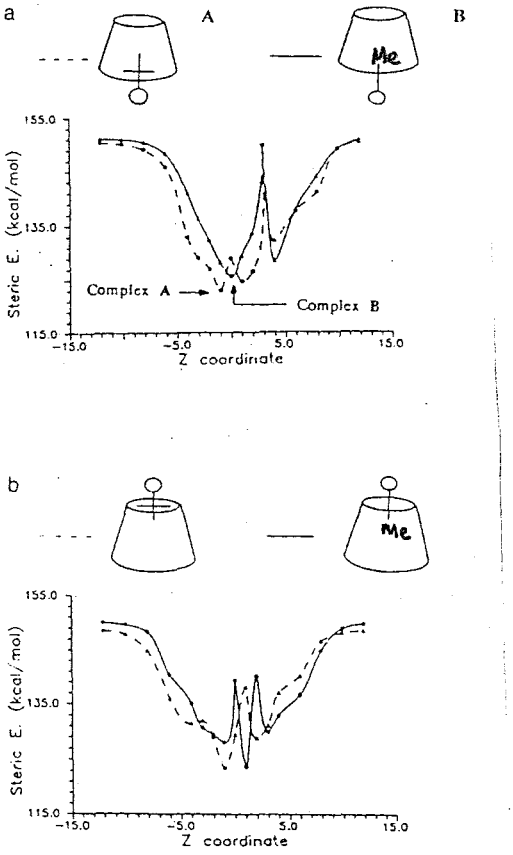

Figure 1.36: Plots of calculated ΔE versus the Z-coordinates for the modelling of the complexes between alkybenzenes and GCD through (a) the wider and (b) the narrower rims. (In both figures, the solid and dashed lines are for the inclusion of the methyl and the *tert*-butyl benzene molecules, respectively)[90].

Lu *et al.* [91] compared computational calculations for the inclusion of 4-nitrophenol by BCD with X-ray crystallographic studies. Examples of the calculations of energy variation during the course of inclusion are shown in Figures 1.37 and 1.38.

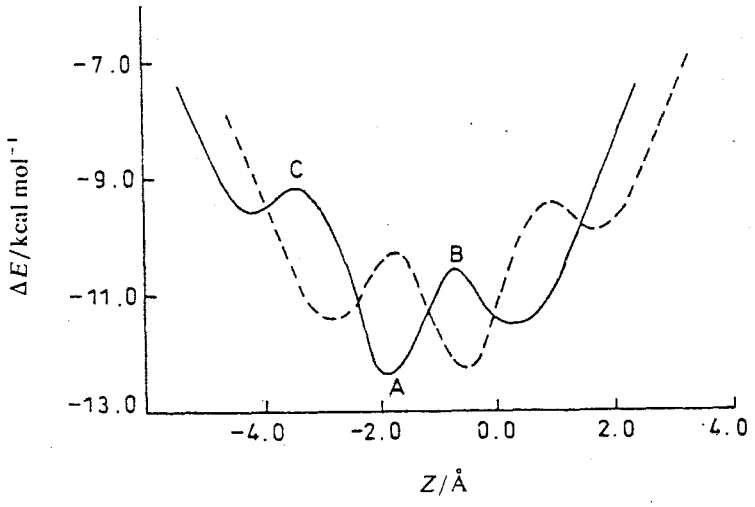

Figure 1.37: Energy profiles for inclusion of 4-nitrophenol by BCD with z-coordinates of gravity of the guest molecule: the solid line is with the NO_2 group and the dashed line OH group at the down side [91].

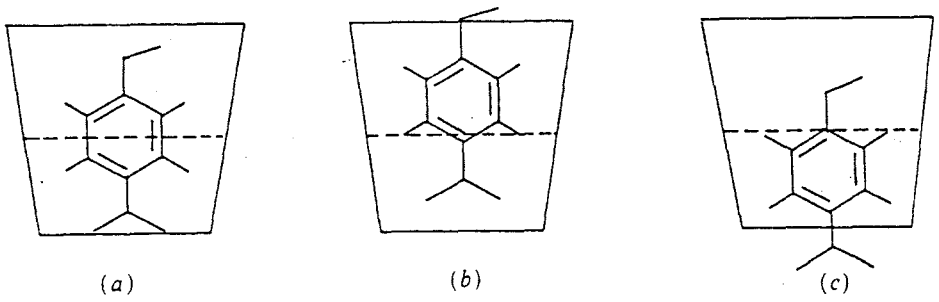

Figure 1.38: Relative positions of 4-nitrophenol and BCD at the energy minima (a) A, (b) B and (c) C [91].

In a study of the inclusion of 3-nitrophenol in ACD [92], the NO_2 group occupied the low dielectric region in the ACD and the –OH group was in the high dielectric region at the wider (secondary OH) mouth of the cavity.

Myles *et al.* [93] have modelled the interaction between the large molecule of the drug indomethacin and BCD.

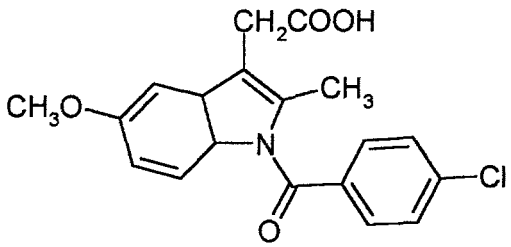

Indomethacin

The preferred structure is a 1 drug : 2 CD complex with the CDs arranged head - to - head and one aromatic ring of the indomethacin molecule in each CD cavity. The -C=O group is at the interface of the two CD cavities. Similar 1 drug : 2 CD complexes are preferred structures for many large guest molecules.

Some results reported [82] for modelling reactions in CD environments are of interest. Furuki *et al.* [94] calculated values of the activation energy for decarboxylation of the phenylcyanoacetate anion. As the reactant was moved into the CD cavity, the E values decreased. The CD cavity can have a solvent–like function ("micro-solvent"), i.e. having properties similar to those in a relatively apolar solvent. Lushkov and Venanzi [95] modelled the hydrolysis of phenylacetate and compared the nucleophilic attacks by OH^-(aq) with that by the two possible alkoxide ions [O_2 and O_3], of the BCD. Attacks by the O_3

hydroxyl lowered the activation barrier by about 40 kJ mol^{-1} compared to attack by OH(aq). Few attempts have been made [82] to model the photolysis of inclusion complexes of cyclodextrins.

1.15 Aims of this research

The main aim of this research is to make a systematic study of the thermal behaviour in the solid state of the isomers of aminobenzoic acid (3-ABA and 4-ABA), and of aminosalicylic acid (3-ASA, 4-ASA and 5-ASA). These compounds have the pharmaceutical uses described in Section 1.4, but the emphasis of this study is on the differences in thermal behaviour (e.g. melting, vaporisation and decarboxylation) caused by the different positioning of the functional groups in these sets of isomers. Their behaviour is to be compared with that of the "parent" benzoic acid (BA) and salicylic acid (SA) as reference substances. The influence of the possible decomposition products: 2-aminophenol (2-AP), 3-aminophenol (3-AP) and 4-aminophenol (4-AP), on the thermal behaviour is also examined.

An additional aim of the study is to study the thermal behaviour of the above isomers after mixing with various cyclodextrins. The pharmaceutical applications of cyclodextrins (Section 1.6.2) for improving the aqueous solubility of drugs and /or enhancing their thermal and photostability by inclusion of part or all of the drug molecule in the cyclodextrin cavity are well known. In this study, three different cyclodextrins (beta-, hydroxypropyl-beta-(modified) and gamma-cyclodextrins) with different size cavities (Table 1.1) are used to investigate the possible formation of inclusion complexes with the ASA isomers and the effects of any such inclusion on the stabilities of the included (guest) molecules.

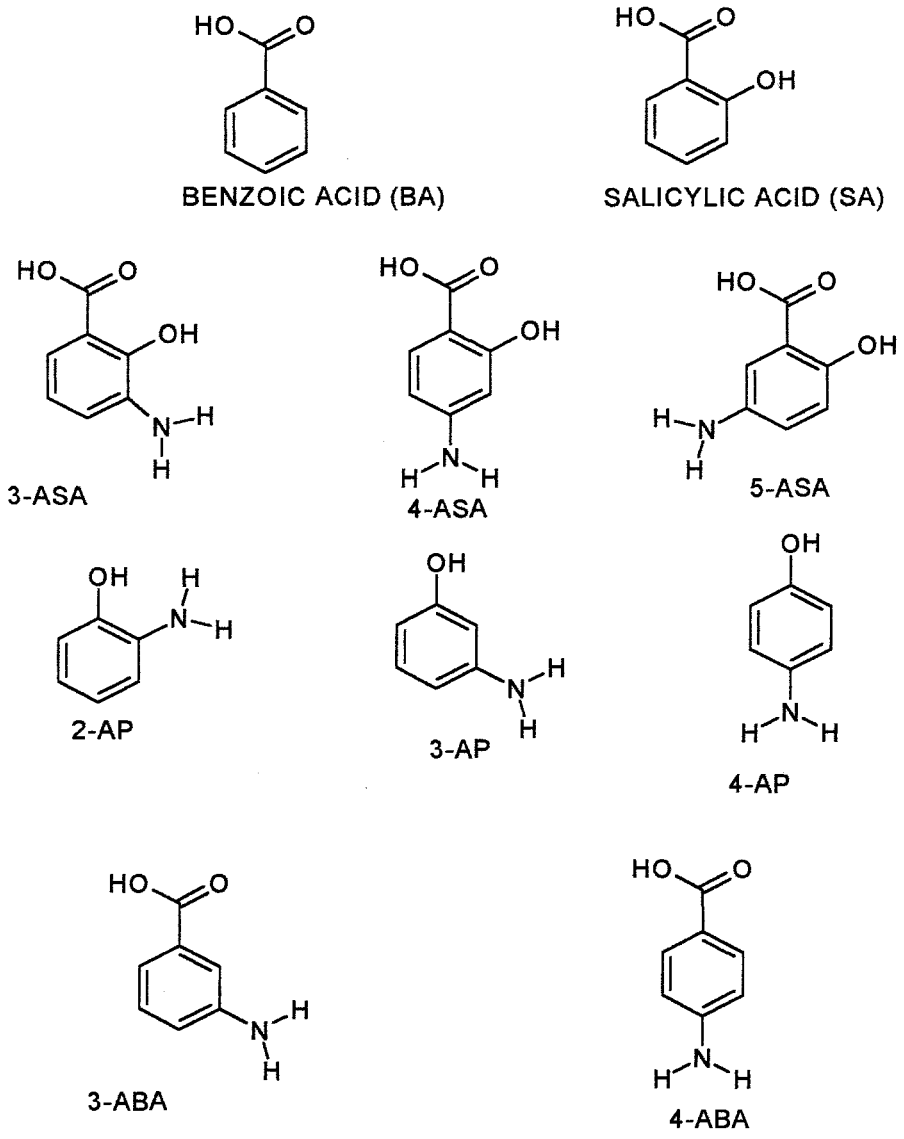

Figure 1.39: The main reactants whose stability has been examined in this project.

2. EXPERIMENTAL

2.1 Materials

Benzoic acid (BA), 4-aminobenzoic acid (4-ABA) and salicylic acid (SA) were obtained from Unilab, Saarchem.(Pty) Ltd. 2-aminophenol (2-AP) and 3-aminophenol (3-AP), 3-aminobenzoic acid (3-ABA) and 3-, 4-, and 5-aminosalicylic acids (3-ASA, 4-ASA and 5-ASA) were obtained from Aldrich Chemical Co. Ltd (UK). 4-Aminophenol (4-AP) was obtained from Riedel-de-Haën Co. Ltd. The samples were used in the form supplied.

The sodium salts of 3-ASA, 4-ASA and 5-ASA were prepared by reacting equivalent amounts of the acids and sodium hydroxide solution. The solutions were left to stand overnight to evaporate slowly. The sodium salts of 3-ASA and 5-ASA were both black, while that of 4-ASA was brownish in colour.

Freshly prepared solutions of the pure sodium salt of 4-ASA are nearly colourless, but on standing they develop an amber and eventually dark brown to black colour. The presence of an amber colour is not necessarily a sign of extensive decomposition [8].

Three different cyclodextrins (beta-, hydroxypropyl-beta-, and gamma-cyclodextrins), with the water contents, molar masses and cavity sizes given below (Table 2.1) were obtained from Wacker-Chemie GmbH (Munich, Germany). The water contents were determined by the Karl Fischer method.

Table 2.1: Details of the cyclodextrins used in this study

Cyclodextrins	Abbreviation	molar mass /g mol-1	water content / %	cavity diameter / nm
Beta-	BCD	1135	14.9	0.8
Gamma-	GCD	297	11.2	1.0
Hydroxypropyl- beta-	HPBCD	1414	9.0	-

2.2 Preparation of drug/cyclodextrin mixtures

Mixtures of the samples and cyclodextrins were prepared in two ways: by physical mixing and kneading.

Physical mixtures were made by shaking and stirring the calculated amounts of the dry powder 'host'(CD) and 'guest' (drug) compounds in a test-tube, avoiding grinding.

Kneaded mixtures were prepared using a suitable solvent, in this case, ethanol. The compounds were weighed and transferred into a suitable container, where they were kneaded with sufficient ethanol to make a paste. The kneading process usually produces more uniform mixtures [31]. The mixtures were then placed in an oven at 40°C to 50°C overnight to dry, followed by gentle grinding. The kneaded and physical mixtures were examined in the same manner as the pure samples. The data obtained from the pure compounds and cyclodextrins were compared with the data for mixtures.

2.3 Instrumentation for thermal analysis

2.3.1 Differential scanning calorimetry (DSC)

A Perkin-Elmer Series 7 Differential Scanning Calorimeter connected to a Thermal Analysis Controller (TAC/DX) was used. Calibration was done using the melting point and enthalpy of melting of indium. Three types of sample pans were used: open pans, sealed aluminium pans (cold-welding press and the appropriate pans supplied by Perkin-Elmer) and stainless-steel pressure capsules (Perkin-Elmer) with copper gaskets. Unless otherwise stated, sample masses were about 2-5 mg and the atmosphere was flowing nitrogen. The heating rate used was usually 10 K min^{-1}. The reference was an empty pan of the same type as that containing the sample.

2.3.2 Thermogravimetry (TG)

Thermogravimetry was carried out on a Perkin-Elmer Series 7 TG, which was calibrated in standard fashion using magnetic standards. Samples, in an open platinum pan, were heated in flowing nitrogen at 10 K min^{-1}. The TG could be connected to a 2000 FTIR (Perkin-Elmer) via a heated interface (Perkin-Elmer). The purge gas, containing the decomposition products in the gaseous state, was all passed through a gas cell for analysis (see Section 1.7).

2.3.3 Hot-stage microscopy (HSM)

An Ortholux microscope, supplied by Ernest Leitz GMBH, Wetzlar, Germany, was used for hot-stage microscopy. The changes in structures and colours of samples could be observed during heating and subsequent cooling.

2.4 Instrumentation for other methods of analysis

2.4.1 X-ray powder diffraction (XRPD)

X-ray diffraction powder analyses were done on the pure materials and on the mixtures with cyclodextrins to check whether inclusion had taken place. Copper K_α radiation (1.5418 A), a voltage of 40 kV, and a current of 20 mA were used. The readings were recorded for 2θ values from 5 to 60 degrees.

2.4.2. Infrared spectroscopic studies (IR)

IR spectroscopic studies were done on the pure materials and on their mixtures. Samples were compressed in KBr discs. This method sometimes causes complexation. Spectra were recorded on a Perkin-Elmer FTIR Spectrum 2000 spectrometer.

2.4.3 Molecular modelling

X-ray crystal structures were retrieved from the Cambridge Crystallographic Data Bank [26]. A Cerius^2 (version 4.5) program was used to manipulate these structures. Monomer units derived from the structures were minimised using a conjugated gradient algorithm [96]. The diameters and lengths of the CD cavities were measured. The maximum dimensions of the potential guest compounds were also measured and used to determine whether the guest compound could, on geometrical grounds only be partially or completely included in the CD cavity.

3. THE THERMAL BEHAVIOUR OF SUBSTITUTED AMINOBENZOIC ACIDS

3.1 Calculation of thermodynamic properties

The expected thermodynamic properties: enthalpies of formation in the solid, liquid and gaseous phases, enthalpies of melting, vaporization and sublimation, and the enthalpies of the decarboxylation reactions of the appropriate (solid) acids, were calculated from tables of group contributions, according to the methods given by Domalski and Hearing [45] and the results of these predictions are given in Table 3.1. These values are used later for the comparison with values determined from experiments.

Table 3.1 Calculated thermodynamic properties of reactants whose stability is examined in this project [45]

Enthalpy changes / kJ mol^{-1}							
	formation			melt	vap.	sublim.	decarb.
	solid(s)	liq.(l)	gas(g)				
benzoic acid	-386.35	-374.34	-294.75	12.01	79.59	91.60	41.84
salicylic acid	-591.13	-579.86	-493.61	11.25	86.25	97.52	32.02
phenol	-165.60	-156.56	-96.00	9.04	60.56	69.60	n/a
2-aminobenzoic acid	-401.73	-380.00	-290.61	21.73	89.39	111.12	39.30
3-aminobenzoic acid	-411.73	-390.00	-290.61	21.73	99.39	121.12	49.30
4-aminobenzoic acid	-415.73	-392.00	-290.61	23.73	101.39	125.12	53.30
3-aminosalicylic acid	-606.51	-585.52	-489.47	20.99	96.05	117.04	29.02
4-aminosalicylic acid	-616.51	-595.52	-489.47	20.99	106.05	127.04	39.02
5-aminosalicylic acid	-620.51	-597.52	-489.47	22.99	108.05	131.04	43.02
2-aminophenol	-183.98	-174.22	-91.86	9.76	82.36	92.12	n/a
3-aminophenol	-183.98	-174.22	-91.86	9.76	82.36	92.12	n/a
4-aminophenol	-183.98	-174.22	-91.86	9.76	82.36	92.12	n/a

1). No correction was given for the different isomers of aminophenol.

2). Decarboxylation of the acids is assumed to be of the form: $RCOOH(s) \rightarrow RH(s) + CO_2(g)$.

3.2 Thermal behaviour of the reference acids: benzoic and salicylic acids

3.2.1 DSC, TG and HSM results

Figures 3.1 and 3.2 show the DSC and TG curves (obtained under the experimental conditions described in Chapter 2) for benzoic acid (BA) and salicylic acid (SA), respectively.

For BA, the TG curve shows a mass-loss starting at about 85°C and by 138°C, with a heating rate of 10 K min^{-1}, 98 % of the original mass has been lost by evaporation/decomposition in a single stage. The DSC curves (uncrimped aluminium pans heated in flowing nitrogen at 10 K min^{-1}) show an endotherm for BA from 115°C to 120°C with ΔH =16 kJ mol^{-1}.

The TG curve for SA (heated at 10 K min^{-1}) shows onset of the mass-loss at about 130°C and the process is almost complete (96 %) in a single stage at about 178°C. The DSC curve for SA shows an endotherm from 158°C to 162°C, with $\Delta H = 23$ kJ mol^{-1}.

Hot-stage microscopic (HSM) observation of benzoic acid (BA), using polarised light, showed a change from colourless to bright colours at 70°C and melting at 108°C. On cooling the molten BA, crystals start to form at 102°C and become stable at 95°C. Hot-stage microscopic studies of salicylic acid (SA) showed an initially dark crystal which turned into a clear crystal at 110°C and melted from 130°C to 145°C. These changes did not produce any measurable DSC effect. On immediate cooling, a chain-like crystal was formed from 92°C to 90°C.

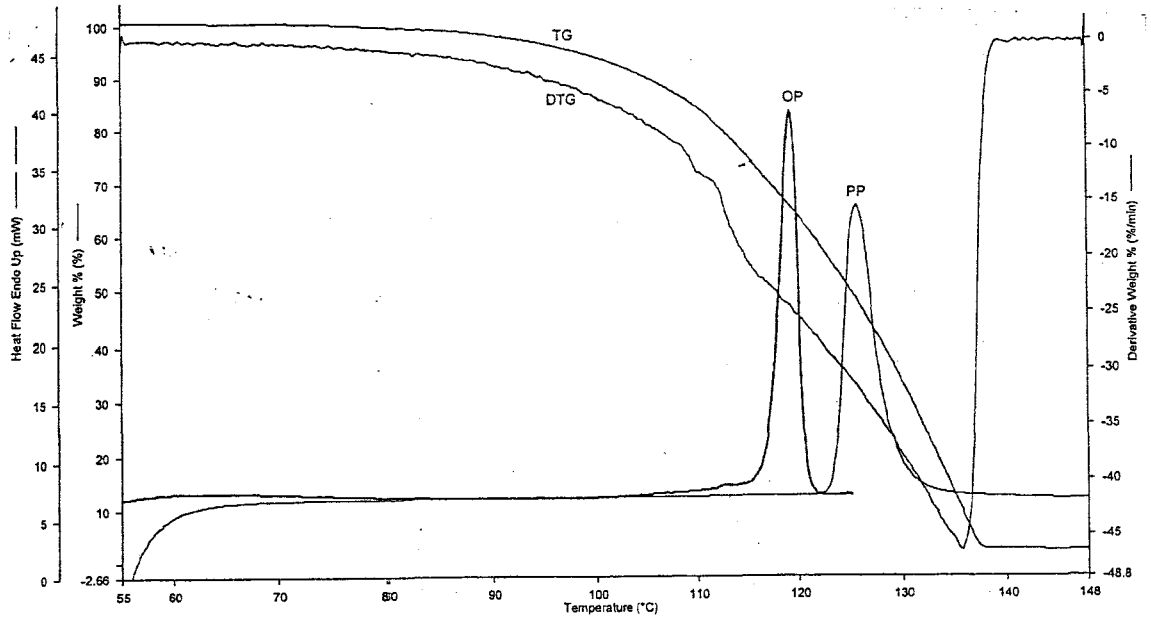

Figure 3.1: TG, DTG and DSC curves for benzoic acid (BA) (heated in flowing nitrogen at 10 K min^{-1}: uncrimped aluminium (op) and sealed pressure pans (pp) for DSC and open platinum pans for TG).

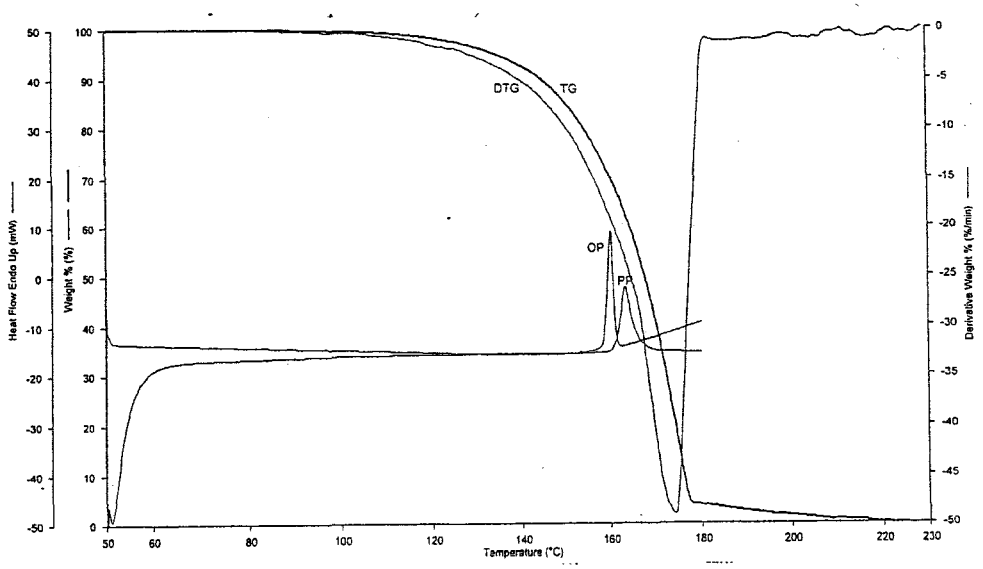

Figure 3.2: TG, DTG and DSC curves for salicylic acid (SA) (heated in flowing nitrogen at 10 K min^{-1}: uncrimped aluminium (op) and sealed pressure pans (pp) for DSC and open platinum pans for TG).

3.2.2 Evaporation studies

Between the melting and boiling points, the isothermal evaporation of many liquids from a constant (uniform) surface-area of sample in a suitable pan is a zero-order rate process [97, 98, 99]. This corresponds to an approximately linear mass-loss with time at a constant temperature and, for a constant heating rate and Arrhenius temperature dependence, to an exponential-type mass-loss with temperature. The TG and DTG curves for benzoic acid (BA) heated at 10 K min^{-1} in flowing N_2 are shown in Figure 3.1. The DTG curve shows an increase in rate of mass-loss around the melting point of benzoic acid at 122 °C (The DSC curves are also shown in Figure 3.1). Using the rate of mass-loss as a measure of the zero-order rate constant, k, for evaporation, an Arrhenius-type plot of ln(k) against 1/T (T in kelvin) for the evaporation process (Figure 3.3) shows a discontinuity associated with melting. Linear regression of the high (>122°C) and low (<122°C) temperature segments gave apparent activation energies of 47 ± 2 kJ mol^{-1} and 67 ± 3 kJ mol^{-1}, respectively. The reported enthalpy of sublimation is 90 ± 1 kJ mol^{-1} [100]. From Table 3.1, the calculated enthalpies of melting, evaporation and sublimation are 12, 80 and 92 kJ mol^{-1}, respectively.

The TG curve for SA (Figure 3.2) shows a single-step mass-loss. A similar Arrhenius-type plot (Figure 3.4) for SA is linear. The apparent activation energy determined from the slope of the plot is 88 ± 1 kJ mol^{-1}. From Table 3.1 the enthalpies of melting, evaporation and sublimation are 11, 86 and 98 kJ mol^{-1}, respectively.

Values of apparent activation energies determined in this way are generally expected [52, 101, 102] to be close to the enthalpies of vaporisation or sublimation.

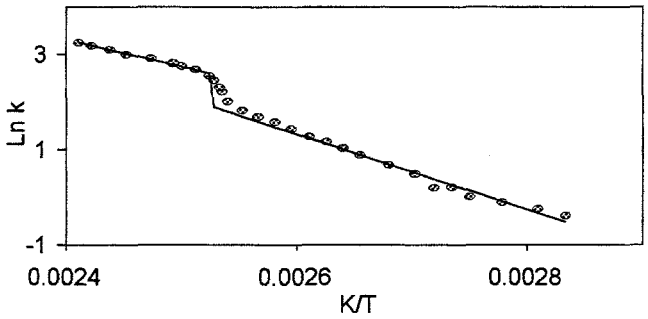

Figure 3.3: Arrhenius-type plot for the evaporation of benzoic acid (BA) (calculated from the TG curve shown in Figure 3.1).

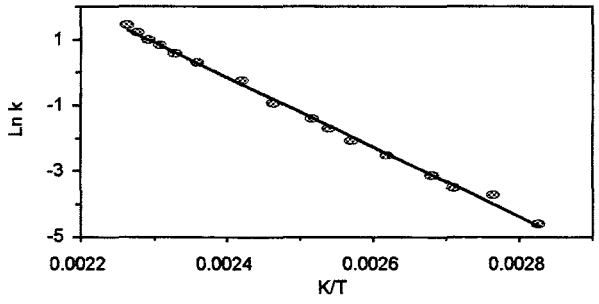

Figure 3.4: Arrhenius-type plot for the evaporation of salicylic acid (SA) (calculated from the TG curve shown in Figure 3.2).

Previous values reported for the enthalpy of sublimation of BA are 87.5 kJ mol^{-1} [51], 90 ± 1 kJ mol^{-1} (at 298 K) [104], 87 kJ mol^{-1} [105], 89 ± 6 kJ mol^{-1} [106] and a range of 88.9 ± 0.3 to 89.3 ± 0.3 kJ mol^{-1} [107]. These values are not significantly different from each other. The reported enthalpy of vaporisation of BA are 69.2 ± 0.1[13] and 66.1 ± 2.0 [14] and for SA is 64.8 kJ mol^{-1} [15].

These thermochemical results for BA and SA are summarised and discussed in Section 3.10.

3.2.3 Evolved gas analysis (EGA) using TG-FTIR

TG-FTIR experiments on the reference acids showed no sign of the decarboxylation process. These results are different to those obtained for 3-ASA (Figure 3.13) and 4-ASA (Figure 3.14) where there are clear indications of formation of carbon dioxide.

Figure 3.5 is a stacked plot for the TG run of the BA in flowing nitrogen, at 10 K min^{-1}. The evolution of some water is observed between 95°C and 150°C with maximum production at 120°C. Evolution of water is always inconclusive because of a variety of possible sources other than the sample (e.g the connecting gas line). The TG curve (Figure 3.1) shows almost complete (98%) evaporation at 158°C. Murata *et al.* [107] reported that benzoic acid sublimes and dimerises in the vapour phase when heated between 50°C and 100°C. The absence of evolution of carbon dioxide confirms that sublimation is not accompanied by significant decomposition.

For SA (Figure 3.6), FTIR shows the evolution of water at about 150°C with maximum at about 180°C and continuing up to about 200°C. The TG curve (Figure 3.2) for SA shows almost complete (96 %) evaporation/decomposition by 178°C. The evolution of water at the higher temperatures indicates some dehydroxylation.

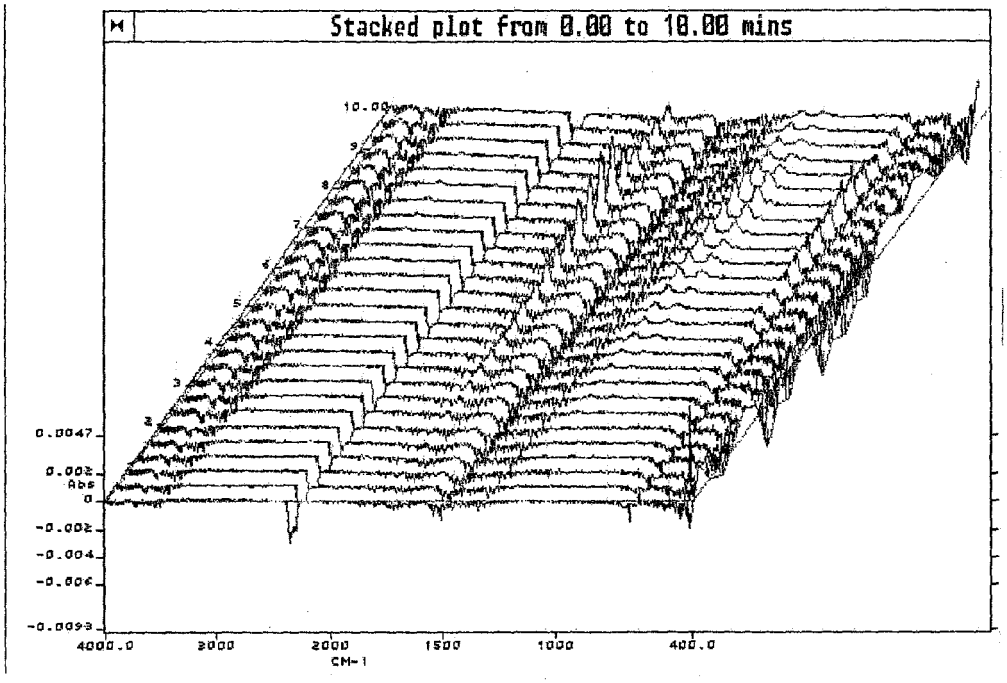

Figure 3.5: A stacked plot of FTIR spectra recorded during a TG run on benzoic acid (heated at 10 K min^{-1} in flowing nitrogen from 50 to 150°C).

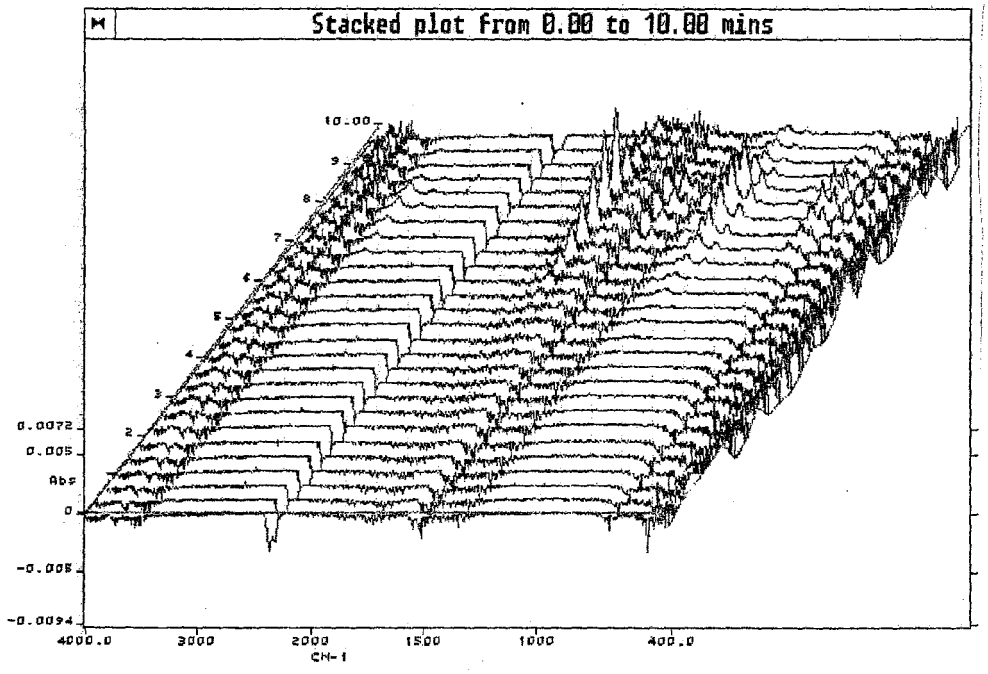

Figure 3.6: A stacked plot of FTIR spectra recorded during a TG run on salicylic acid (heated at 10 K min^{-1} in flowing nitrogen from 50 to 150°C).

3.3 Thermal behaviour of the aminobenzoic acids (ABA)

3.3.1 TG , DSC and HSM results

On decarboxylation, all of the aminobenzoic acid isomers should give aniline (liquid). The TG curves for 3-ABA (m. pt = 171-174°C) (Figure 3.7) and 4-ABA (m. pt = 181-188°C) [19] (Figure 3.9) heated in flowing nitrogen at 10 K min^{-1} are similar. Onset of mass-loss is at about 100°C.

For 3-ABA, mass-loss is rapid until about 90 % loss at about 270°C. There is then a slow mass-loss which is still incomplete at 540°C (not shown in Figure 3.7). The DSC curves (Figure 3.7) for 3-ABA (heated in nitrogen at 10 K min^{-1}) showed a small broad endotherm, onset 153°C, ΔH about 15 J g^{-1}, followed by sharper endotherm, onset 170°C, that was overlapped by sharp and strong exotherm. Immediately on completion of this complex set of peaks (182°C), the sample was cooled at 10 K min^{-1} and the cooling curve showed an exotherm (ΔH = -197 J g^{-1}) with onset temperature at 152°C. On reheating the same cooled sample (Figure 3.8), a broader endotherm without any obvious overlapping exotherm was observed, onset at 170°C (ΔH = 202 J g^{-1}). This was followed by yet another small endotherm, onset 177°C (ΔH =5 J g^{-1}). Evolved gas analysis (EGA) by FTIR did not reveal the formation of carbon dioxide or any other gaseous product.

For 4-ABA, mass-loss is rapid until 95 % loss at about 220°C (Figure 3.9). There is then a slow mass-loss still incomplete by 420°C. The DSC curves for 4-ABA (Figure 3.9) showed a sharp endotherm at 185°C. On cooling, an exotherm occurs at about 148°C to 150°C. Reheating the cooled sample (Figure 3.10) gave an endotherm at about 177°C. Evolved gas analysis by FTIR (Figure 3.12) did reveal formation of carbon dioxide (CO_2) from 185°C to 240°C.

Hot-stage microscopic (HSM) observation of 3-ABA showed nucleation of particles from 130°C to 138°C. Melting occurs from 140°C to 148°C and evaporation is observed from 158°C to 164°C. On cooling, crystal formation took place slowly between 135°C and 130°C and a stable crystal formed between 105°C and 100°C. On reheating a cooled sample, a brightly coloured formation is seen between 145°C and 150°C, which formed a band-like crystal on cooling again. 4-ABA showed nucleation from 115°C to 150°C and melting occurs at 165°C followed by rapid evaporation. On cooling, coloured chain-like crystals were formed at 150°C.

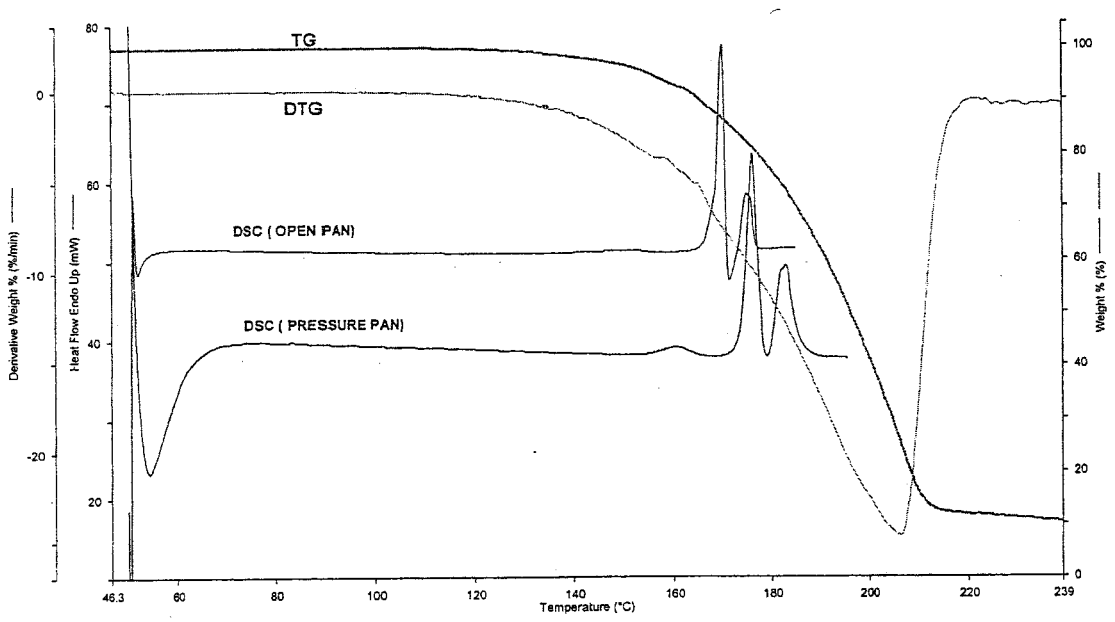

Figure 3.7: TG, DTG and DSC curves for 3-ABA (heated in flowing nitrogen at 10 K min^{-1}: uncrimped aluminium (op) and sealed pressure pans (pp) for DSC and open platinum pans for TG).

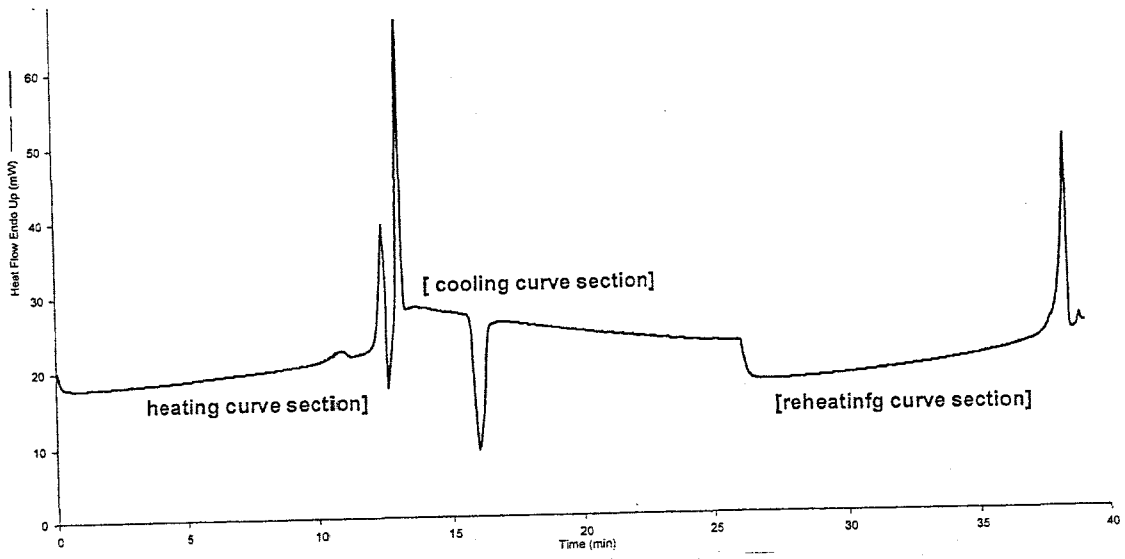

Figure 3.8: DSC curves for the multiple-step run of 3-ABA: (a) first heating, (b) cooling and (c) reheating (heated at10 K min^{-1} in flowing nitrogen in an uncrimped aluminium pan).

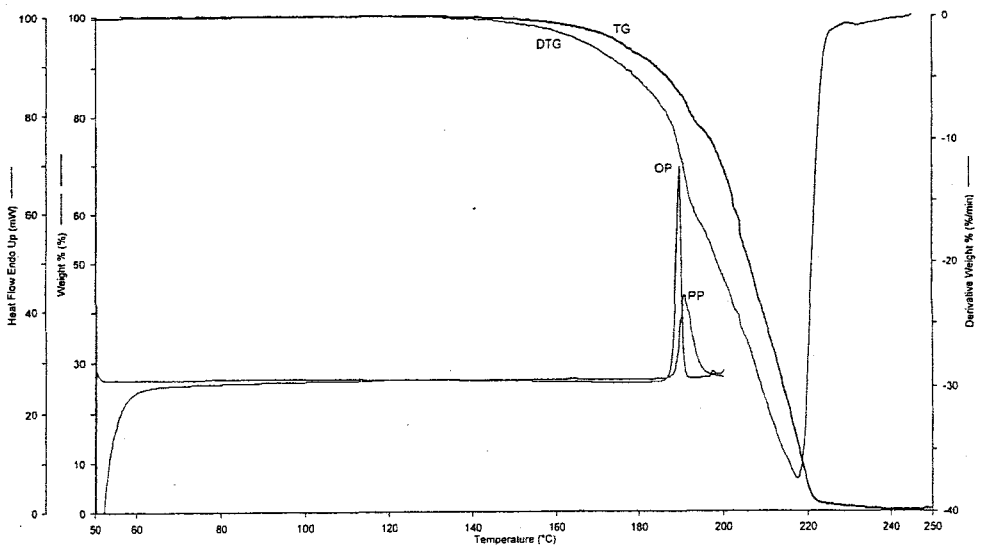

Figure 3.9: TG, DTG and DSC curves for 4-ABA (heated in flowing nitrogen at 10 K min^{-1}: uncrimped aluminium (op) and sealed pressure pans (pp) for DSC and open platinum pans for TG).

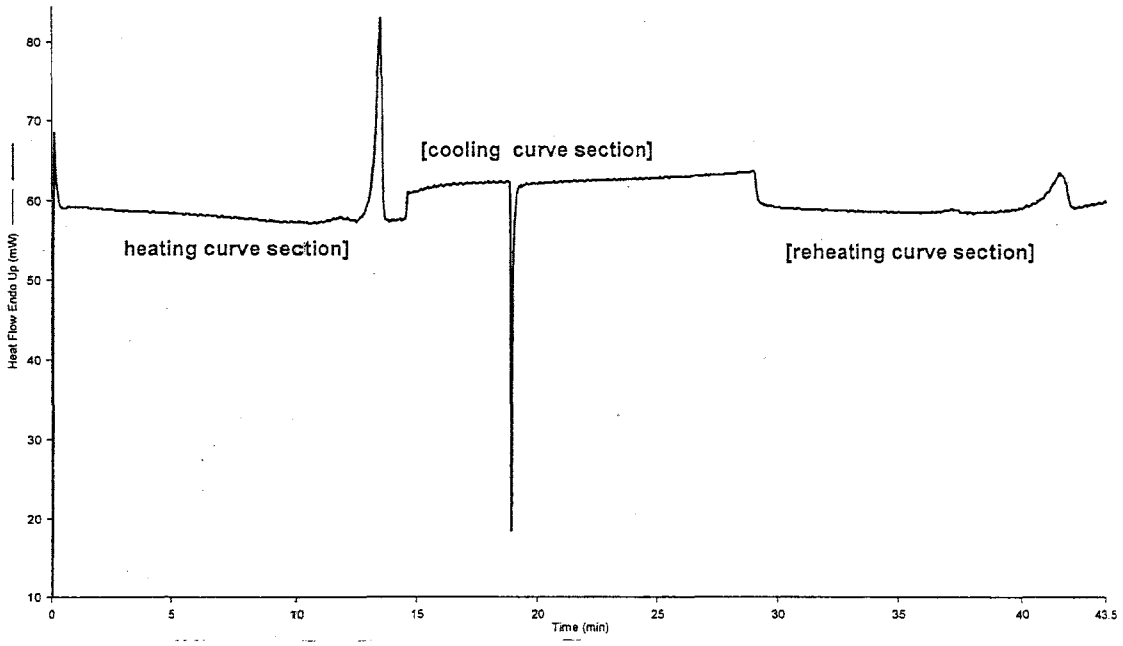

Figure 3.10: DSC curves for the multiple-step run of 4-ABA: (a) first heating, (b) cooling and (c) reheating (heated at 10 K min^{-1} in flowing nitrogen in uncrimped aluminium pan).

3.3.2 Evaporation studies

Arrhenius-type plots for the evaporation of 3-ABA and 4-ABA are shown in Figure 3.11. The apparent activation energies for evaporation of 3-ABA and 4-ABA were determined from their slopes to be 98 ± 2 k J mol^{-1} and 63 ± 2 k J mol^{-1}, respectively. From Table 3.1, the enthalpies of melting, vaporisation and sublimation of 3-ABA are 22, 99 and 121 kJ mol^{-1}, respectively. Values for 4-ABA are 24, 101 and 125 kJ mol^{-1}, respectively (Table 3.1). So, for 3-ABA, the measured activation energy is close to the enthalpy of vaporisation, but the value for 4-ABA is considerably lower.

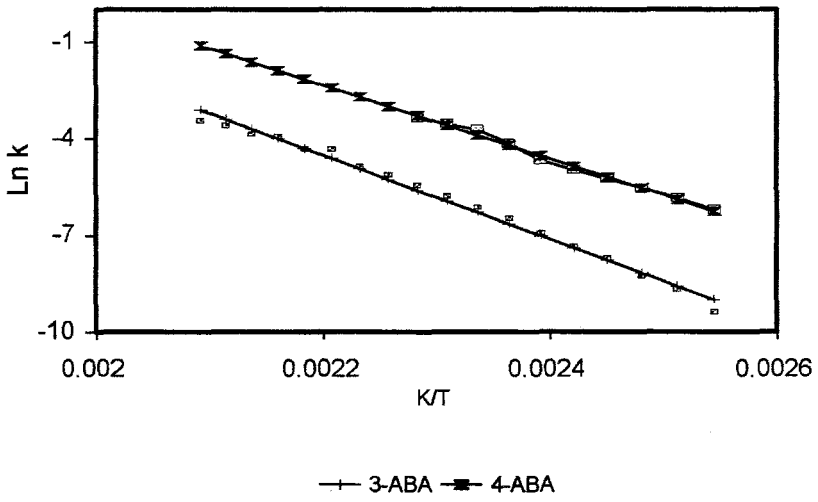

Figure 3.11: Arrhenius-type plots for the evaporation of 3-ABA and 4-ABA (calculated from the TG curves shown in Figures 3.7 and 3.9).

3.3.3 Evolved gas analysis (EGA) by TG-FTIR

The stacked plot of FTIR spectra recorded (Figure 3.12) for 4-ABA during a TG run showed that decarboxylation occurred between about 190°C and 240°C (after 14.0 to 19.0 minutes), with maximum evolution of CO_2 at 220°C (after 17.0 minutes). These observations correspond to the results shown by the TG curve (Figure 3.9). A similar experiment on 3-ABA showed no evolution of CO_2.

The difference in behaviour could be attributed to the stabilizing presence of the amino-group in the meta position. The decarboxylations of a variety of benzoic acid derivatives were studied by Chung-Tang *et al.*[58] and they reported that most of the derivatives with an electron donating group at the meta position did not easily decompose (see Section 1.5).

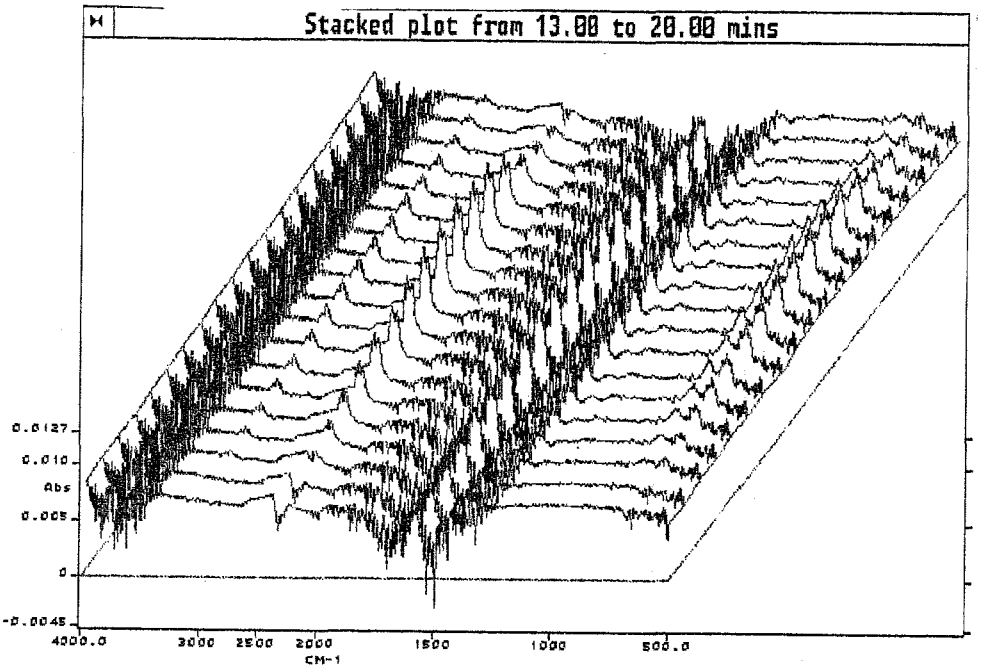

Figure 3.12: A stacked plot of FTIR spectra recorded during a TG run on 4-ABA (heated at 10 K min^{-1} in flowing nitrogen from 50 to 250°C).

3.4 Thermal behaviour of the aminosalicylic acids (ASAs)

3.4.1 TG, DSC and HSM results

Generally, it is expected that the aminosalicylic acids will decompose by decarboxylation to form the corresponding aminophenols. The decarboxylation of 3-aminosalicylic acid is expected to give 2-aminophenol; 4-aminosalicylic acid to give 3-aminophenol; and 5-aminosalicylic acid to give 4-aminophenol. Decarboxylation (see Table 3.1) is an endothermic process and so are melting and evaporation. The calculated enthalpies of decarboxylation of solid 3-ASA, 4-ASA and 5-ASA are 29, 39 and 43 kJ mol^{-1}, respectively. The sum of the enthalpies of melting and decarboxylation for 3-ASA, 4-ASA and 5-ASA are 50, 60 and 66 kJ mol^{-1}, respectively.

The TG and DTG curves for 3-ASA (Figure 3.13), heated in flowing nitrogen at 10 K min^{-1}, show a single-stage mass-loss with onset temperature at about 180°C and decomposition/evaporation is almost complete (95 %) at 240°C. The DSC curve in an uncrimped aluminium pan (Figure 3.13) showed an endotherm, onset at about 220°C, followed immediately by an exotherm. The use of a sealed pressure pan gave better resolution of the endotherm, onset at 239°C ($\Delta H = 61$ kJ mol^{-1}). The reported melting point (manufacturer's specification) for 3-ASA is 240°C.

The TG and DTG curves for 4-ASA (Figure 3.14), heated in flowing nitrogen at 10 K min^{-1}, show a two-stage mass-loss (total 100 %), with the discontinuity after about 30 % mass-loss at close to the reported [9] melting point of 4-ASA (139°C-141°C). The manufacturer's specification is 147°C, with decomposition. Hansen *et al.* [108] reported the melting point values as being uncertain with various authors giving different results, ranging from 135-140°C (with decomposition) to 149-151°C (with decomposition). The CO_2 content, calculated from the formula of 4-ASA, is about 28.8 %, i.e. close to the mass-loss at the discontinuity, but evolved gas analysis by FTIR (Section 3.4.2) showed that evolution of CO_2 occurred during the latter stage (i.e. above 140°C) of the TG curve. The DSC curve for 4-ASA (Figure 3.14), under similar experimental conditions, shows several overlapping endotherms. The first (small) endotherm has onset (under these conditions) at about 110°C, the second at about 115°C, and the third at about 125°C, becoming complex and shifting to exothermic at about 132°C. On cooling from 155°C and rescanning the sample, a more compact complex endotherm with onset about 115°C was recorded. The expected product of decarboxylation, 3-AP, melts in the range 115°C to 121°C.

The TG and DTG curves for 5-ASA (Figure 3.15) show 100% mass-loss in a single stage with onset (under the experimental conditions described) at about 190°C and the DTG curve shows a maximum at close to 270°C, corresponding to the reported melting point of 5-ASA. A DSC curve for 5-ASA heated in an uncrimped aluminium pan (Figure 3.15) showed an endotherm, onset 278°C, ΔH = 89 kJ mol^{-1}. On using a sealed pressure pan, a well-resolved endotherm, onset temperature at 282°C, ΔH = 67 kJ mol^{-1} was obtained. On cooling after the first melt and reheating, no endotherm was observed. Evolution of CO_2 was not detected using TG-FTIR. The reported melting point (manufacturer's notes) for 5-ASA is 280°C and for 4-AP is 182°C.

Hot-stage microscopic studies (HSM) of 3-ASA showed a brown coloration at 235°C to 240°C. No further changes were observed on cooling and reheating of the sample. HSM of 4-ASA showed nucleation of crystals at 100°C. This became faster at 115°C and was complete at 120°C. For 5-ASA, HSM observation showed a colour change to a brown stable crystal at about 270°C to 285°C. No further changes were observed on cooling and reheating of the sample.

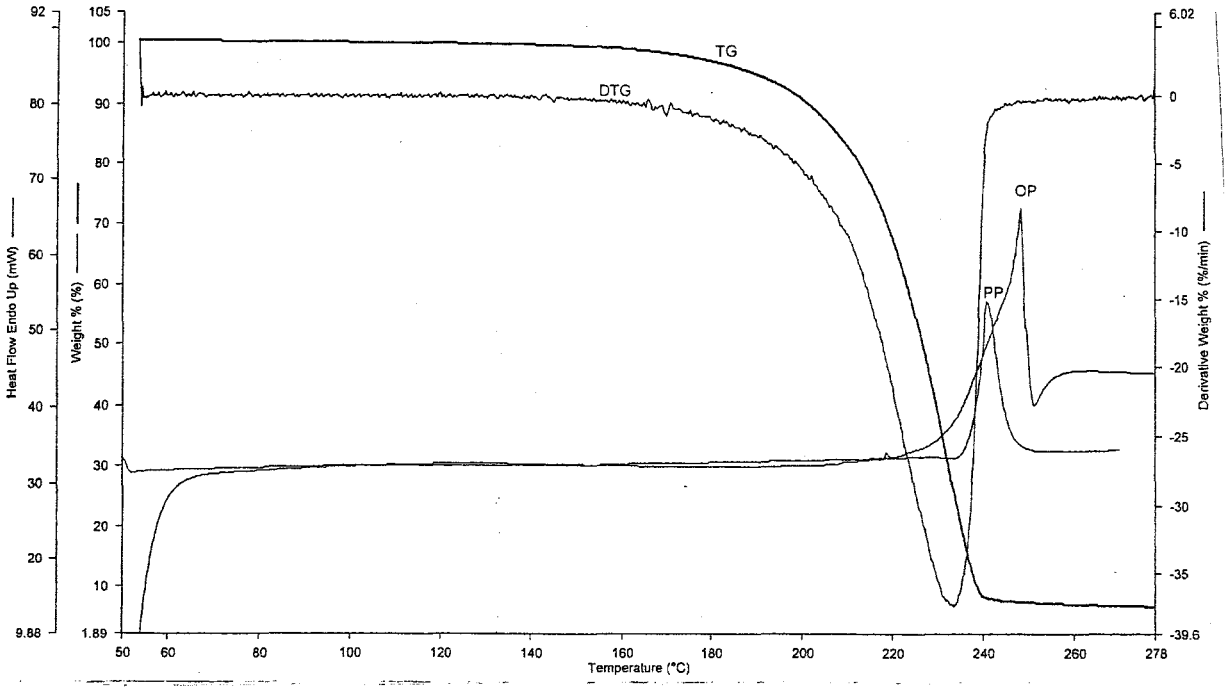

Figure 3.13: TG, DTG and DSC curves for 3-ASA, (heated in flowing nitrogen at 10 K min^{-1}: uncrimped aluminium (op) and pressure sealed pans (pp) for DSC and open platinum pans for TG).

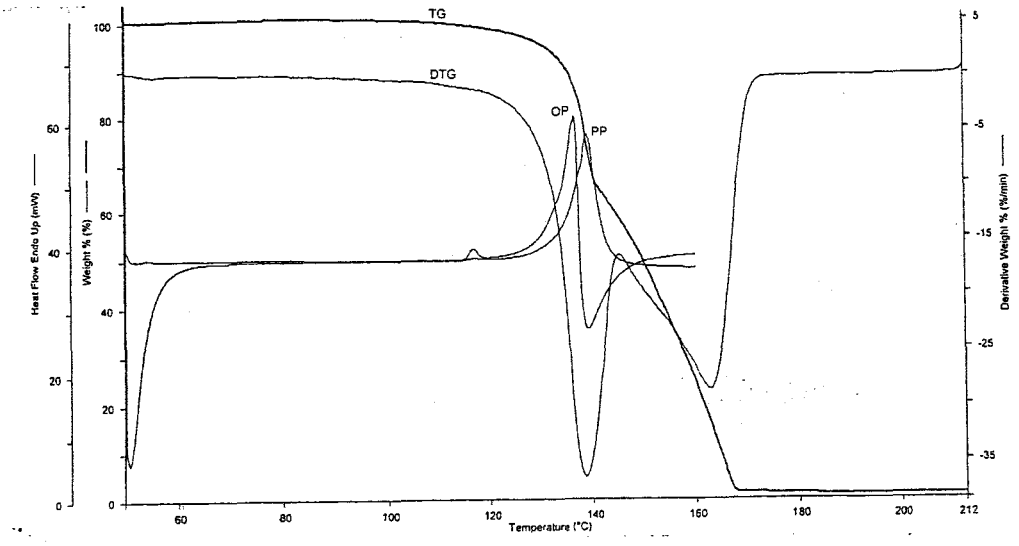

Figure 3.14: TG, DTG and DSC curves for 4-ASA, (heated in flowing nitrogen at 10 K min^{-1}: uncrimped aluminium (op) and sealed pressure pans (pp) for DSC and open platinum pans for TG).

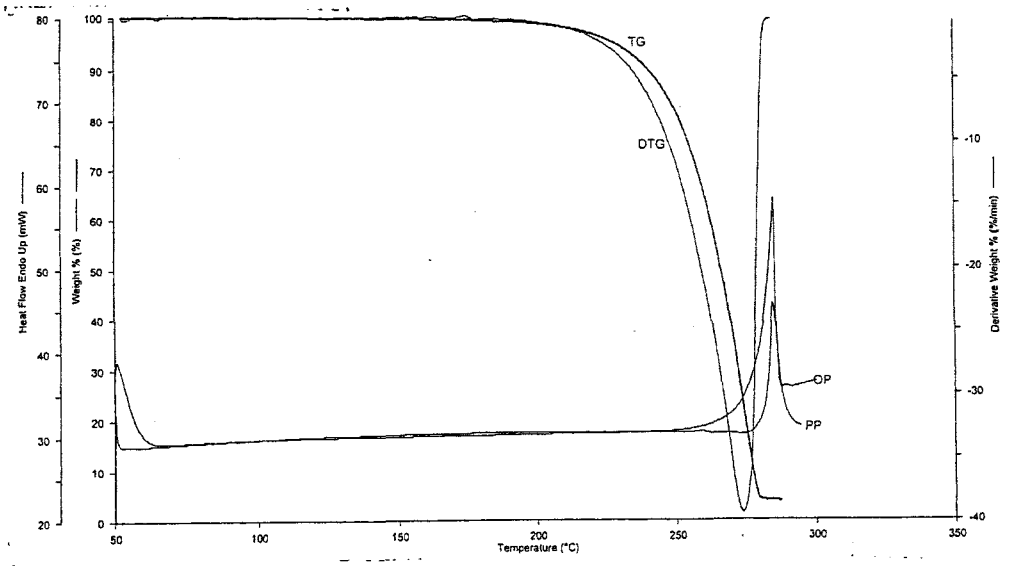

Figure 3.15: TG, DTG and DSC curves for 5-ASA, (heated in flowing nitrogen at 10 K min^{-1}: uncrimped aluminium (op) and sealed pressure pans (pp) for DSC and open platinum pans for TG).

3.4.2 Evolved gas analysis (EGA) of the aminosalicylic acids using TG-FTIR

TG-FTIR was used to determine the gases evolved (Section 1.7) during the heating of 3-ASA, 4-ASA, and 5-ASA. The TG curve for 3-ASA showed a one-stage decomposition process (Figure 3.14). Comparison of the DSC and TG curves (Figure 3.14) showed that the DSC endotherm is observed at temperatures (onset 237°C) near the completion of the TG mass-loss. The FTIR stacked plot (Figure 3.17) showed onset of the evolution of carbon dioxide gas after 17.5 minutes. Because the heating rate was 10°C min^{-1} and the initial temperature was 50°C, this onset temperature is about 225°C. The evolution of carbon dioxide continued with a maximum at about 21.0 minutes (260°C) and evolution was still being observed at 24.0 minutes (290°C). At this temperature (290°C), the TG curve

shows almost complete mass loss (95%). The decarboxylation process thus occurs near the temperature of the endotherm (230°C to 250°C) observed on the DSC curve.

The TG curve for 4-ASA (Figure 3.14) shows at least two-stages of mass-loss (Section 3.4.1) with a discontinuity at around 140°C. The DSC curve for 4-ASA (Figure 3.14) shows an endotherm, onset about 120°C, which is better resolved in a sealed pressure pan (ΔH = 46 kJ mol^{-1}). The mass-loss for 4-ASA at the TG discontinuity is approximately 29 %, which is close to the mass-loss expected for the release of CO_2. The TG-FTIR showed, however, that this agreement is only coincidental. The stacked plot of FTIR spectra (Figure 3.17) recorded during a TG run on 4-ASA (starting temperature 50°C and heating rate 10 K min^{-1}), showed that CO_2 evolution occurred between 130°C and 170°C with maximum production at 150°C. The Gram-Schmidt reconstructions (Figure 3.18) (see also pages 26,27) for the overall gas formation and the evolution of carbon dioxide confirm the formation of carbon dioxide only. The temperature of melting of 4-ASA is about 130°C.

The TG-FTIR analysis of 5-ASA showed no carbon dioxide evolution.

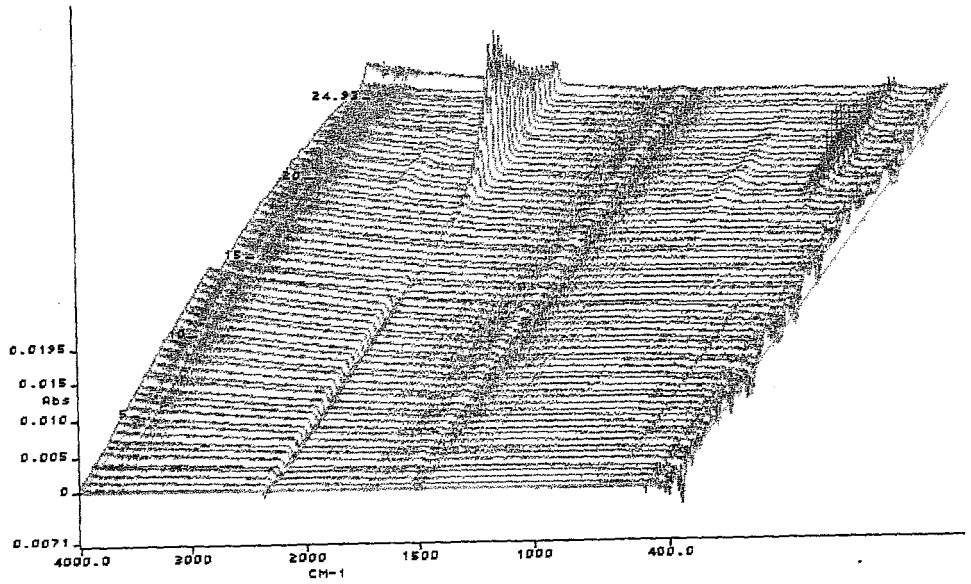

Figure 3.16: A stacked plot of FTIR spectra recorded during a TG run on 3-ASA (heated at 10 K min^{-1} in flowing nitrogen from 50 to 300°C).

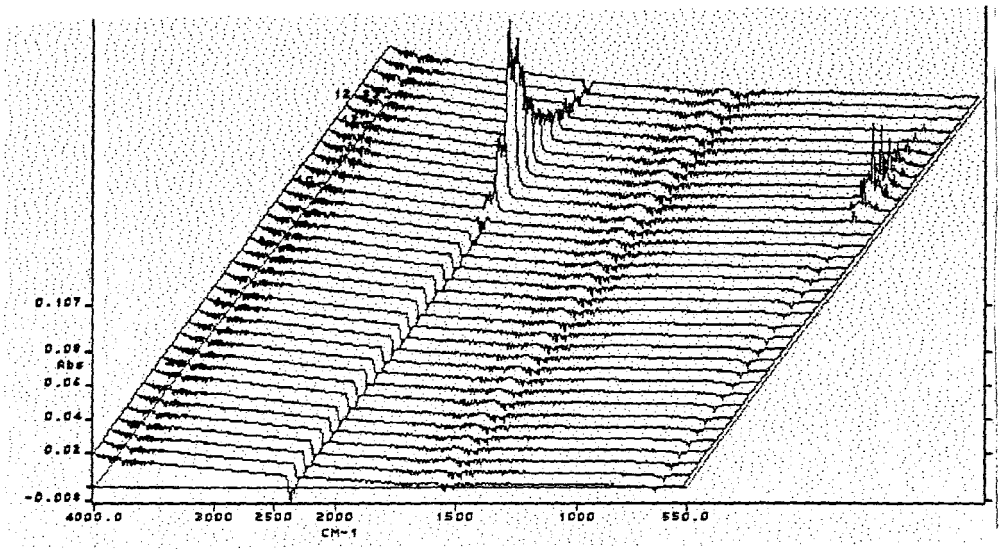

Figure 3.17: A stacked plot of FTIR spectra recorded during a TG run on 4-ASA (heated at 10 K min^{-1} in flowing nitrogen from 50 to 180°C).

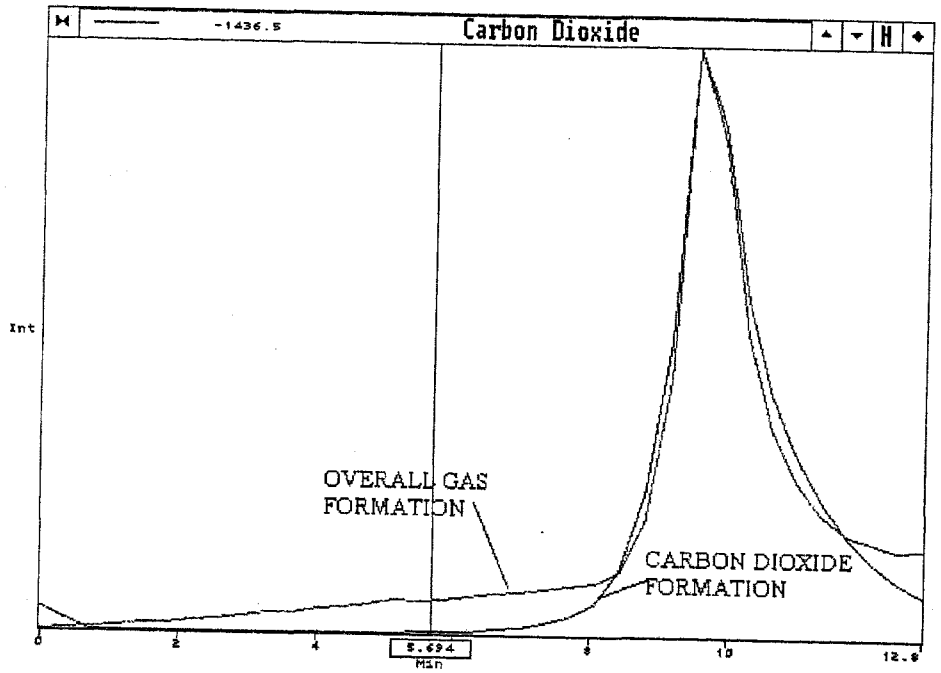

Figure 3.18: The Gram-Schmidt reconstruction curves for the overall gas formation and for the evolution of CO_2, recorded during a TG run (heated at 10 K min^{-1} in flowing nitrogen).

Results for the thermal behaviour of the three isomers of aminosalicylic acid are summarised in Table 3.2.

Table 3.2 Thermal behaviour of the aminosalicyclic acids

	m.pt /°C	TG /°C	CO_2 evolution (max.)/°C	DTG max. /°C	DSC (pp) endotherm onset /°C	ΔH/ kJ mol^{-1}
3-ASA	240	one-stage 180-240	225-290 (250)	235	239	61
4-ASA	130	two-stage 100-135 135-170	130-170 (150)	138-165	110 (complex)	-
5-ASA	270	one-stage 160-280	none detected	270	282	67

All the ASAs show onset of mass losses at temperatures well below the reported melting points. The maxima of the DTG curves occur close to the melting points (Table 3.2).

The thermal stabilities of the three isomers are related to their melting temperatures. Studies done by Chung *et al.* [58] showed that crystal packing in organic compounds is dominated by hydrogen-bonding and that, in aminobenzoic acid derivatives, the presence of polar carboxyl-groups enhances decarboxylation (see Section 1.5 and 3.11). Resonance structures (Figure 1.8 and 1.10) contribute to the molecular structures of these isomers in varied percentages. The more polar the contributing resonance structures are, the faster the rate of decomposition [25].

Evaporation (i.e either sublimation or vaporisation), melting and decarboxylation are all endothermic processes. TG cannot detect melting and cannot distinguish between evaporation and decarboxylation (or other type of decomposition). EGA by TG-FTIR permits the detection of decarboxylation. Decarboxylation could take place in the solid, molten or gaseous states. If it occurs in gaseous state, the endothermic effect will not be detectable by DSC. The endothermic effect of evaporation is generally too broad for reliable detection and measurement using DSC in open pans. Use of sealed pressure pans for DSC generally changes the processes occurring.

3.4.3 Evaporation studies

The Arrhenius-type plot for the evaporation of 3-ASA (Figure 3.19) is approximately linear. From its slope, the apparent activation energy was determined to be 116 ± 3 k J mol^{-1}. From Table 3.1, calculated enthalpies of melting, vaporisation and sublimation are 21, 96 and 117 kJ mol^{-1}, respectively.

The Arrhenius-type plot for 4-ASA (Figure 3.20) has two linear segments, corresponding approximately to the two-stage mass-loss shown in the TG curve. Linear regression for the low (<150°C) and the high (>150°C) temperature segments gave apparent activation energies of evaporation of 175 ± 7 kJ mol^{-1} and 59 ± 1 kJ mol^{-1}, respectively. From Table 3.1, the calculated enthalpies of sublimation, melting and vaporisation are 21, 127 and 106 kJ mol^{-1}, respectively.

The Arrhenius-type plot for 5-ASA (Figure 3.21) is based upon a single-stage mass-loss. The apparent activation energy of evaporation was calculated to be 158 ± 4 kJ mol^{-1}. From Table 3.1, the calculated enthalpies of melting, vaporisation and sublimation are 23, 108 and 131 kJ mol^{-1}, respectively. Results for the evaporation studies are summarised in Table 3.3.

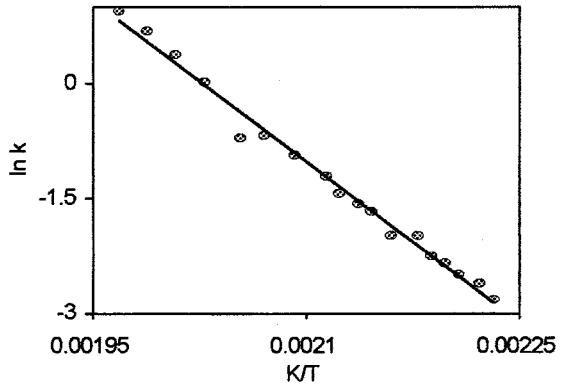

Figure 3.19: The Arrhenius-type plot for evaporation of 3-ASA (calculated from the TG curve shown in Figure 3.13).

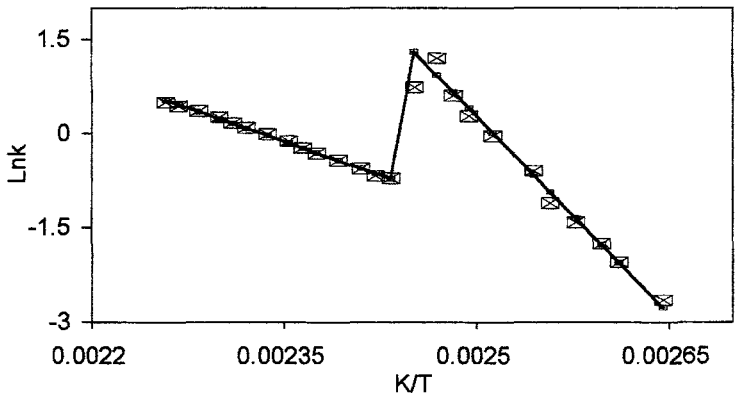

Figure 3.20: The Arrhenius-type plots for evaporation of 4-ASA (calculated from the TG curve shown in Figure 3.14).

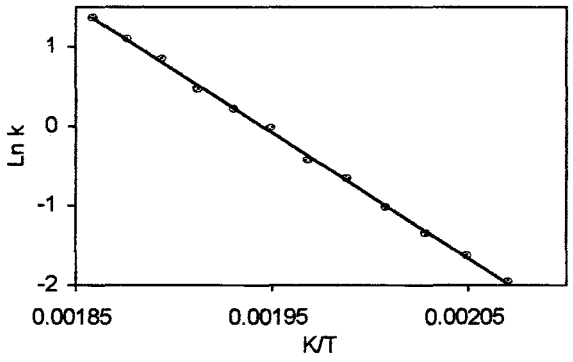

Figure 3.21: The Arrhenius-type plot for evaporation of 5-ASA (calculated from the TG curve shown in Figure 3.16).

Table 3.3 Summary of the apparent activation energies, E_{vap}, for evaporation of the compounds shown (from Arrhenius-type plots) and the enthalpy values from Table 3.1 calculated for related processes

Enthalpies/ kJ mol^{-1}						
		Calculated	Table 3.1			
		$E_{vap.}$	melt	vap.	sublim	decarb.
BA	low	67 ±3	12	80	92	42
	high	47 ± 2				
SA		88 ± 1	11	86	98	32
3-ABA		98 ± 2	22	99	121	49
4-ABA		63 ± 2	24	101	125	53
3-ASA		116 ± 3	21	96	117	29
4-ASA	low	175 ± 7	21	106	127	39
	high	59 ±1				
5-ASA		158 ± 4	23	108	131	43

The values of E_{vap} for SA, 3-ABA and 3-ASA are close to the calculated enthalpies of vaporisation, while E_{vap} for 5-ASA is closer to the enthalpy of sublimation. The results for BA, 4-ABA and 4-ASA are not as straightforward. Both 4-ABA and 4-ASA do undergo decarboxylation.

3.5 Correction of enthalpy measurements for accompanying mass losses

Riesen *et al.* [65] have pointed out that corrections are required when DSC measurements in an open pan are accompanied by mass-losses due to sublimation, evaporation or decomposition. Mass-losses can be avoided by using sealed pressure pans, but this changes the pressure and thus, usually, the processes under

consideration. Mass-losses from TG curves can be related to DSC measurements at the corresponding temperature to correct the enthalpy measurements to those for the actual mass at that temperature.

Riesen *et al.* [65] used measurements on anthracene as an example. Anthracene has a melting point of 220 °C, but begins to sublime below this temperature. The enthalpy of melting calculated from the initial mass was found to be 134 J g^{-1}. This value was much lower than the literature value of 161 J g^{-1}. On normalisation of the enthalpy value to the actual sample mass at the onset temperature of the endotherm, a value of 160 J g^{-1} was obtained. The effect of applying similar procedures to relate the enthalpy measurements for benzoic acid derivatives to the actual masses of the samples was explored in this study. The results are summarised in Table 3.4.

Table 3.4 Values for the enthalpies of melting of the benzoic acid derivatives corrected for the actual sample mass

Compound	BA	SA	4-ABA	3-ASA	4-ASA	5-ASA
Initial sample mass / mg	3.945	3.298	2.146	1.132	2.440	1.511
Onset temp. of endotherm/ °C	120	158	186	225	125	265
Mass-loss before endotherm/ %	35	25	19	32	29	52
Enthalpy change / kJ mol^{-1}						
Normalised to initial mass	16	23	25	93	39	66
Normalised to actual mass	25	31	31	232	55	114
Calc. enthalpy of melting (Table3.1)/ kJ mol^{-1}	12	11	24	21	21	23
Enthalpies of melting in pressure pan/kJ mol^{-1}	15	24	24	61	46	67

The results in Table 3.3 illustrate the difficulty of separating the concurrent processes of evaporation and melting (with the additional possibility of decarboxylation). Because the TG curves show mass-losses continuing through the temperature regions of the endotherms, the estimated enthalpy values based on initial sample masses are the lower limit and would increase if allowance was made for mass losses (Table 3.4).

Modulated temperature DSC was not available to test its ability to resolve these processes. The difference in thermal behaviour of aminobenzoic acids and aminosalicylic acids is that decomposition of aminosalicylic acids may also involve dehydroxylation in addition to melting, sublimation, evaporation and decarboxylation.

3.6 Thermal behaviour of the sodium salts of 3-ASA, 4-ASA and 5-ASA

The preparation of the sodium salts of the aminosalicylic acid isomers is described in Section 2.1.

3.6.1 The sodium salt of 3-ASA

The DSC curve for the sodium salt of 3-ASA (Figure 3.22) shows two endotherms. The first is broad with onset at 91 °C ($\Delta H = 91$ kJ mol^{-1}). The second is a complex endotherm with an initial sharp endotherm at an onset temperature of 254 °C, followed by a broad endotherm with a slow return to the baseline.

The TG and DTG curves in nitrogen (Figure 3.23) show a mass-loss from 100 °C to 170 °C (about 5%) and a mass-loss from 240 °C to 340 °C of 45%, with a discontinuity after 35 % mass-loss at about 280 °C, which was followed by a slow

mass-loss that was not complete at 500°C. The calculated mass-loss for decarboxylation is 23.8% of anhydrous salt. The initial mass-loss of 5%, if assumed to be water, corresponds approximately to a hemi-hydrate (3-NH_2-C_6H_3(OH)COONa.0.5H_2O). Many sodium salts of organic acids decompose to form sodium carbonate. The calculated mass loss for the anhydrous sodium salt to form Na_2CO_3 is 39.0 % (Figure 3.26).

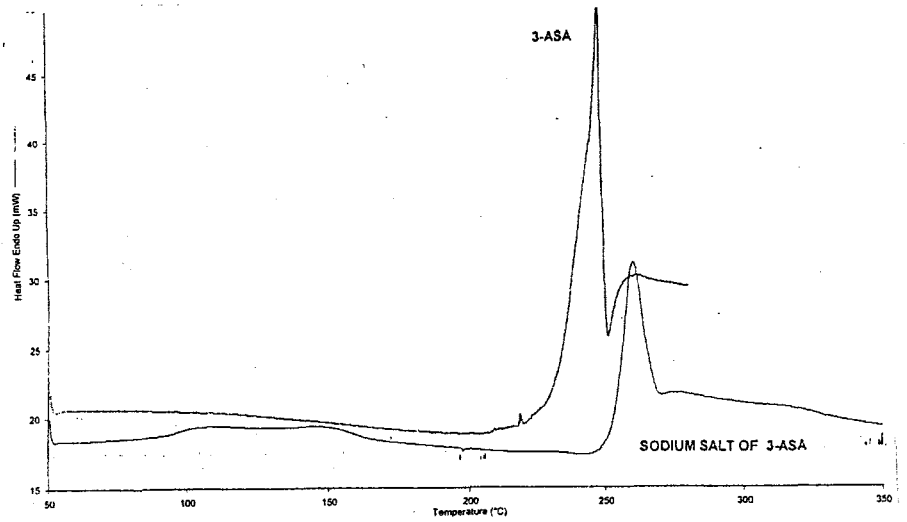

Figure 3.22: DSC curves for 3-ASA and the sodium salt of 3-ASA (heated in flowing nitrogen in an uncrimped aluminium pan at 10 K min^{-1}).

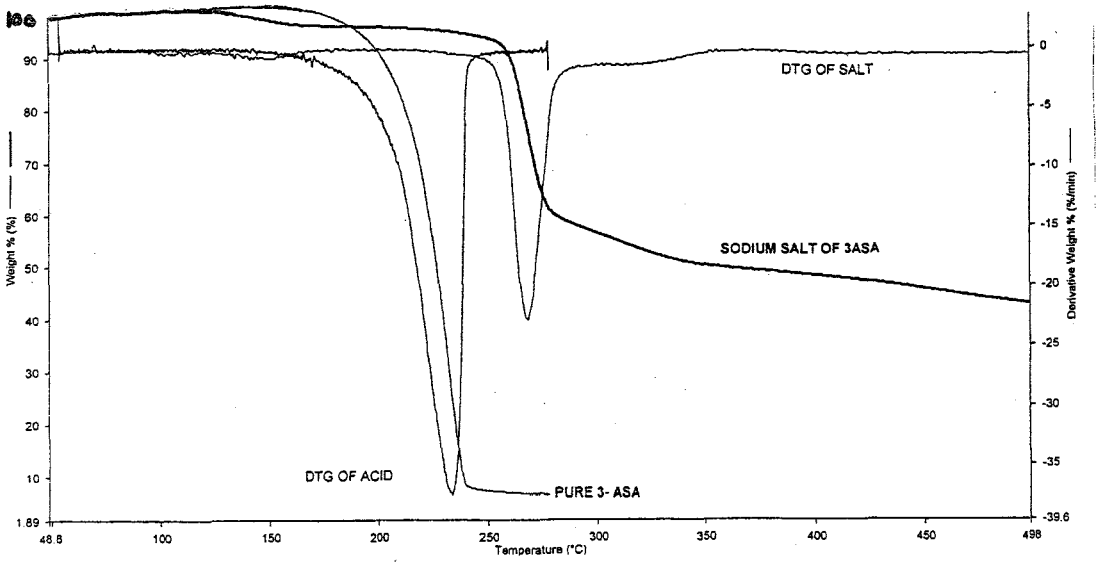

Figure 3.23: TG and DTG curves for 3-ASA and the sodium salt of 3-ASA (heated in flowing nitrogen in an open platinum pan at 10 K min^{-1}).

The sodium salt of 3-ASA (black in colour) showed similar decomposition patterns in flowing oxygen as in that of flowing nitrogen (Figure 3.24). The only difference was observed at about 250°C, where there is a sharp mass-loss in flowing oxygen. The residual sample did not change colour.

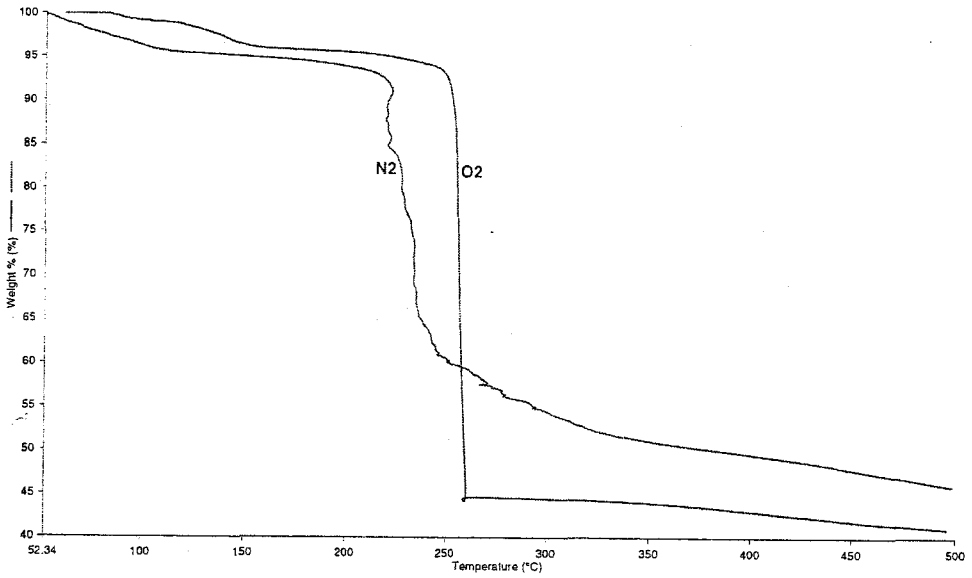

Figure 3.24: TG curves for the sodium salt of 3-ASA in oxygen (O_2) and in nitrogen (N_2) (heated in open platinum pans at 10 K min^{-1}).

Evolved gas analysis (EGA) by TG-FTIR in nitrogen shows formation of both water and carbon dioxide (Figure 3.25). Carbon dioxide is produced at three different stages: the first below 150°C, the second between 200°C and 300°C and the third stage is continuous formation up to 500°C. The thermal behaviour of the salt is quite different from that of the sodium salts of 4-ASA and 5-ASA. The FTIR results in Figure 3.25 correspond to the TG curve shown in Figure 3.23.

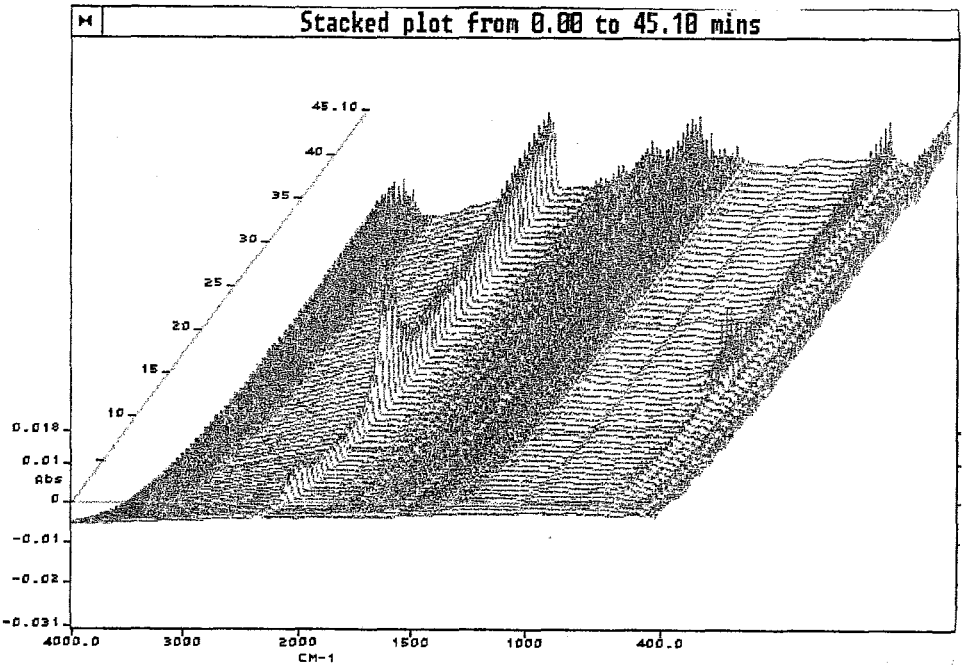

Figure 3.25: A stacked plot of the FTIR spectra recorded during a TG (Figure 3.23) run on the sodium salt of 3-ASA in nitrogen (heated at 10 K min^{-1} from 50 to 500°C).

X-ray powder diffraction patterns for the sodium salt of 3-ASA, its residue after heating to 500 °C and that of pure sodium carbonate are given in Figure 3.26. The XRPD pattern of the residue after heating is quite different from that of the original salt and is not very different from that of pure Na_2CO_3. This supports the formation of some Na_2CO_3 on heating the salt. The original black colour of the salt did not change on heating as happened for the sodium salt of 4-ASA.

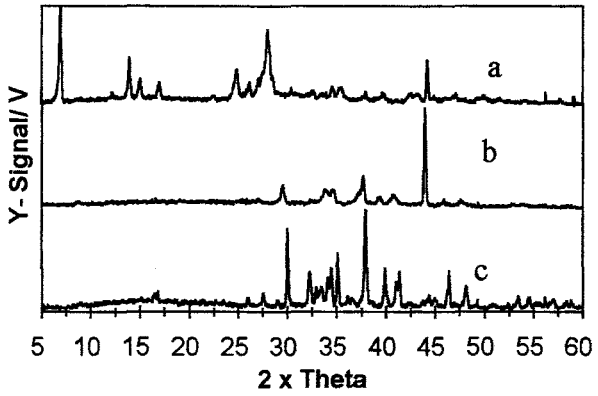

Figure 3.26: The XRPD patterns for (a) the sodium salt of 3-ASA, (b) the residue of the sodium salt of 3-ASA after heating to 500°C and (c) the pure sodium carbonate.

3.6.2 The sodium salt of 4-ASA

The DSC curve for the sodium salt of 4-ASA, showed two endotherms occurring far below the melting point of 4-ASA (Figure 3.27). The first endotherm is broad and appears between 50°C and 100°C, where a sharper endotherm begins (100°C to 110°C). The endotherm between 50°C and 100°C is accompanied by a two-stage mass-loss in the TG curve (Figure 3.28). There was an initial mass-loss between 40°C and 50°C of about 2 % followed by another mass-loss of about 20 % from 50°C to 100°C and then a two-stage mass-loss from 230°C to 330°C (total mass-loss of 9.0 %). Calculations done using the mass-loss of 20% between 50°C and 100°C gave the number of moles of water in the salt to be about 2.4. Wesolowski [9] has reported the formation of a dihydrate ($4\text{-}NH_2\text{-}C_6H_3(OH)COONa.2H_2O$). The expected mass-loss for dehydration of the dihydrate is 17.1 %. By about 650°C, the total mass loss is about 38.0 %. The calculated mass loss for decarboxylation of the dehydrated salt is 25.0% and the

calculated mass-loss for decarboxylation of the hydrated salt is 21%. Therefore, the residue of about 62.0 % could be sodium carbonate (Figure 3.33). Comparison with the TG curve for pure 4-ASA shows that the salt is thermally more stable than the acid.

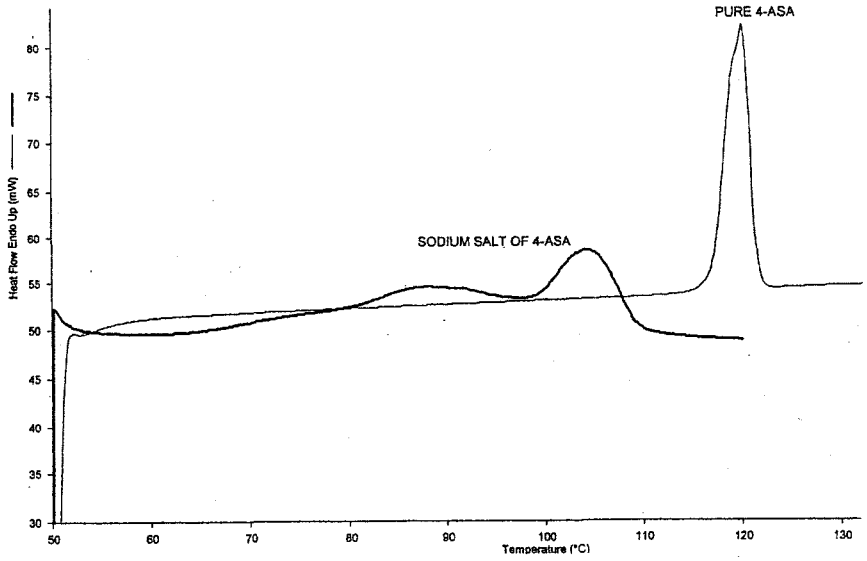

Figure 3.27: DSC curves for 4-ASA and the sodium salt of 4-ASA (heated in flowing nitrogen in uncrimped aluminium pans at 10 K min^{-1}).

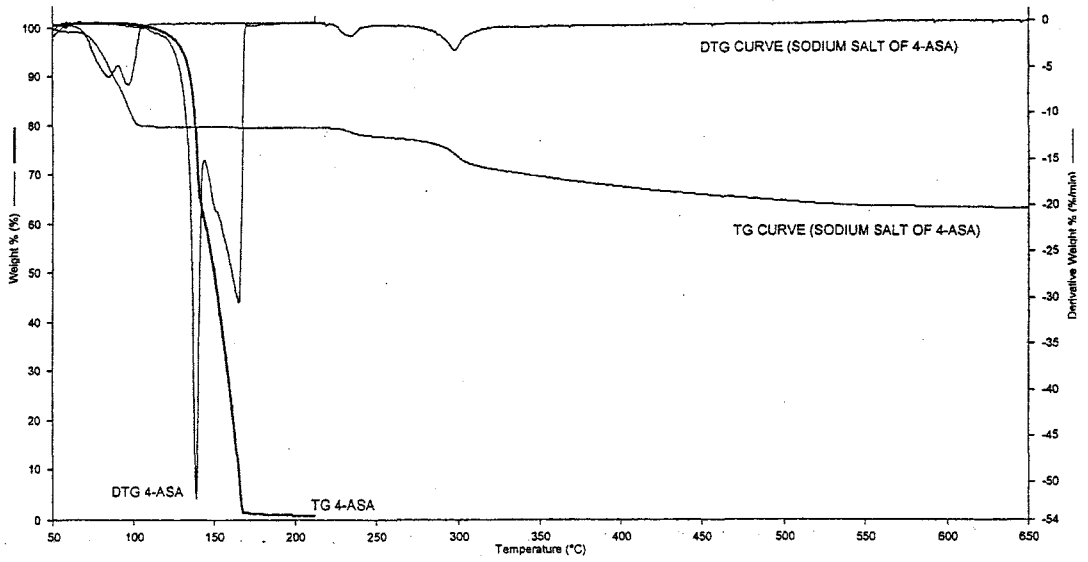

Figure 3.28: TG and DTG curves for 4-ASA and the sodium salt of 4-ASA (heated in flowing nitrogen in an open platinum pan at 10 K min^{-1}).

The TG curves for the sodium salt of 4-ASA in oxygen and in nitrogen are similar up to the onset of very rapid decomposition (heated at 10 K min^{-1} in open platinum pans) (Figure 3.29). Contrary to the observation seen in both sodium salts of 3-ASA and 5-ASA, this salt changed its colour from brownish to whitish colour. There is, as was observed in the sodium salt of 3-ASA, a sharp decomposition at about 250°C.

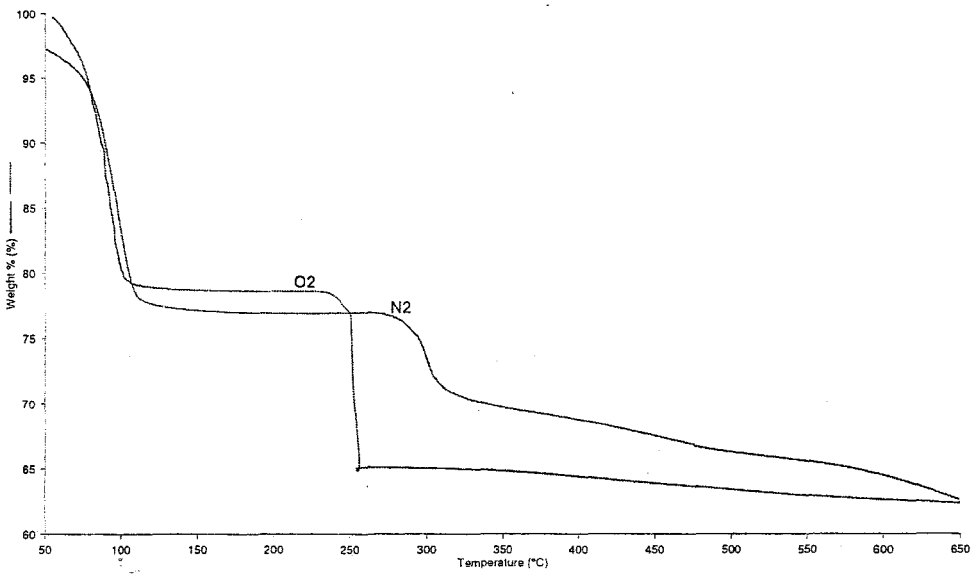

Figure 3.29: TG curves for the sodium salt of 4-ASA in oxygen (O_2) and in nitrogen (N_2) (heated in open platinum pans at 10 K min^{-1}).

A TG-FTIR run (Figure 3.30) for the sodium salt of 4-ASA showed the evolution of CO_2, and hence the occurrence of decarboxylation at temperatures higher than 250°C. The evolution of carbon dioxide continued and showed no maximum by 650°C. The mass-loss starting at 250°C is thus related to the formation of carbon dioxide. The GSR plot (Figure 3.31) for the formation of carbon dioxide shows slow release at lower temperatures and more rapid release after 50 minutes (550°C). A similar plot (Figure 3.32) for the evolution of H_2O shows that this occurs between 90°C and 130°C, at a heating rate of 10 K min^{-1}.

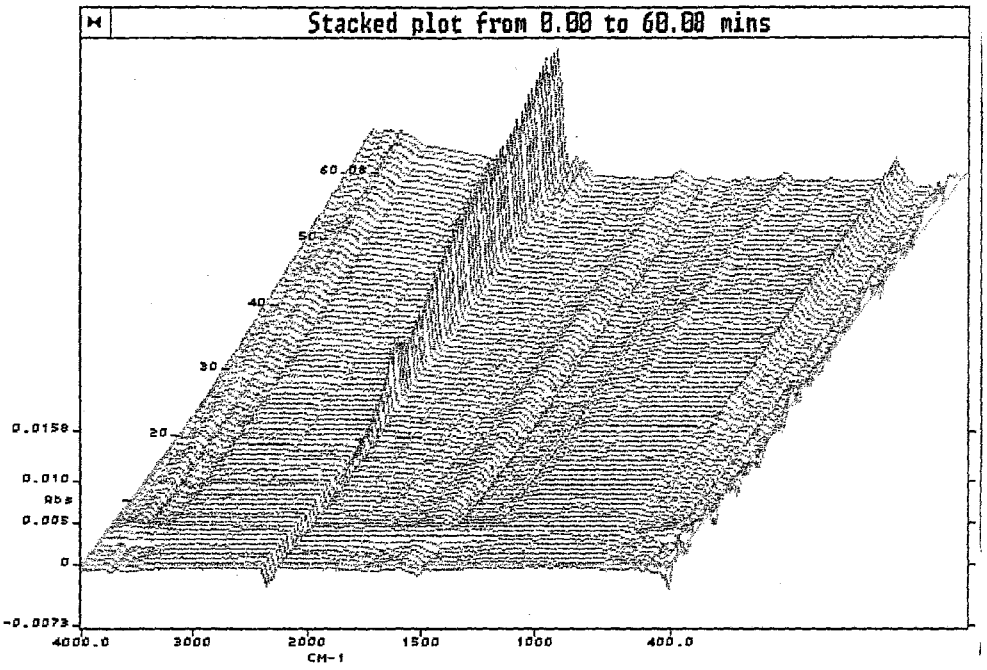

Figure 3.30: A stacked plot of the FTIR spectra recorded during a TG run (Figure 3.28) on the sodium salt of 4-ASA (heated in an open platinum pan in nitrogen at 10 K min^{-1} from 50 to 650°C).

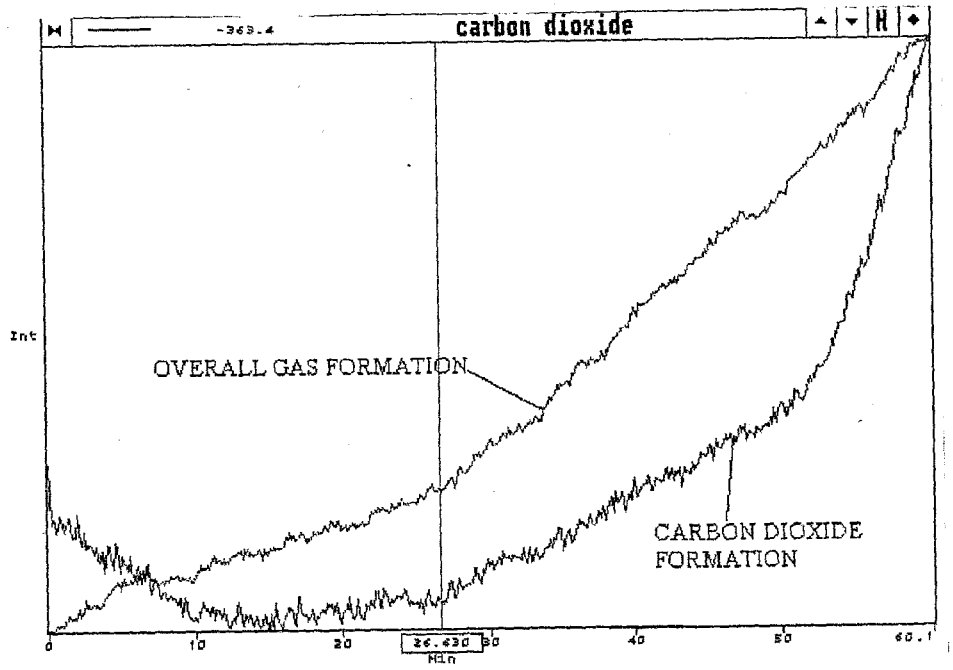

Figure 3.31: The Gram-Schmidt reconstruction (GSR) curve for the overall release of gases and the evolution of CO_2 from sodium salt of 4-ASA (heated in flowing nitrogen at 10 K min^{-1}).

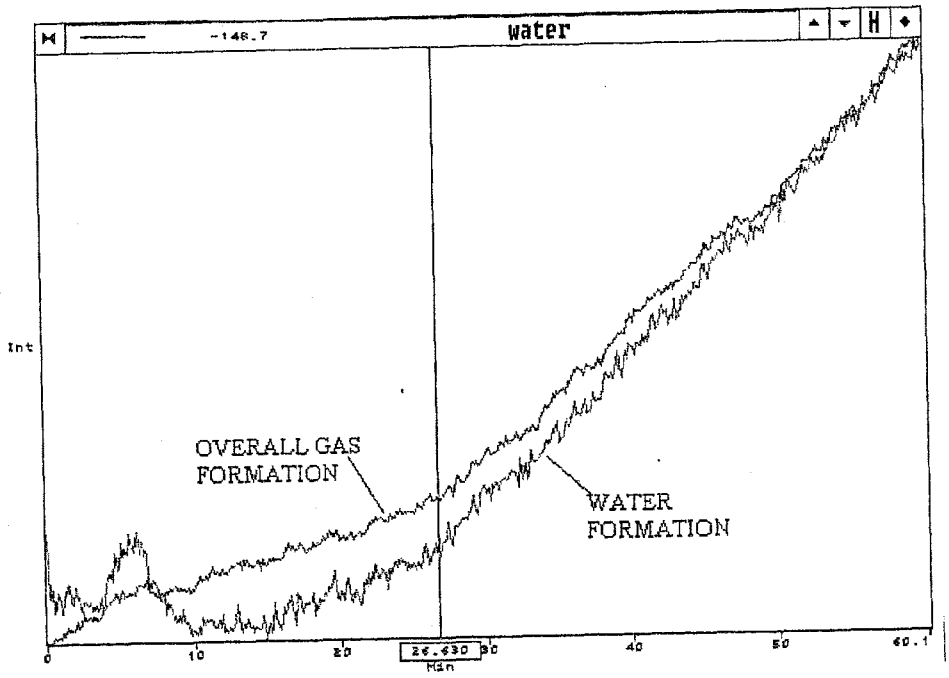

Figure 3.32: The Gram-Schmidt reconstruction (GSR) curve for the overall release of gas and the evolution of H_2O from the sodium salt of 4-ASA (heated in flowing nitrogen at 10 K min^{-1}).

X-ray powder diffraction patterns of the sodium salt of 4-ASA, the residue after heating to 650°C and pure Na_2CO_3 are shown in Figure 3.33. The XRPD pattern for the residue and for pure Na_2CO_3 are very similar. The results showed the decomposition of the salt (which is accompanied by a colour change from brownish to white) results in the formation of sodium carbonate after heating up to 650°C.

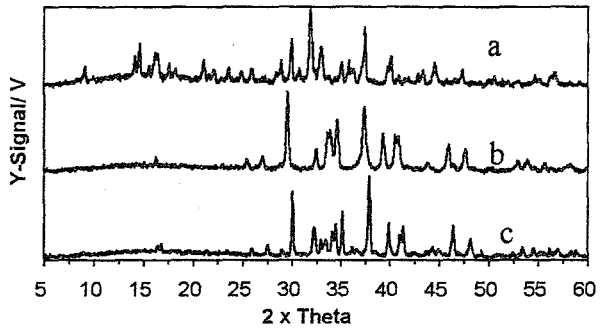

Figure 3.33: XRPD patterns for (a) the sodium salt of 4-ASA, (b) the residue of sodium salt of 4-ASA after heating to 650 °C and (c) pure sodium carbonate.

3.6.3 The sodium salt of 5-ASA

A DSC curve (Figure 3.34) for the sodium salt of 5-ASA showed a broad endotherm between 110 °C and 150 °C. The TG curve (Figure 3.35) showed a two-stage process from 80 °C to 140 °C with a total mass-loss of 12 %. This was followed by a slow mass-loss between 140 °C and 500 °C. The total mass-loss by 500 °C is about 25 %.

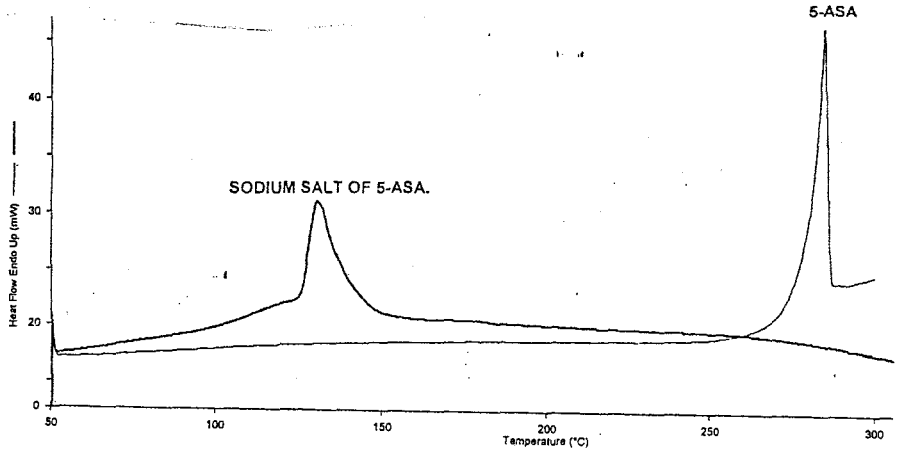

Figure 3.34: DSC curves for 5-ASA and the sodium salt of 5-ASA (heated in flowing nitrogen in uncrimped aluminium pans at 10 K min^{-1}).

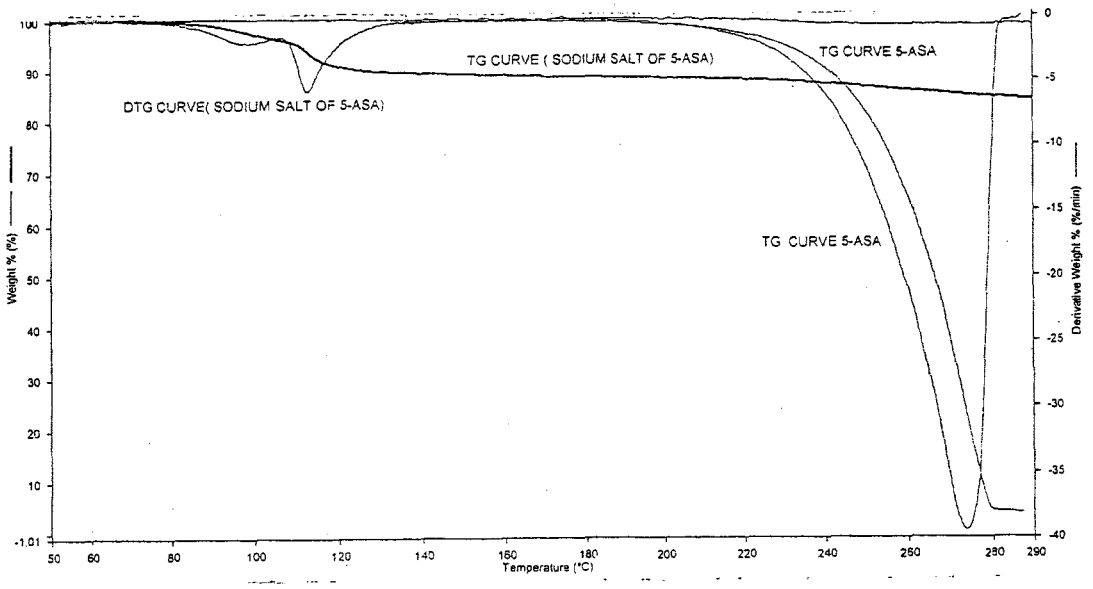

Figure 3.35: TG and DTG curves for 5-ASA and the sodium salt of 5-ASA (heated in flowing nitrogen in an open platinum pan at 10 K min^{-1}).

The TG and DTG curves (Figure 3.36) for the sodium salt of 5-ASA in oxygen and in nitrogen (heated in open platinum pans at 10 K min^{-1}) are very similar. The total mass-loss at 500 °C is 25 %. In this sodium salt, there is no sharp decomposition/oxidation in oxygen at 250 °C as was observed for the sodium salts of 3-ASA and 4-ASA.

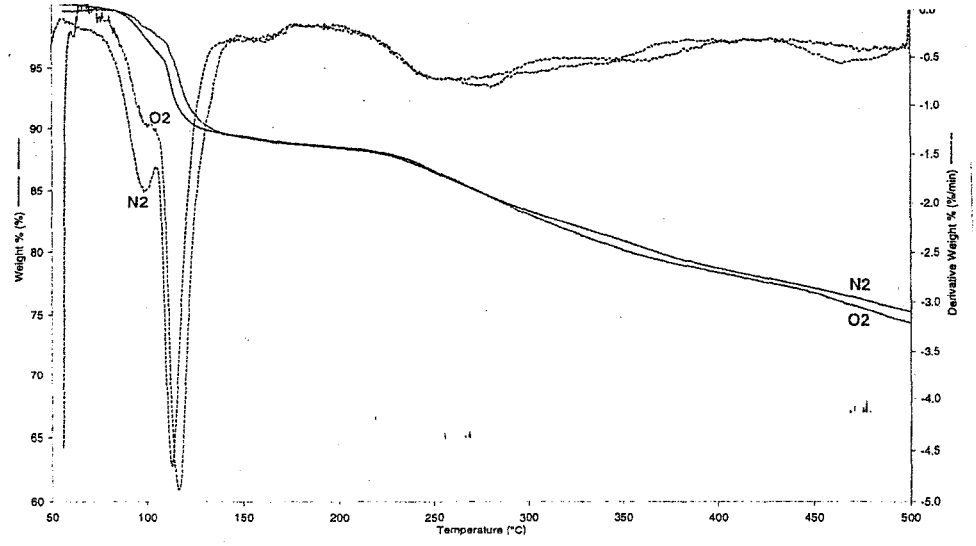

Figure 3.36: TG and DTG curves for the sodium salt of 5-ASA in oxygen (O_2) and in nitrogen (N_2) (heated in open platinum pans at 10 K min^{-1}).

TG-FTIR analysis of the gases evolved during heating of the salt did not show any decarboxylation process. Calculations from the 12% mass-loss in the TG curve for the salt, if assumed to be water, gave 1.4 moles of water (5-NH_2-C_6H_3(OH)COONa.1.4H_2O). The calculated mass-loss for decarboxylation of the dehydrated salt is 25.1% and for the formation of sodium carbonate is 39.0% (Figure 3.37).

X-ray powder diffraction patterns of the sodium salt of 5-ASA, the residue after heating to 650°C, and of pure Na_2CO_3 are shown in Figure 3.37. The XRPD patterns are all different from each other. The residue of the heated salt did not change in colour. The results showed that the salt (5-NH_2-C_6H_3(OH)COONa.1.4H_2O) did not form sodium carbonate after heating up to 650°C.

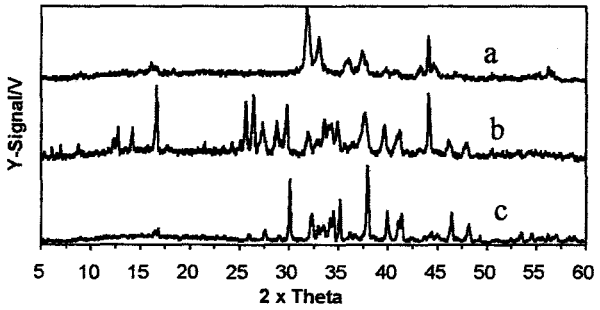

Figure 3.37: XRPD patterns for (a) a sodium salt of 5-ASA, (b) a residue of heated sodium salt of 5-ASA and (c) a pure sodium carbonate.

Results for the sodium salts of 3-ASA, 4-ASA and 5-ASA are summarised in Table 3.5. Most of the DSC endotherms were complex. Different hydrates were found for the three salts and hence their dehydrations were different. Dehydration is a two-stage process for the 4-ASA and 5-ASA salts. The process of

decarboxylation for the salts of 3-ASA and 4-ASA occurred over a wide range of temperatures. Decarboxylation of the 5-ASA salt could not be detected. Generally, preparation of the sodium salts of these acids improved the thermal stability of the compounds.

Table3.5 Thermal behaviour of the sodium salts of aminosalicylic acids

Sodium salt of	No. of moles H_2O	TG /°C	CO_2 evolution	DTG max./°C	DSC (op) endotherm onset /°C	ΔH /kJmol^{-1}
3-ASA	0.5	100-170 240-340	100-500	150 and 275	91 and 254	91 complex
4-ASA	2.4	50-100 230-330	 250-650	80 and 100 (doublet) 240 300	50 and 100	complex
5-ASA	1.4	80-140	none detected	90 and 110 (doublet)	110	complex

3.7 Thermal behaviour of the aminophenols (AP)

3.7.1 DSC and TG results

Decarboxylation of the aminosalicylic acids should lead to the formation of the corresponding aminophenols, so their thermal behaviour was also investigated. The DSC curves for the aminophenols, 2-AP, 3-AP and 4-AP, under similar experimental conditions to those described above, are shown in Figures 3.38, 3.39 and 3.40, respectively. All the DSC curves showed sharp endotherms when samples were heated in uncrimped aluminium pans, but these endotherms became

broader when sealed pressure pans were used. The onset temperatures for the endotherms for 2-AP, 3-AP and 4-AP are 170°C, 118°C and 183°C, respectively, using uncrimped aluminium pans. Using sealed pressure pans these onset temperatures were 175°C, 120°C and 185°C, respectively. The reported melting temperatures of the aminophenols are: 2-AP, 174-177°C; 3-AP, 124-126°C and 4-AP, 186°C (manufacturer's notes), so that these endotherms can be associated with melting of the compounds.

The use of sealed pressure pans prevents other processes such as evaporation from occurring during melting of the samples. On cooling a sample that had been heated in an uncrimped pan immediately after the melting endotherm and rescanning the sample, the area of the endotherm was greatly decreased, indicating that melting was accompanied by decomposition and/or loss of sample by evaporation.

The TG curves for the aminophenols (Figure 3.38, 3.39 and 3.40) showed onset of mass loss at about 110°C for all three isomers. The rates of mass-loss, shown by the DTG curves in the given Figures, were similar for 2-AP and 4-AP, with that for 3-AP being slower.

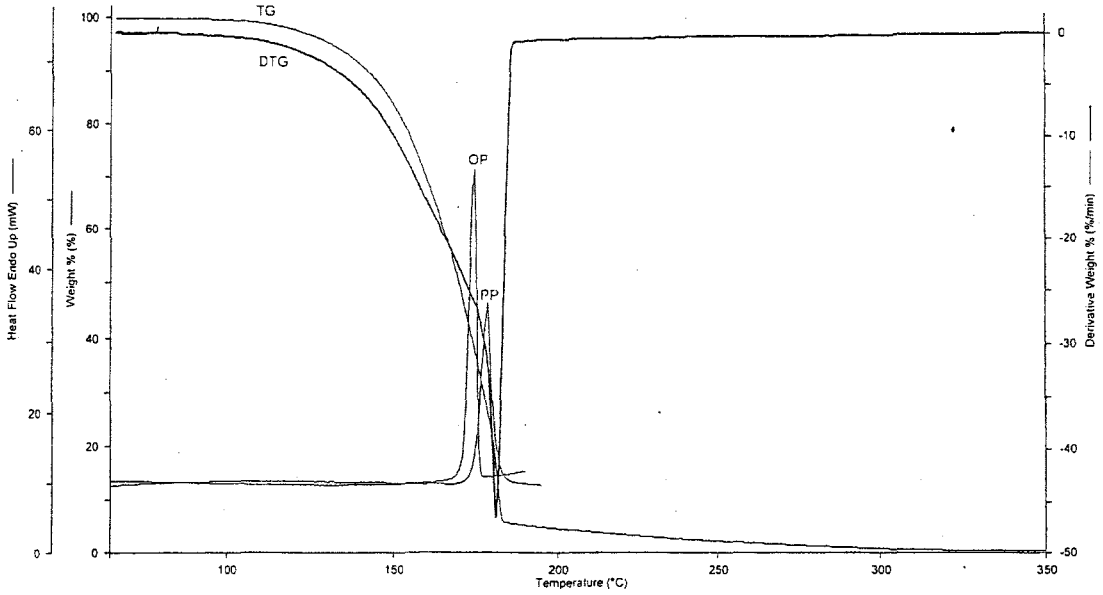

Figure 3.38: TG, DTG and DSC curves for 2-AP (heated in flowing nitrogen at 10 K min^{-1}: op = uncrimped aluminium and pp = sealed pressure pans for DSC: open platinum pans for TG).

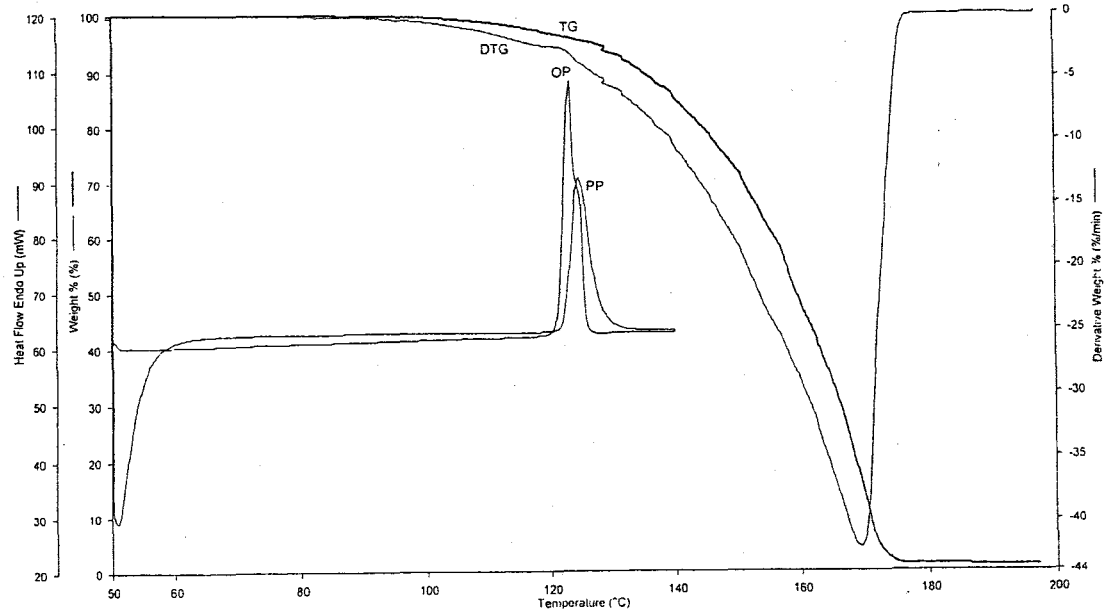

Figure 3.39: TG, DTG and DSC curves for 3-AP (heated in flowing nitrogen at 10 K min^{-1}: uncrimped aluminium (op) and sealed pressure pans (pp) for DSC: open platinum pans for TG).

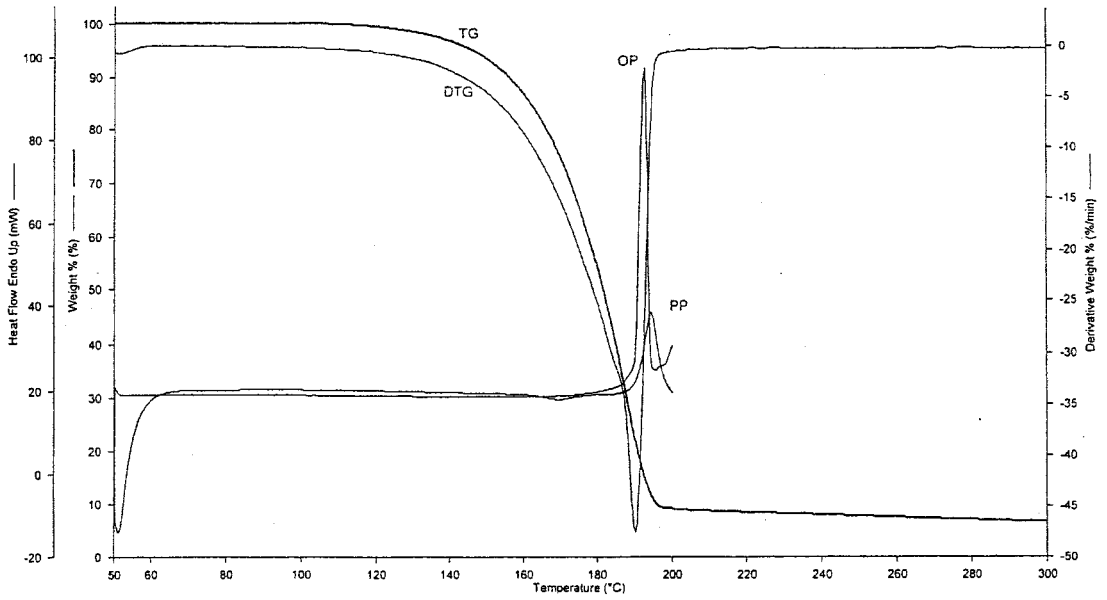

Figure 3.40: TG, DTG and DSC curves for 4-AP (heated in flowing nitrogen at 10 K min^{-1}: uncrimped aluminium (op) and sealed pressure pans (pp) for DSC: open platinum pans for TG).

3.7.2 Evaporation studies of the aminophenols

The DTG curves for the aminophenols were used (as described in Section 3.2.2) to construct the Arrhenius-type plots shown in Figure 3.41. The values of the apparent activation energies of evaporation for 2-AP, 3-AP and 4-AP from the plots are 81 ± 2, 71 ± 6, and 92 ± 1 kJ mol^{-1}, respectively. From Table 3.1, the estimated enthalpy changes, with no provision for the differences in the isomers, are: melting 10 kJ mol^{-1}, vaporisation 82 kJ mol^{-1}, and sublimation 92 kJ mol^{-1}. The apparent activation energies are thus close to the range of the calculated enthalpies of vaporisation and sublimation.

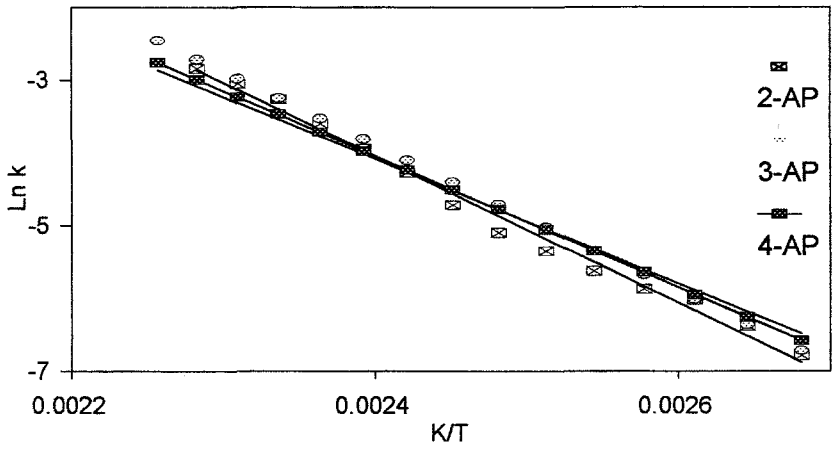

Figure 3.41: Arrhenius-type plots for the evaporation of the aminophenols (calculated from the TG curves in Figures 3.38, 3.39 and 3.40).

Results for the thermal behaviour of the isomers of aminophenols are summarised in Table 3.6.

Table 3.6 Thermal behaviour of the aminophenols

APs	m.pt /°C	T_{onset} of mass loss in TG/°C	DTG max. mass-loss	T_{onset} (DSC (pp) endotherm/°C	ΔH_{melt} / kJ mol^{-1}	E_{vap} / kJ mol^{-1}
2-AP	174-177	110	175	175	29	81 ± 2
3-AP	124-126	110	170	120	24	71 ± 6
4-AP	186	110	190	185	23	92 ± 1

3.7.3 Correction of enthalpy measurements for accompanying mass losses

The onset temperatures of the melting endotherms for the three aminophenols differed considerably from each other (from DSC runs using uncrimped aluminium pans). The mass-losses in the corresponding TG curves are much higher for 2-AP

and 4-AP than for 3-AP so that greater corrections need to be applied to the measured enthalpies of melting (see Table 3.7).

Table 3.7 Summary of the enthalpy values of the aminophenols corrected for the actual sample mass

Compound	2-AP	3-AP	4-AP
Mass of sample/ mg	2.383	3.011	3.821
Onset temp. of endotherm/ °C	170	118	187
Reported m.pt/ °C	174-177	124-126	186
Mass-loss before the endotherm/ %	45	2	68
Enthalpy / kJ mol^{-1}			
1. Normalised to initial mass	34	25	30
2. Normalised to actual mass	61	26	93
Calc. enthalpy of melting (Table 3.1)*	10	10	10
Enthalpies in sealed pressure pan/kJ mol^{-1}	29	24	23

* No provision for the differences in isomers.

The values of the enthalpies of melting obtained experimentally are much higher than the calculated values and the predictions, in this case with no provision for the differences in isomers, are apparently unreliable.

3.8 Thermal behaviour of mixtures of the aminosalicylic acids with their corresponding aminophenols

3.8.1 DSC results

Decarboxylation of the aminosalicylic acids leads to the formation of the corresponding aminophenols. Because of the possibility of such processes occurring, it was of interest to examine the thermal behaviour of equimolar

mixtures of the aminosalicylic acids with the corresponding aminophenols, by comparing the DSC and TG curves for the mixtures with those of the pure components. This is an admittedly exaggerated situation, but the behaviour of the ASAs in the presence of large amounts of potential degradation products can serve as a guide to the possible influences of smaller amounts of such a compounds.

The DSC curve (Figure 3.42) for a 1:1 molar ratio mixture of 3-ASA/2-AP showed several overlapping endotherms. The first endotherm is fairly sharp and has onset temperature at about 169 °C and $\Delta H = 94$ J g^{-1} (mass of the mixture taken). This is followed by broad endotherms (180 °C to 260 °C). Melting of 2-AP, represented by the first endotherm, thus affects the melting process of 3-ASA.

The DSC curve for a 1:1 molar ratio mixture of 4-ASA/3-AP (Figure 3.43) showed a complex overlapping endotherm, with onset about 110 °C and complete by about 130°C. The melting of 3-AP at about 110 °C thus has a marked effect on the thermal behaviour of 4-ASA.

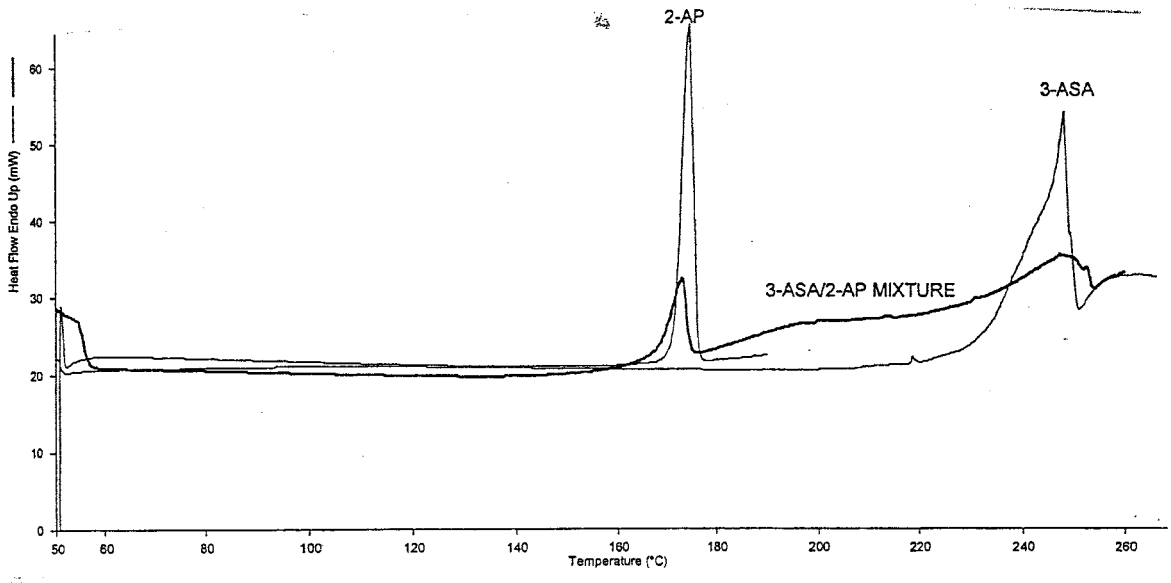

Figure 3.42: DSC curves for 3-ASA, 2-AP and a 1:1 molar mixture of 3-ASA/2-AP (heated in flowing nitrogen at 10 K min^{-1} in uncrimped aluminium pans).

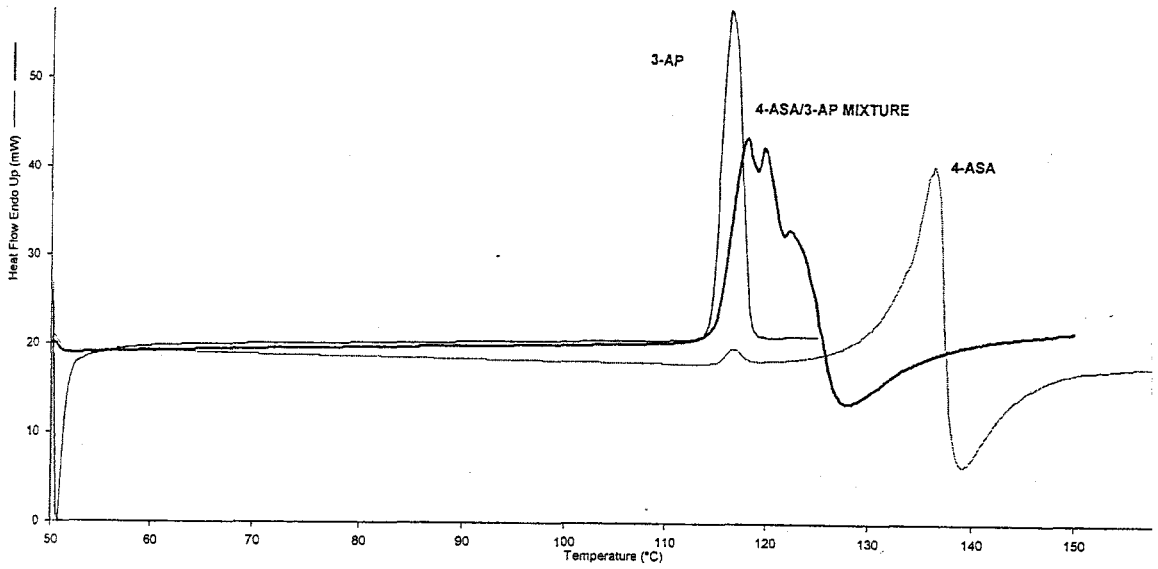

Figure 3.43: DSC curves for 4-ASA, 3-AP and a 1:1 molar mixture of 4-ASA/3-AP (heated in flowing nitrogen at 10 K min^{-1} in uncrimped aluminium pans).

The DSC curve of a 1:1 molar ratio mixture of 5-ASA/4-AP (Figure 3.44) shows two endotherms. The first is sharper with onset about 170°C and is followed by a broader endotherm, onset about 195°C and complete by about 240°C (ΔH_1 = 164 J g^{-1}; ΔH_2 =190 J g^{-1} (Total ΔH = 354 J g^{-1}). Calculated ΔH from linear combination is 374 J g^{-1}. The normal endotherm for 4-AP at 179°C was thus lowered to 170°C in the mixture. The melting of 4-AP is affected by the presence of 5-ASA and also changes the subsequent thermal behaviour of 5-ASA.

From the above results it can be seen that decarboxylation of the aminosalicylic acids to form the corresponding (lower melting and hence liquid) aminophenols, even in small amounts, initially will have marked effects on the subsequent thermal behaviour of the remaining aminosalicylic acids.

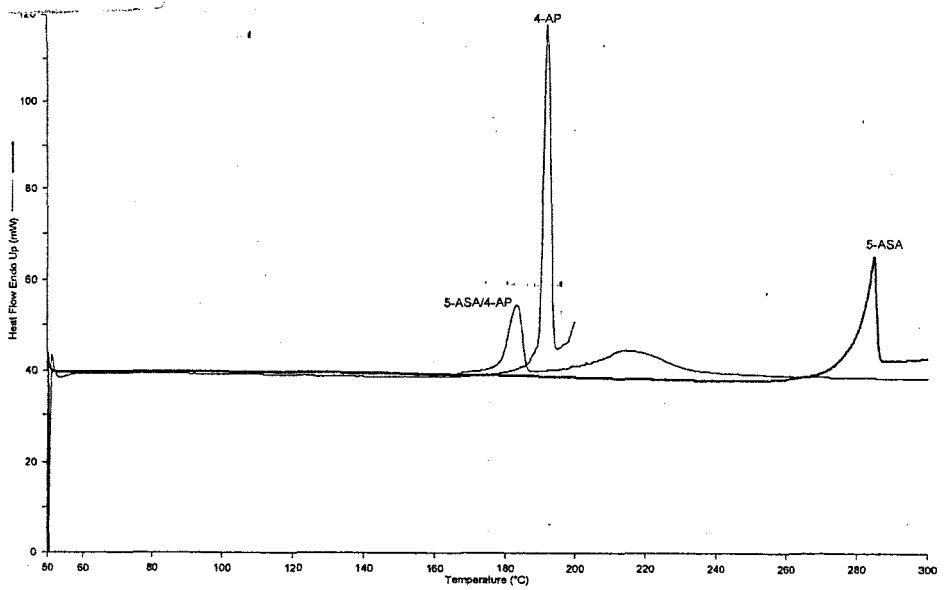

Figure 3.44: DSC curves for 5-ASA, 4-AP and a 1:1 molar mixture of 5-ASA/4-AP (heated in flowing nitrogen in uncrimped aluminium pans at 10 K min^{-1}).

3.8.2 Evolved gas analysis (EGA) of the mixtures

Figure 3.45 shows the three-dimensional stacked plot of FTIR spectra recorded during heating of a mixture of 3-ASA and its possible degradation product 2-AP. The result is similar to that for pure 3-ASA (Figure 3.16) where the process of decarboxylation commences at about 250°C and evolution of carbon dioxide continues up to 350°C.

4-ASA is clearly affected by the presence of the decomposition product, 3-AP (Figure 3.46). Carbon dioxide (CO_2) is evolved after barely 2.5 minutes (75°C) and reaches a maximum at 4.0 minutes (90°C). Only a small amount of carbon dioxide is being produced after 7.0 minutes (120°C).

5-ASA which did not show any decarboxylation in its pure form, also showed no decarboxylation in the presence of 4-AP.

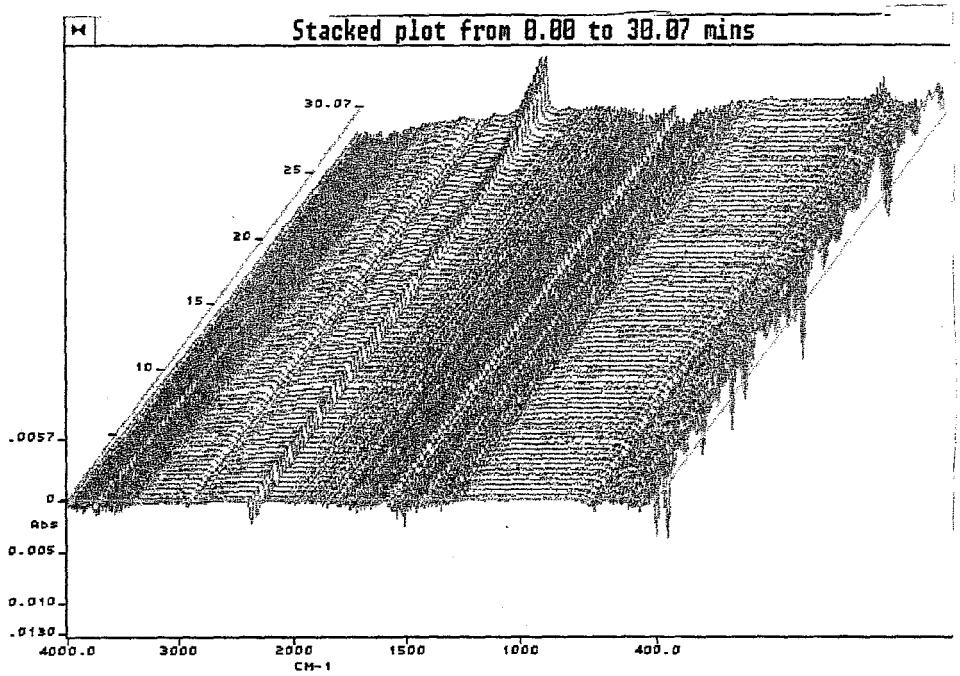

Figure 3.45 A stacked plot of FTIR spectra recorded during a TG run on a mixture of 3-ASA and 2-AP (heated at 10 K min^{-1} in flowing nitrogen from 50 to 350°C).

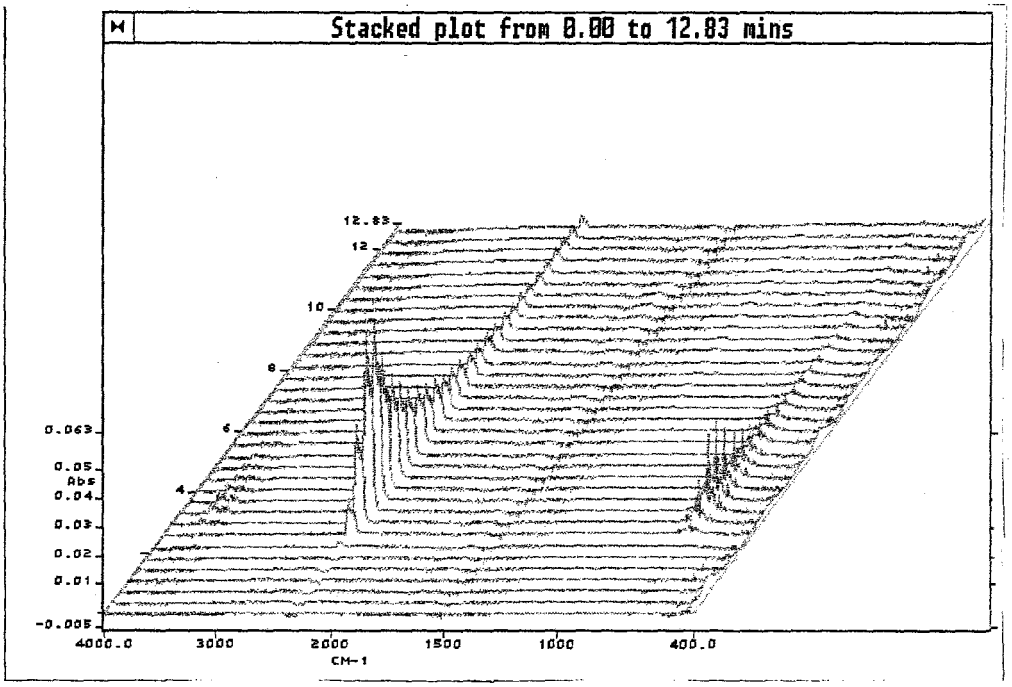

Figure 3.46: A stacked plot of FTIR spectra recorded during a TG run on a mixture of 4-ASA and 3-AP (heated at 10 K min^{-1} in flowing nitrogen from 50 to 180°C).

A more detailed study of the influence of 3-AP (and, possibly, other additives) on the decarboxylation of 4-ASA would be of interest.

3.9 Thermal behaviour of the aminobenzoic acid derivatives in an oxygen environment

3.9.1 Introduction

The environment in which the sample is analysed is a very important aspect in the thermal analysis of solid compounds. Environments may be inert (nitrogen, argon, helium), oxidizing (oxygen or air), reducing (hydrogen, carbon monoxide) or reactive (hydrogen chloride, hydrogen fluoride, etc.). In addition to its reactive or protective function, the choice of the purge gas depends to a certain extent on the cost, availability, thermal conductivity, purity and density [109].

In oxygen or air, the rate of oxidation will depend upon the exposed surface area of the sample and whether the products are volatile, or likely to form solid layers on surfaces that are likely to restrict further oxidation.

3.9.2 DSC and TG results for the reference acids (BA and SA)

The DSC curves for benzoic acid (BA) and salicylic acid (SA) showed endotherms similar to those obtained in nitrogen. The DSC curve for BA (uncrimped aluminium pans in flowing oxygen at 10 k min^{-1}) shows an endotherm from 120°C to 128°C and ΔH = 17 kJ mol^{-1}. The corresponding values in nitrogen were 115°C to 120°C with ΔH = 16 kJ mol^{-1}. The TG curves in oxygen (Figure 3.47) were similar to those in nitrogen shown in Figure 3.1. The irregularities in the TG curves due to evaporation/sublimation seemed to be more marked.

The DSC and TG curves for SA (in flowing oxygen and at 10 K min^{-1}) (Figure 3.48) were also similar to those obtained in nitrogen (Figure 3.2). The values for the endotherms were from 154°C to 164°C, ΔH = 22 kJ mol^{-1} in oxygen and from

158 °C to 162 °C with $\Delta H = 23$ kJ mol^{-1} in nitrogen.

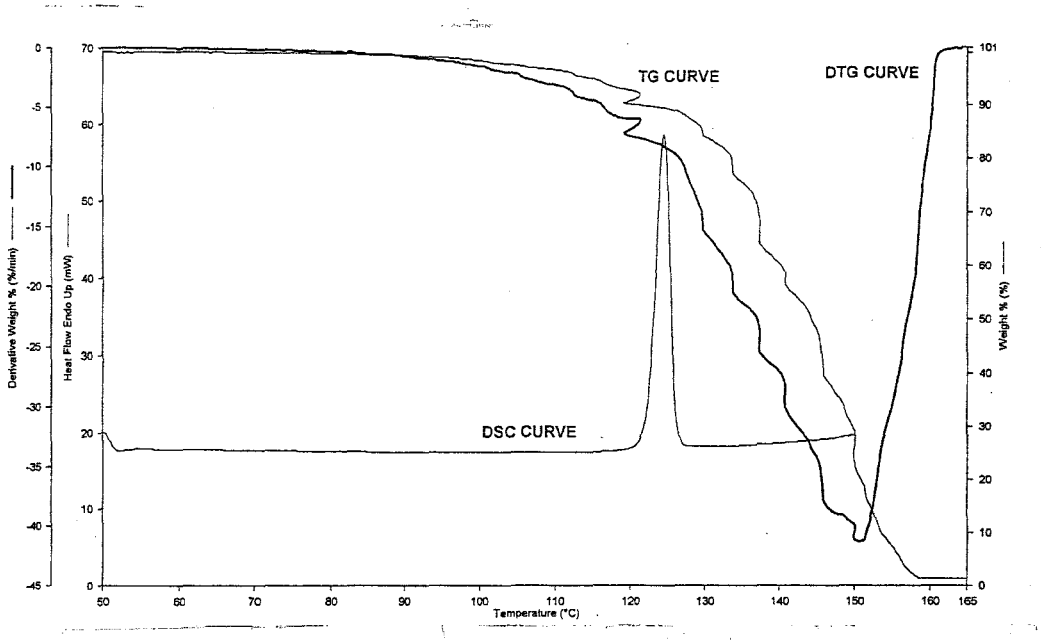

Figure 3.47: The DSC, TG and DTG curves for benzoic acid (BA) (heated in flowing oxygen at 10 K min^{-1}: uncrimped aluminium for DSC and open platinum pan for TG).

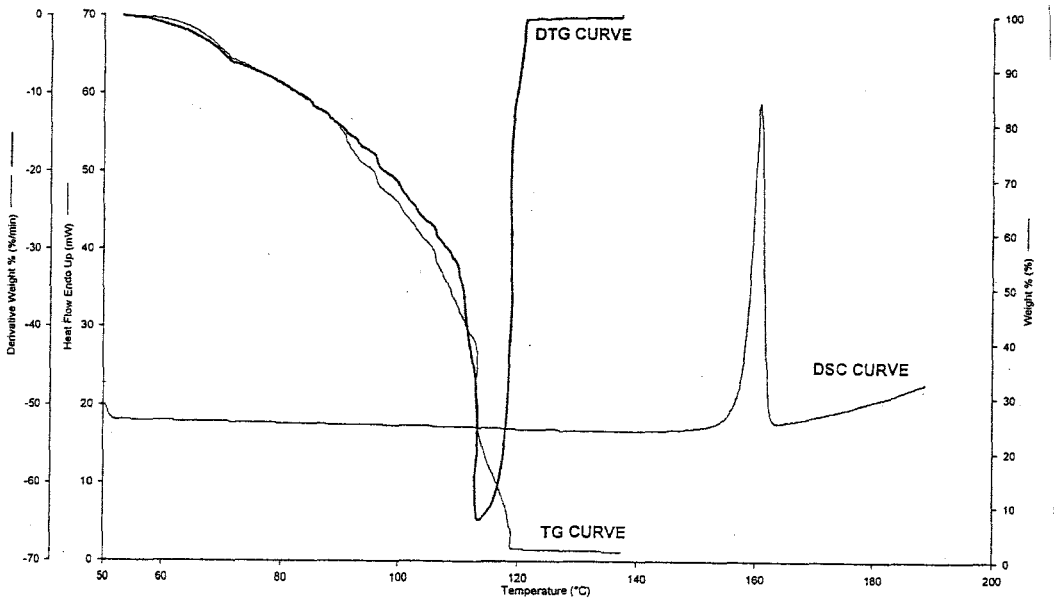

Figure 3.48: The DSC, TG and DTG curves for salicylic acid (SA) (heated in flowing oxygen at 10 K min^{-1}: uncrimped aluminium for DSC and open platinum pan for TG).

3.9.3 DSC and TG results for the aminosalicylic acids (ASA)

The DSC curves for 3-ASA heated at 10 K min^{-1} in oxygen showed (Figure 3.49) a complex exotherm, with a major peak from 235 °C to 247 °C, ($\Delta H = 44$ kJ mol^{-1}) followed by further complex exotherms. The TG curves showed that the mass-loss starts at about 200 °C and about 25% of the original mass remains at 260 °C (Figure 3.49). The corresponding run under flowing nitrogen (see Figure 3.13) showed that the mass remaining around 240 °C is about 5%. The exothermic processes seen in the DSC curve are thus accompanied by mass losses.

The TG and DTG curves for 4-ASA heated at 10 K min^{-1} in oxygen (Figure 3.50) were similar to those obtained in nitrogen (see Section 3.4.1 and Figure 3.14). The DSC curve for 4-ASA heated in oxygen is initially similar to that in nitrogen. It shows overlapping endotherms with onset at about 115 °C and at about 136 °C, followed immediately by a sharp exotherm. The DSC curve under nitrogen showed several overlapping endotherms with onset temperatures at about 110 °C, about 115 °C, and at about 125 °C becoming complex and shifting to exothermic at about 132 °C (Figure 3.14).

The DSC and TG curves for 5-ASA heated at 10 K min^{-1} in oxygen are different to those obtained in nitrogen. The DSC curve shows an exotherm from 267 °C to 299 °C, with $\Delta H = -153$ kJ mol^{-1} (Figure 3.51). This exotherm has the same onset temperature, 278 °C, as that of the endotherm observed in flowing nitrogen. The TG curve (Figure 3.50) shows that the mass-loss starts at 200 °C and at around 255 °C, 25% of the original mass remains. Comparison of the DSC and TG/DTG curves suggests that the DSC exotherm occurred after the major mass-loss had taken place, but this may be as a result of differences in the exposure of the sample to the oxygen in the DSC and the TG experiments.

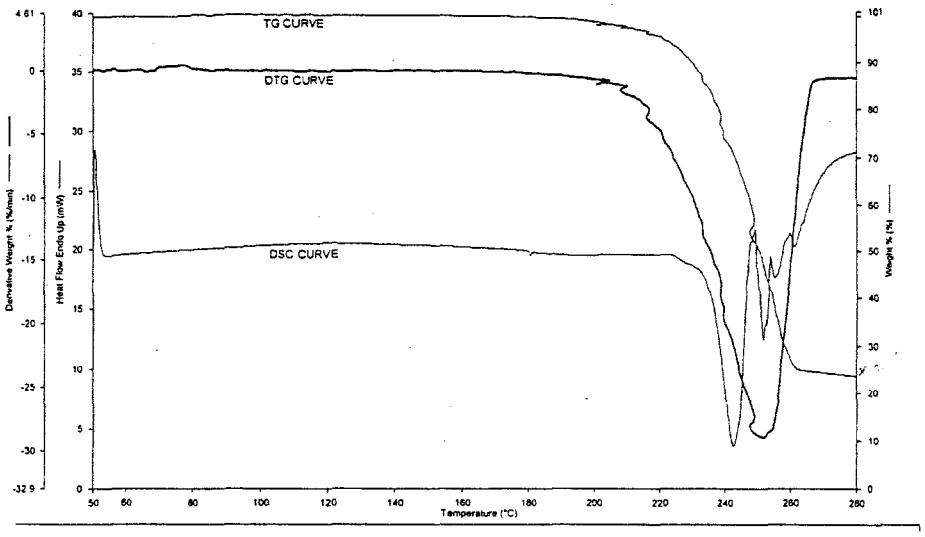

Figure 3.49: The DSC, TG and DTG curves of 3-ASA (heated in flowing oxygen at 10 K min^{-1} in open platinum pan for TG and uncrimped aluminium pan for DSC runs).

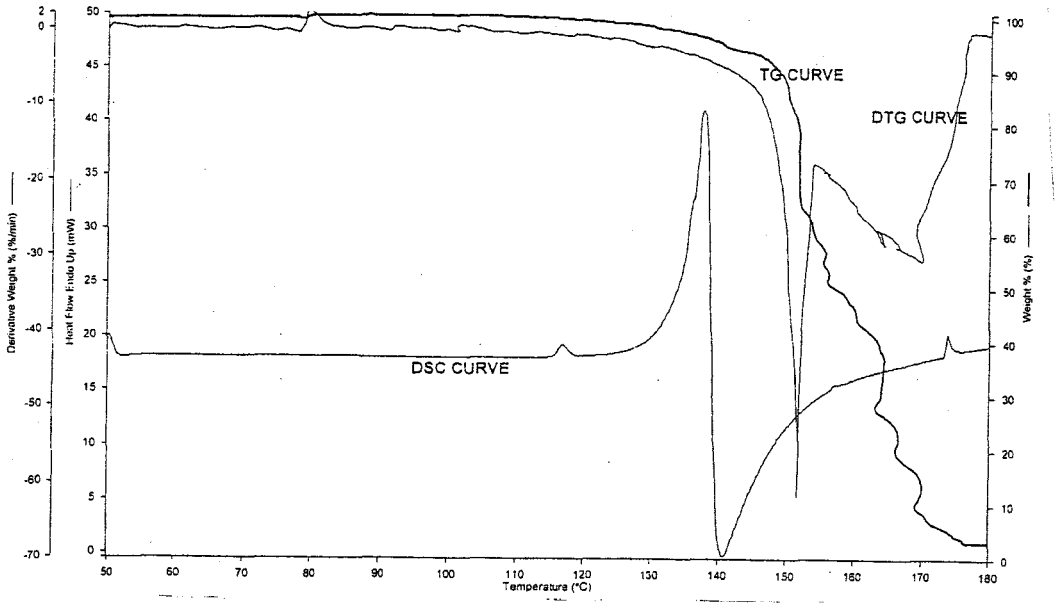

Figure 3.50: The DSC, TG and DTG curves of 4-ASA (heated in flowing oxygen at 10 K min^{-1} in open platinum pan for TG and uncrimped aluminium pan for DSC runs).

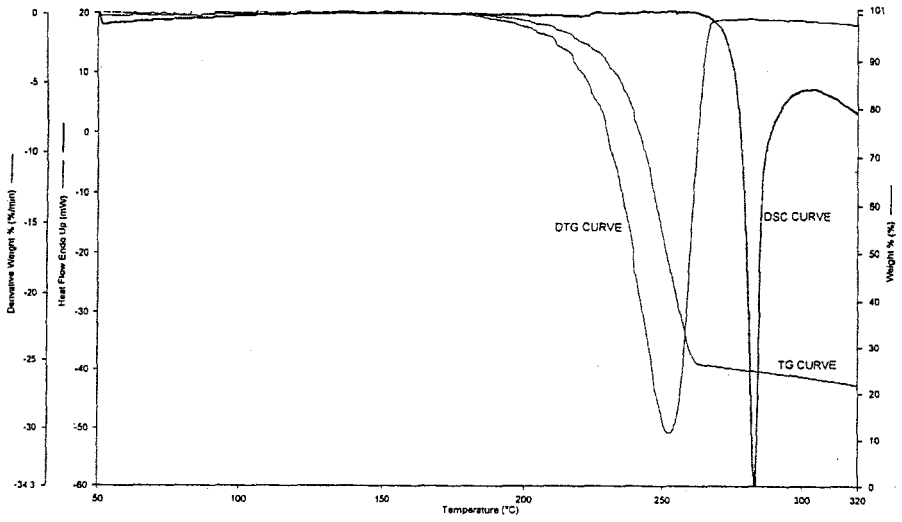

Figure 3.51: The DSC, TG and DTG curves of 5-ASA (heated in flowing oxygen at 10 K min^{-1} in open platinum pan for TG and uncrimped aluminium pan for DSC runs).

FTIR spectra of the residues from the TG runs on 3-ASA and 5-ASA were recorded and are shown in Figures 3.52 and 3.53.

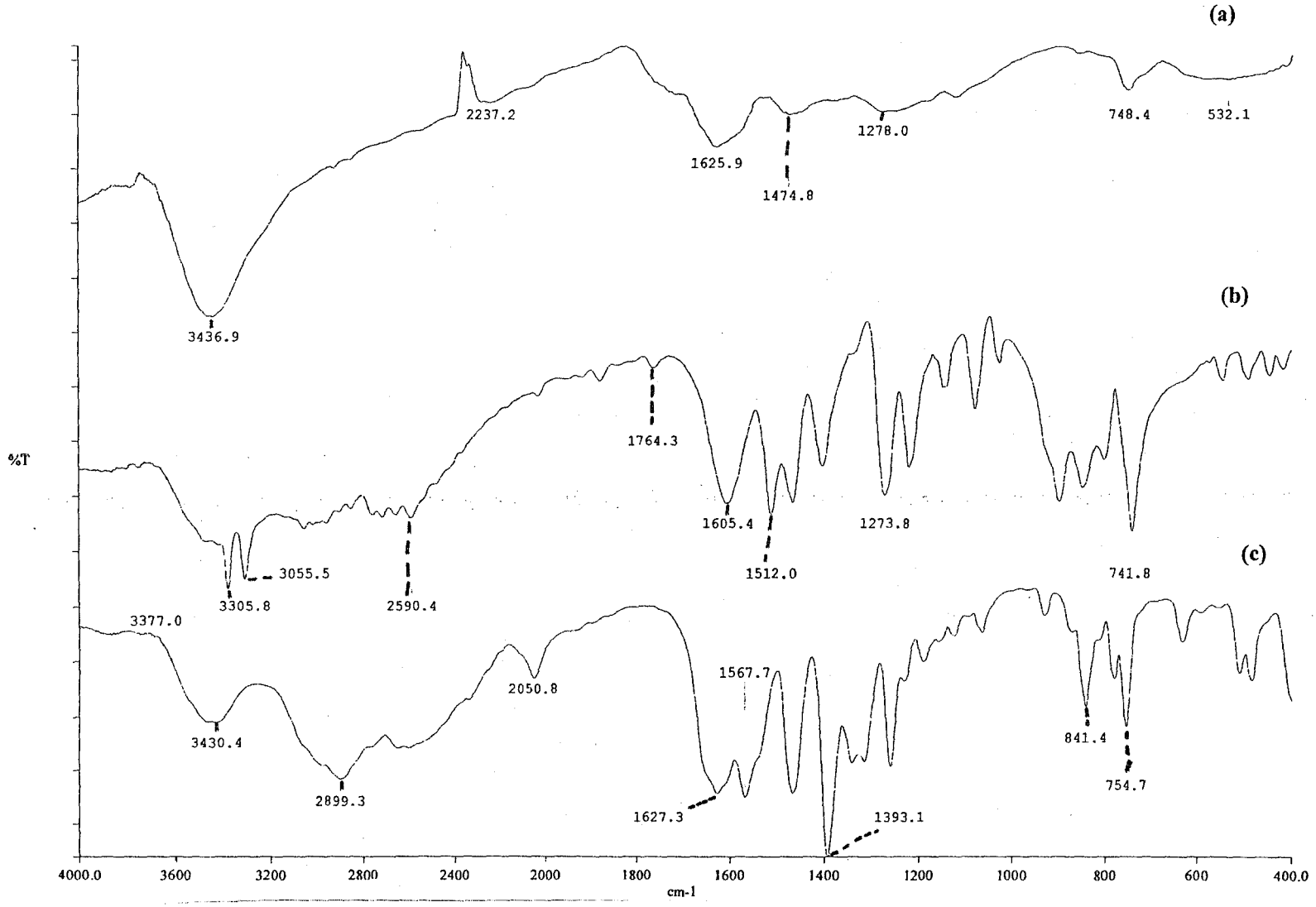

Figure 3.52: FTIR spectra of (a) the residue after heating of 3-ASA in oxygen, (b) a possible degradation product 2-AP and (c) the original 3-ASA.

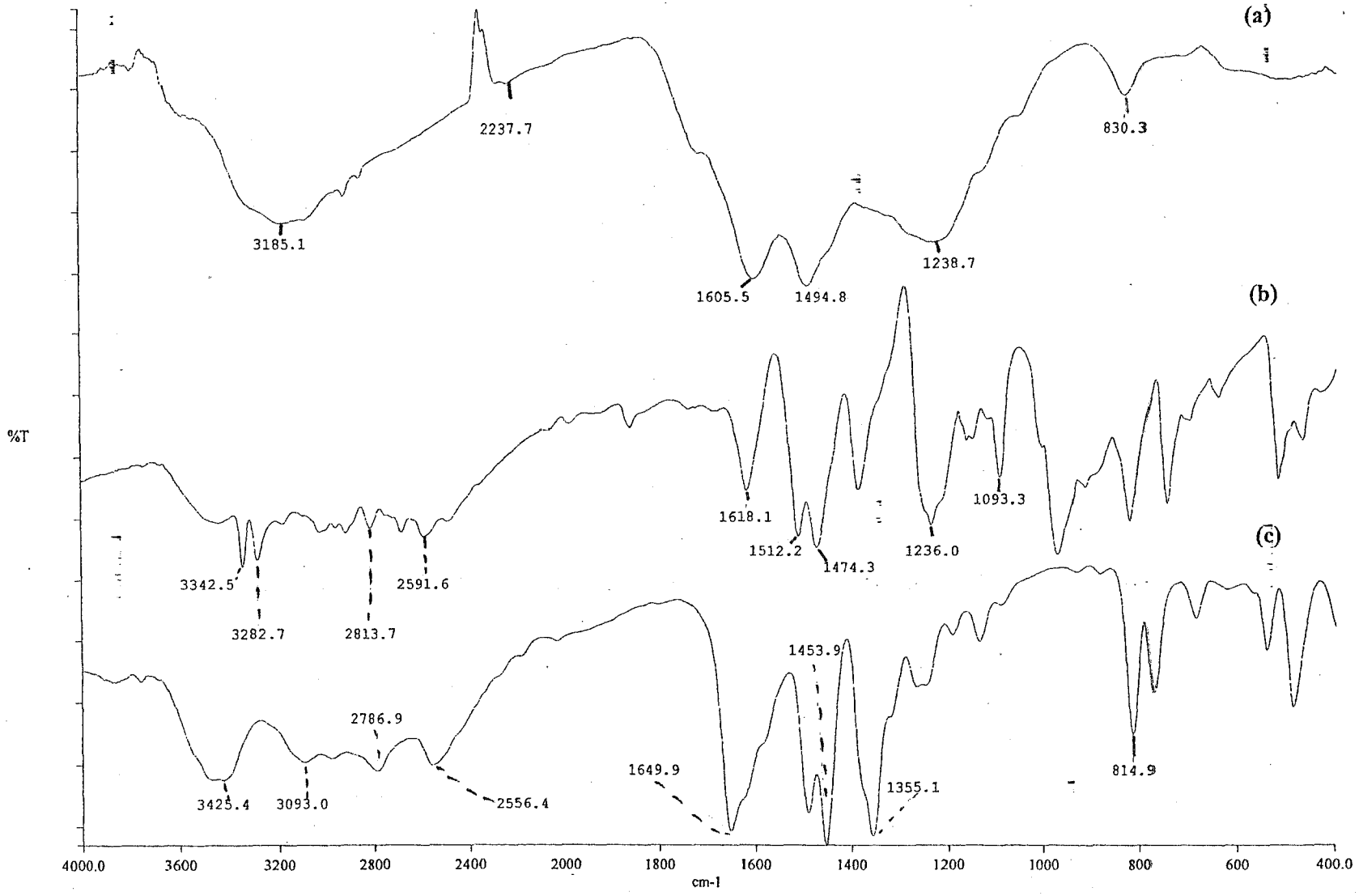

Figure 3.53: FTIR spectra of (a) the residue after heating of 5-ASA in oxygen, (b) a possible degradation product 4-AP, and (c) the original 5-ASA.

3.9.4 Discussion

An oxygen environment affected the thermal behaviour of 3-ASA and 5-ASA but not of BA, SA and 4-ASA. Once again, the thermal behaviour of 4-ASA deviated very much from that of the other isomers, 3-ASA and 5-ASA.

In nitrogen, the compounds, other than 3-ASA and 5-ASA, appear to evaporate or sublime without significant decomposition. The temperature range over which this volatilization occurs varies from compound to compound. When volatilization occurs at low temperatures, the presence of oxygen instead of nitrogen has no significant effect. For those compounds that volatilize (some with decomposition) at higher temperatures (about 200°C) some oxidation occurs, as shown by the exotherms in the DSC curves. Oxidation results in unidentified residues that were less volatile than the original samples but could not be identified from their FTIR spectra.

3.10 General Discussion

3.10.1 Trends

All of the compounds studied show complex thermal behaviour, particularly when heated in open or uncrimped sample pans. The thermal events observed in the DSC curves are nearly all endothermic and the onset temperatures of the main endotherms are usually close to the reported melting points of the compounds.

The thermal behaviour of the compounds in sealed pressure pans was compared with that in open pans. The enthalpies of sublimation and vaporisation are not readily measured from DSC curves.

TG curves for most of the compounds show onset of mass losses at temperatures

well below those for the initial endotherms in the DSC curves. This is an indication of ready sublimation under the conditions used in TG (open pan, 10 K min^{-1}, flowing nitrogen).

The rates of mass loss were used to estimate the apparent activation energies of evaporation, whether by sublimation or by vaporisation of the liquid, or both. These values were compared with the calculated values in Table 3.1.

The enthalpies measured from the DSC curves were corrected where possible for the actual sample mass obtained from the TG curve at the temperature corresponding to the onset of the thermal event [65]. This correction usually makes a great difference to the estimated values.

3.10.2 The reference acids (BA and SA)

The thermochemical results for benzoic acid (BA) and salicylic acid (SA) are summarized in Tables 3.8 and 3.9.

Table 3.8 Enthalpies of melting of benzoic acid (BA) and salicylic acid (SA)

Pan	Open		Cold-welded Al		Sealed pressure		Calc.(Table 3.1)
Acid	T_{onset} /°C	ΔH/ kJ mol^{-1}	T_{onset} /°C	ΔH/ kJ mol^{-1}	T_{onset} /°C	ΔH/ kJ mol^{-1}	ΔH/ kJ mol^{-1}
BA	159	23.1	159	24.8	160	24.4	11.3
SA	117	16.4	123	17.7	123	14.8	12.0

Table 3.9 Apparent activation energies, E_{vap}, for evaporation of benzoic acid (BA) and salicylic acid (SA)

			From Table 3.1 ΔH/kJ mol^{-1}		
Compound (m.pt)	T.range /°C	E_{vap} / kJ mol^{-1}	vap.	sublim.	decarb.
BA (120°C)	80 - 120	67 ± 3	79.6	91.6	41.8
	120 - 145	47 ± 2			
SA (158°C)	100 - 162	88 ± 1	86.3	97.5	32.0

Comparison of the behaviour of BA and SA is of interest. Introduction of the -OH group results in a decreased melting point and a decreased molar enthalpy of melting, not predicted by Table 3.1 calculations.

The values of E_{vap} lie within the range of values predicted for sublimation and vaporisation. The behaviour of BA is interesting because it shows a discontinuity in the Arrhenius-type plot at temperatures close to its melting point. TG-FTIR measurements on BA (Section 3.2.3 and Figure 3.5) did not detect any formation of carbon dioxide.

There are various ways in which one could interpret E_{vap}. In terms of classical picture of the energy barrier to be overcome in the process, the increased hydrogen bonding possible in SA would be expected to increase this barrier for evaporation in agreement with higher value for SA. A more empirical interpretation on the basis of the temperature coefficient of the later process considered could be derived from a similar molecular explanation of increased hydrogen bonding in SA.

Both BA and SA evaporate without decarboxylation, or oxidation in air or oxygen.

3.10.3 The aminobenzoic acids (ABA)

The thermochemical results for the aminobenzoic acids are summarised in Table 3.10.

Table 3.10 Enthalpies of melting of the aminobenzoic acids (ABAs)

Pan	open Al		Cold-welded Al		Sealed pressure		Calc. Table 3.1
Compound	T_{onset} /°C	ΔH/ kJ mol^{-1}	T_{onset} /°C	ΔH/ kJ mol^{-1}	T_{onset} /°C	ΔH/ kJ mol^{-1}	ΔH/ kJ mol^{-1}
3-ABA	170	-	-	-	175	-	21.7
4-ABA	188	24.8	183	24.1-34.3	189	23.7	23.7

Values for the enthalpy of melting of 3-ABA are not included, due to complexity of the endotherms in the DSC curve (Figure 3.5). For 4-ABA, agreement between the experimental and predicted enthalpies of melting is good.

Table 3.11 Apparent activation energies, E_{vap}, of the evaporation of the aminobenzoic acids (ABAs)

			(From Table 3.1) ΔH/kJ mol^{-1}		
Compound (m.pt)	T_{range} / °C	E_{vap}/ kJ mol^{-1}	Vap.	Sublim.	Decarb.
3-ABA (171-174°C)	120 - 170	102 ± 2	99	121	49
4-ABA (183-189°C)	160 - 210	110 ± 4	101	125	53

The values of $E_{vap,}$ estimated from the TG curves, are closest to the predicted values of the enthalpies of vaporisation which are not very different for the two isomers.

Although the melting points and the values of E_{vap} for the two isomers are similar, the marked differences (seen in the DSC curves) in the melting behaviour of 3-ABA results in difference in susceptibility to decarboxylation (found only for 4-ABA).

3.10.4 The aminosalicylic acids (ASAs)

The thermochemical results for the aminosalicylic acids (ASAs) are summarised in Tables 3.12 and 3.13.

Table 3.12 Enthalpies of melting of the aminosalicylic acids (ASAs)

Pan	Open Al		Cold-welded Al		Sealed pressure		Calc. Table 3.1
Acid	T_{onset} /°C	ΔH/ kJ mol^{-1}	T_{onset} /°C	ΔH/ kJ mol^{-1}	T_{onset} /°C	ΔH/ kJ mol^{-1}	ΔH/ kJ mol^{-1}
3-ASA	244	92.8	239	64.7	239	61.2	21.0
4-ASA	133	25.6	131	40.4	136	46.1	21.0
5-ASA	258	88.6	270	67.2	282	67.0	23.0

Agreement between measured and predicted values of the enthalpies of melting is poor. The variation between isomers is also much greater than in the predicted values and this could indicate inadequate allowance for isomeric effects in the predictions. This is supported by the large difference in the melting temperature of 4-ASA compared to the other isomers.

Table 3.13 Apparent activation energies, E_{vap}, for the evaporation of the aminosalicylic acids (ASAs)

			(From Table 3.1) ΔH/kJ mol^{-1}		
Acid (m.pt)	T_{range} / °C	E_{vap}/ kJ mol^{-1}	Vap.	Sublim.	Decarb.
3-ASA (243°C)	175-240	116 ± 3	96	117	29
4-ASA (131 -136°C)	130-150 150-180	174 ± 7 59 ± 1	106	127	39
5-ASA (270°C)	210-270	135 ± 2	108	131	43

The agreement between the values of E_{vap} estimated from the TG curves for 3-ASA and 5-ASA and the values predicted for the enthalpies of sublimation (Table 3.1) is good. The TG curve for 4-ASA is very different to those for the other isomers, indicating that more complex processes are involved.

There is evidence from TG-FTIR that carbon dioxide is evolved by 3-ASA between 225°C and 300°C (Figure 3.11) and for 4-ASA between 130°C and 170°C (Figure 3.12). No carbon dioxide evolution was observed for 5-ASA.

The behaviour of three isomers in oxygen (see Section 3.9.3) was very different, although they all appeared to undergo some oxidation. For all the compounds studied, significant reaction with oxygen required that complete volatilisation should not have occurred below about 200°C.

3.10.5 The aminophenols (AP)

The thermochemical results for the aminophenols (AP) are summarised in Tables 3.14 and 3.15.

Table 3.14 Enthalpies of melting of the aminophenols (AP)

Pan→	Open Al		Cold-welded Al		Sealed pressure		Calc.Table 3.1
Phenol	T_{onset} /°C	ΔH/ kJ mol^{-1}	T_{onset} /°C	ΔH/ kJ mol^{-1}	T_{onset} /°C	ΔH/ kJ mol^{-1}	ΔH/ kJ mol^{-1}
2-AP	176	23.4	172	33.0-34.9	175	29.0	9.8
3-AP	121	25.2	116	24.4	123	24.0	9.8
4-AP	190	29.5	183	29.2-31.5	190	22.7	9.8

The melting point of 3-AP is very much lower than those of other isomers. The experimental values of the enthalpies of the melting of the aminophenols are much higher than the predicted values in Table 3.1. The variation from one isomer to the other, is not as dramatic as the variation of the melting points. No provision for the differences between isomers is available in the predictions.

Table 3.15 Apparent activation energies, E_{vap}, for the evaporation of the aminophenols (AP)

			From Table 3.1/ ΔH/kJ mol^{-1}	
Phenol (m.pt)	T range / °C	E_{vap}/ kJ mol^{-1}	Vap.	Sublim.
2-AP (170°C)	100-170	81± 2	82.4	92.1
3-AP (115-120°C)	100-190	71 ± 6	82.4	92.1
4-AP (182°C)	122-172	92 ± 1	82.4	92.1

Because of the small, and constant predicted enthalpy of melting, the predicted enthalpies of vaporisation and sublimation are very different. The experimental values of $E_{vap.}$ are closest to $\Delta H_{vap.}$ for 2-AP and 3-AP, but closest to $\Delta H_{sublim.}$ as might be expected, for the isomer with the highest melting point, namely 4-AP.

3.11 The relationship between crystal structure and thermochemical properties

Any relationship of this sort will, undoubtedly, be very complex, but it is worth trying to find some qualitative trends.

Molecules are held together in a crystal structure by hydrogen bonding and other forces such as van der Waals interactions (see Section 1.5). Hydrogen bonding can be intra-molecular and/or inter-molecular. The strength of inter-molecular hydrogen bonds will have a large influence on the crystal structure of the compound. The positions of the substituent groups in aromatic compounds and the possible resonance structures [58] which are a measure of the delocalization of electrons, will also affect the crystal packing of the compound. The variety of contributing resonance structures has been used as an explanation for the greater tendency for decarboxylation in 4-ASA [25]. The study showed marked differences in the nature of the molecular species of the ASAs in the solid state [27]. The presence of zwitterionic molecules in both 3-ASA and 5-ASA could be the major cause of strong bonds between their molecules resulting in relatively high melting points.

Physical incorporation of 3-AP in 4-ASA [54] catalysed the decarboxylation process. These observations were confirmed in the experiments done in Section 3.8.2, where the temperature of decarboxylation of 4-ASA was lowered from 150°C to 90°C on incorporating 3-AP.

4. THE THERMAL BEHAVIOUR OF SOME CYCLODEXTRINS

4.1 Introduction

The three cyclodextrins chosen for this study (see Section 2.1) were beta-cyclodextrin (BCD), hydroxypropyl-beta-cyclodextrin (HPBCD) and gamma-cyclodextrin (GCD). Their general properties are given in Table 1.1 in Section 1.6.2. The main features of interest are repeated in Table 4.1.

4.2 DSC and TG studies

The DSC, TG and DTG curves (heating rate 10 K min^{-1} from 50°C to 250°C in flowing nitrogen) for BCD, HPBCD and GCD are shown in Figures 4.1, 4.2 and 4.3, respectively.

The DSC curve (Figure 4.1) for BCD showed an endotherm between 50°C and 120°C, with an onset temperature at 76°C and $\Delta H = 266$ kJ mol^{-1}. The TG and DTG curves show a single mass-loss. The mass-loss between 50°C and 90°C was 11.4 %. On the assumption that this is the removal of water, the mass-loss corresponds to 8.0 moles of water per mole of BCD ($BCD.8H_2O$). A small reversible transition exotherm, not accompanied by a mass-loss (as shown by the TG curve), was observed around 220°C in the DSC curve.

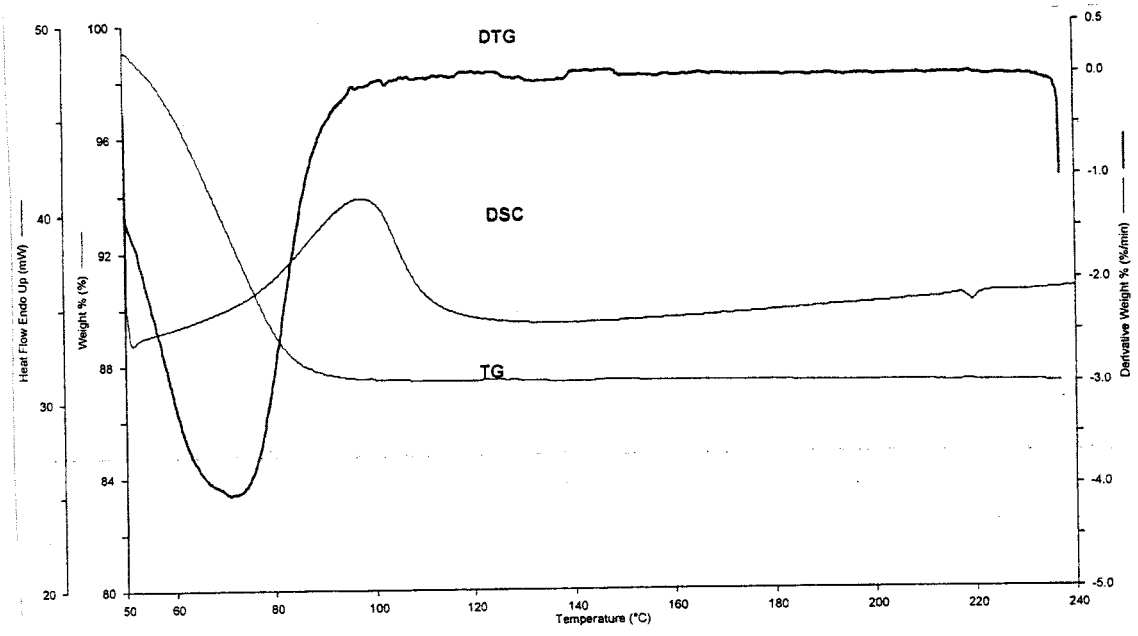

Figure 4.1: DSC, TG and DTG curves for BCD (heated in flowing nitrogen at 10 K min^{-1}: uncrimped aluminium pan for DSC and open platinum pan for TG).

Bilal *et al.* [110] studied the thermal decomposition of the BCD-water complex. Their sample of BCD contained 14 % H_2O by mass.

They determined (using solution calorimetry) that to remove one mole of water from one mole of BCD required $\Delta H = 10.50$ kJ per mole of anhydrous BCD.

$$BCD.nH_2O(s) \rightarrow BCD.(n\text{-}1)H_2O(s) + H_2O(l).$$

The ΔH value obtained from the DSC curve was 385 J (g BCD)$^{-1}$ or 50.2 kJ (mol H_2O)$^{-1}$.

$$BCD.nH_2O(s) \rightarrow BCD.(n-1)H_2O(s) + H_2O(g).$$

The difference: 50.2 - 10.5 kJ = 39.7 kJ is close to the enthalpy of vaporisation of water at 100 °C which is 40.6 kJ mol^{-1}.

No definite hydrate of BCD exists and the maximum water content depends upon the temperature and the water-vapour pressure. The number of water molecules per BCD at 29 ± 1 °C is reported to be 10 to 12 [37, 78]. The sample of BCD used in this study thus contains slightly less water (8 water molecules per BCD unit). The enthalpy of dehydration (266 kJ (mol BCD)$^{-1}$) corresponds then to 33.3 kJ (mol H_2O)$^{-1}$.

The DSC curve (Figure 4.2) for HPBCD showed an endotherm (assumed to be dehydration) between 60 °C and 110 °C, ΔH = 64 kJ mol^{-1}. The TG and DTG curves showed a single-stage mass-loss of 6.0 % between 45 °C and 90 °C. This value corresponds to 5.0 of water moles per mole of HPBCD (HPBCD.$5H_2O$). There was a very small double reversible transition exotherm at about 170 °C, which was not accompanied by a mass-loss, as shown by the TG curve. The measured enthalpy of dehydration of 64 kJ (mol HPBCD)$^{-1}$ thus corresponds to 12.8 kJ (mol H_2O)$^{-1}$.

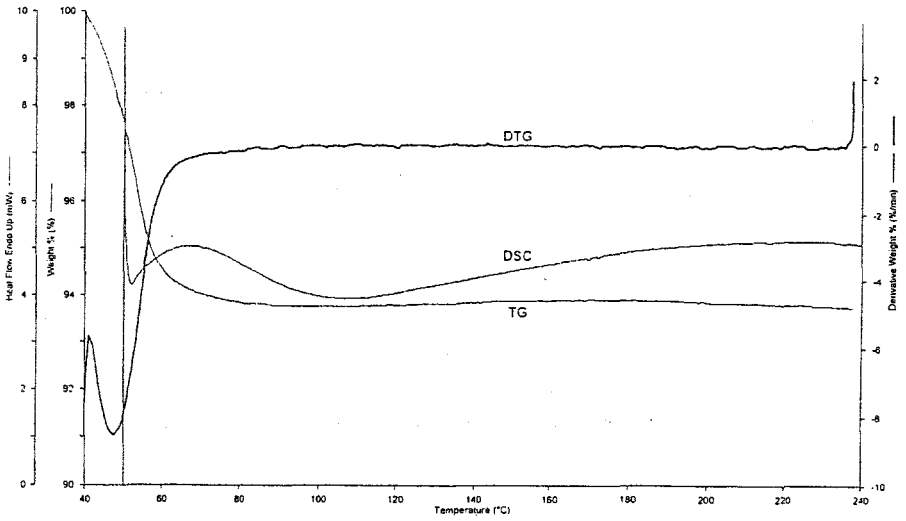

Figure 4.2: DSC, TG and DTG curves for HPBCD (heated in flowing nitrogen at 10 K min^{-1}: uncrimped aluminium pan for DSC and open platinum pan for TG).

The DSC curve for GCD (Figure 4.3) showed a broad endotherm between 60 °C and 110 °C, ΔH = 73 kJ mol^{-1}. The TG curve showed a single-stage mass-loss of 9.0 % and the number of moles of water is then 7.0 per mole of GCD ($GCD.7H_2O$). There was a very small reversible transition endotherm in the DSC curve at around 230 °C, which is not accompanied by a mass-loss. The enthalpy of dehydration of GCD is thus 10.4 kJ $(mol\ H_2O)^{-1}$.

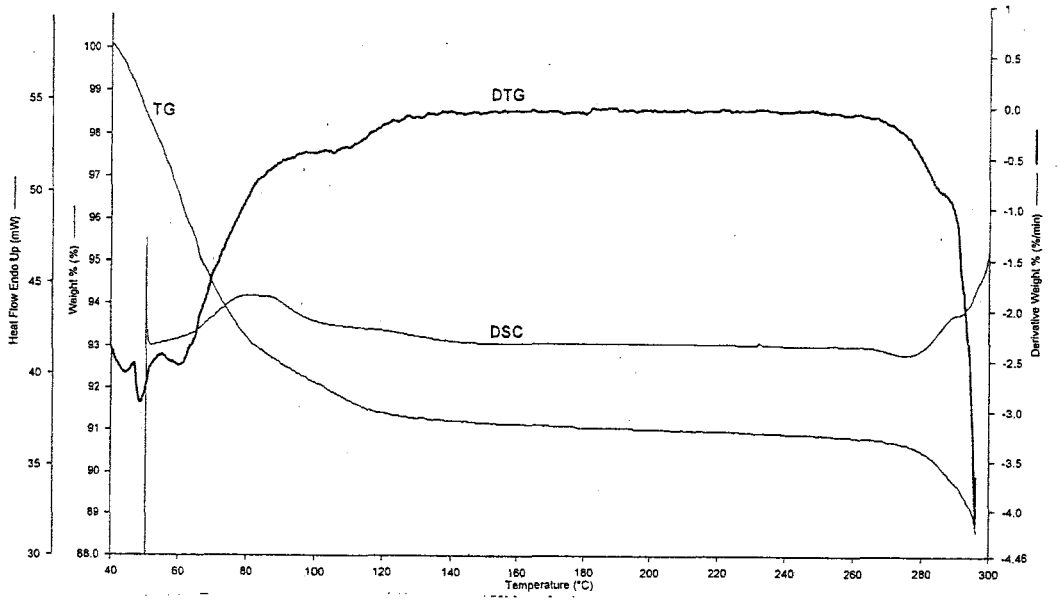

Figure 4.3: DSC, TG and DTG curves for GCD (heated in flowing nitrogen at 10 K min^{-1}: uncrimped aluminium pan for DSC and open platinum pan for TG).

The results for the thermal behaviour of the CDs are summarised in Table 4.1. The table also gives the values of the total water content of the CDs determined by the Karl Fischer method. The values determined by this method are higher than those determined by the TG method, which suggests that not all of the water may be removed during the thermal treatment described. Giordano *et al.* [37] reported that strongly bonded water is released at higher temperatures (°C).

In very qualitative terms, the enthalpy of dehydration of the CDs, calculated per mole of H_2O, decreases as the size of the molecular cavity of the CD increases, or as BCD is modified by substitution.

Table 4.1: The thermal behaviour of the cyclodextrins used in this study.

			DSC		TG				Karl Fischer
CDs	cavity diameter/ nm	molar mass / g mol^{-1}	T_{onset} /°C	ΔH /kJ $(mol\ CD)^{-1}$	T_{range} /°C	Mass loss /%	ΔH / kJ$(mol\ H_2O)^{-1}$	ΔH /J $(g\ CD)^{-1}$	H_2O content /%
BCD	0.8	1135	76	266	40-125	11.4	33.3	234	14.9
HPBCD	-	1414	53	64	40-120	6.0	12.8	45	9.0
GCD	1.0	1297	65	73	40-120	9.0	10.4	56	11.2

Enthalpy of vaporisation of water at 100 °C is 40.6 kJ mol^{-1}.

5. THE THERMAL BEHAVIOUR OF MIXTURES OF THE REFERENCE ACIDS (BA AND SA) WITH THE CYCLODEXTRINS

5.1 Introduction

The thermal behaviour of benzoic acid and of salicylic acid has been described in Section 3.2.1. The thermal behaviour of the three cyclodextrins used in this study is described in Section 4.2.

DSC and TG runs were done on 1:1 molar ratio physical and kneaded mixtures (prepared as described in Chapter 2) of the reference acids: benzoic acid (BA) and salicylic acid (SA) with beta-cyclodextrin (BCD), hydroxypropyl-beta-cyclodextrin (HPBCD) and gamma-cyclodextrin (GCD). The DSC and TG curves for the mixtures were compared with those for the pure acids and the pure CDs. The thermal behaviour of the mixtures can provide an indication of inclusion of guest molecules into the cavity of cyclodextrin, although other types of interaction cannot be ruled out. Generally, the kneaded mixtures would be expected to show greater changes in thermal behaviour. The main, but not entirely conclusive, indication of interaction, is the disappearance of the melting endotherm of the guest in the DSC curves of the mixture. In ideal situations one could determine the amount of interaction by varying the proportions of guest to host and using any measured enthalpy of melting as an indication of the amount of guest that has not interacted. Inclusion of a guest in a CD cavity will generally displace all or some of the water originally in the cavity, so changes in the expected dehydration endotherms of the CDs in the DSC curves of the mixtures may be an additional indication of inclusion.

Care has to be taken to explore the possible influences of the kneading process, which can also alter the water content of the CDs.

Confirmation of indications of interactions such as inclusion requires use of additional techniques such as IR and XRPD. The most conclusive evidence comes from single-crystal X-ray structure determinations. Indications of the formation of a non-crystalline powder from XRPD measurements, are also not conclusive evidence of inclusion, because of grinding and/or kneading can affect crystallinity.

5.2 Mixtures of benzoic acid (BA) with the cyclodextrins

Figure 5.1 shows the DSC curves for the physical and kneaded mixtures of BA with BCD. The DSC curve for BCD shows the dehydration endotherm from 50 °C to 120 °C, with ΔH = 266 kJ mol^{-1} and a reversible transition exotherm around 220 °C (see Figure 4.1 and Table 4.1). The DSC curve for BA shows a sharp melting endotherm (ΔH = 16 kJ mol^{-1}, onset 117 °C). The DSC curve for the physical mixture shows a dehydration endotherm from 64 °C to 104 °C, with ΔH = 238 kJ $(mol\ BCD)^{-1}$ and a much decreased endotherm at onset 122 °C (m. pt of BA) with ΔH = 14 kJ $(mol\ BA)^{-1}$. The kneaded mixture showed a dehydration endotherm at about 60 °C to 111 °C with ΔH = 243 kJ $(mol\ BCD)^{-1}$ and very small endotherm onset 122 °C with ΔH about 1 kJ $(mol\ BA)^{-1}$. The decrease in the endotherm associated with the melting of BA is an indication of an interaction between BA and BCD.

The TG and DTG curves (Figure 5.2 and 5.3) show an initial mass-loss for the physical mixture from 48 °C to 80 °C of 12 %. The total mass-loss at 125 °C is about 20 %, i.e. a further 8 %. This further loss is less than the expected value for

almost complete evaporation/decomposition of 10 % by mass of BA in the mixture, but the total of 20% is very close to that expected from the behaviour of the individual constituents. The TG curve for the kneaded mixture shows an initial mass-loss of 8.5 % from 50°C to 80°C. This value is slightly less than the expected value of 10 % (given above). The total mass-loss is 13.5 % (i.e. a further loss of 5 %), which is less than the expected value of 20%. The measured values are compared with the expected values, calculated from the proportions of the constituents of the mixtures in Table 5.1.

Interaction between BA and BCD is indicated in both the physical and the kneaded mixtures as shown by both the DSC and TG results. At the very least, this interaction causes a decrease in the extent and rate of evaporation of BA.

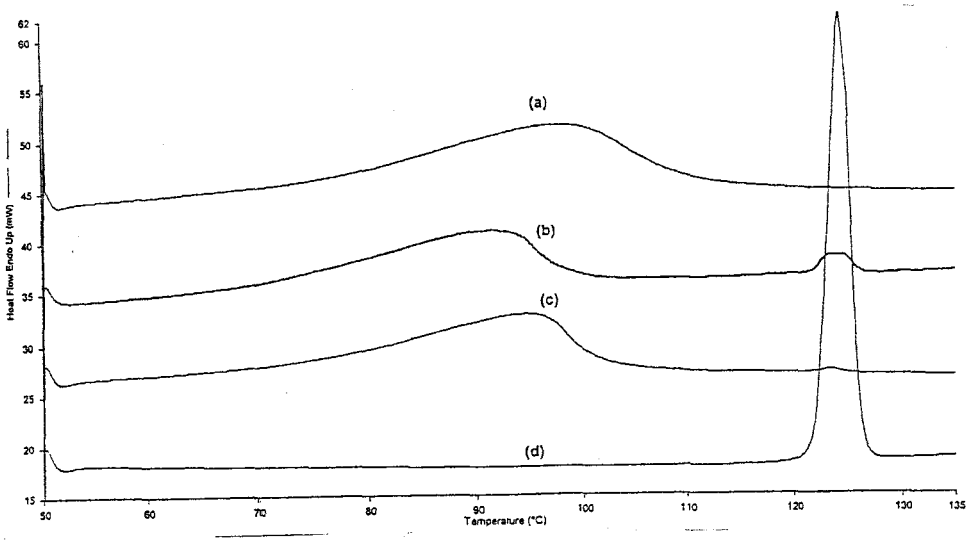

Figure 5.1: DSC curves for the pure components and for mixtures of BA with BCD: (a) pure BCD, (b) physical mixture, (c) kneaded mixture and (d) pure BA (heated in flowing nitrogen at 10 K min^{-1} in uncrimped aluminium pans).

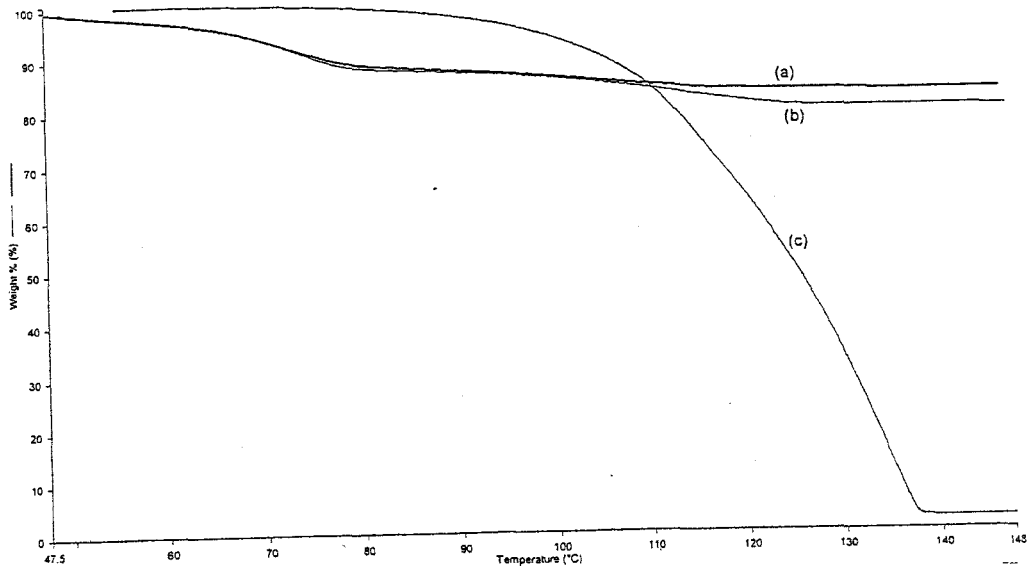

Figure 5.2: TG curves for BA and for mixtures of BA with BCD: (a) kneaded mixture, (b) physical mixture and (c) pure BA (heated in flowing nitrogen at 10 K min^{-1} in open platinum pans).

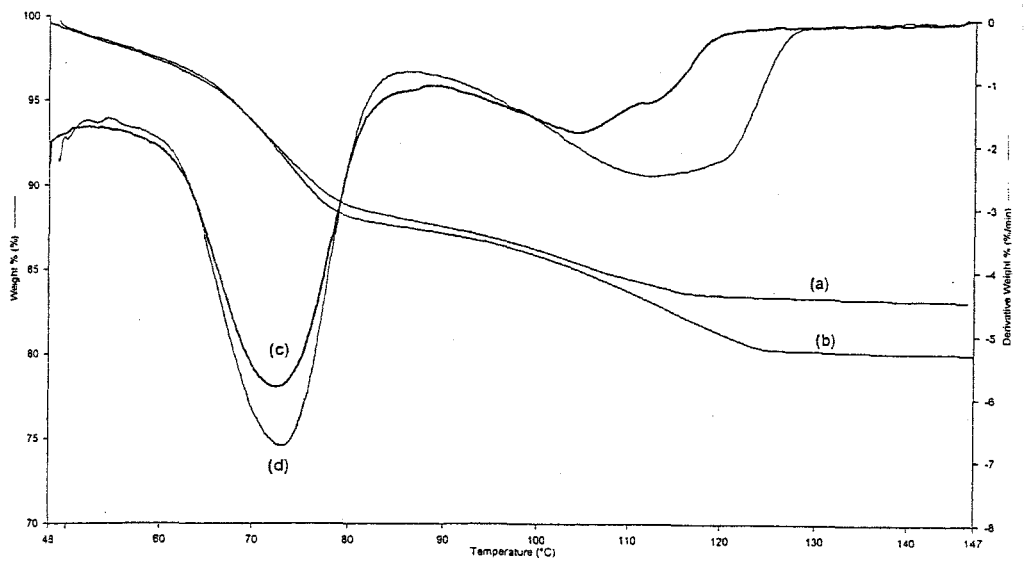

Figure 5.3: TG and DTG curves for the mixtures of BA with BCD: TG curves (a) kneaded mixture and (b) physical mixture and DTG curves: (c) kneaded mixture and (d) physical mixture (heated in flowing nitrogen at 10 K min^{-1} in open platinum pans).

Figure 5.4 shows the DSC curves for the physical and the kneaded mixtures of BA with HPBCD. The DSC curve for HPBCD shows an endotherm from 55°C to 100°C with $\Delta H = 64$ kJ mol^{-1} (see Figure 4.2 and Table 4.1). It also shows a very small double reversible transition exotherm around 170°C, not accompanied by a mass-loss, as shown by the TG curve. The DSC curve for the physical mixture shows a broad dehydration endotherm from 53°C to 111°C, with $\Delta H = 158$ kJ $(mol\ HPBCD)^{-1}$ and no endotherm associated with the melting of BA. The absence of the endotherm associated with the melting of BA is an indication of interaction between BA and HPBCD. Similar results for the kneaded mixture show the absence of the endotherm associated with the melting of BA, but there is a broad dehydration endotherm from 53°C to 102°C, with $\Delta H = 63$ kJ $(mol\ HPBCD)^{-1}$.

The TG and DTG curves (Figure 5.5 and 5.6) show that the mass-losses are greatly decreased in both, the physical and the kneaded mixtures. For the physical mixture, the mass-loss from 48°C to 95°C of about 6 % is close to the expected value of 5.5 % for the loss of water from the mixture containing 92.1 % by mass of HPBCD. The total mass-loss of 7 % at 140°C (i.e a further loss of 1%), is significantly less than the expected value for almost complete evaporation /decomposition of 8 % by mass of BA in the mixture. For the kneaded mixture, the initial mass-loss is about 5 % from 50°C to 110°C. This value is similar to that of the physical mixture. The total mass-loss of about 6 % (i.e loss of a further 1 %) is less than the expected value for 8 % mass-loss of BA from the mixture. The conclusion reached from both DSC and TG curves is that there is significant interaction between BA and HPBCD. These results are summarised in Table 5.1.

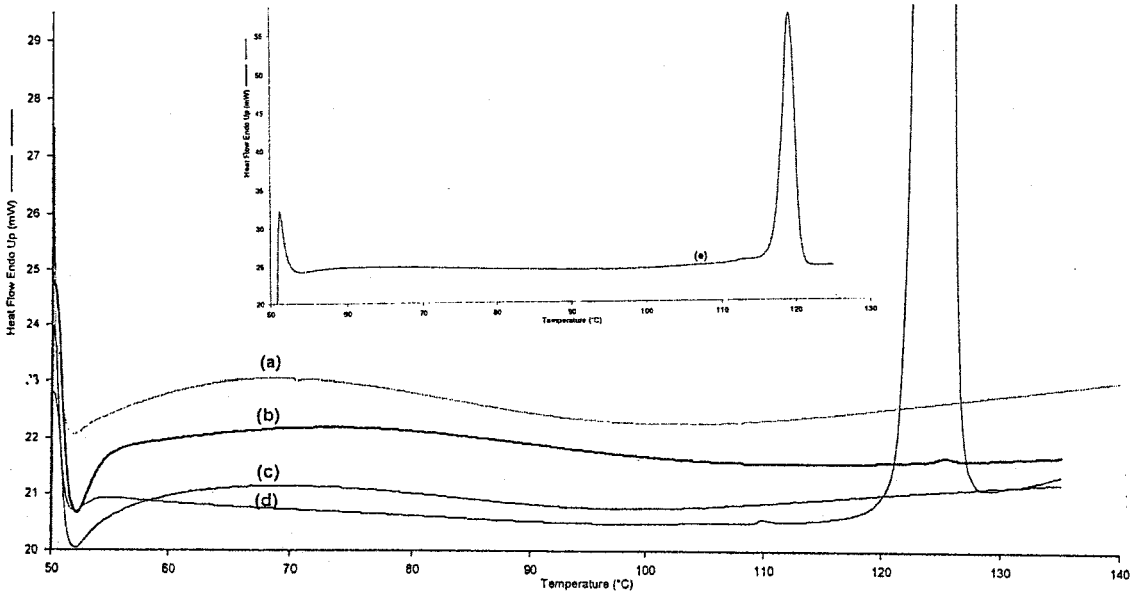

Figure 5.4: DSC curves for the pure components and for mixtures of BA with HPBCD: (a) pure HPBCD, (b) physical mixture, (c) kneaded mixture and (d) pure BA (e) enlarged y-axis scale for curve (d) (heated in flowing nitrogen at 10 $Kmin^{-1}$ in uncrimped aluminium pans).

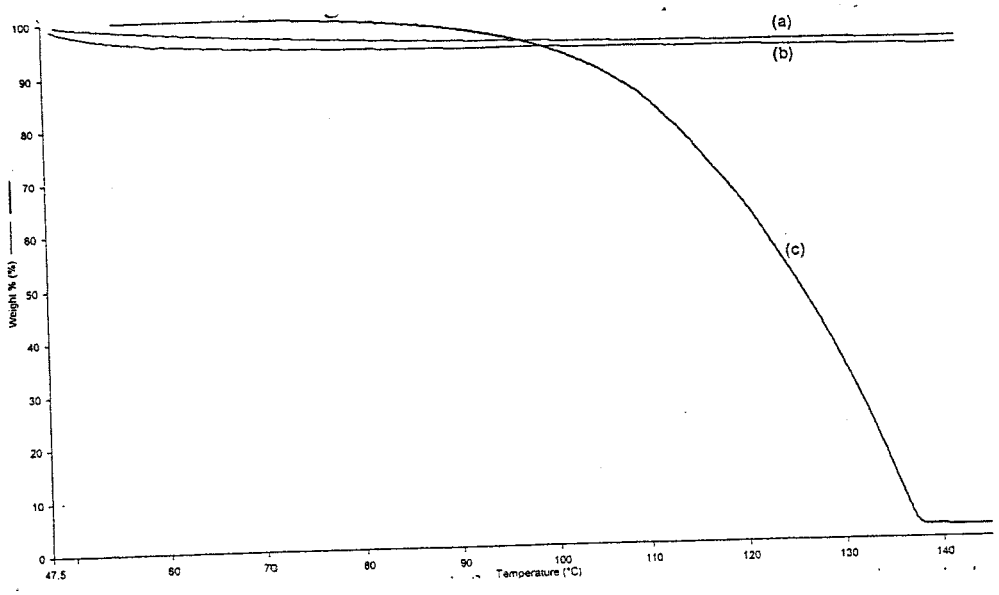

Figure 5.5: TG curves for BA and for mixtures with HPBCD: (a) kneaded mixture (b) physical mixture and (c) pure BA (heated in flowing nitrogen at 10 K min^{-1} in open platinum pans).

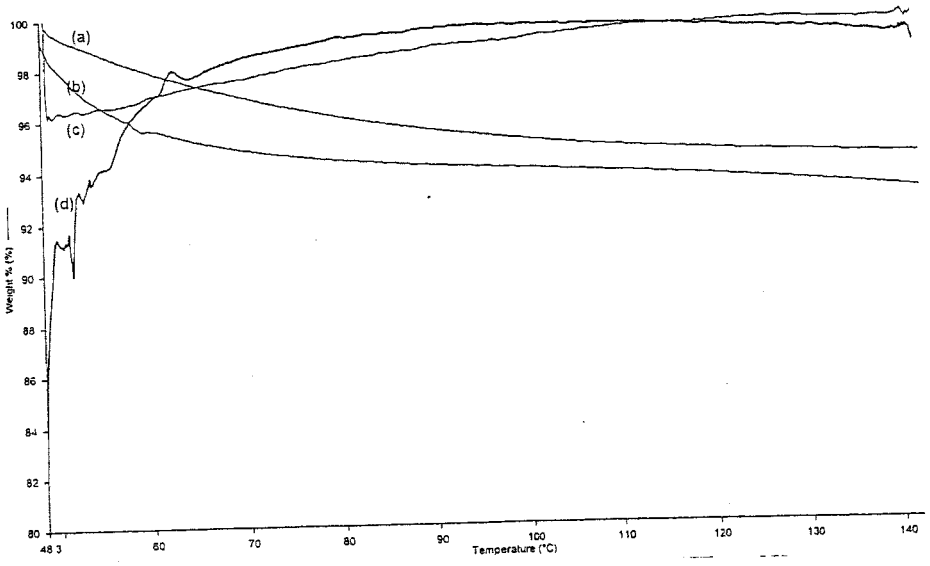

Figure 5.6: TG and DTG curves for mixtures of BA with HPBCD: TG curves: (a) kneaded mixture and (b) physical mixture and DTG curves: (c) kneaded mixture and (d) physical mixture (heated in flowing nitrogen at 10 K min^{-1} in open platinum pans).

Figure 5.7 shows the DSC curves for the physical and the kneaded mixtures of BA with GCD. The DSC curve for pure GCD shows a broad dehydration endotherm from 60 °C to 110 °C, with $\Delta H = 73$ kJ mol^{-1}. There is also a very small reversible transition endotherm around 230 °C (Figure 4.3). The DSC curve for the physical mixture shows two endotherms: a dehydration endotherm from 62 °C to 97 °C, with ΔH about 74 kJ (mol GCD)$^{-1}$ and an endotherm with onset at 62 °C, with ΔH about 20 kJ (mol BA)$^{-1}$. The DSC curve for the kneaded mixture shows no dehydration endotherm as well as no endotherm associated with the melting of BA. Results for the kneaded mixture show that there is greater interaction between BA and GCD than in the physical mixture.

The TG and DTG curves for the physical and kneaded mixtures are shown in Figure 5.8 and 5.9. The initial mass-loss for the physical mixture is 10 % from 55 °C to 110 °C. This is close to the value of 8.2 % expected for the loss of water from GCD in the mixture containing 91.4 % by mass of GCD. There is no additional mass-loss at about 140 °C, hence no mass-loss related to evaporation of BA. For the kneaded mixture, the initial mass-loss of 4 % from 42 °C to 70 °C is less than the expected 8.2 % (see above). The total mass-loss at 140 °C is about 5 % (i.e. a further loss of 1 %). Evaporation of all the BA would lead to a mass-loss of 8.6 %. There is thus an extensive interaction between BA and GCD in the kneaded mixtures as shown by both the DSC and TG results, which are summarised in Table 5.1.

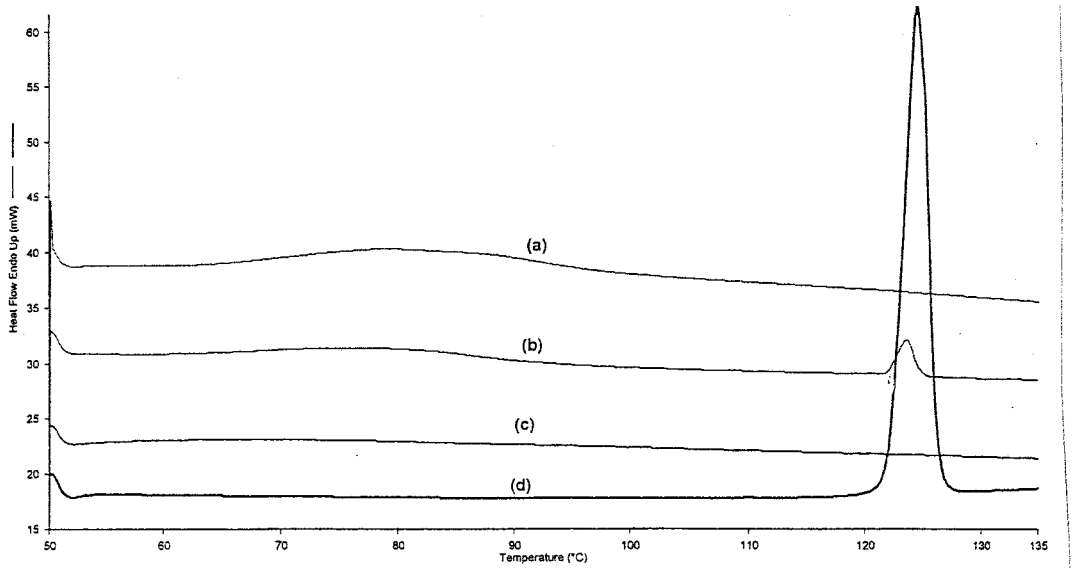

Figure 5.7: DSC curves for the pure components and for mixtures of BA with GCD: (a) pure GCD, (b) physical mixture, (c) kneaded mixture and (d) pure BA (heated in flowing nitrogen at 10 K min^{-1} in uncrimped aluminium pans).

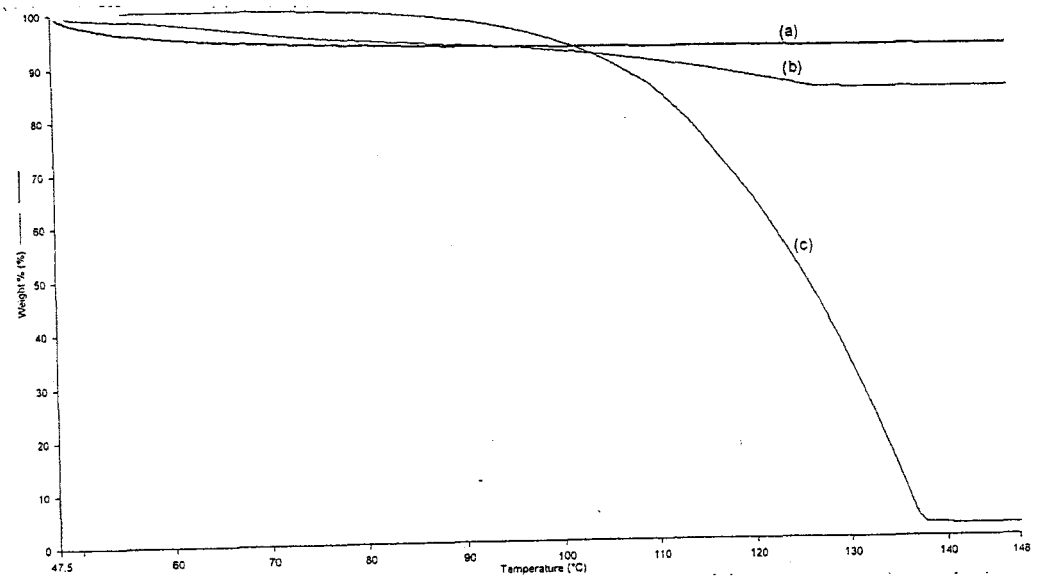

Figure 5.8: TG curves for pure BA and for mixtures with GCD: (a) kneaded mixture, (b) physical mixture and (c) pure BA (heated in flowing nitrogen at 10 K min^{-1} in open platinum pans).

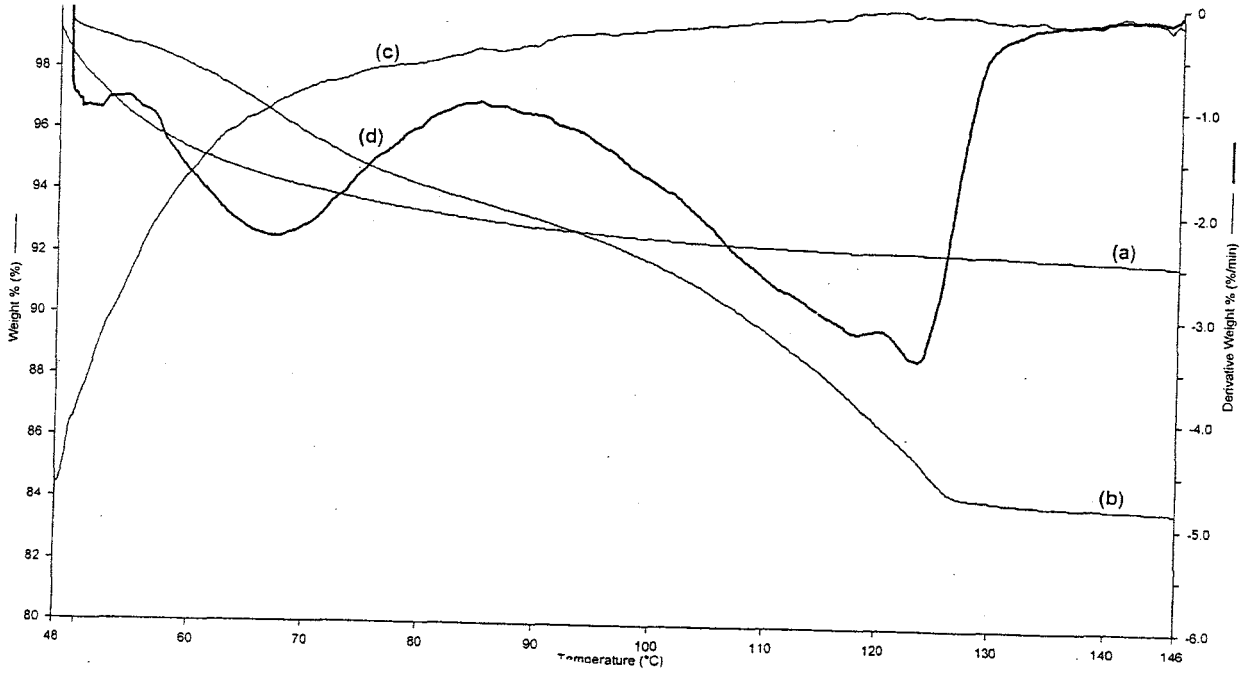

Figure 5.9: TG and DTG curves for mixtures of BA with GCD: TG curves: (a) kneaded mixture and (b) physical mixture and DTG curves: (c) kneaded mixture and (d) physical mixture (heated in flowing nitrogen at 10 K min^{-1} in open platinum pans).

5.3 Mixtures of salicylic acid (SA) with the cyclodextrins

Figure 5.10 shows the DSC curves for the physical and the kneaded mixtures of SA with BCD. The DSC curve for pure BCD has been described in Section 4.1 and for pure SA in Section 3.2. The DSC curve for the physical mixture shows two endotherms: a dehydration endotherm from 61 °C to 114 °C, with $\Delta H = 281$ kJ (mol BCD)$^{-1}$ and an endotherm with onset at 144 °C, with $\Delta H = 9$ kJ (mol SA)$^{-1}$. The reversible transition endotherm at 220 °C is also present. The DSC curve for the kneaded mixture shows a broad double (overlapped) dehydration endotherm from 63 °C to 118 °C, with $\Delta H = 74$ kJ (mol BCD)$^{-1}$. This double endotherm is similar to the DTG curve (Figure 5.8). There is no endotherm related to the melting of SA, but the reversible transition endotherm is observed around 220 °C. The absence of the endotherm associated with the melting of SA is an indication of an interaction between SA and BCD.

The TG and DTG curves for the physical and kneaded mixtures of SA with BCD are shown in Figures 5.11 and 5.12. The TG curve for the physical mixture shows a mass-loss of 12% between 46 °C and 80 °C. The DTG curve shows a two-stage mass-loss, the first between 46 °C and 60 °C (4%) and the second between 60 °C and 80 °C (8%). The overall mass-loss from 60 °C to 80 °C is close to the expected value of 10% for the loss of water from the BCD in the mixture containing 89.2% BCD. The total mass-loss at 140 °C is about 22% (i.e. a further loss of 10%). This is close to the expected value for almost complete evaporation/decomposition of 11% SA by mass in the mixture. The TG curve for the kneaded mixture shows mass-losses to occur in three stages from 47 °C to 130 °C (confirmed by the DTG curve). The mass-loss from 47 °C to 50 °C is about 1%, the mass-loss from 50 °C to 80 °C is about 3% and the last mass loss is about 7% from 80 °C to 130 °C.

Mass was lost slowly after this temperature (130°C) and by 220°C, a total of 16% (i.e. a further loss of 3%) had been lost. This is less than the 11% which would have accompanied the complete evaporation/decomposition of SA. The changes in thermal behaviour of the individual components in the mixture indicate interaction between the two compounds. These results are summarised in Table 5.1.

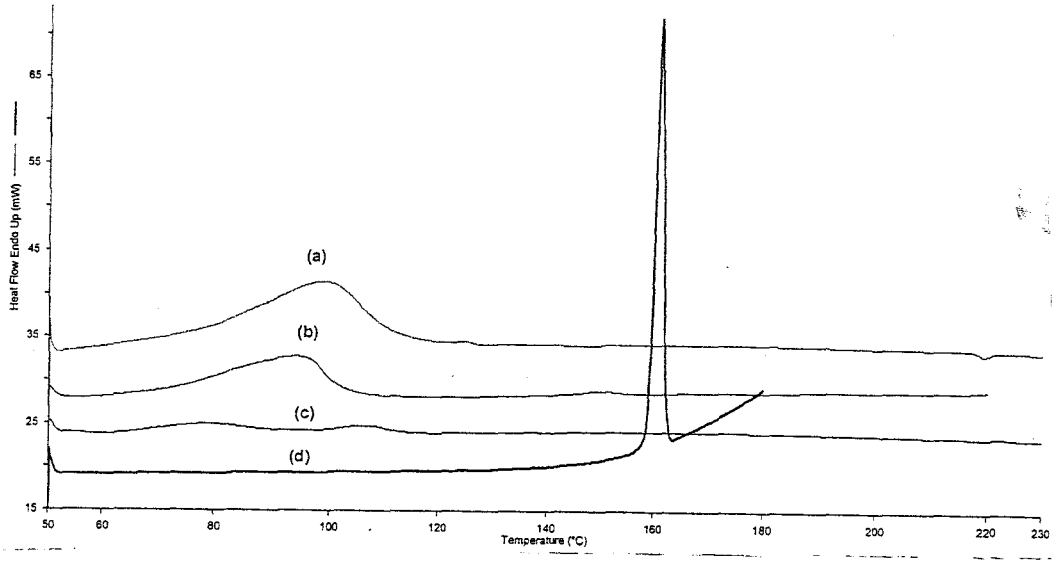

Figure 5.10: DSC curves for the pure components and for mixtures of SA with BCD: (a) pure BCD, (b) physical mixture, (c) kneaded mixture and (d) pure SA (heated in flowing nitrogen at 10 K min^{-1} in uncrimped aluminium pans).

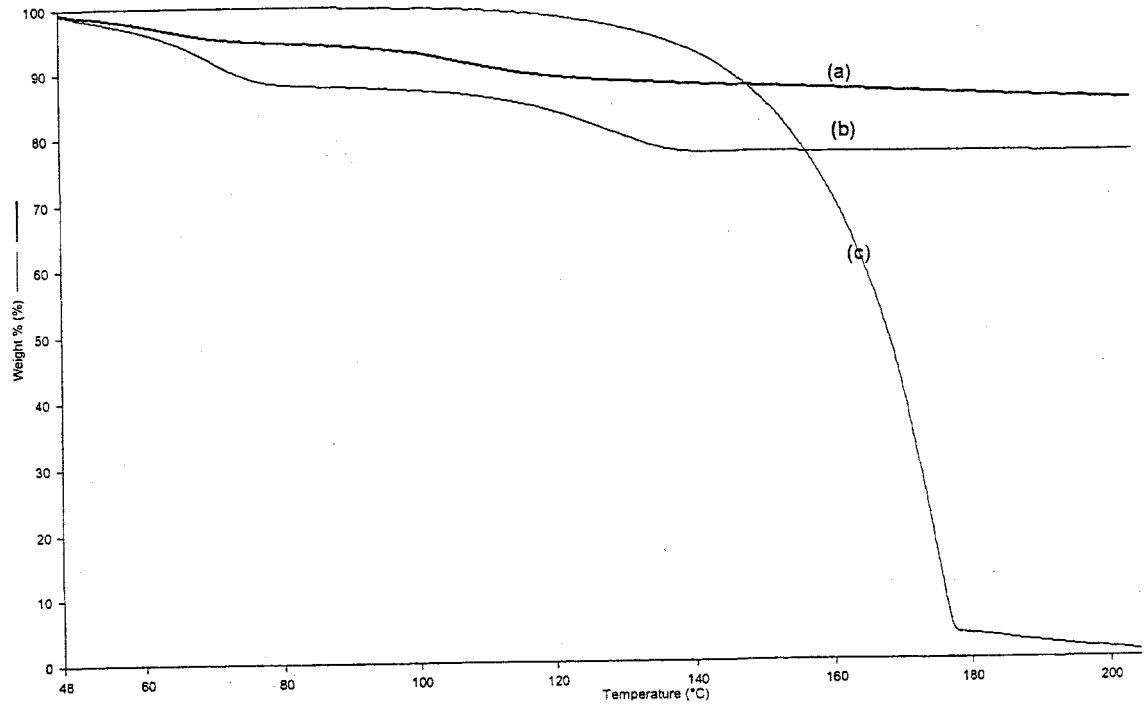

Figure 5.11: TG curves for SA and for mixtures with BCD: (a) kneaded mixture, (b) physical mixture and (c) pure SA (heated in flowing nitrogen at 10 K min^{-1} in open platinum pans).

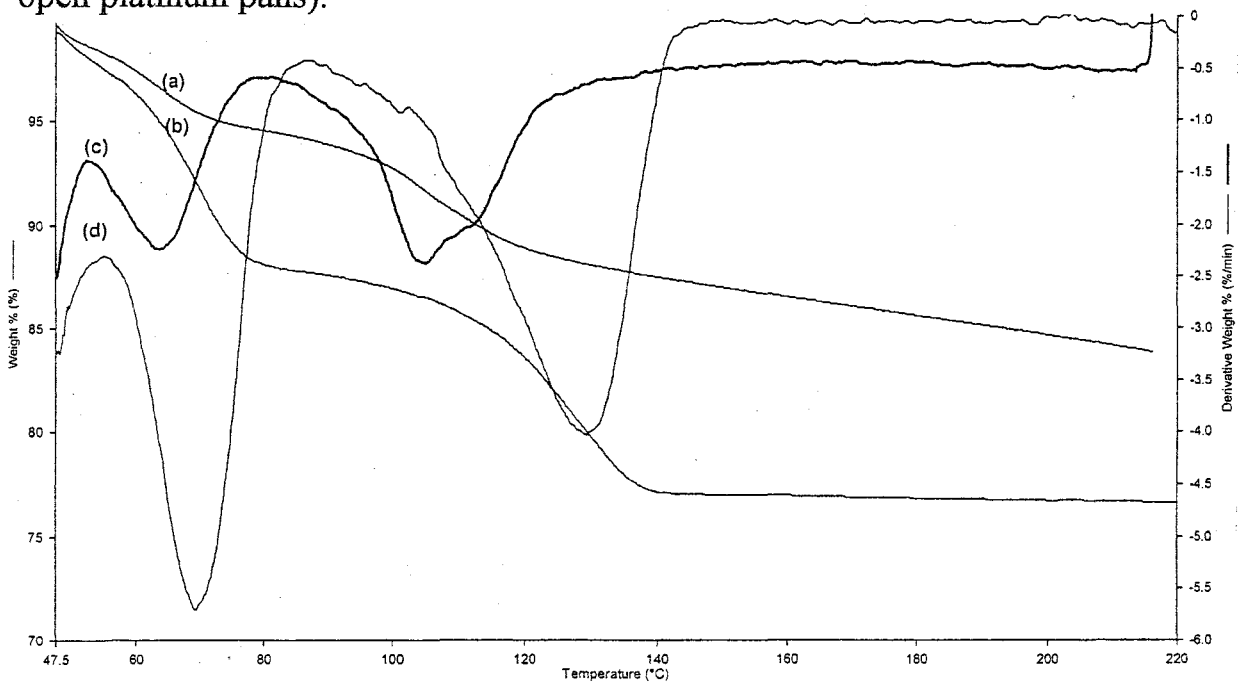

Figure 5.12: TG and DTG curves for mixtures of SA with BCD: TG curves: (a) kneaded mixture and (b) physical mixture, and DTG curves: (c) kneaded mixture and (d) physical mixture (heated in flowing nitrogen at 10 K min^{-1} in open platinum pans).

Figure 5.13 shows the DSC curves for the physical and the kneaded mixtures of SA with HPBCD. The DSC curve for pure HPBCD has been described in Section 4.1. The DSC curve for the physical mixture shows a dehydration endotherm from 53°C to 80°C, with ΔH = 19 kJ (mol HPBCD)$^{-1}$ and no other endotherm was observed. The DSC curve for the kneaded mixture did not show any endotherm associated either with dehydration of the HPBCD or the melting of SA.

TG and DTG curves for the physical and kneaded mixture are shown Figure 5.14 and 5.15. The physical mixture undergoes a mass-loss from 45°C to 70°C of about 5 % and another mass-loss from 70°C to 120°C of 7 %. This total mass-loss of 12 % is much higher than the expected mass-loss of 5.5 % for the loss of water in pure HPBCD in the mixture containing 91.1 % by mass of HPBCD. The curve also does not show any mass-loss above 140°C. For the kneaded mixture, the mass-loss from 48°C to 120°C is 2 %, which is less than the value expected of 5.5%. The total mass-loss of 5% by 220°C, is less than the expected value for the complete evaporation/decomposition of 9% by mass of HPBCD in the mixture. The thermal behaviour indicates interaction between SA and HPBCD. These results are summarised in Table 5.1.

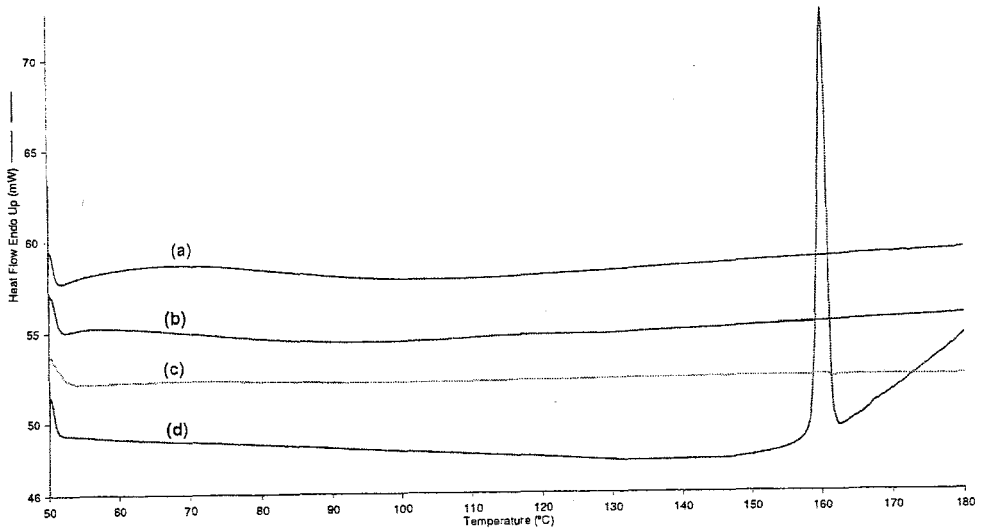

Figure 5.13: DSC curves for the pure components and for mixtures of SA with HPBCD: (a) pure HPBCD, (b) physical mixture, (c) kneaded mixture and (d) pure SA (heated in flowing nitrogen at 10 K min^{-1} in uncrimped aluminium pans).

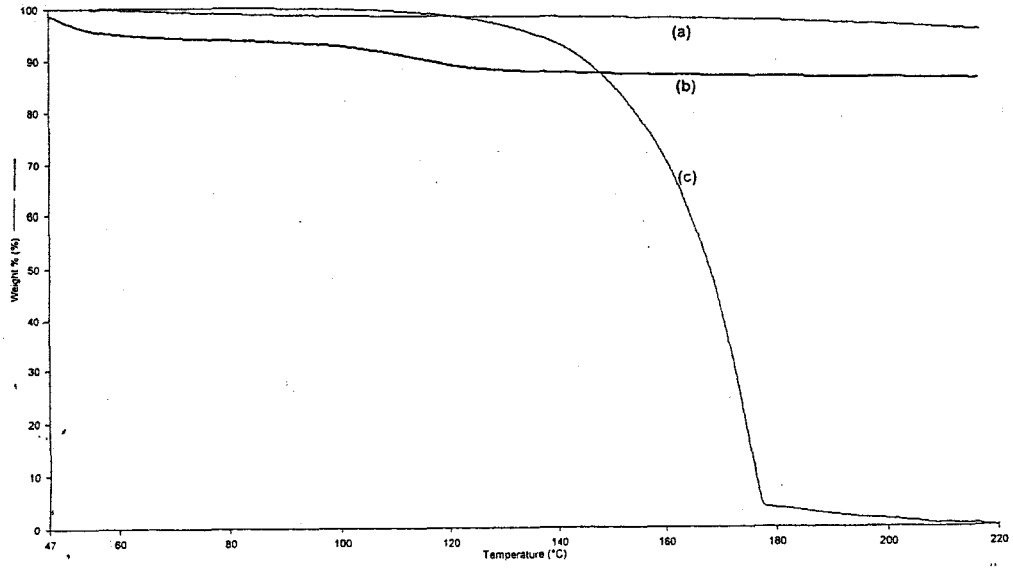

Figure 5.14: TG curves for SA and for mixtures with HPBCD: (a) kneaded mixture, (b) physical mixture and (c) pure SA (heated in flowing nitrogen at 10 K min^{-1} in open platinum pans).

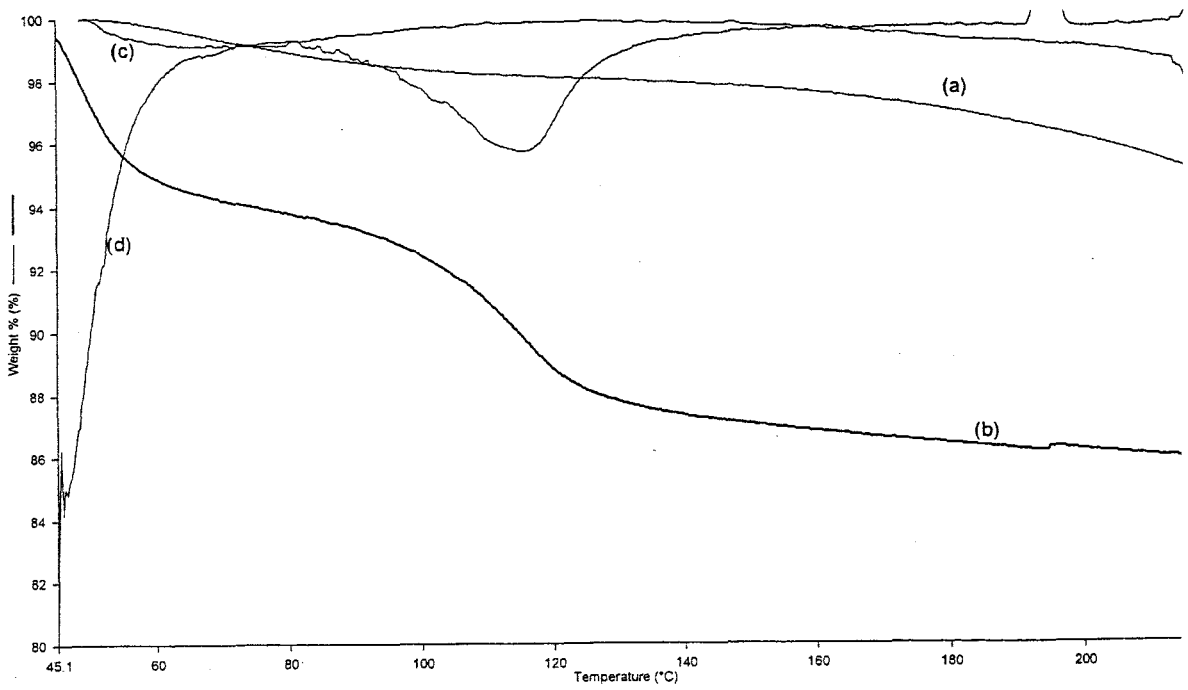

Figure 5.15: TG and DTG curves for mixtures of SA with HPBCD: TG curves: (a) kneaded mixture and (b) physical mixture and DTG curves: (c) kneaded mixture and (d) physical mixture (heated in flowing nitrogen at 10 K min^{-1} in open platinum pans).

Figure 5.16 shows the DSC curves for the physical and the kneaded mixtures of SA with GCD. The DSC curve for pure GCD shows a dehydration endotherm from 60 °C to 110 °C, with $\Delta H = 73$ kJ mol^{-1} and small endotherm around 230 °C (Figure 4.3 and Table 4.1). The DSC curve for the physical mixture shows a dehydration endotherm from 61 °C to 130 °C, with $\Delta H = 123$ kJ $(mol\ GCD)^{-1}$ and an endotherm, with onset at 141 °C and $\Delta H = 2$ kJ $(mol\ SA)^{-1}$. The DSC curve for the kneaded mixture shows only a dehydration endotherm from 61 °C to 145 °C, with $\Delta H = 119$ kJ $(mol\ GCD)^{-1}$. The absence of the endotherm associated with the melting of SA in the curve for the kneaded mixture is an indication of interaction between SA and GCD.

The TG and DTG curves for the physical and the kneaded mixtures of SA with GCD are shown in Figure 5.17 and 5.18. The TG curve for the physical mixture shows a mass-loss of 5% from 50°C to 85°C, followed by another mass-loss of 9% between 85°C and 140°C. The total mass-loss by 140°C is 14%. The mass-losses expected from the behaviour of the components would be 8.1% and 9.6%. For the kneaded mixture, the mass-loss (shown by the DTG curve to occur in two stages), is about 5%, with the first loss being 2% and then followed by mass-loss of 3%. This is less than the expected value of 8% for the loss of water from pure GCD in the mixture containing 90.4% by mass of GCD. A mass-loss related to the total evaporation/decomposition of the 9.6% SA is not observed and this indicates that an interaction has occurred. These results are summarised in Table 5.1.

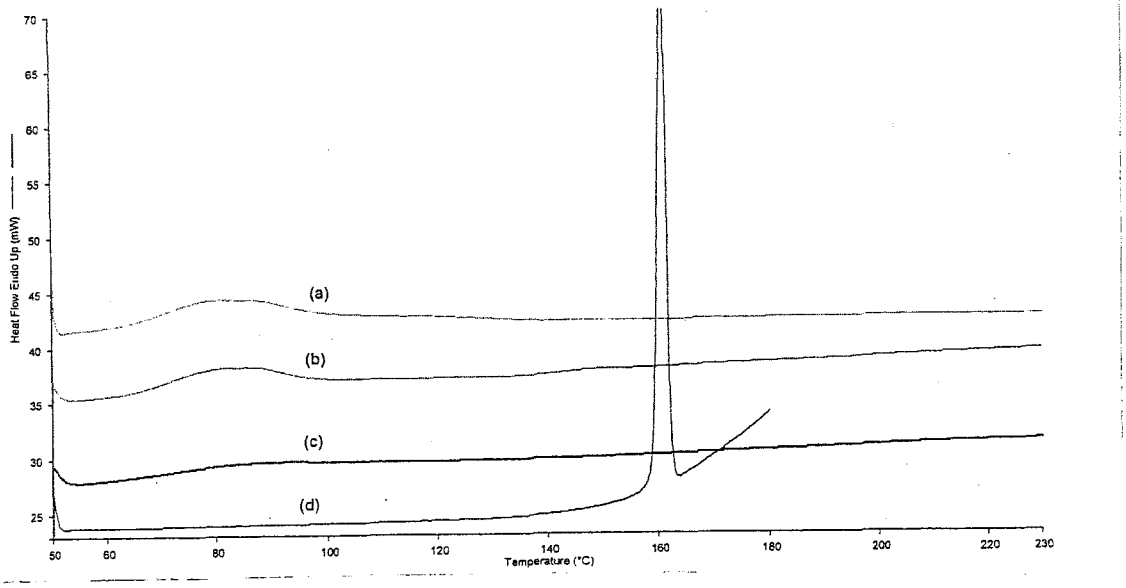

Figure 5.16: DSC curves for the pure components and for mixtures of SA with GCD: (a) pure GCD, (b) physical mixture, (c) kneaded mixture and (d) pure SA (heated in flowing nitrogen at 10 K min^{-1} in uncrimped aluminium pans).

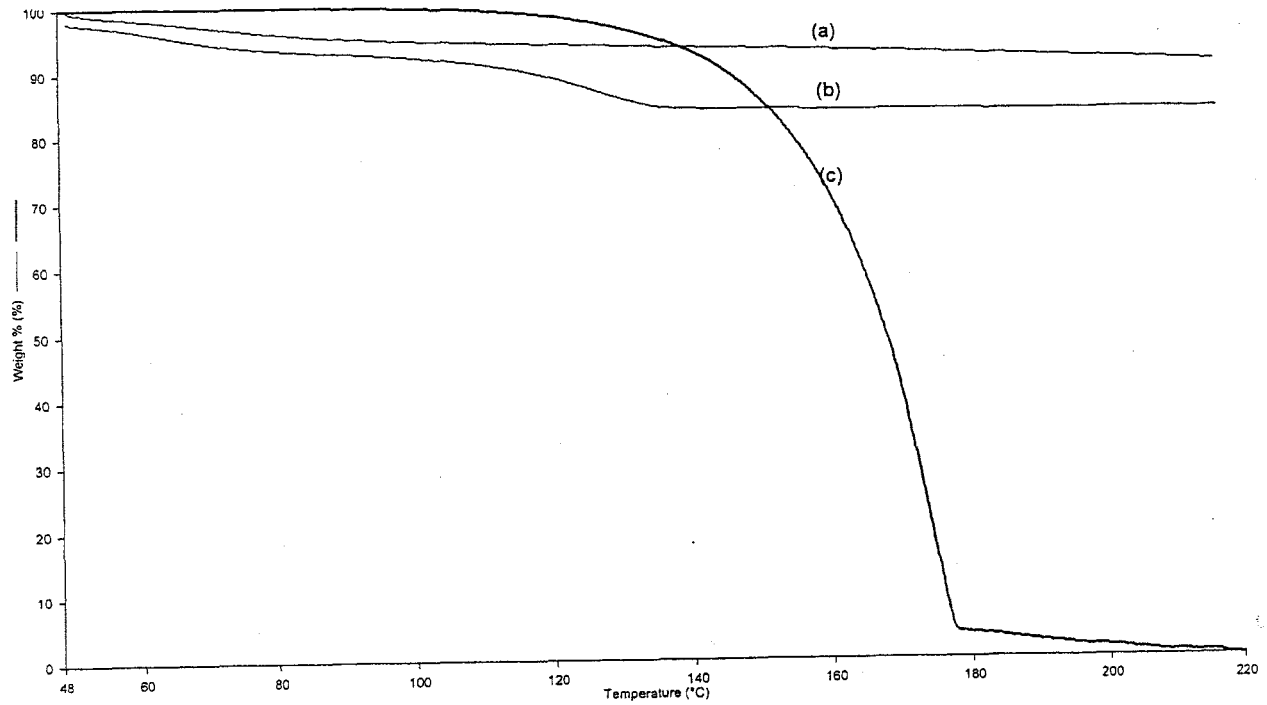

Figure 5.17: TG curves for SA and for mixtures with GCD: (a) kneaded mixture, (b) physical mixture and (c) pure SA (heated in flowing nitrogen at 10 K min^{-1} in open platinum pans).

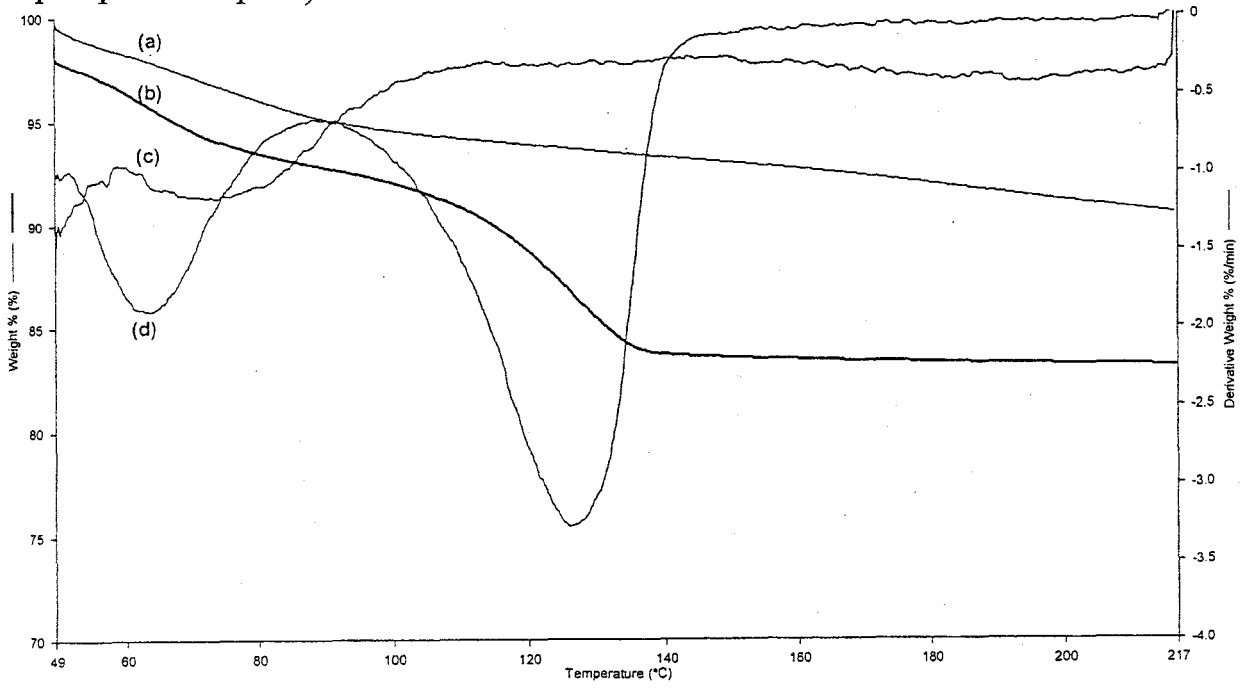

Figure 5.18: TG and DTG curves for mixtures of SA with GCD: TG curves: (a) kneaded mixture and (b) physical mixture and DTG curves: (c) kneaded mixture and (d) physical mixture (heated in flowing nitrogen at 10 K min^{-1} in open platinum pans).

5.4 Discussion

The results summarised in Table 5.1 indicate that there are interactions in 1:1 molar ratio mixtures of BA and SA with all three cyclodextrins. Changes in thermal behaviour are generally greater for kneaded mixtures than for physical mixtures. The main change is disappearance of the melting endotherm of BA or of SA in the DSC curves for the kneaded mixtures. In some mixtures, the endotherms corresponding to dehydration of the CD were decreased in size. This could result from displacement of water from the cavity of the CD by inclusion of BA or SA, or a decrease in the energy requirements for dehydration in the presence of BA or SA. The exception to this trend is the behaviour of the SA/GCD mixtures where the enthalpy of dehydration was increased. This could indicate the inclusion of additional atmospheric moisture during the mixing process or formation of hydrate of guest molecule which then is included in the CD cavity.

HPBCD had the greatest effect on the behaviour of both BA and SA, even in physical mixtures. Physical mixing of SA was more successful in producing interaction than physical mixing of BA. It would appear, very qualitatively, that the additional -OH group in SA enhances interaction with CDs.

Table 5.1 Summary of the expected and observed thermal behaviour of 1:1 molar ratio mixtures of BA and SA with cyclodextrins (p = physical mixture and k = kneaded mixture)

1:1 molar ratio mixtures		Expected			Observed			
Mixture	% acid by mass	% mass loss CD	ΔH dehyd. / kJ (mol CD)$^{-1}$	ΔH_{melt} / kJ (mol acid)$^{-1}$		% mass loss CD	ΔH dehyd. / kJ (mol CD)$^{-1}$	ΔH_{melts} /kJ (mol acid)$^{-1}$
BA/BCD	9.7	10.3	266	16	p	12.0	234	14
					k	8.5	243	1
BA/HPBCD	7.9	5.5	64	16	p	6	158	0
					k	5	6 3	0
BA/GCD	8.6	8.2	73	16	p	10	74	20
					k	4	0	0
SA/BCD	10.8	10.2	266	23	P	12	281	9
					k	13	74	0
SA/HPBCD	8.9	5.5	64	23	p	12	19	0
					k	2	0	0
SA/GCD	9.6	8.1	73	23	p	14	123	2
					k	5	119	0

6. THE THERMAL BEHAVIOUR OF MIXTURES OF THE AMINOSALICYLIC ACIDS (3-ASA, 4-ASA AND 5-ASA) WITH THE CYCLODEXTRINS

6.1 Introduction

The thermal behaviour of aminosalicylic acids has been described in Section 3.4 and the thermal behaviour of the three cyclodextrins used in the this study is described in Section 4.2.

DSC (using uncrimped aluminium pans) and TG (using open platinum pans) runs were done on 1:1 molar ratio physical and kneaded mixtures (prepared as described in Chapter 2) of 3-ASA, 4-ASA and 5-ASA with beta-cyclodextrin (BCD), hydroxypropyl-beta-cyclodextrin (HPBCD) and gamma-cyclodextrin (GCD). The DSC and TG curves for the mixtures were compared with those for the pure acids and pure CDs recorded under similar conditions. The thermal behaviour of the mixtures can provide an indication of inclusion of guest molecules in the cyclodextrin cavity, although other types of interaction cannot be ruled out (see discussions in Section 5.1). Changes in the dehydration endotherm of the CDs at temperatures from 50°C to 120°C and changes in the melting endotherm of the potential guest compound, including complete disappearance of the endotherm, are useful guides to changes occurring after mixing of the two compounds. Generally, the kneaded mixtures would be expected to show greater changes in thermal behaviour than the physical mixtures. If no interaction takes place, the areas of the CD dehydration endotherms and the ASA melting endotherms in the DSC curves for the mixtures should be directly related to the amounts of these constituents in the mixtures.

6.2 Mixtures of 3-aminosalicylic acid (3-ASA) with the cyclodextrins

Figure 6.1 shows the DSC curves for the physical and the kneaded mixtures of 3-ASA with BCD. The DSC curve for pure BCD shows a dehydration endotherm from 50 °C to 120 °C, with ΔH = 266 kJ (mol BCD)$^{-1}$ and a reversible transition exotherm around 220 °C (Figure 4.2 and Table 4.1). The DSC curve for 3-ASA in an uncrimped aluminium pan (Figure 3.8) shows an endotherm with onset at 220 °C, followed by an exotherm. The DSC curve for the physical mixture shows a dehydration endotherm between 70 °C and 110 °C (ΔH = 252 kJ (mol BCD)$^{-1}$ and a broad endotherm with ΔH = 59 kJ (mol 3-ASA)$^{-1}$ overlapping with the BCD reversible transition exotherm around 220 °C. The curve for the kneaded mixture exhibits no dehydration endotherm, but shows the BCD reversible transition exotherm around 220 °C near the onset of a broad 3-ASA melting endotherm at 229 °C (ΔH = 69 kJ (mol 3-ASA)$^{-1}$. The broadening of the endotherm associated with the melting of 3-ASA is an indication of some interaction in both mixtures. The disappearance of the dehydration endotherm for BCD in the DSC curve for the kneaded mixture could indicate that the water has been displaced from the BCD cavity during the kneading process. This displacement could be by 3-ASA molecules or by the kneading solvent (ethanol). If the latter was the reason, some indication should be seen of the endothermic removal of the solvent.

The TG and DTG curves (Figure 6.2 and 6.3) for the mixtures of 3-ASA with BCD confirm the displacement of water from the BCD cavity by the kneading process and show no indication that the kneading solvent was retained. The physical mixture showed an initial mass-loss (50 °C to 90 °C) of about 8.5 %. This is close to the expected value of 10.0 % for the loss of water in pure BCD from the mixture containing 86.5 % by mass of BCD. The total mass-loss for the physical mixture

of 20.0 % by about 240°C (i.e. a further loss of 11.5 %) is close to that expected for almost complete evaporation/decomposition of 13.5 % by mass of 3-ASA in the mixture. In the TG curve of the kneaded mixture, the initial mass-loss is 2.0 % and the total mass-loss is 14.0 % (i.e a further loss of 12.0%). This is close to the expected for almost complete evaporation/ decomposition of 13.5% by mass of 3-ASA in the mixture. Thus BCD does not appear to have a very significant effect on the thermal stability of 3-ASA in the physical mixture or kneaded mixture.

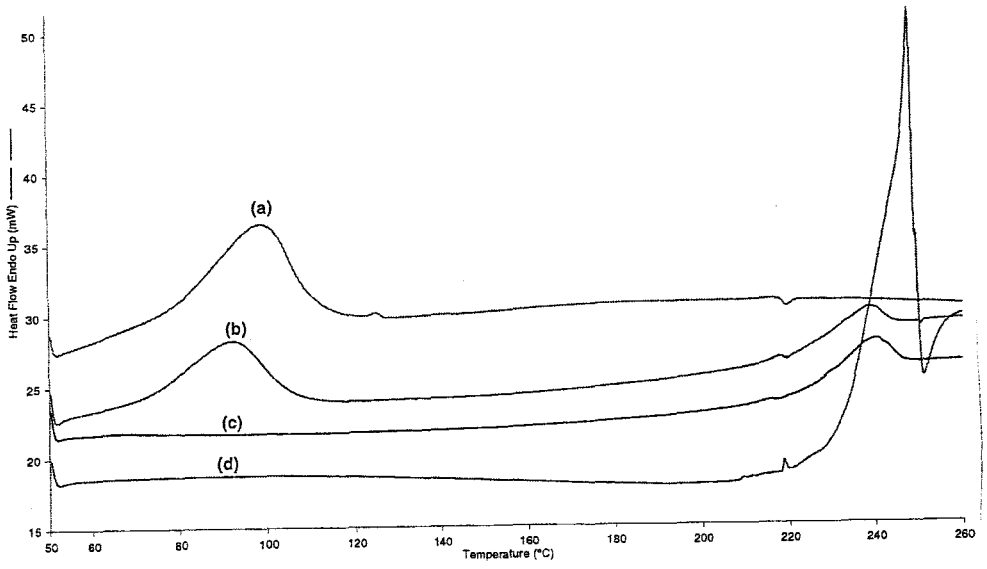

Figure 6.1: DSC curves for the pure components and for mixtures of 3-ASA with BCD: (a) pure BCD, (b) physical mixture, (c) kneaded mixture and (d) pure 3-ASA (heated in flowing nitrogen at 10 K min^{-1} in uncrimped aluminium pans).

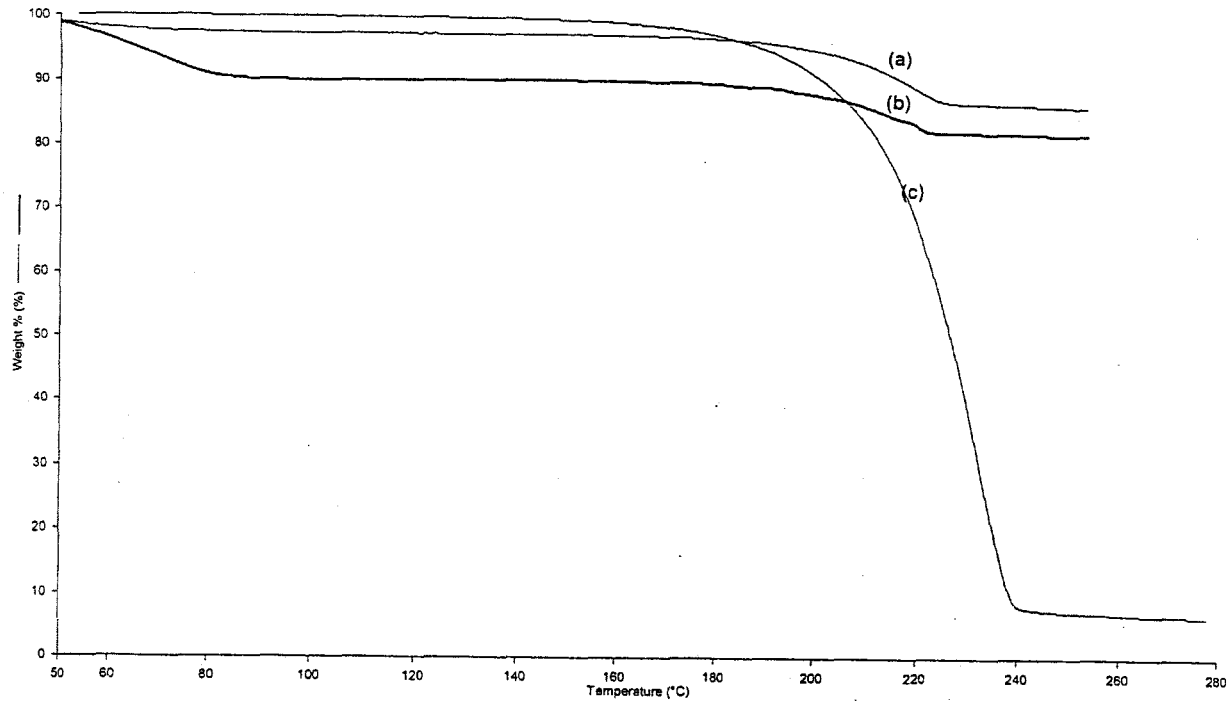

Figure 6.2: TG curves for 3-ASA and for mixtures of 3-ASA with BCD: (a) kneaded mixture (b) physical mixture and (c) pure 3-ASA (heated in flowing nitrogen at 10 K min^{-1} in open platinum pans).

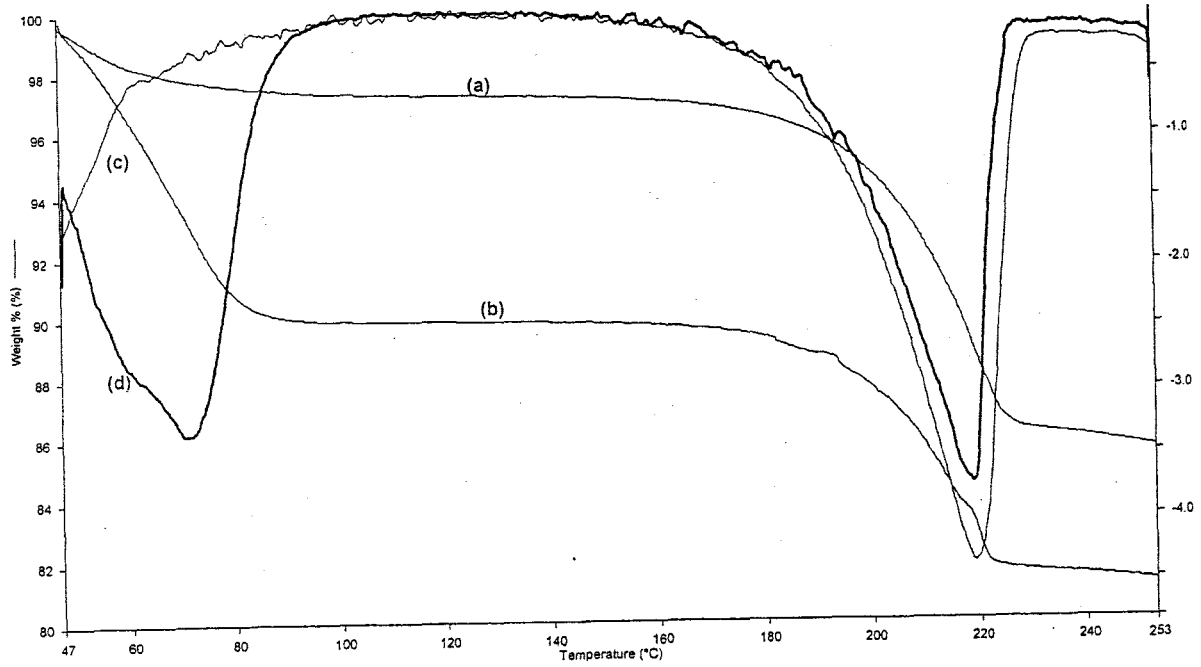

Figure 6.3: TG and DTG curves for mixtures of 3-ASA with BCD: TG curves: (a) kneaded mixture and (b) physical mixture, and DTG curves: (c) kneaded mixture and (d) physical mixture (heated in flowing nitrogen at 10 K min^{-1} in open platinum pans).

Figure 6.4 shows the DSC curves for the physical and kneaded mixtures of 3-ASA with HPBCD. The DSC curve for HPBCD shows an endotherm from 55°C to 100°C with $\Delta H = 64$ kJ mol^{-1} (Figure 4.2 and Table 4.1). It also shows a very small reversible transition exotherm at around 170°C, not accompanied by a mass-loss. The DSC curve for the physical mixture shows a dehydration endotherm with $\Delta H = 100$ kJ $(mol\ HPBCD)^{-1}$ and a much decreased melting endotherm from 218°C to 230°C with $\Delta H = 5$ kJ $(mol\ 3\text{-}ASA)^{-1}$. The curve for the kneaded mixture shows a dehydration endotherm from 53°C to 97°C with $\Delta H = 61$ kJ $(mol\ HPBCD)^{-1}$. No endotherm associated with the melting of 3-ASA is visible. The decrease in the dehydration endotherm of HPBCD and the virtual disappearance of the melting endotherm of 3-ASA are indications of interaction in the mixtures. The increased value for the dehydration endotherm of the physical mixture could indicate that the remaining water in the cavity interacts with the ASA present, thus inhibiting its removal.

The TG and DTG curves for the mixtures of 3-ASA and HPBCD are shown in Figure 6.5 and 6.6. The initial mass-loss of the physical mixture is 5 % between 40°C and 65°C. This is close to the expected value of 5.4 % for loss of water in pure HPBCD from a mixture containing 91.1 % by mass of HPBCD. The total mass-loss of 14.5 % at about 250°C (i.e. a further loss 9.5 %) is close to that expected for almost complete evaporation/decomposition of 8.9 % by mass of 3-ASA in the mixture. For the kneaded mixture, the initial mass-loss is similarly 5% between 40°C and 75°C and the total mass-loss was 14.0 % at about 250°C (i.e. a further loss of 9 %). The above results show no significant differences between physical and kneaded mixtures.

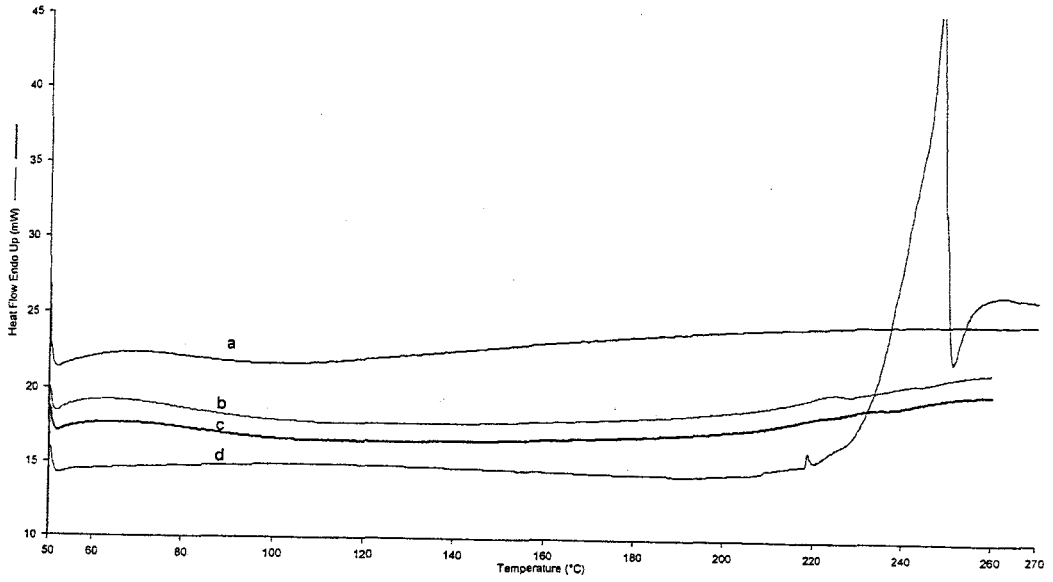

Figure 6.4: DSC curves for the pure components and for mixtures of 3-ASA with HPBCD: (a) pure HPBCD, (b) physical mixture, (c) kneaded mixture and (d) pure 3-ASA (heated in flowing nitrogen at 10 K min^{-1} in uncrimped aluminium pans).

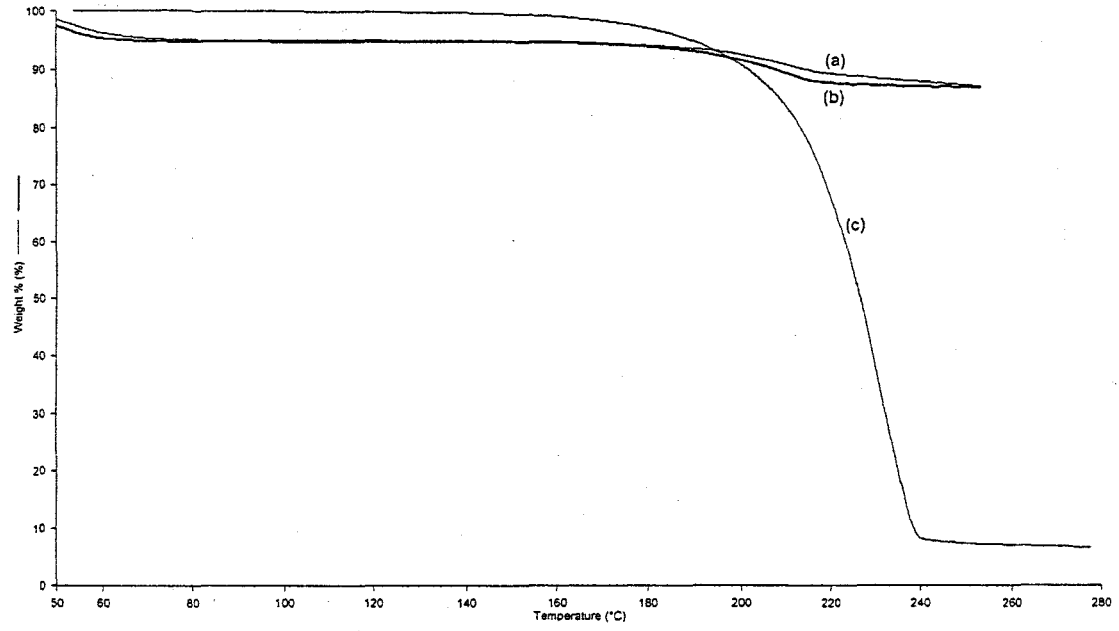

Figure 6.5: TG curves for 3-ASA and for mixtures with HPBCD: (a) kneaded mixture, (b) physical mixture and (c) pure 3-ASA (heated in flowing nitrogen at 10 K min^{-1} in open platinum pans).

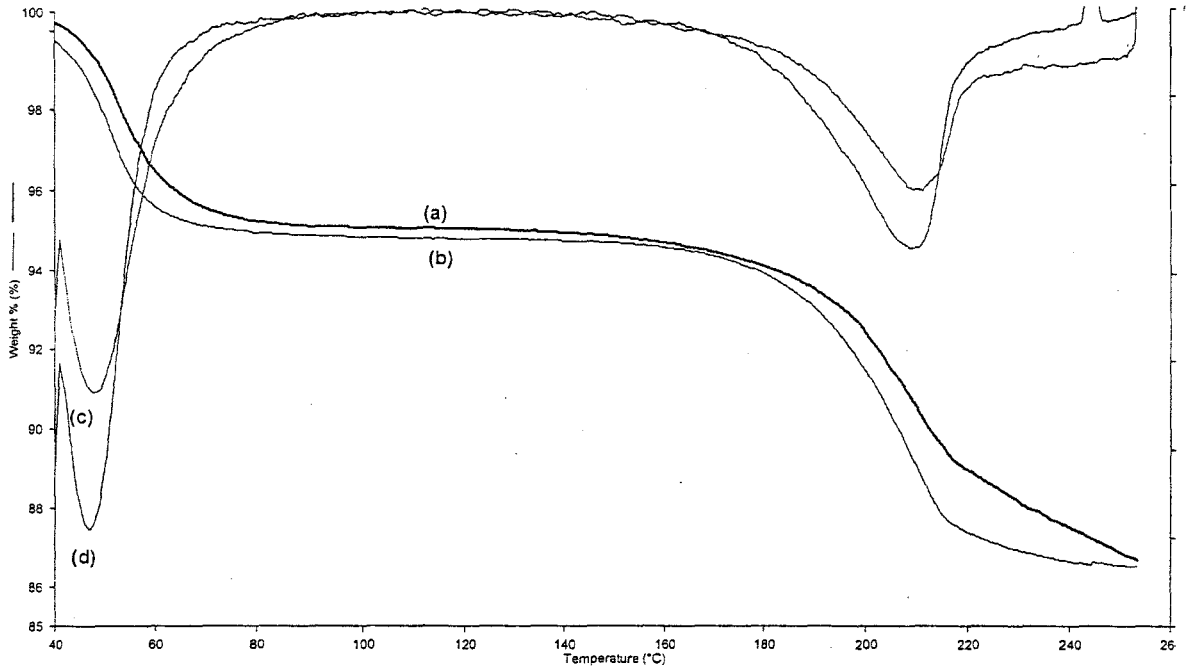

Figure 6.6: TG and DTG curves for mixtures of 3-ASA with HPBCD: TG curves: (a) kneaded mixture and (b) physical mixture, and DTG curves: (c) kneaded mixture and (d) physical mixture (heated in flowing nitrogen at 10 K min^{-1} in open platinum pans).

DSC curves for the physical and the kneaded mixtures of 3-ASA with GCD are shown in Figure 6.7. The DSC curve for pure GCD shows a broad dehydration endotherm from 60 °C to 110 °C, with $\Delta H = 73$ kJ mol^{-1}. There is also a very small reversible transition endotherm in the DSC curve around 230 °C (Figure 4.3 and Table 4.1). The DSC curve for the physical mixture shows a dehydration endotherm between 60 °C and 139 °C with $\Delta H = 163$ kJ(mol GCD)$^{-1}$ and an endotherm associated with melting of 3-ASA (onset 226 °C) with $\Delta H = 69$ kJ (mol 3-ASA)$^{-1}$. For the kneaded mixture, the dehydration endotherm is from 53 °C to 102 °C with $\Delta H = 65$ kJ (mol GCD)$^{-1}$ and a small broad endotherm at onset 223 °C with $\Delta H = 10$ kJ (mol 3-ASA)$^{-1}$. Broadening of the melting endotherm for 3-ASA is an indication of interaction in the mixtures. The decreased enthalpy values for

dehydration of GCD in the kneaded mixtures is an indication of water displacement from the GCD cavity by either 3-ASA or the kneading solvent (ethanol).

TG and DTG curves (Figure 6.8 and 6.9) for the mixtures of 3-ASA with GCD support the displacement of water from the cavity of the GCD by the kneading process. The physical mixture showed an initial mass-loss from 40°C to 110°C of about 7.0 %. This is close to the expected value of 8.1 % for the loss of water in pure GCD from the mixture containing 89.4 % by mass of GCD. The total mass-loss of 19 % at about 220°C (i.e. a further loss of 12 %) is close to that expected for almost complete evaporation/decomposition of 11 % by mass of 3-ASA in the mixture. In the TG curve of the kneaded mixture, there is a smaller initial mass-loss of 3% and the total mass-loss is 14 % (a further loss of 11%). This is close to the value of 10.6% for almost complete evaporation/decomposition of 3-ASA in the mixture. These results are summarised in Table 6.1.

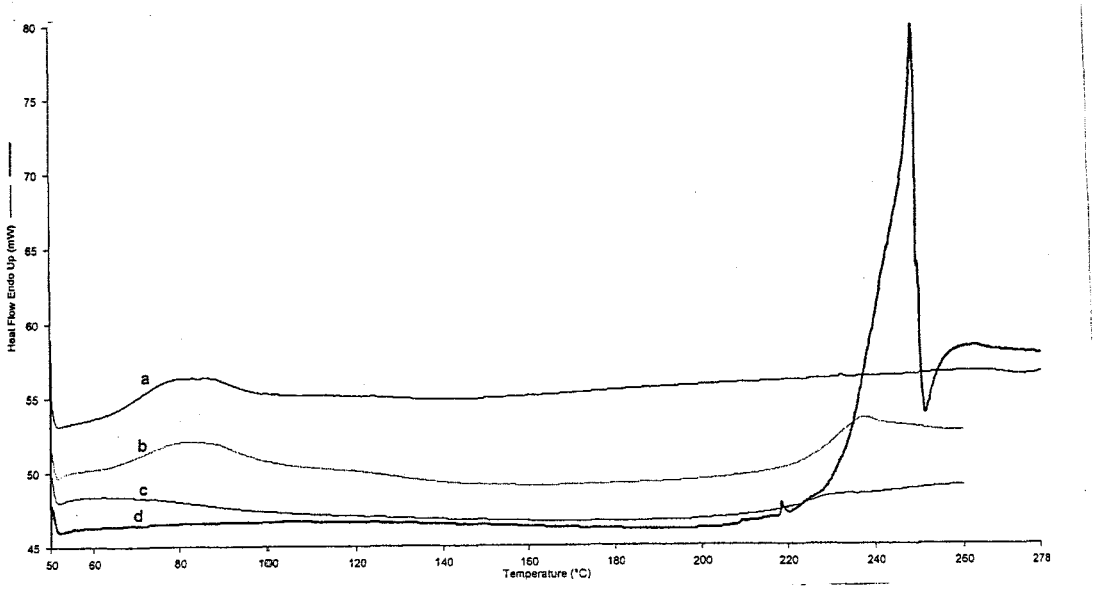

Figure 6.7: DSC curves for the pure components and for mixtures of 3-ASA with GCD: (a) pure GCD, (b) physical mixture, (c) kneaded mixture and (d) pure 3-ASA (heated in flowing nitrogen at 10 K min^{-1} in uncrimped aluminium pans).

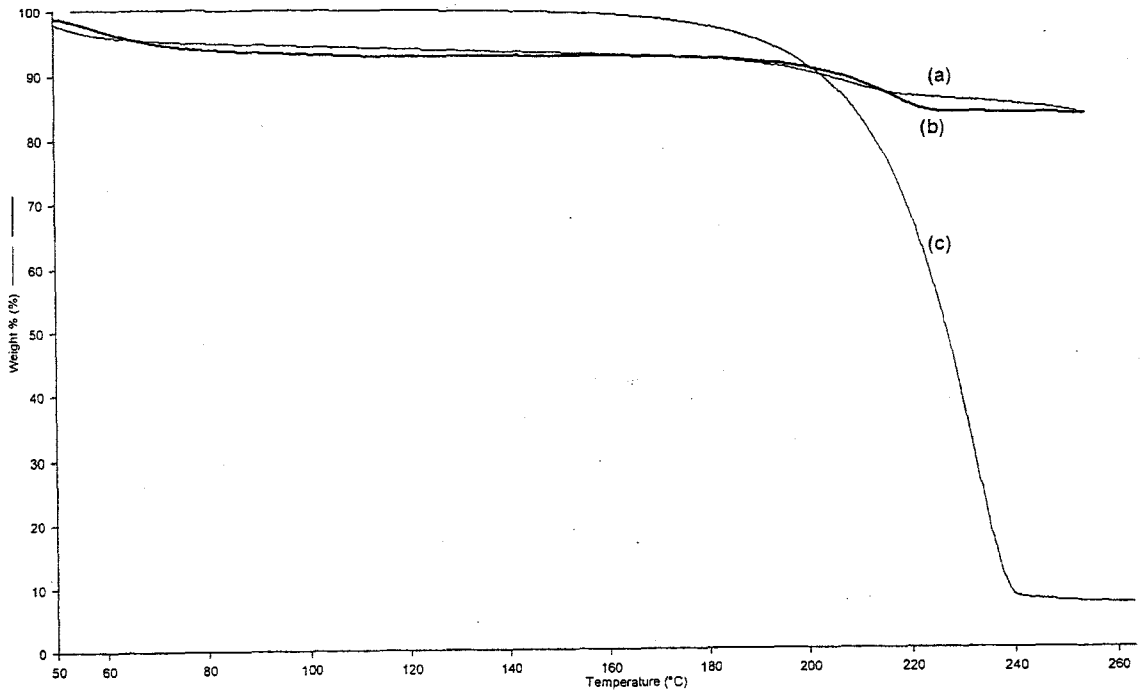

Figure 6.8: TG curves for 3-ASA and for of 3-ASA mixtures with GCD: (a) kneaded mixture, (b) physical mixture and (c) pure 3-ASA (heated in flowing nitrogen at 10 K min^{-1} in open platinum pans).

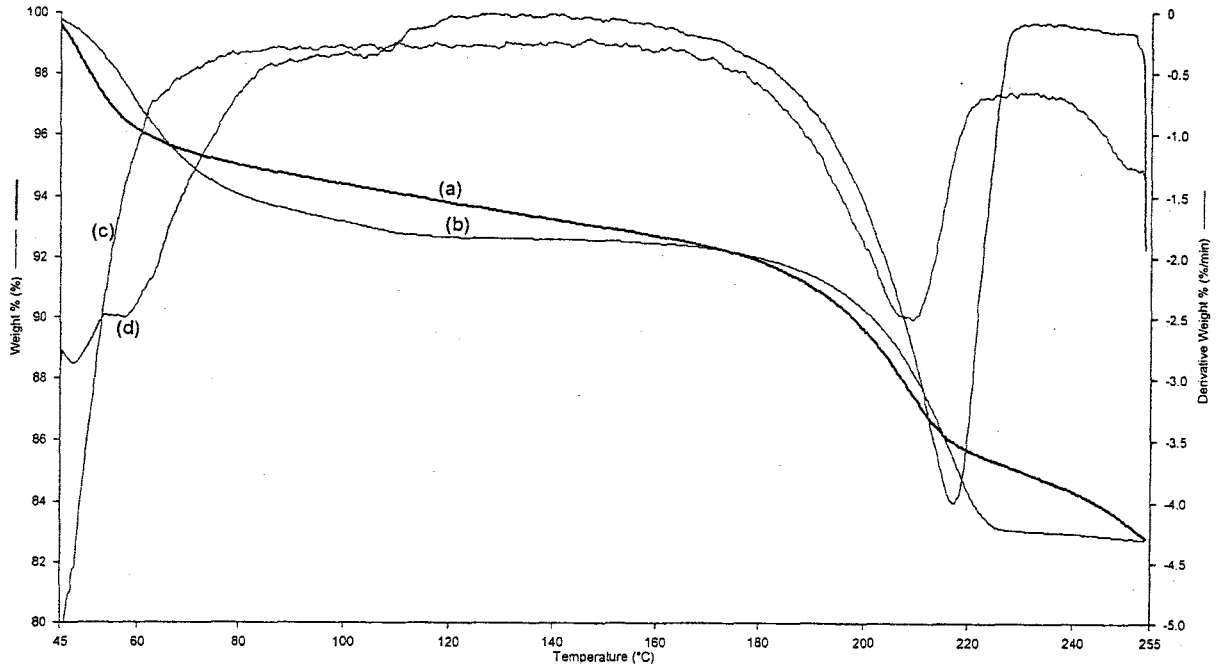

Figure 6.9: TG and DTG curves for mixtures of 3-ASA with GCD: TG curves: (a) kneaded mixture and (b) physical mixture, and DTG curves: (c) kneaded mixture and (d) physical mixture (heated in flowing nitrogen at 10 K min^{-1} in open platinum pans).

6.3 Mixtures of 4-aminosalicylic acid (4-ASA) with the cyclodextrins

Figure 6.10 shows the DSC curves for the physical and the kneaded mixtures of 4-ASA with BCD. The DSC curve for pure BCD shows a dehydration endotherm from 50 °C to 120 °C with ΔH = 266 kJ (mol BCD)$^{-1}$ (Figure 4.1 and Table 4.1). It also shows a reversible transition exotherm around 220 °C. The DSC curve for pure 4-ASA shows a melting endotherm with onset 133 °C and ΔH = 26 kJ mol^{-1}. The DSC curve for the physical mixture shows a dehydration endotherm from 64 °C to 102 °C with ΔH = 184 kJ (mol BCD)$^{-1}$. There was no evidence of the normal melting endotherm of 4-ASA at about 133 °C but there was a double endotherm (complex) (onset 156 °C) with combined ΔH = 32 kJ (mol 4-ASA)$^{-1}$. The curve for the kneaded mixture showed a dehydration endotherm from 73 °C to 108 °C with ΔH = 181 kJ (mol BCD)$^{-1}$ and a broad complex endotherm from 148 °C to 164 °C with ΔH = 14 kJ (mol 4-ASA)$^{-1}$. The absence of endotherms associated with the melting of 4-ASA is an indication of an interaction between 4-ASA and BCD. This is supported by the slight decrease in the enthalpy values for the dehydration of BCD that could indicate the displacement of water in the CD cavity by a guest compound.

The TG and DTG curves (Figures 6.11 and 6.12) for the physical and kneaded mixtures of 4-ASA and BCD show the apparent stability of 4-ASA in both mixtures. The TG curve for the physical mixture showed an initial mass-loss of 5.5 %, which is far less than the expected value of 10 % for the loss of water in pure BCD from the mixture containing 88.1% by mass of BCD. The total mass-loss for the physical mixture of 15 % at about 200 °C (a further loss of 9.5%) is less than the expected value for almost complete evaporation/ decomposition of 11.9 % by mass of 4-ASA in the mixture. The TG curve for the kneaded mixture shows

an even lower initial mass-loss from 47°C to 90°C of about 2 %. The total mass-loss of 10 % (a further loss of 8.5 %) around 230°C is much lower that the expected 11.9 % for almost complete evaporation/decomposition of 4-ASA in the mixture. The results for both mixtures indicate an interaction between 4-ASA and BCD.

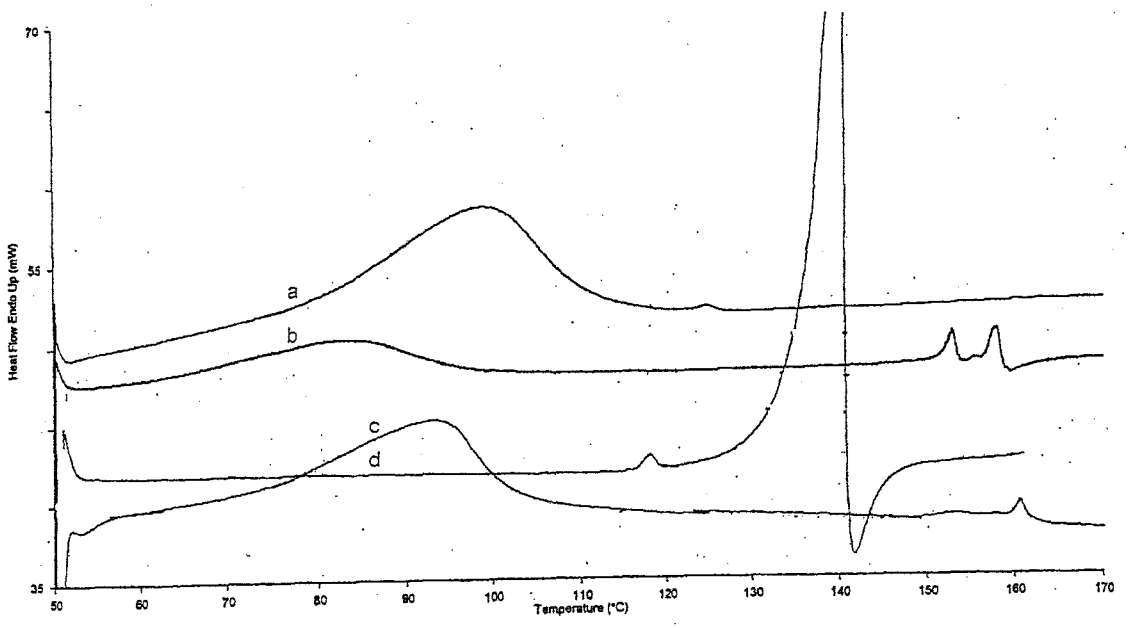

Figure 6.10: DSC curves for the pure components and for mixtures of 4-ASA with BCD: (a) pure BCD, (b) physical mixture, (c) kneaded mixture and (d) pure 4-ASA (heated in flowing nitrogen at 10 K min^{-1} in uncrimped aluminium pans).

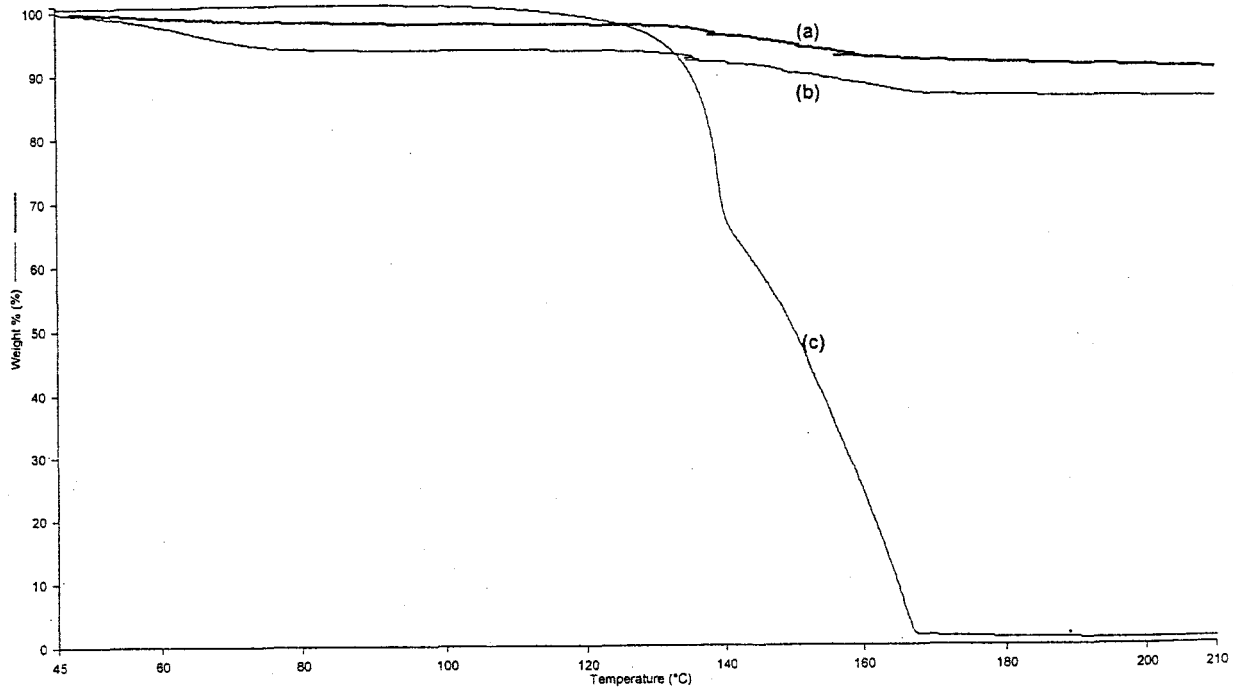

Figure 6.11: TG curves for 4-ASA and for mixtures with BCD: (a) kneaded mixture, (b) physical mixture and (c) pure 4-ASA (heated in flowing nitrogen at 10 K min^{-1} in open platinum pans).

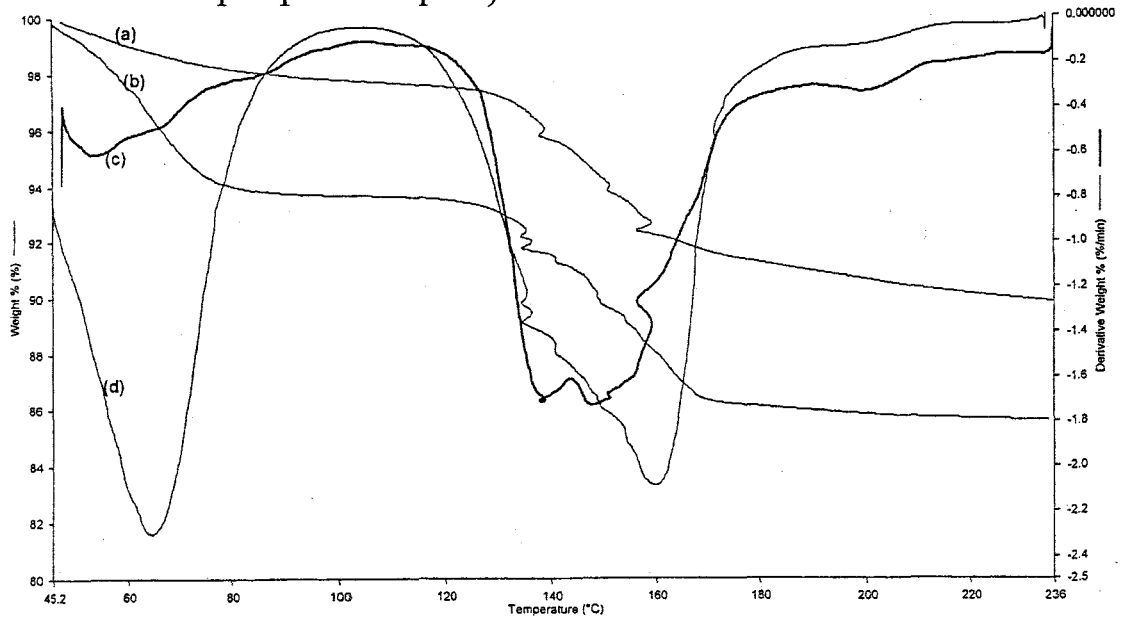

Figure 6.12: TG and DTG curves for mixtures of 4-ASA with BCD: TG curves: (a) kneaded mixture and (b) physical mixture and DTG curves: (c) kneaded mixture and (d) physical mixture (heated in a flowing nitrogen at 10 K min^{-1} in open platinum pans).

Figure 6.13 shows DSC curves for the physical and the kneaded mixtures of 4-ASA with HPBCD. The DSC curve for pure HPBCD shows an endotherm from 55°C to 100°C with $\Delta H = 64$ kJ mol^{-1} (Figure 4.2 and Table 4.1). It also shows a small reversible transition exotherm at about 170°C, not accompanied by mass-loss. The DSC curve for the physical mixture shows a dehydration endotherm with $\Delta H = 36$ kJ $(mol\ HPBCD)^{-1}$ and a broad endotherm (onset 108°C) with $\Delta H = 89$ kJ $(mol\ 4\text{-}ASA)^{-1}$. No endotherms or exotherms were observed for the kneaded mixture.

The broadening of the melting endotherm for 4-ASA in the DSC curve for the physical mixture and the decrease in the enthalpy value are all indications of interaction between 4-ASA and HPBCD. The complete absence of expected features in the DSC curve for the kneaded mixture is a strong indication of interaction between the two compounds in the mixtures.

The TG and DTG curves for the physical and kneaded mixtures of 4-ASA with HPBCD are shown in Figure 6.14 and 6.15. The initial mass-loss for the physical mixture is 5.5 % between 40°C and 110°C. This is close to the expected value of 5.4 % for the loss of water in pure HPBCD from the mixture of 90.2 % by mass of HPBCD. The total mass-loss of 13 % (i.e. a further loss of 7.5 %) around 220°C is close to the expected value for almost complete evaporation/decomposition of 9.8 % by mass of 4-ASA in the mixture. For the kneaded mixture, the TG curve shows the initial mass-loss of 1 %, which is much lower than the expected value. The total mass-loss of 5.5 % (a further loss of 4.5 %) is also much lower than the expected value of 9.8 %. The observations from these TG and DTG curves support the occurrence of interaction between 4-ASA and HPBCD in kneaded mixtures.

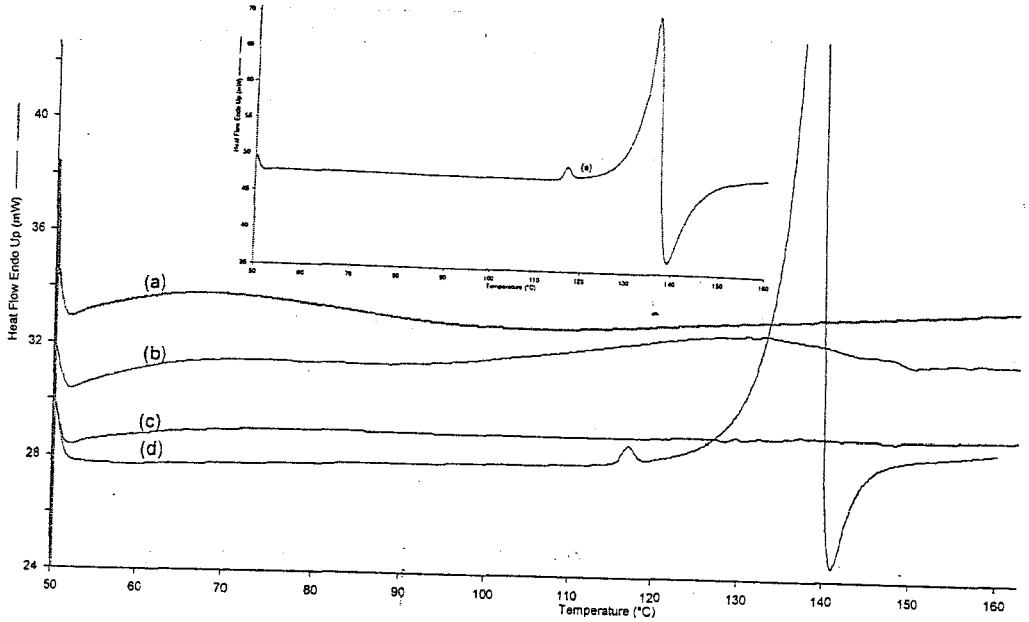

Figure 6.13: DSC curves for the pure components and for mixtures of 4-ASA with HPBCD: (a) pure HPBCD, (b) physical mixture, (c) kneaded mixture and (d) pure 4-ASA (e) enlarged scale for curve (d) (heated in flowing nitrogen at 10 K min^{-1} in uncrimped aluminium pans).

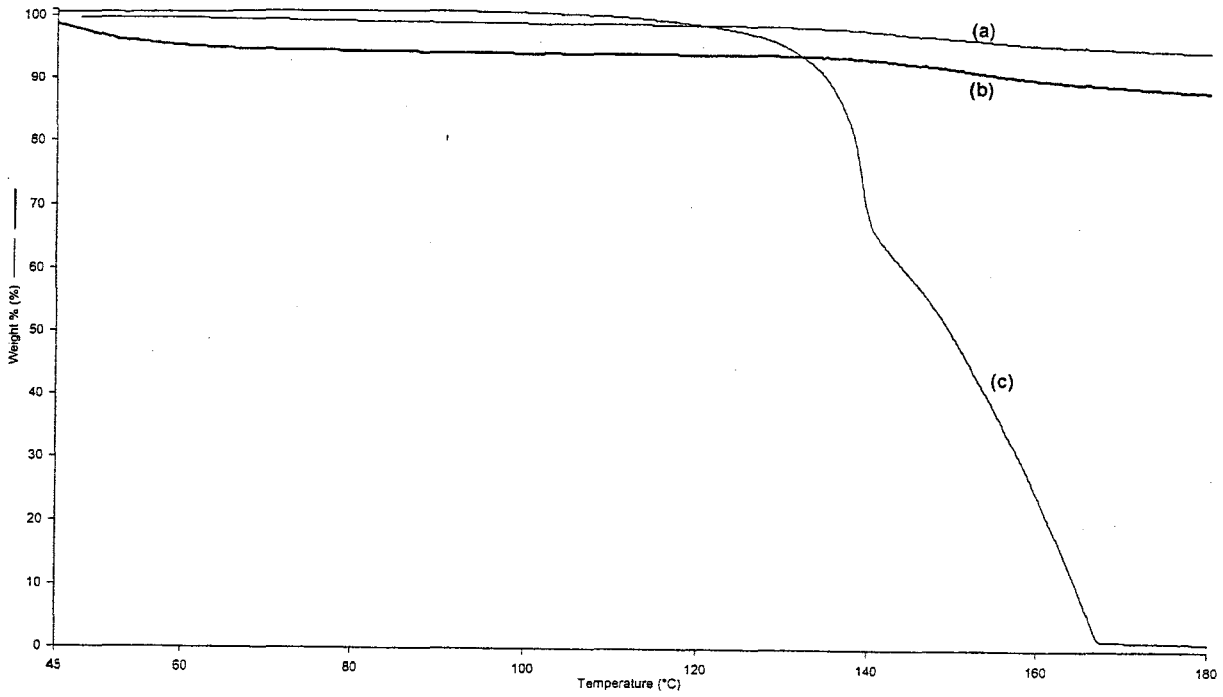

Figure 6.14: TG curves for 4-ASA and for mixtures with HPBCD: (a) kneaded mixture, (b) physical mixture and (c) pure 4-ASA (heated in flowing nitrogen at 10 K min^{-1} in open platinum pans).

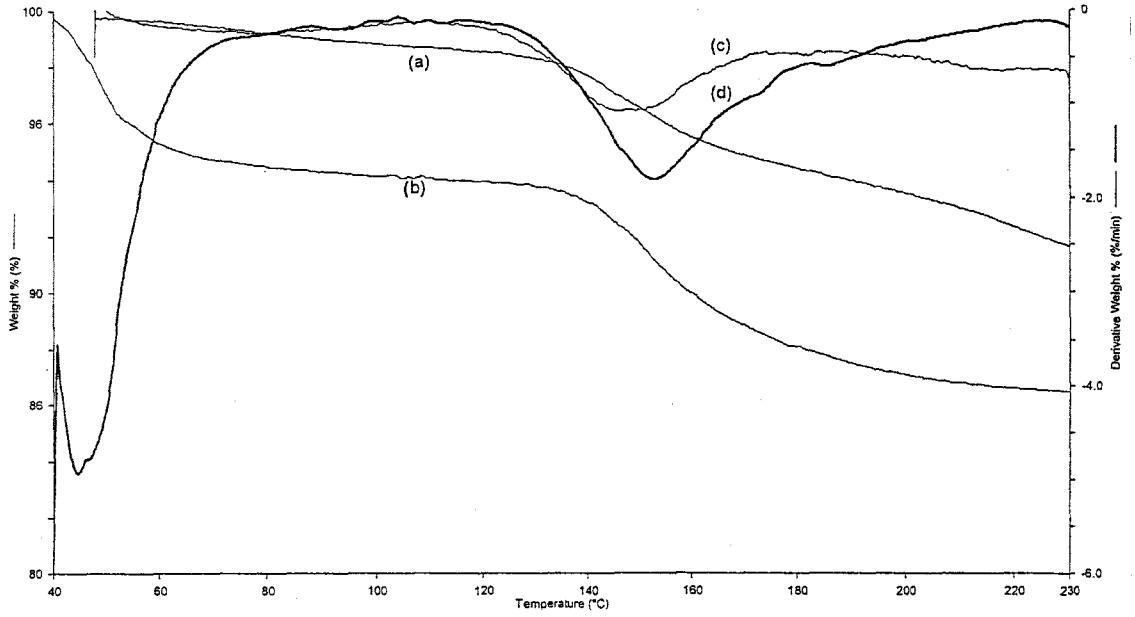

Figure 6.15: TG and DTG curves for mixtures of 4-ASA with HPBCD: TG curves: (a) kneaded mixture and (b) physical mixture and DTG curves: (c) kneaded mixture and (d) physical mixture (heated in flowing nitrogen at 10 K min^{-1} in open platinum pans).

Figure 6.16 shows the DSC curves for the physical and kneaded mixtures of 4-ASA with GCD. The DSC curve for pure GCD shows a broad dehydration endotherm from 60 °C to 110 °C, with $\Delta H = 73$ kJ mol^{-1}. There is also a very small reversible transition endotherm in the DSC curve around 230 °C (Figure 4.3 and Table 4.1). The DSC curve for the physical mixture shows a dehydration endotherm from 64 °C to 101 °C with $\Delta H = 69$ kJ $(mol\ GCD)^{-1}$ and no endotherm at 122 °C associated with melting of 4-ASA. For the kneaded mixture, there is only one endotherm (dehydration) from 53 °C to 99 °C with $\Delta H = 182$ kJ $(mol\ GCD)^{-1}$. The absence of the endotherm associated with the melting of 4-ASA is

an indication of interaction of the 4-ASA with GCD.

TG and DTG curves (Figure 6.17 and 6.18) for physical and kneaded mixtures of 4-ASA with GCD support the occurrence of interaction between these two compounds in both mixtures. For the physical mixture, the initial mass-loss (40 °C to 100 °C) of about 5.0 % is less than the expected value of 8.0 % loss of water in pure GCD in the mixture containing 89.4 % mass of GCD. The total mass-loss at about 180 °C of 16 % (i.e a further loss of 11%) is close to that expected for almost complete evaporation/decomposition of 10.6 % of 4-ASA by mass. The TG curve for the kneaded mixture showed an initial mass-loss of 12 % from 40 °C to 70 °C which is higher than the expected value of 8.0 %. The total mass-loss at around 180 °C is 18 % (i.e. a further loss of 6 %) which is much less than the expected of 10.6 %, but the overall expected and found values are similar. The results are summarised in Table 6.2

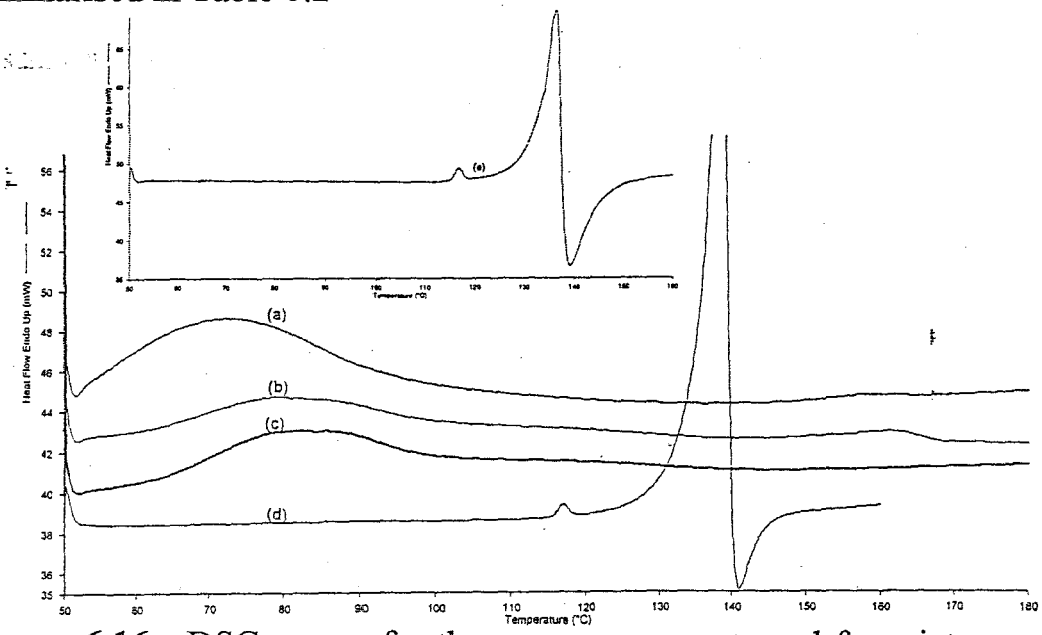

Figure 6.16: DSC curves for the pure components and for mixtures of 4-ASA with GCD: (a) pure GCD, (b) physical mixture, (c) kneaded mixture and (d) pure 4-ASA (e) enlarged y-axis scale for curve (d) (heated in flowing nitrogen at 10 K min^{-1} in uncrimped aluminium pans).

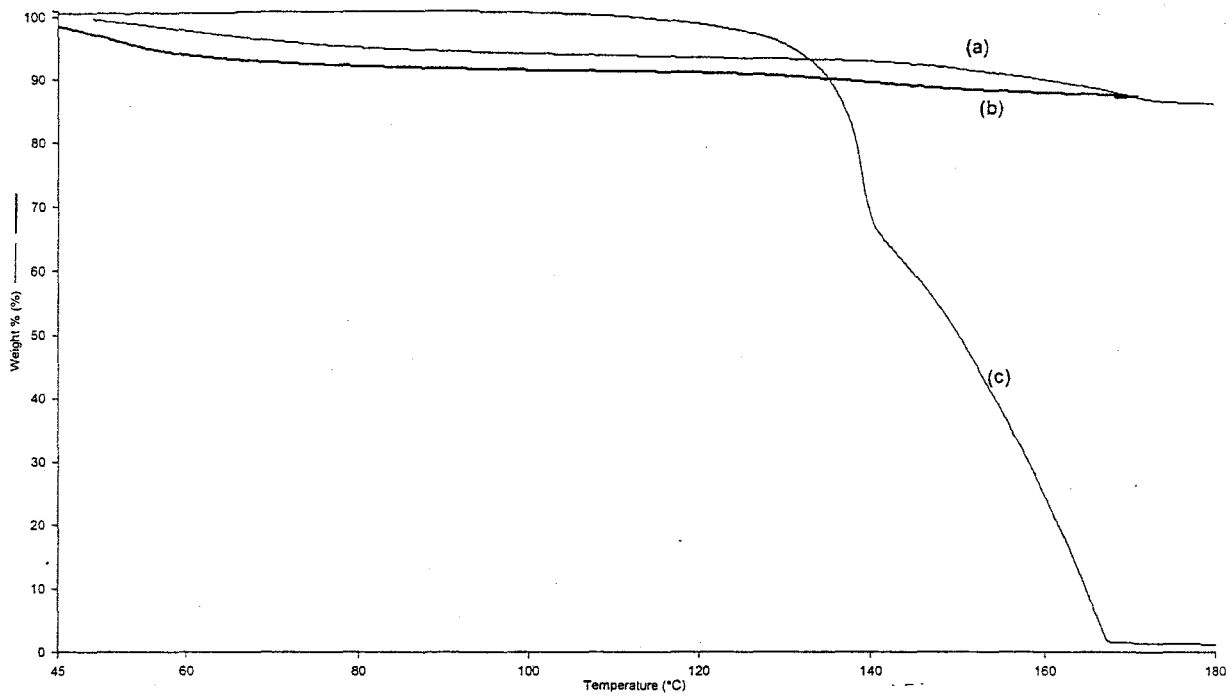

Figure 6.17: TG curves for 4-ASA and for mixtures of 4-ASA with GCD: (a) kneaded mixture, (b) physical mixture and (c) pure 4-ASA (heated in flowing nitrogen at 10 K min^{-1} in open platinum pans).

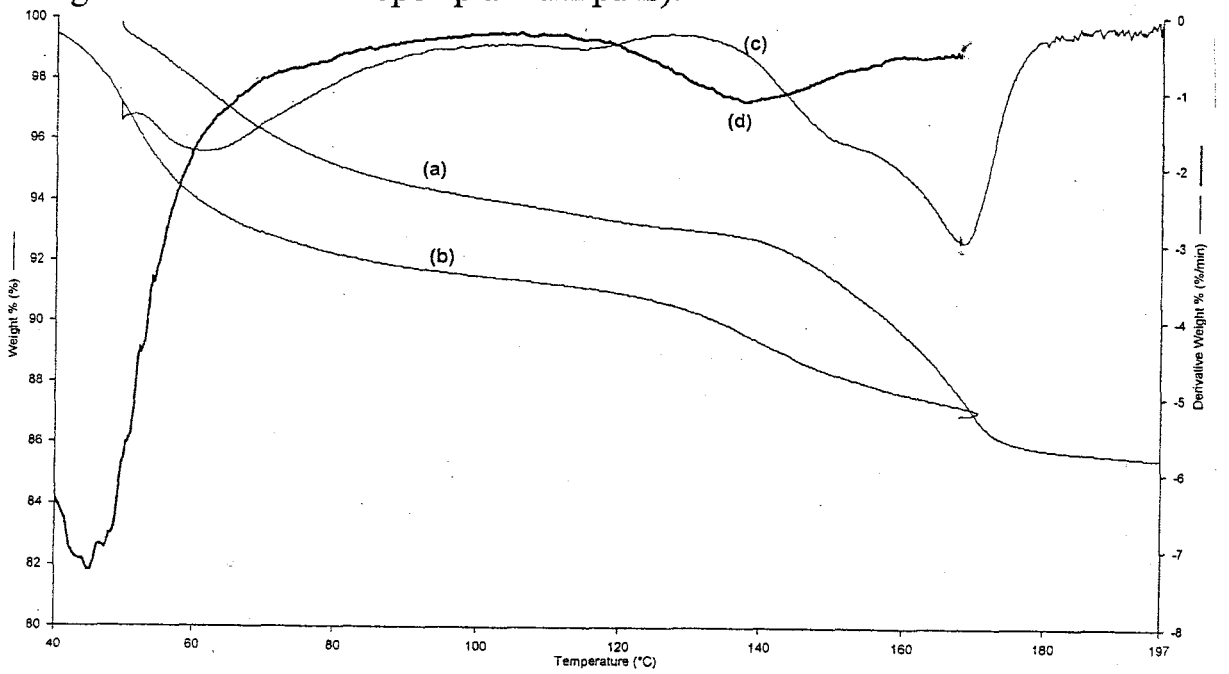

Figure 6.18: TG and DTG curves for mixtures of 4-ASA with GCD: TG curves: (a) kneaded mixture and (b) physical mixture, and DTG curves: (c) kneaded mixture and (d) physical mixture (heated in flowing nitrogen at 10 K min^{-1} in open platinum pans).

6.4 Mixtures of 5-aminosalicylic acid (5-ASA) with the cyclodextrins

Figure 6.19 shows the DSC curves for the physical and the kneaded mixtures of 5-ASA and BCD. The DSC curve for BCD shows a dehydration endotherm from 50°C to 120°C with ΔH = 266 kJ mol^{-1} and a reversible transition exotherm around 220°C (Figure 4.1 and Table 4.1). The DSC curve for 5-ASA shows an endotherm with ΔH = 89 kJ mol^{-1} and onset 278°C (Figure 3.10). The DSC curve for the physical mixture shows a dehydration endotherm from 66°C to 114°C with ΔH = 255 kJ $(mol\ BCD)^{-1}$, a reversible transition exotherm around 220°C ,and a broad endotherm associated with the melting of 5-ASA with onset at 254°C and ΔH = 119 kJ $(mol\ 5\text{-}ASA)^{-1}$. The kneaded mixture shows a dehydration endotherm from 66°C to 109°C with ΔH =199 kJ $(mol\ BCD)^{-1}$, a reversible exotherm around 220°C, and an endotherm associated with melting of 5-ASA with onset at 260°C and ΔH = 122 kJ $(mol\ 5\text{-}ASA)^{-1}$. The broadening of the endotherms and the decreased enthalpy values indicate some interaction between 5-ASA and BCD.

The TG and DTG curves for the mixtures of 5-ASA with BCD are shown in Figures 6.20 and 6.21. The TG curve for the physical mixture shows an initial mass-loss of 13 %, which is slightly higher than the expected value of 10 % for the loss of water in pure BCD from the mixture containing 88.1% by mass of BCD. The total mass-loss at about 300°C is 24 % (i.e a further 11%) which is close to the expected mass of 11.9% for almost complete evaporation/ decomposition of 5-ASA in the mixture. The kneaded mixture shows an initial mass-loss of 12 %. The DTG curve shows two stages: the first mass-loss is 2% and the second mass-loss is 10 %. The total mass-loss at about 300°C is 38 % (i.e. a further loss of 26%) which is far higher than the expected mass-loss of 11.9 % for almost complete evaporation/decomposition of 5-ASA in the mixture. At high

temperatures both melting of 5-ASA and decomposition of the CD could be occurring together. Therefore, the dehydration of the CD is best used as indicator in investigating interaction between 5-ASA and BCD.

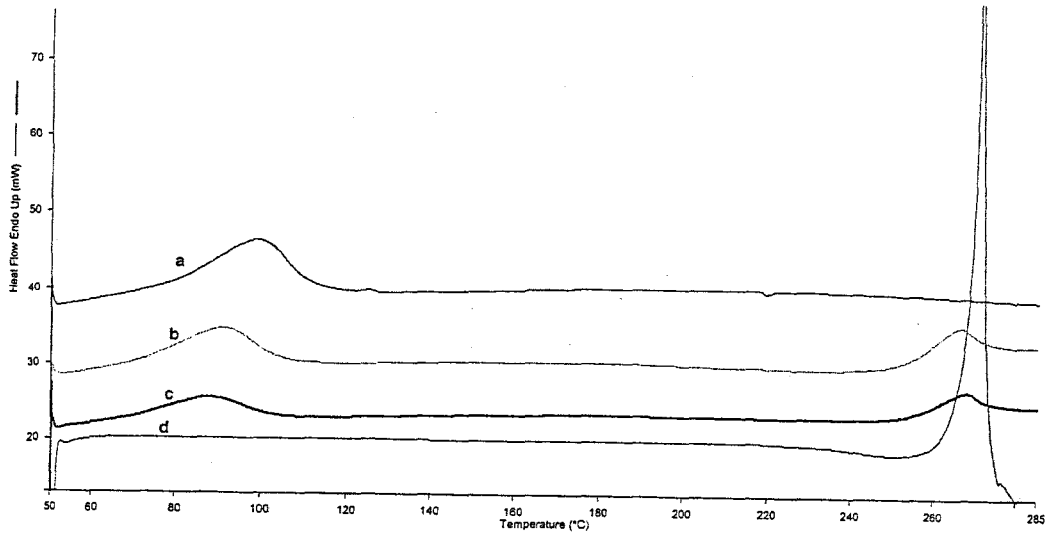

Figure 6.19: DSC curves of the pure components and for mixtures of 5-ASA with BCD: (a) pure BCD, (b) physical mixture, (c) kneaded mixture and (d) pure 5-ASA (heated in flowing nitrogen at 10 K min^{-1} in uncrimped aluminium pans).

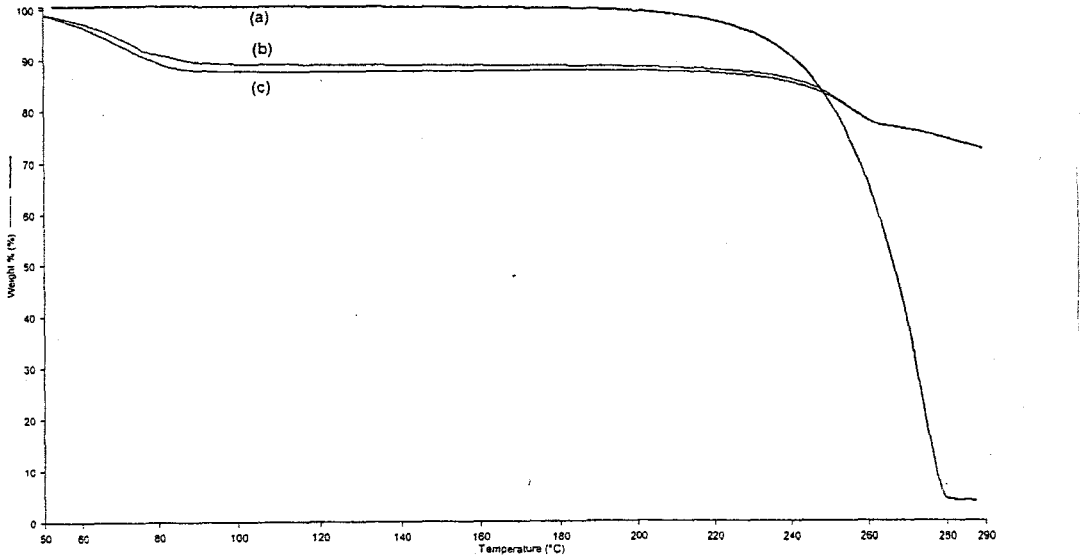

Figure 6.20: TG curves for 5-ASA and mixtures with BCD: (a) pure 5-ASA, (b) kneaded mixture and (c) physical mixture (heated in flowing nitrogen at 10 K min^{-1} in open platinum pans).

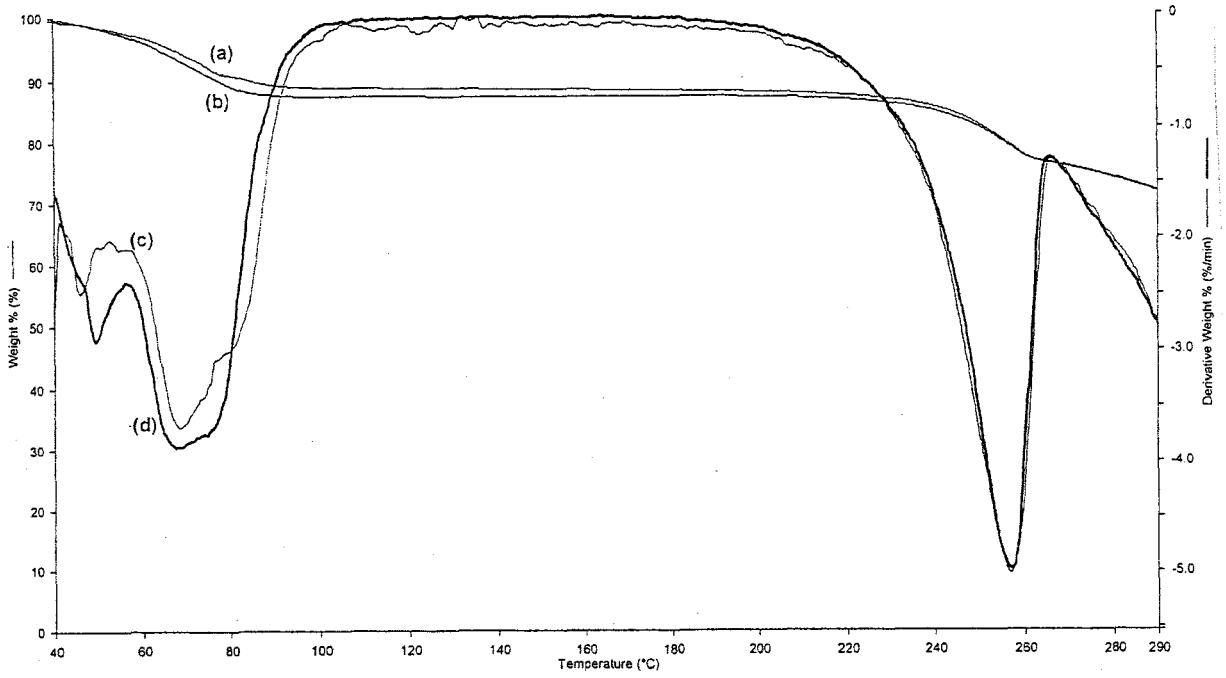

Figure 6.21: TG and DTG curves for mixtures of 5-ASA with BCD: TG curves: (a) kneaded mixture and (b) physical mixture, and DTG curves: (c) kneaded mixture and (d) physical mixture (heated in flowing nitrogen at 10 K min^{-1} in open platinum pans).

Figure 6.22 shows the DSC curves for the physical and the kneaded mixtures of 5-ASA with HPBCD. The DSC curve for pure HPBCD shows an endotherm from 55°C to 100°C with ΔH = 64 kJ mol^{-1} and a small double reversible transition endotherm, not accompanied by mass loss, at 170°C (Figure 4.2 and Table 4.1). The DSC curve for the physical mixture shows only a decreased dehydration endotherm from 55°C to 99°C with ΔH = 72 kJ $(mol\ HPBCD)^{-1}$. The kneaded mixtures show an endotherm from 148°C to 169°C with ΔH = 52 kJ $(mol\ 5\text{-}ASA)^{-1}$ and a reversible transition exotherm around 210°C. There is a small broad endotherm, onset 240°C in the melting region. The absence or decreased size of the endotherm associated with the melting of 5-ASA is an indication of interaction between 5-ASA and HPBCD.

The TG and DTG curves for the physical and the kneaded mixtures of 5-ASA and HPBCD are shown in Figures 6.23 and 6.24. The TG curve for the physical mixture shows an initial mass-loss of 13.5 % between 40 °C and 80 °C. The DTG curve shows this mass-loss to be a two-stage process. This value (13.5 %) is much higher than the expected value of 5.4 % for the loss of water in pure HPBCD from the mixture of 90.2 % by mass of HPBCD. The total mass-loss at 300 °C is 26 % (i.e a further loss of 12.5 %). This is higher than the expected value of 9.8% for almost complete evaporation/decomposition of 5-ASA in the mixture. The last mass-loss was in two stages as shown by DTG curve. The TG curve for the kneaded mixture shows an initial mass loss of 6 %. This is slightly higher than the expected value. The total mass-loss of 32 % (i.e a further loss of 26 %) is also higher than expected. This is attributed to both 5-ASA and HPBCD decomposing at almost the same temperatures.

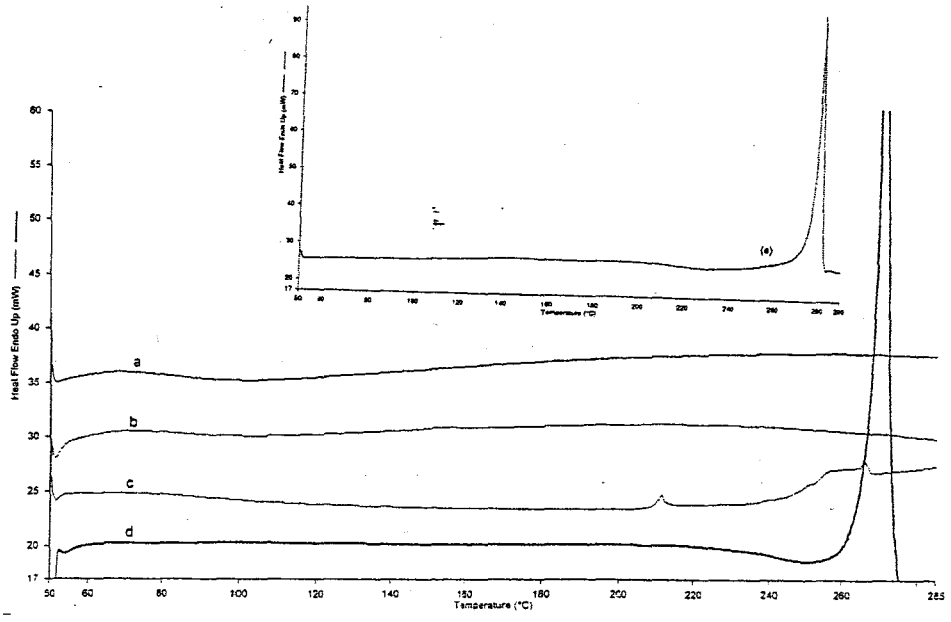

Figure 6.22: DSC curves of the pure components and for mixtures of 5-ASA with HPBCD: (a) pure HPBCD, (b) physical mixture, (c) kneaded mixture and (d) pure 5-ASA (e) enlarged y-axis scale for curve (d) (heated in flowing nitrogen at 10 K min^{-1} in uncrimped aluminium pans).

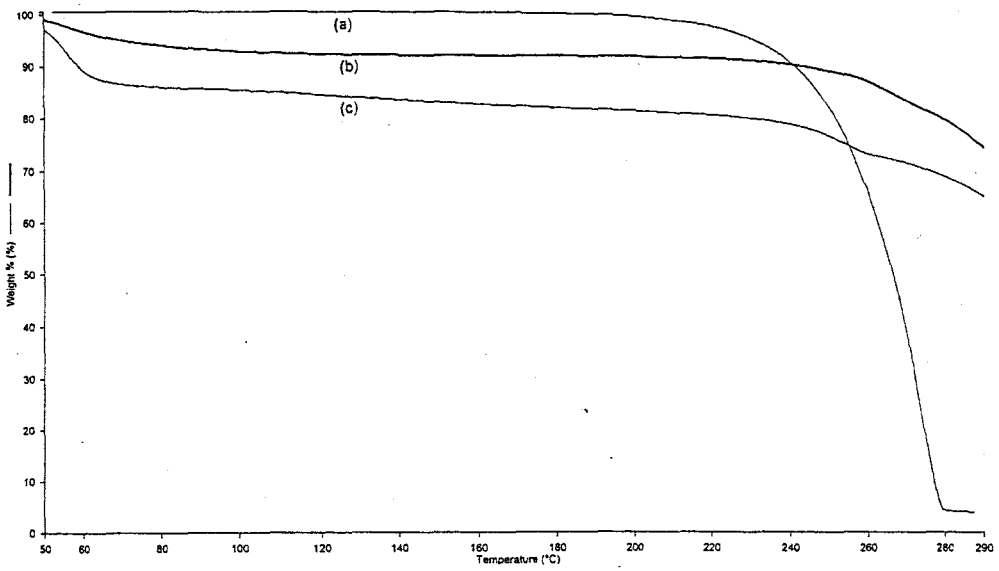

Figure 6.23: TG curves for 5-ASA and mixtures of 5-ASA with HPBCD: (a) pure 5-ASA, (b) kneaded mixture and (c) physical mixture (heated in flowing nitrogen at 10 K min^{-1} in open platinum pans).

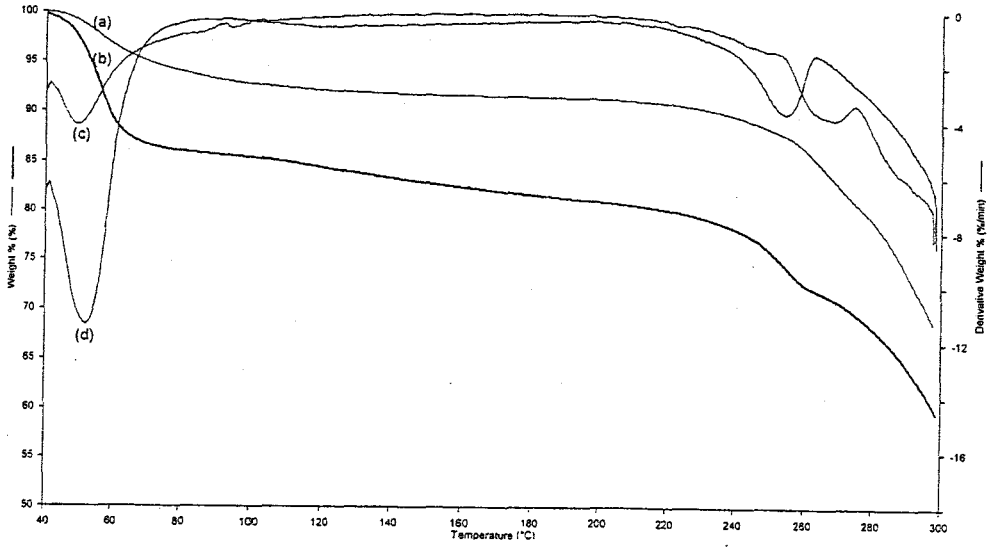

Figure 6.24: TG and DTG curves for mixtures of 5-ASA with HPBCD: TG curves: (a) kneaded mixture and (b) physical mixture, and DTG curves: (c) kneaded mixture and (d) physical mixture (heated in flowing nitrogen at 10K min^{-1} in open platinum pans).

Figure 6.25 shows the DSC curves for the physical and the kneaded mixtures of 5-ASA with GCD. The DSC curve for pure GCD shows a broad dehydration endotherm from 60°C to 110°C, with $\Delta H = 73$ kJ mol^{-1} and a very small reversible transition endotherm, not accompanied by mass-loss, around 230°C (Figure 4.3 and Table 4.1). The DSC curve for the physical mixture shows a dehydration endotherm from 62°C to 95°C, with $\Delta H = 61$ kJ $(mol\ GCD)^{-1}$ and broad endotherm associated with the melting of 5-ASA with onset 254°C and $\Delta H = 80$ kJ $(mol\ 5\text{-}ASA)^{-1}$. The DSC curve for the kneaded mixture shows a dehydration endotherm from 55°C to 98°C with $\Delta H = 120$ kJ $(mol\ GCD)^{-1}$ and a broad endotherm with onset 246°C, with $\Delta H = 67$ kJ $(mol\ 5\text{-}ASA)^{-1}$. There is also a reversible transition exotherm around 220°C.

The TG and DTG curves (Figure 6.26 and 6.27) show that the physical mixture undergoes an initial mass-loss of 5.0 % (from 50°C to 120°C), which is less than the expected value of 8.0 % for the loss of water in pure GCD in the mixture containing 89.4 % by mass of the GCD. The total mass-loss of 16 % (a further 11%) at about 270°C, is close to the expected value for the almost complete evaporation/decomposition of 11 % mass of 5-ASA in the mixture. The kneaded mixture shows an initial mass loss of 5 % which is less than expected. The total mass-loss at about 270°C is 9.5 % (a further loss of 4.5 %) which is also less than the expected value.

These results from both DSC and TG curves indicate some interaction between 5-ASA and GCD in both mixtures and are summarised in Table 6.3

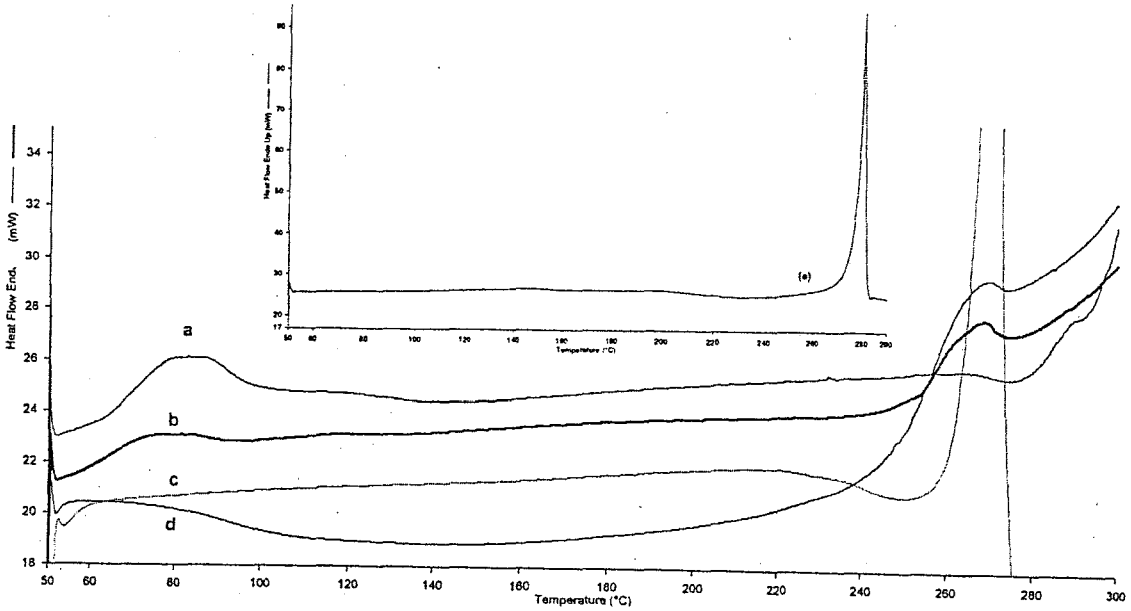

Figure 6.25: DSC curves of the pure components and for mixtures of 5-ASA with GCD: (a) pure GCD, (b) physical mixture, (c) kneaded mixture and (d) pure 5-ASA (e) enlarged y-axis scale for curve (d) (heated in flowing nitrogen at 10 K min^{-1} in uncrimped aluminium pans).

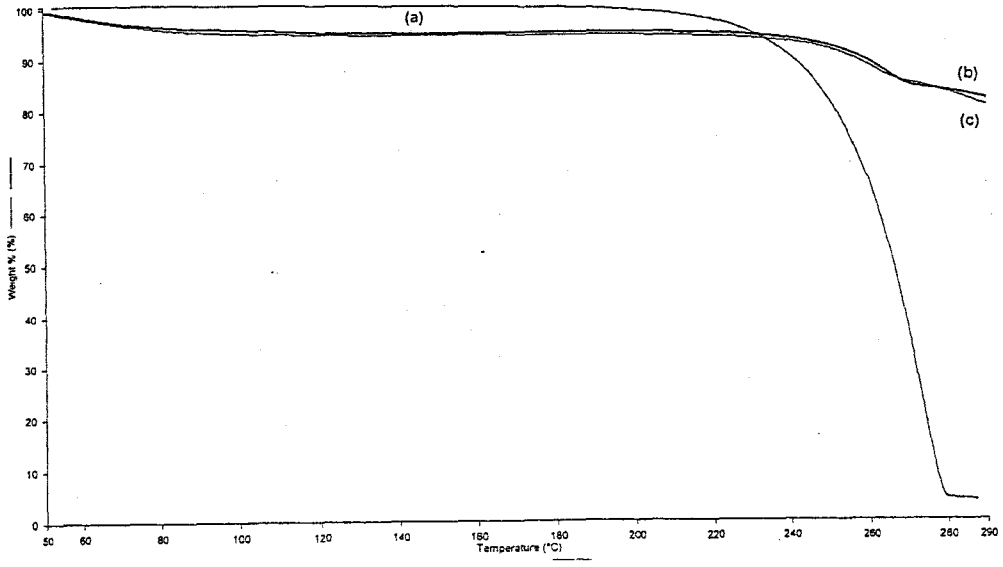

Figure 6.26: TG curves for 5-ASA and mixtures of 5-ASA with GCD: (a) pure 5-ASA, (b) kneaded mixture and (c) physical mixture (heated in flowing nitrogen at 10 K min^{-1} in open platinum pans).

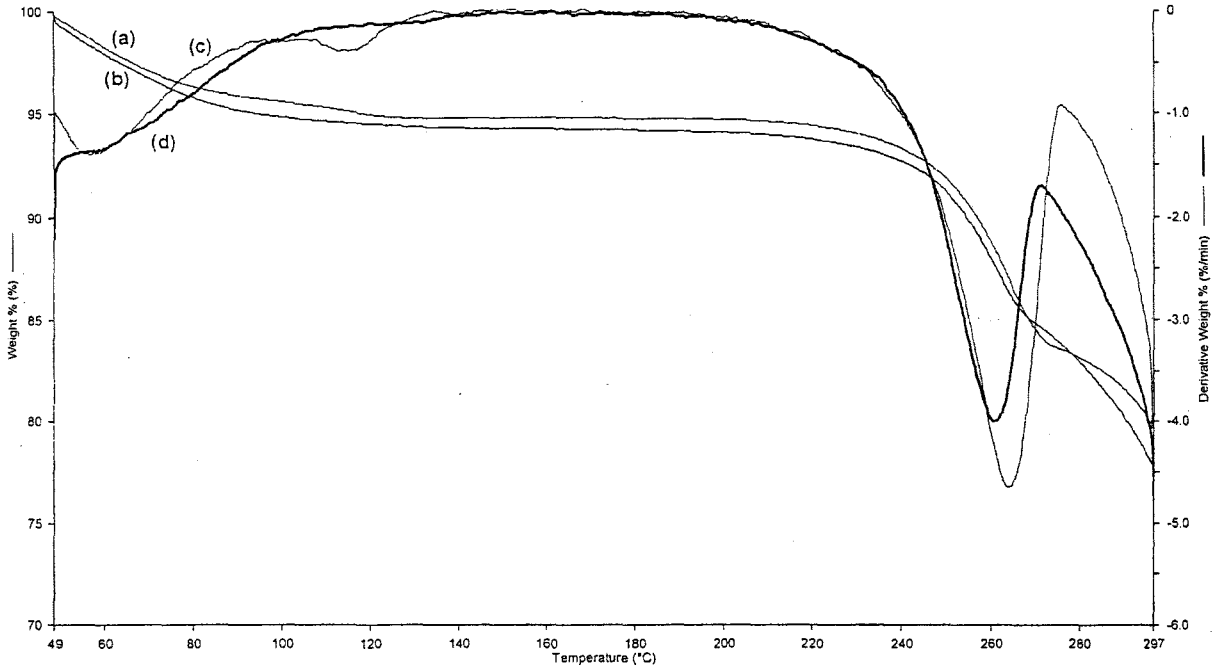

Figure 6.27: TG and DTG curves for mixtures of 5-ASA with GCD: TG curves: (a) kneaded mixture and (b) physical mixture, and DTG curves: (c) kneaded mixture and (d) physical mixture (heated in flowing nitrogen at 10 K min^{-1} in open platinum pans).

Table 6.1 Summary of the expected and observed thermal behaviour of 1:1 molar ratio mixtures of 3-ASA with the cyclodextrins (p = physical mixture and k= kneaded mixture)

1:1 molar ratio mixtures		Expected			Observed			
Mixture	% acid by mass	% mass loss CD	ΔH dehyd. / kJ (mol CD)$^{-1}$	ΔH_{melt} /kJ (mol acid)$^{-1}$		% mass loss CD	ΔH dehyd. / kJ (mol CD)$^{-1}$	ΔH_{melts} /kJ (mol acid)$^{-1}$
3-ASA/BCD	11.9	10.0	266	92.8	P	8.5	252	59
					k	2.0	0	69
3-ASA/HPBCD	9.8	5.4	64	92.8	p	5.0	100	5
					k	5.0	61	0
3-ASA/GCD	10.6	8.1	73	92.8	p	7.0	163	69
					k	3.0	65	10

Table 6.2 Summary of the expected and observed thermal behaviour of 1:1 molar ratio mixtures of 4-ASA with the cyclodextrins (p = physical mixture and k = kneaded mixture)

1:1 molar ratio mixtures		Expected			Observed			
Mixture	% acid by mass	% mass loss CD	ΔH dehyd. / kJ (mol CD)$^{-1}$	ΔH_{melt} / kJ (mol acid)$^{-1}$		% mass loss CD	ΔH dehyd. /kJ (mol CD)$^{-1}$	ΔH_{melts} /kJ (mol acid)$^{-1}$
4-ASA/BCD	11.9	10.0	266	25.6	p	5.5	184	32
					k	2.0	181	14
4-ASA/HPBCD	9.8	5.4	64	25.6	p	5.5	36	89
					k	1.0	0	0
4-ASA/GCD	10.6	8.1	73	25.6	p	5.0	69	0
					k	12.0	182	0

Table 6.3 Summary of the expected and observed thermal behaviour of 1:1 mole ratio mixtures of 5-ASA with the cyclodextrins (p= physical mixture and k = kneaded mixture)

1:1 molar ratio mixtures		Expected			Observed			
Mixture	% acid by mass	% mass loss CD	ΔH dehyd. / kJ (mol CD)$^{-1}$	ΔH_{melt} /kJ (mol acid)$^{-1}$	% mass loss CD		ΔH dehyd. / kJ (mol CD)$^{-1}$	ΔH_{melts} / kJ (mol acid)$^{-1}$
5-ASA/BCD	11.9	10.0	266	88.6	p	13.0	255	199
					k	12.0	199	122
5ASA/HPBCD	9.8	5.4	64	88.6	p	13.5	72	0
					k	6.0	52	0
5-ASA/GCD	10.6	8.1	73	88.6	p	5.0	61	80
					k	6.0	120	67

6.5 Discussion

The following conclusions can be drawn from the results summarised in Tables 6.1, 6.2, and 6.3.

Generally, as expected, the kneaded mixtures show greater changes in thermal behaviour from that of the individual components than do the physical mixtures but the changes in the physical mixtures are also significant. There is evidence that kneading process can displace water from the CDs.

From thermal analysis it is, of course, not possible to separate the interactions caused by mixing from those produced by subjecting the mixture (be it physical or kneaded) to a heating programme. It is here that XRD and IR results (see Sections 7, 8 and 9) on unheated mixtures can provide important information at the molecular level. Determining whether some kind of interaction may have occurred is relatively simple compared to determining the nature of the interaction. From thermal analysis, the disappearance of the melting endotherms of the ASAs in the DSC curves of the mixtures with the CDs is the main indicator of an interaction.

TG can support the indications of DSC by providing quantitative information on the water content of the CD, which could be expected to be changed by the occurrence of inclusion. TG can also reveal the extent of evaporation/ decomposition of the guest from the mixture. The guest must, of course, undergo some thermal event, such as melting or vaporisation at temperatures below those at which CD itself degrades [111].

Szente [111] has formulated some of the questions which need to be answered concerning the nature of the interactions of the mixtures of potential guests with

host CDs. These include determining whether the guest actually enters the CD cavity and how much of the guest remains outside the cavity. An additional aspect, seen in the present study, is the fate of water molecules already hosted within the CD cavity when the CD is mixed with another potential guest substance. Various possibilities of interaction exist. The guest can replace all the water and this expelled water can be lost from the mixture during, or soon after, the mixing process. This would be clearly shown by both disappearance of the dehydration endotherm from the DSC curves of the mixtures and the absent, or decreased, initial mass loss in the TG curves.

The next possibility would be that all, or most, of the water expelled from the CD cavities remains, although more loosely-bound, in the mixture and is released on heating with a similar mass-loss to that for the individual CD, but a decreased enthalpy of dehydration. Alternatively, some of the water molecules may share the CD cavity with the guest molecule, G, forming a type of hydrate, $G.nH_2O$, stabilised within the cavity and behaving differently to pure guest, G.

Another possibility is that the guest molecules may only enter the cavity during the heating programme when the water molecules are expelled. Because dissociation of host-guest complexes will be endothermic and the formation of host-guest complexes could be close to thermally neutral, an apparent disappearance of, or marked decrease in the size of, the dehydration endotherm for the host CD could be observed.

Comparison of the effects of the different CDs on the behaviour of individual ASA isomers shows that HPBCD has the greatest interaction with 3-ASA and 5-ASA, followed by GCD, while BCD generally shows the least interaction. For 4-ASA,

the effect of GCD seems to be more marked than for 3-ASA and 5-ASA. Reasons for these observations must involve the cavity sizes of the CDs and the molecular structures of the acids.

6.6 Thermal behaviour of kneaded cyclodextrins

There is a possibility that the kneading process can displace water from the cavity of the CDs and thus affect their thermal behaviour.

Samples of cyclodextrins BCD, HPBCD and GCD were kneaded with ethanol (as described in Section 2.2) but in absence of any other potential guest substance. The DSC curves for kneaded cyclodextrins did not show the expected dehydration endotherms and reversible transitions at 220°C. The TG curves (Figure 6.28, 6.29 and 6.30) show mass-losses at temperatures between 50°C and 75°C. The percentage mass-losses for the kneaded CDs were found to be 11.5%, 4.4% and 7.0% for BCD, HPBCD and GCD, respectively, compared to the original values of 11.4%, 6.0% and 9.0%, respectively (Table 4.1).

The possibility could be that the water expelled from the CD cavities remains, although more loosely-bound, in the mixture and is released on heating with a similar or lower mass-loss than that for the individual CD, but no enthalpy of dehydration [111].

The IR spectra (Figures 6.31, 6.32 and 6.33) of the kneaded samples are very similar to the spectra of the original samples, except for BCD where the band at 1520 cm^{-1} in the original is absent in the kneaded sample. X-ray powder diffraction patterns before and after kneading are compared in Section 7.1.

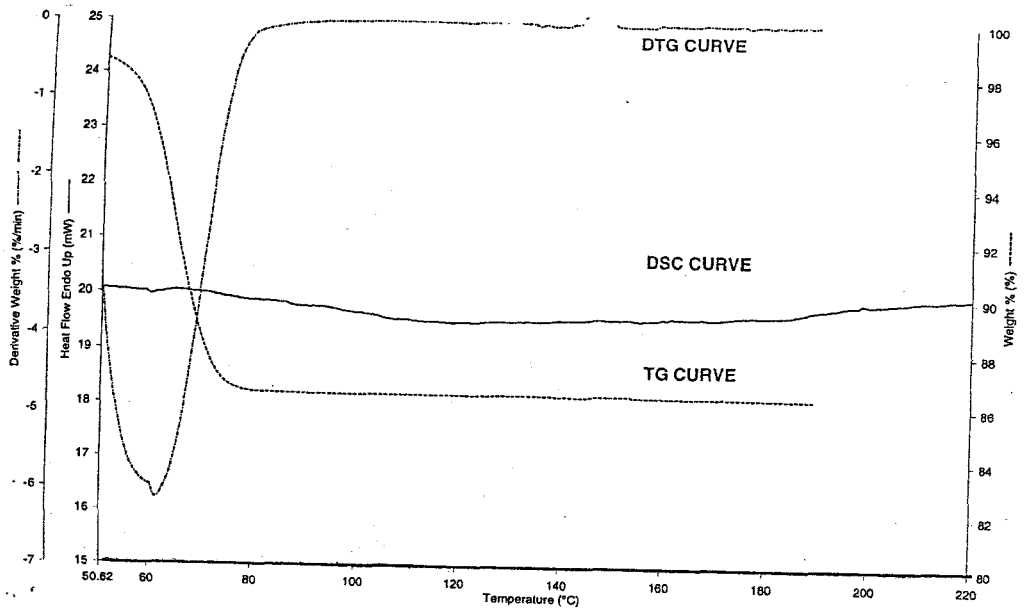

Figure 6.28: The DSC, TG and DTG curves for BCD after kneading with solvent only and drying (heated in flowing nitrogen at 10 K min^{-1}: uncrimped aluminium for DSC and open platinum pan for TG).

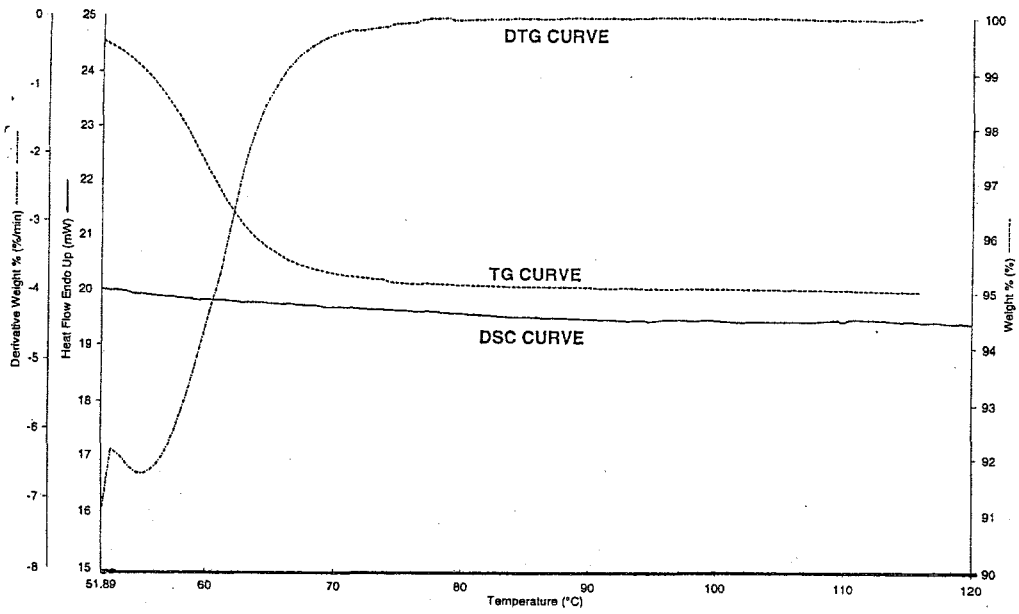

Figure 6.29: The DSC, TG and DTG curves for HPBCD after kneading with solvent only and drying (heated in flowing nitrogen at 10 K min^{-1}: uncrimped aluminium for DSC and open platinum pan for TG).

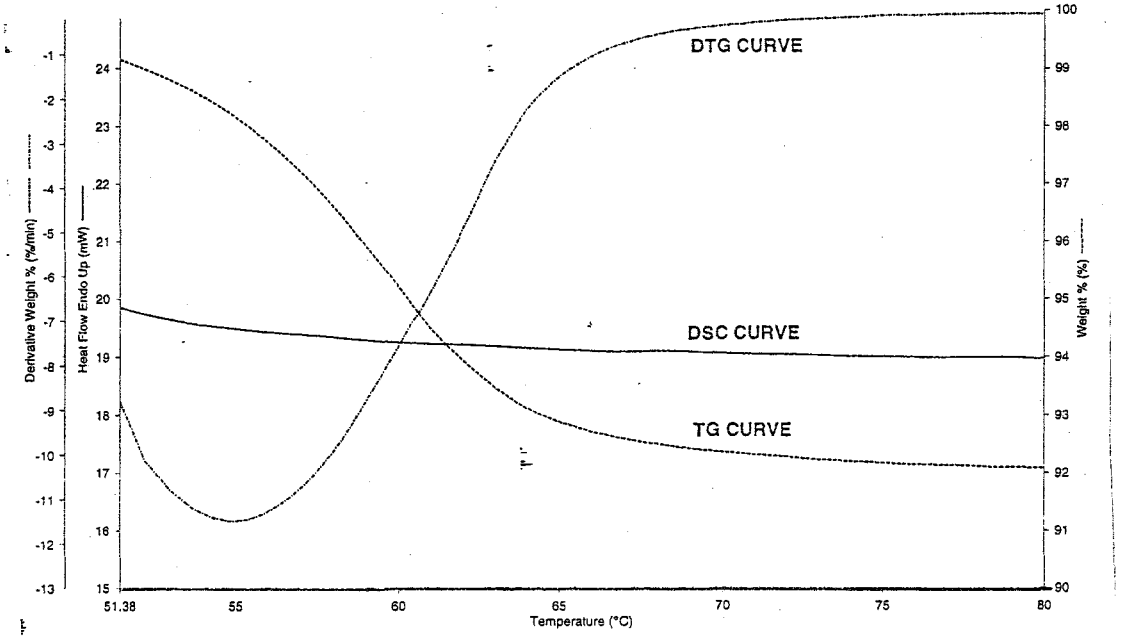

Figure 6.30: The DSC, TG and DTG curves for GCD after kneading with solvent only and drying (heated in flowing nitrogen at 10 K min^{-1}: uncrimped aluminium for DSC and open platinum pan for TG).

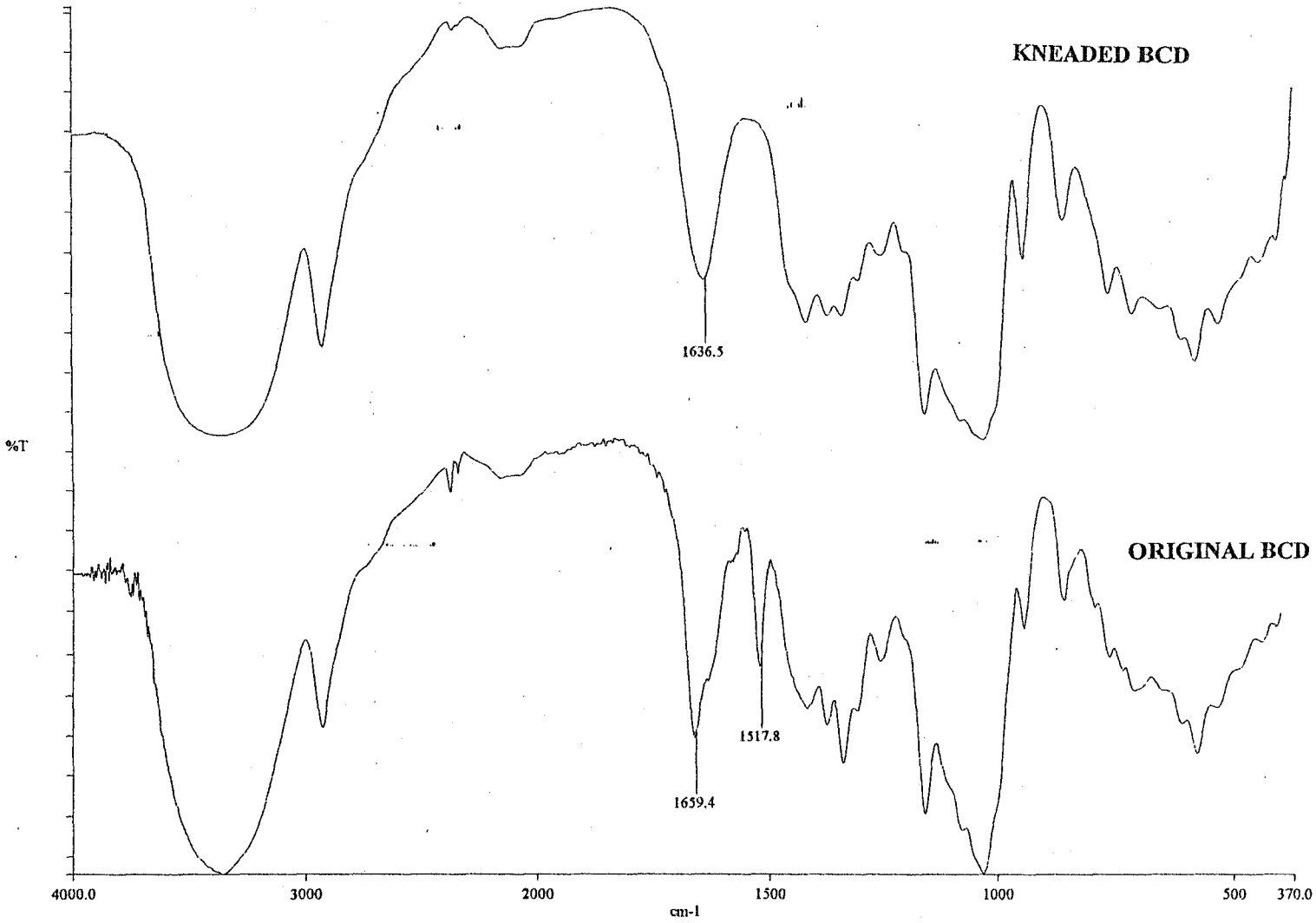

Figure 6.31: IR spectra of the original and kneaded BCD samples.

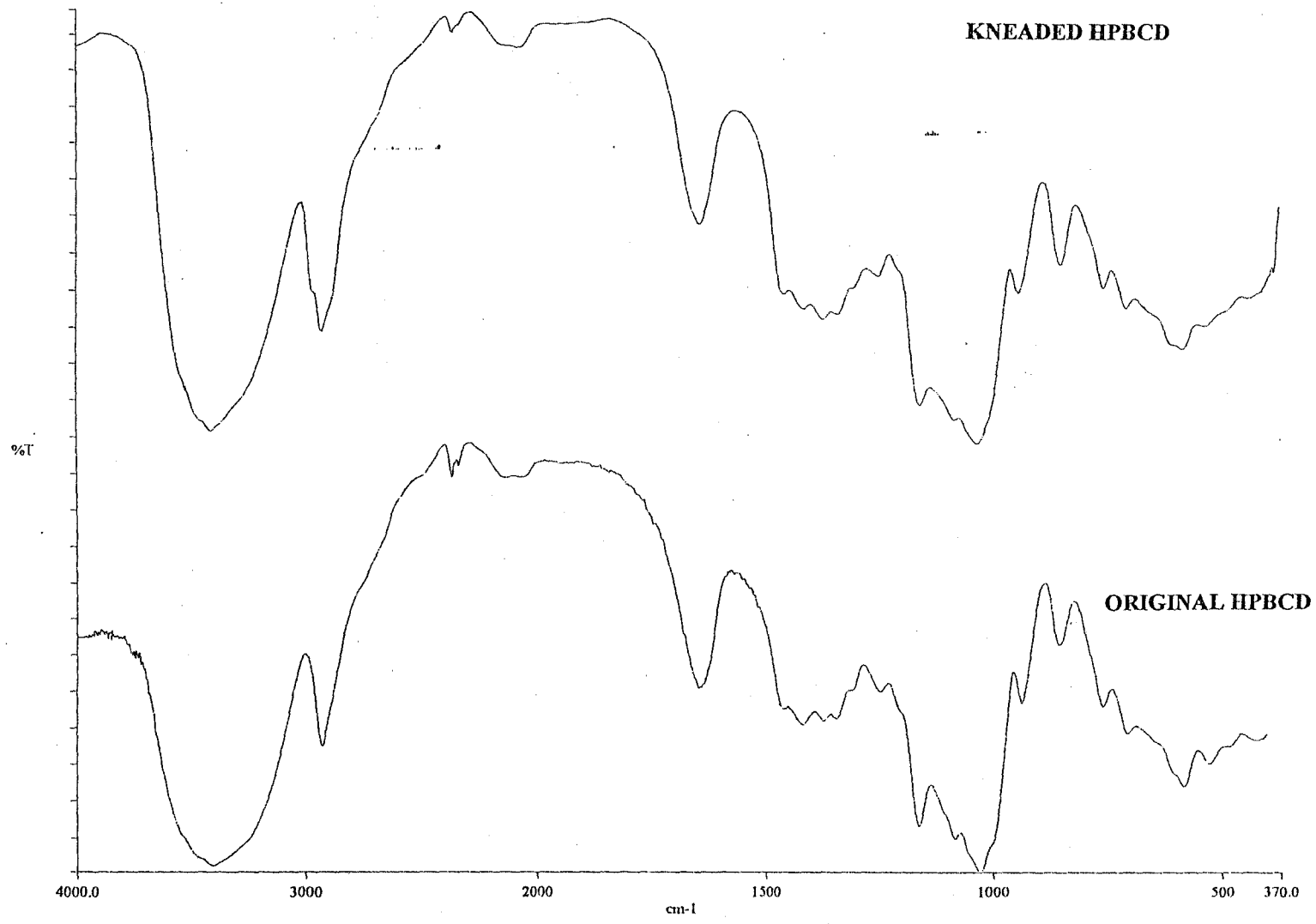

Figure 6.32: IR spectra of the original and kneaded HPBCD samples.

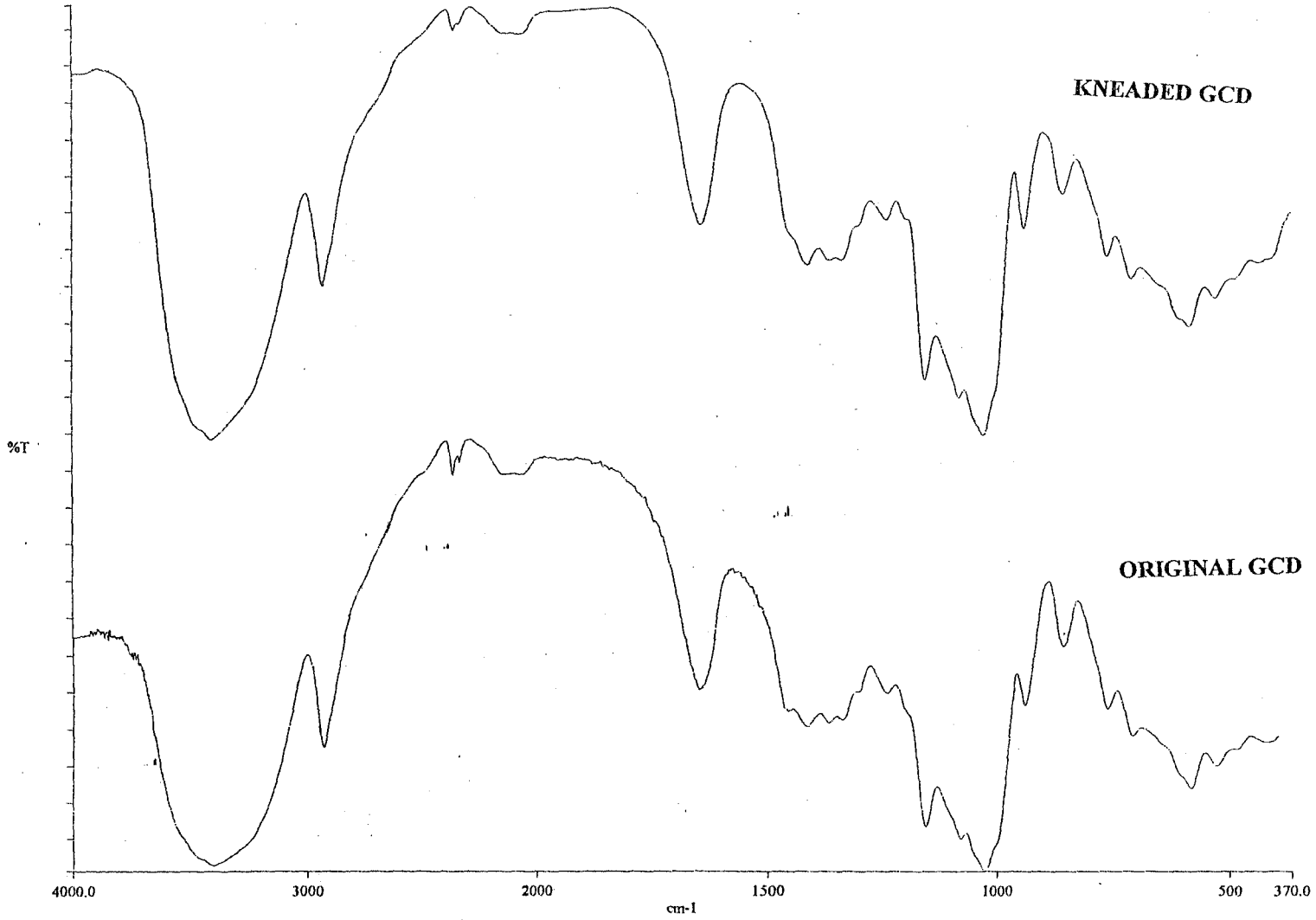

Figure 6.33: IR spectra of the original and kneaded GCD samples.

7. X-RAY POWDER DIFFRACTION STUDIES OF MIXTURES OF THE REFERENCE ACIDS (BA AND SA) WITH THE CYCLODEXTRINS

7.1 The cyclodextrins

X-ray powder diffraction patterns (recorded as described in Section 2.4.1) were used to check the possible interactions of the reference acids (BA and SA) with the three cyclodextrins (BCD, HPBCD and GCD). The X-ray powder patterns for the three cyclodextrins are shown in Figure 7.1. BCD is the most crystalline of the three and HPBCD the least. Interaction between a guest molecule and a cyclodextrin host will usually change the crystalline structure of the CD and hence the X-ray diffraction pattern. Crystalline compounds give clear and sharp X-ray diffraction patterns, while amorphous compounds give diffuse diffraction patterns. The diffuse nature of an X-ray powder pattern of a host/guest mixture may also be an indication of inclusion of the guest molecule into the cavity of the host compound.

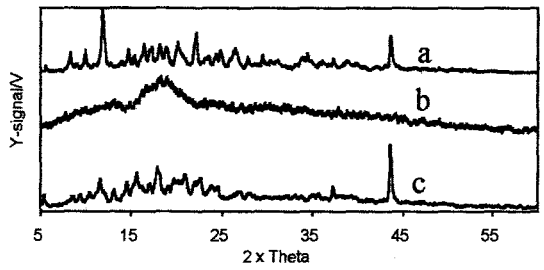

Figure 7.1: X-ray powder diffraction patterns for (a) BCD, (b) HPBCD, and (c) GCD.

It is also possible that the kneading process (Section 2.2 and Section 6.6) using ethanol as a solvent could affect the crystallinity of the CDs. Samples of the CDs

were thus treated in a similar manner to the kneading process, and X-ray diffraction patterns of the resulting powders were recorded under the same conditions as for the original samples (Figure 7.2).

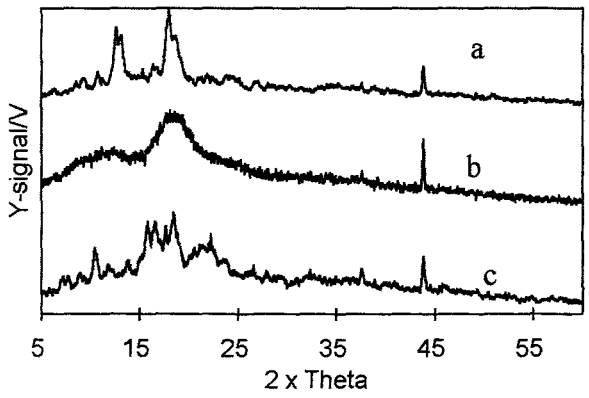

Figure 7.2: X-ray powder diffraction patterns for (a) BCD, (b) HPBCD and (c) GCD after kneading with solvent only and drying (Section 2.2).

The XRPD patterns of the CDs after kneading do indicate changes in crystallinity. BCD appears to be slightly less crystalline, HPBCD more crystalline and GCD is little changed. These changes need to be taken into consideration when comparing physical and kneaded mixtures. The effects of the kneading solvent on CDs were examined further using DSC, TG and IR (Section 6.6).

7.2 Mixtures of benzoic acid (BA) with the cyclodextrins

Figure 7.3 shows the X-ray powder diffraction patterns of the pure components and of the mixtures of benzoic acid with BCD. The XRPD patterns for both physical and kneaded mixtures are different from each other and from those of the pure components. The kneaded mixture is the least crystalline. Indications are

that there is significant interaction between BA and BCD.

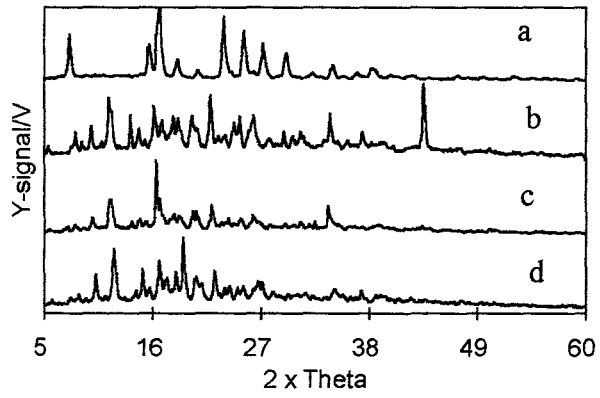

Figure 7.3: X-ray powder diffraction patterns for (a) BA, (b) BCD, (c) BA/BCD physical mixture, and (d) BA/BCD kneaded mixture (mixtures are 1:1 molar ratios).

Figure 7.4 shows X-ray powder diffraction patterns of the pure components and of the mixtures of BA with HPBCD. The XRPD pattern for HPBCD is diffuse to start with so changes are difficult to determine. The physical mixture shows a diffraction peak at about $2\theta = 17°$ which is characteristic of BA. This peak is not evident in the kneaded mixture, so the possibility of interaction after kneading exists.

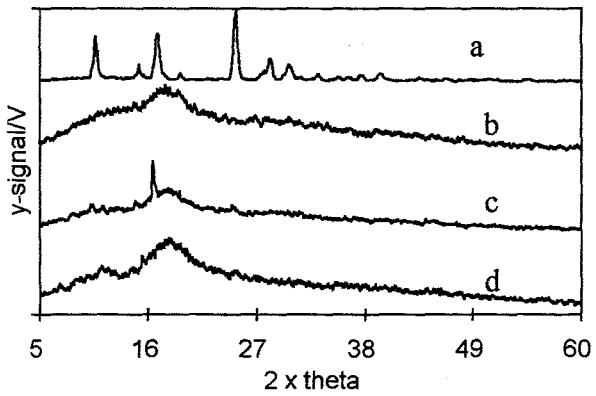

Figure 7.4: X-ray powder diffraction patterns for (a) BA, (b) HPBCD, (c) BA/HPBCD physical mixture, and (d) BA/HPBCD kneaded mixture.

Figure 7.5 shows the X-ray powder patterns of the pure components and of the mixtures of BA with GCD. The most intense peak of the GCD pattern at about $2\theta = 43°$ disappears in the XRPD patterns of the mixtures, while the most intense peak for BA at about $2\theta = 25°$ is present. This suggests that some crystalline BA remains unaffected.

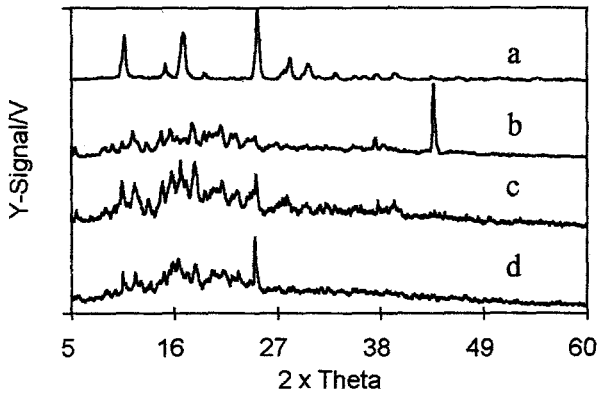

Figure 7.5: X-ray powder diffraction patterns for (a) BA, (b) GCD, (c) BA/GCD physical mixture, and (d) molar BA/GCD kneaded mixture.

The three cyclodextrins differ in their degree of crystallinity as well as their cavity size (see Table 4.1). Both of these factors could influence the possible inclusion of BA. In general the crystallinity of the host appears to be decreased by the formation of mixtures.

7.3 Mixtures of salicylic acid (SA) with the cyclodextrins (CDs)

Figure 7.6 shows the X-ray powder diffraction patterns of the pure components and of the 1:1 molar ratio mixtures of salicylic acid (SA) with BCD. The XRPD patterns of both physical and kneaded mixtures are quite different from those of the pure components and from each other. As usual, the kneaded mixtures show the greater changes.

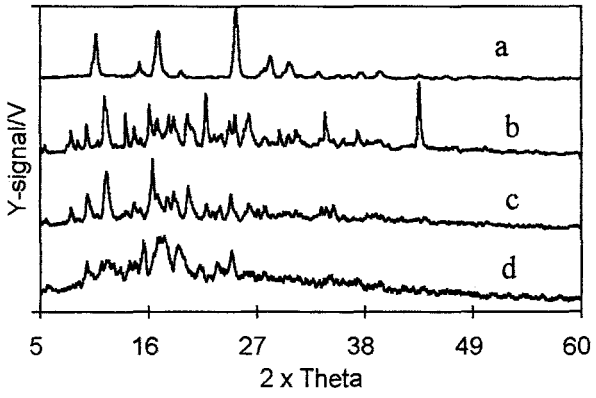

Figure 7.6: X-ray powder diffraction patterns for (a) SA, (b) BCD, (c) SA/BCD physical mixture, and (d) SA/BCD kneaded mixture.

Figure 7.7 shows the X-ray diffraction patterns of the pure components and of the mixtures of SA with HPBCD. XRPD patterns for the physical and the kneaded mixtures are diffuse and similar to HPBCD. The absence of any of the lines for SA is an indication of possible interaction between SA and HPBCD. Behaviour is very similar to that of BA/HPBCD.

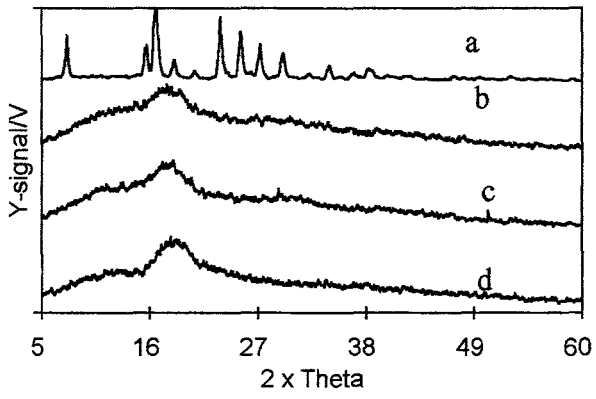

Figure 7.7: X-ray powder diffraction patterns for (a) SA, (b) HPBCD, (c) SA/HPBCD physical mixture, and (d) SA/HPBCD kneaded mixture..

Figure 7.8 shows the X-ray diffraction patterns of the pure components and of the mixtures of SA with GCD. The XRPD pattern for the kneaded mixture is more diffuse than that of the physical mixture. The XRPD pattern for the physical mixture is also different from those of the pure components. The prominent peak for GCD at about $2\theta = 43°$ is missing in the XRPD patterns for both mixtures. The XRPD patterns for both mixtures indicate interaction between SA and GCD. Behaviour is similar to that of BA/GCD.

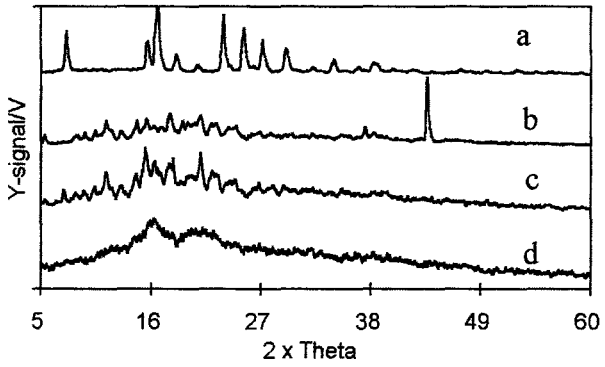

Figure 7.8: X-ray powder diffraction patterns for (a) SA, (b) GCD, (c) SA/GCD physical mixture, and (d) SA/GCD kneaded mixture.

Figure 7.9 compares the XRPD patterns for the physical and kneaded mixtures of BA with BCD and similar mixtures of SA with BCD. The changes observed in the XRPD powder patterns of BCD on mixing with SA are similar to those found for mixtures of BCD with BA. The patterns for the kneaded mixtures differ more than those of the physical mixtures.

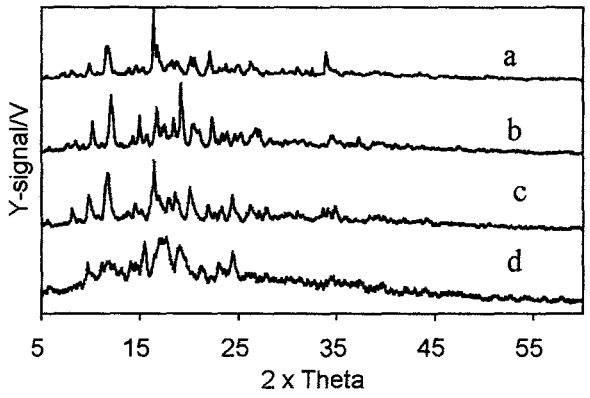

Figure 7.9: X-ray powder diffraction patterns for (a) BA/BCD physical mixture, (b) BA/BCD kneaded mixture, (c) SA/BCD physical mixture, and (d) SA/BCD kneaded mixture.

8. X-RAY POWDER DIFFRACTION STUDIES OF MIXTURES OF AMINOSALICYLIC ACIDS (ASAs) WITH CYCLODEXTRINS (CDs)

8.1 Introduction

The approach used was the same as in Section 7. The XRPD patterns for 1:1 molar ratio physical and kneaded mixtures of 3-ASA, 4-ASA and 5-ASA with the three CDs (BCD, HPBCD and GCD) were recorded and compared with the patterns of the pure components. The powder patterns for the three isomers of ASA are compared in Figure 8.1. The three patterns are very different.

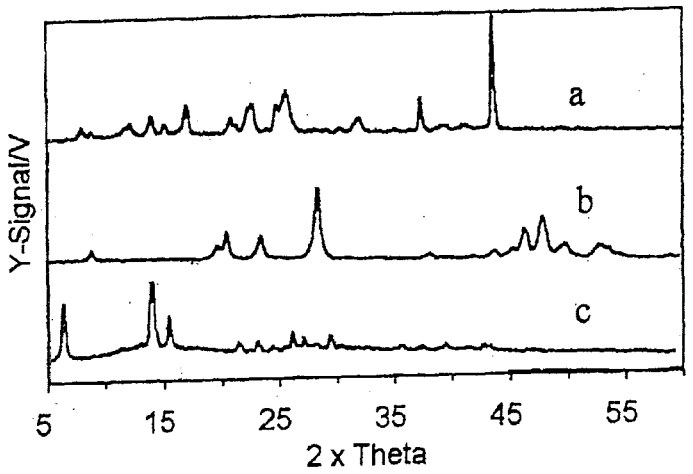

Figure 8.1: X-ray powder diffraction patterns for (a) 3-ASA, (b) 4-ASA, and (c) 5-ASA.

8.2 Mixtures of 3-ASA with cyclodextrins

Figure 8.2 shows the X-ray powder diffraction patterns of the pure components and of mixtures of 3-ASA with BCD. The XRPD pattern for pure 3-ASA is quite different from those of the mixtures. The patterns for the kneaded and the physical mixtures are similar, but the pattern of the kneaded mixture is less detailed than that

that of the physical mixture. Interesting features are the high intensity peaks at about $2\theta = 43°$ in the patterns of both 3-ASA and BCD and the persistence of this peak in the mixtures. The large peak at about $2\theta = 12°$ for BCD also persists in the mixtures.

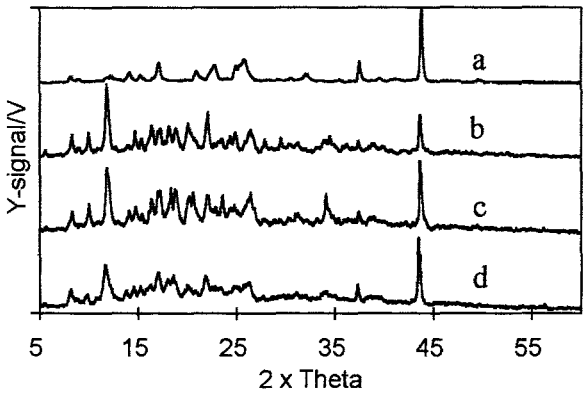

Figure 8.2: X-ray powder diffraction patterns for (a) 3-ASA, (b) BCD, (c) 3-ASA/BCD physical mixture, and (d) 3-ASA/BCD kneaded mixture.

Figure 8.3 shows the X-ray powder diffraction patterns of the pure components and of the mixtures of 3-ASA with HPBCD. The XRPD pattern for HPBCD is diffuse and this shows its amorphous nature. The pattern for the physical mixture shows the main diffraction lines associated with 3-ASA while the pattern for the kneaded mixture is different from those of pure components but indicates a higher degree of crystallinity in a new crystal structure. This could indicate that the kneading process has led to the formation of a crystalline 3-ASA/HPBCD complex.

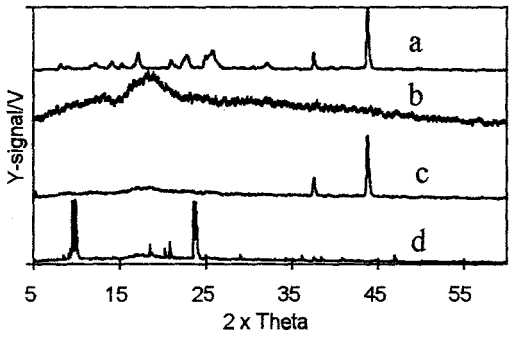

Figure 8.3: X-ray powder diffraction patterns for (a) 3-ASA, (b) HPBCD, (c) 3-ASA/HPBCD physical mixture, and (d) 3-ASA/HPBCD kneaded mixture.

Figure 8.4 shows the X-ray powder diffraction patterns of the pure components and of the mixtures of 3-ASA with GCD. The coincidence of the strong peak at about $2\theta = 43°$ in the patterns of both 3-ASA and GCD complicates the interpretation of the patterns of the mixtures because this peak persists in the patterns of both the kneaded and physical mixtures. The pattern for the physical mixture could be mainly superposition of the patterns of the pure components. The pattern for the kneaded mixture is more diffuse, but some unaffected crystalline 3-ASA or GCD could be present.

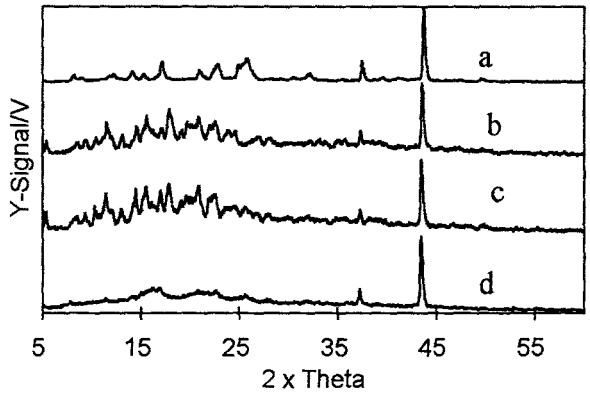

Figure 8.4: X-ray powder diffraction patterns for (a) 3-ASA, (b) GCD, (c) 3-ASA/GCD physical mixture, and (d) 3-ASA/GCD kneaded mixture.

8.3 Mixtures of 4-ASA with the cyclodextrins.

Figure 8.5 shows the X-ray powder diffraction patterns of the pure components and of the mixtures of 4-ASA with BCD. Individual components show well-resolved crystalline patterns. The pattern for the physical mixture is fairly similar to that of pure BCD with the major peaks related to pure 4-ASA not apparent. The pattern for the kneaded mixture is still crystalline but different from that of the physical mixture. The strong peak at $2\theta = 43°$, characteristic of BCD, persists in both mixtures.

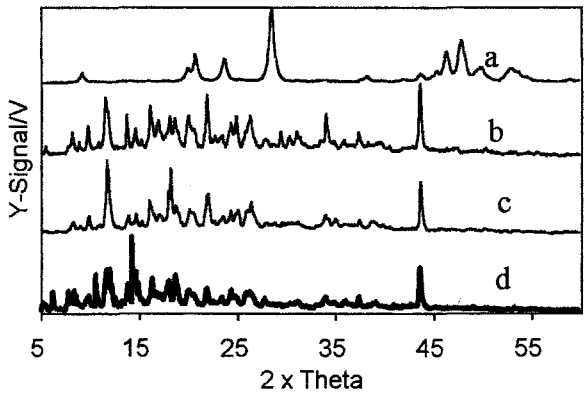

Figure 8.5: X-ray powder diffraction patterns for (a) 4-ASA, (b) BCD, (c) 4-ASA/BCD physical mixture, and (d) 4-ASA/BCD kneaded mixture.

Figure 8.6 shows the X-ray powder diffraction patterns of the pure components and of the mixtures of 4-ASA with HPBCD. The pattern of both mixtures show a strong peak at about $2\theta = 43°$ which is not a feature of the pattern of either 4-ASA or HPBCD. It is a feature though of the more crystalline cyclodextrins. Some of the features in the pattern of the physical mixture could be from some unaffected crystalline 4-ASA.

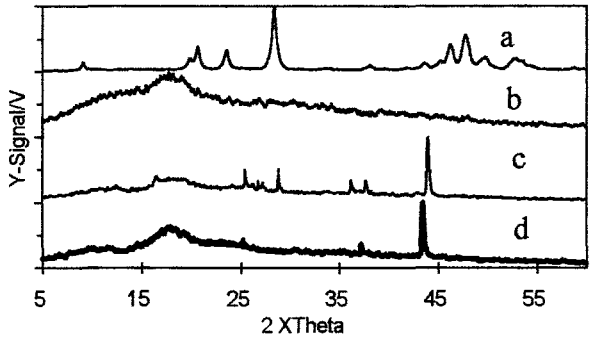

Figure 8.6: X-ray powder diffraction patterns for: (a) 4-ASA, (b) HPBCD, (c) 4-ASA/HPBCD physical mixture, and (d) 4-ASA/HPBCD kneaded mixture.

Figure 8.7 shows the X-ray powder diffraction patterns of the pure components and of the mixtures of 4-ASA with GCD. The increased detail in the high angle regions of the patterns of the physical and the kneaded mixtures suggests that extensive structural changes have occurred on mixing of the components and that the kneading process has enhanced these.

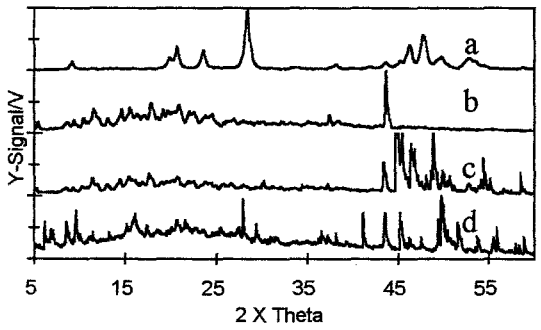

Figure 8.7: X-ray powder diffraction patterns for (a) 4-ASA, (b) GCD, (c) 4-ASA/GCD physical mixture, and (d) 4-ASA/GCD kneaded mixture.

8.4 Mixtures of 5-ASA with the cyclodextrins.

Figure 8.8 shows the X-ray powder diffraction patterns of the pure components and of the mixtures of 5-ASA with BCD. The X-ray powder diffraction pattern of 5-ASA is different from, and simpler than, that of 4 -ASA. The XRPD patterns for both the physical and the kneaded mixtures are similar to that of pure BCD and contributions from pure crystalline 5-ASA are not evident.

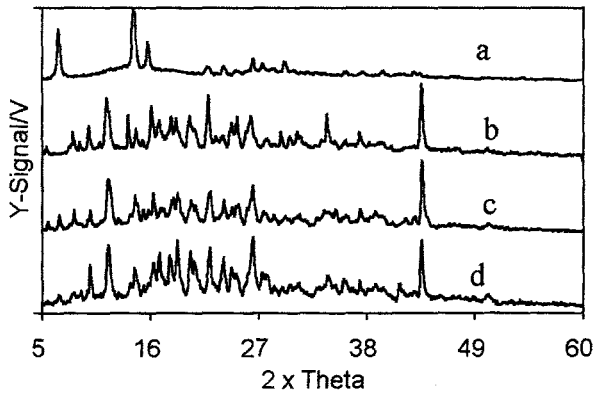

Figure 8.8: X-ray powder diffraction patterns for (a) 5-ASA, (b) BCD, (c) 5-ASA/BCD physical mixture, and (d) 5-ASA/BCD kneaded mixture.

Figure 8.9 shows the X-ray powder diffraction patterns of the pure components and of the mixtures of 5-ASA with HPBCD. The differences between the patterns of the kneaded mixture and the physical mixture are very marked and indicate significant interaction between the two compounds with the formation of crystalline substances. The sort of changes observed are similar, but not identical, to those observed for 4-ASA/HPBCD mixtures.

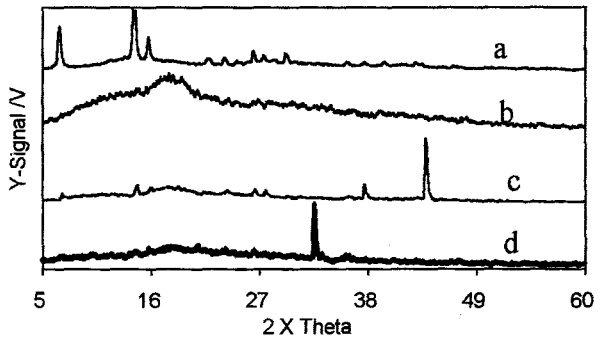

Figure 8.9: X-ray powder diffraction patterns for (a) 5-ASA, (b) HPBCD, (c) 5-ASA/HPBCD physical mixture, and (d) 5-ASA/HPBCD kneaded mixture.

Figure 8.10 shows the X-ray powder diffraction patterns of the pure components and of the mixtures of 5-ASA with GCD. The patterns for both mixtures are similar to those for pure GCD with the kneaded mixture showing fewer details than the physical mixture. The changes observed are very different from those observed for 4-ASA/GCD mixtures, but resemble those for 3-ASA/GCD mixtures.

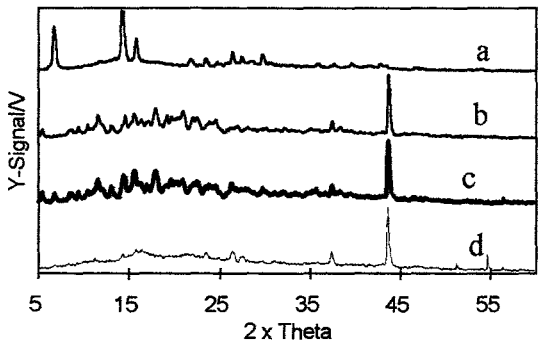

Figure 8.10: X-ray powder diffraction patterns for: (a) 5-ASA, (b) GCD, (c) 5-ASA/GCD physical mixture, and (d) 5-ASA/GCD kneaded mixture.

Figures 8.11, 8.12 and 8.13 compare the XRPD patterns of the kneaded mixtures of the three ASA isomers with each of the three cyclodextrins.

Figure 8.11 shows the patterns for the ASAs with BCD. The XRPD patterns for these mixtures are all different from each other and from that of pure BCD (see Figure 7.1). The pattern for the 3-ASA/BCD mixture is the least crystalline and that for the 5-ASA/BCD mixture the most crystalline.

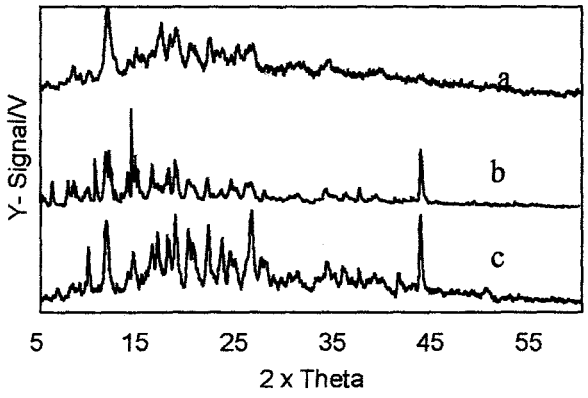

Figure 8.11: X-ray powder diffraction patterns for the kneaded mixtures of: (a) 3-ASA, (b) 4-ASA, and (c) 5-ASA with BCD.

Figure 8.12 shows the XRPD patterns of the kneaded mixtures of the three ASA isomers with HPBCD. For all the mixtures the patterns show that their patterns are more diffuse that the XRPD patterns for the pure components (Figure 8.1). The pattern for the kneaded mixture of 3-ASA with HPBCD is the most diffuse.

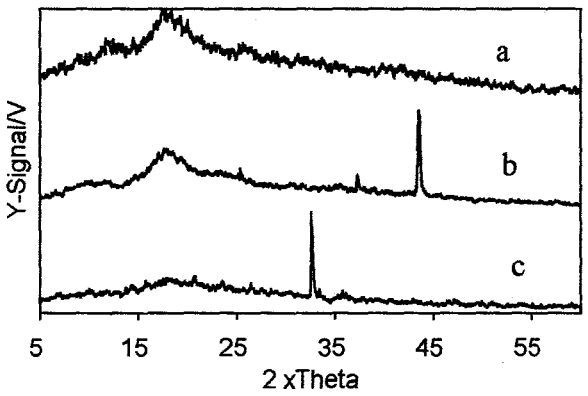

Figure 8.12: X-ray powder diffraction patterns for the kneaded mixtures of (a) 3-ASA, (b) 4-ASA, and (c) 5-ASA with HPBCD.

Figure 8.13 shows the XRPD patterns for the three ASA isomers with GCD. The XRPD pattern for the mixture of 4-ASA with GCD shows the greatest crystallinity. The region of $2\theta = 40°$ to $60°$ is more detailed than in pure 4-ASA (Figure 8.1). The XRPD patterns for 3-ASA and 5-ASA with GCD are much more diffuse.

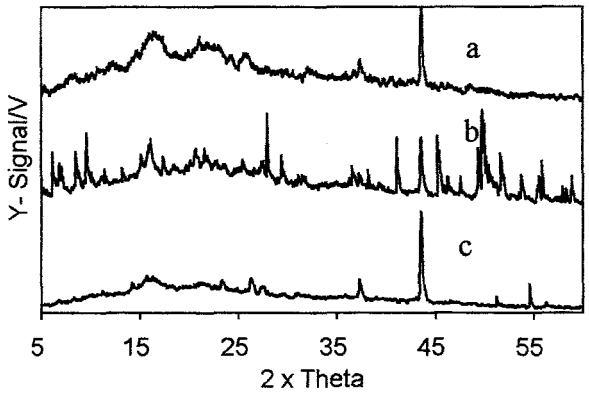

Figure 8.13: X-ray powder diffraction patterns for the kneaded mixtures of (a) 3-ASA, (b) 4-ASA, and (c) 5-ASA with GCD.

8.5 Discussion

Presumably, obtaining a crystalline diffraction pattern for a mixture, which differs significantly from the patterns of the guest substance and from that of the host CD (if it is crystalline), is a better indication of inclusion than obtaining a diffuse pattern. Care is needed however, in interpreting results because the kneading solvent can affect the crystallinity (see Section 7.1). This influence could occur in the kneaded mixtures of 4-ASA with BCD and with GCD.

9. INFRARED SPECTROSCOPIC STUDIES ON THE REFERENCE ACIDS (BA AND SA) AND THEIR MIXTURES WITH CYCLODEXTRINS

9.1 Infrared studies

Confirmation of the formation of host-guest inclusion complexes relies on a variety of complementary evidence. The thermal behaviour of mixtures of potential guests, prepared under conditions likely to favour inclusion, such as the kneading process described in Section 2.2, may suggest that inclusion has occurred. Such indications can be explored further using techniques such as X-ray powder diffraction (see Sections 7 and 8) and infrared spectroscopy (this and the following sections).

The use of infrared spectroscopy (IR) is not always suitable for the study of inclusion because the absorption bands arising from the cyclodextrin structure may interfere with the bands of any included molecule. The C=O (carbonyl carbon) absorption region (around 1700 cm^{-1}) is not, however, usually interfered with and most researchers have made use of this region to study the interactions of the guest and host compounds [112]. It should also be noted that the cyclodextrins have a characteristic band at 1640 cm^{-1} because of the presence of some moisture [76].

Physical and kneaded mixtures were prepared as described in Section 2.2 and infrared spectra were recorded as described in Section 2.4.2 for the pure components and for the mixtures.

9.2 The IR spectra of the cyclodextrins

The IR spectra of BCD, HPBCD and GCD are compared in Figure 9.1. A broad absorption band at 3600-3100 cm^{-1}, with a shoulder at 2920 cm^{-1} is observed for

all three CDs. For HPBCD and GCD there are absorption bands at 2360 cm^{-1}, and at 2366 cm^{-1} for BCD. A band at 1646 cm^{-1} was observed for both HPBCD and GCD, but for BCD the band was at 1663 cm^{-1}. A unique absorption band at 1521 cm^{-1} was also observed for BCD. The slight variations in the absorption bands for CDs could be as a result of the different structures of the compounds, especially the amorphous nature of the HPBCD.

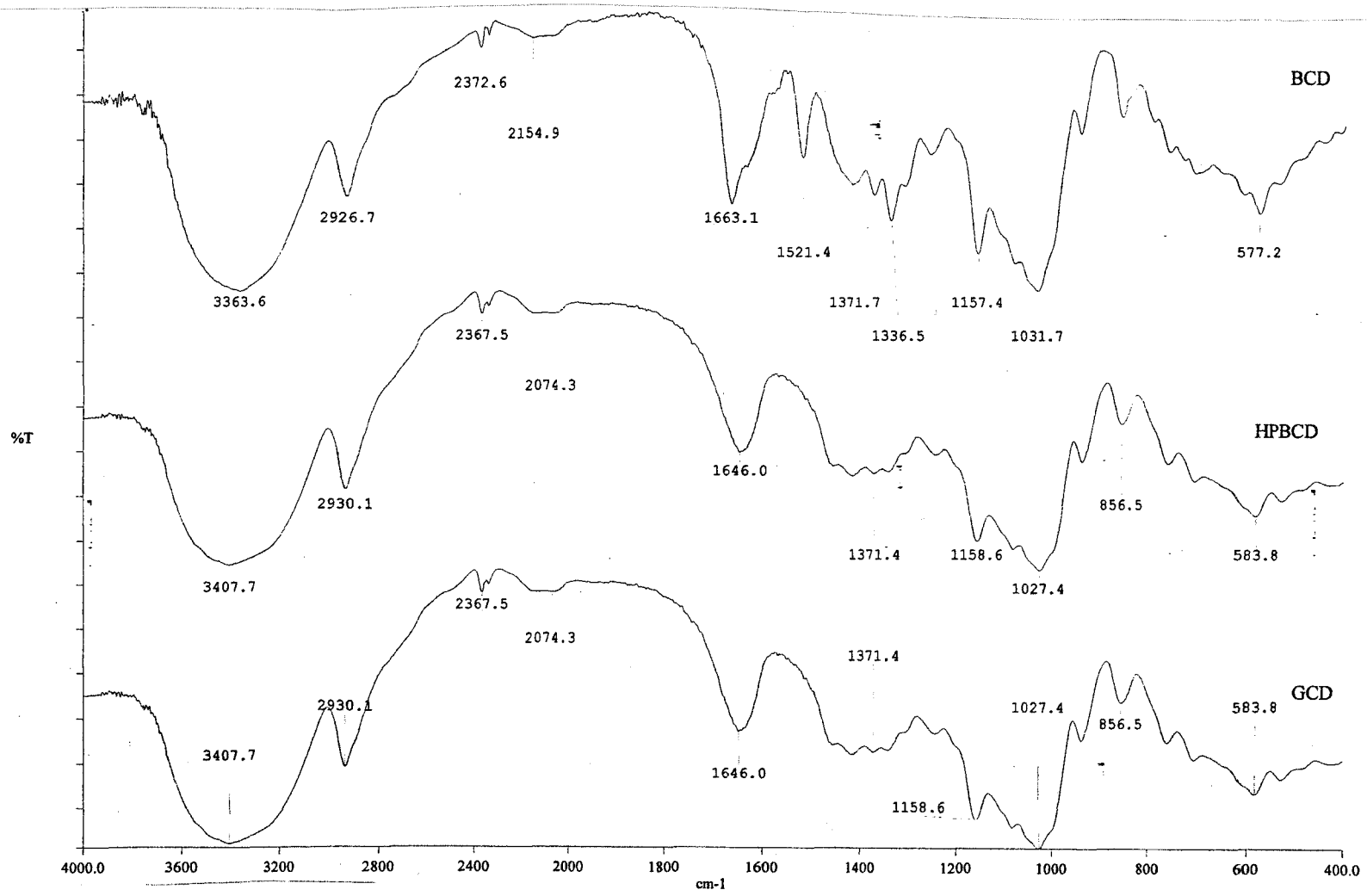

Figure 9.1: Infrared spectra of the cyclodextrins: (a) BCD, (b) HPBCD and (c) GCD .

9.3 Mixtures of benzoic acids (BA) with the cyclodextrins

The infrared spectra of BA, BCD and their physical and kneaded mixtures are shown in Figure 9.2. The spectra of the physical and the kneaded mixtures are very similar to each other and to that of BCD except for the region from about 1200-800 cm^{-1}. The band at 1688 cm^{-1} in the spectrum of BA is associated with the carbonyl-carbon absorption and changes in this band are useful in monitoring the interaction process. There is also a broad absorption in this range in the spectrum of BCD (max. at 1661 cm^{-1}). In the physical mixture, the apparent maximum of the superimposed contributing bands is at 1656 cm^{-1} and in the kneaded mixture, this maximum is at 1663 cm^{-1}. The region between this band and the next band that is common to all three spectra at about 1158 cm^{-1} shows the greatest effect of interactions.

The IR spectra of BA, HPBCD and their physical and kneaded mixtures are shown in Figure 9.3. The physical and the kneaded mixture differ from each other in the C = O absorption region and in the band at about 2930 cm^{-1}. The C=O absorption bands are observed at 1706 cm^{-1} and 1645 cm^{-1} (doublet band) for the physical mixture and for the kneaded mixture the absorption band is also a doublet at 1643 cm^{-1}. The band for the kneaded mixture has thus shifted slightly towards lower wave numbers.

The IR spectra of BA, GCD and their physical and kneaded mixtures are shown in Figure 9.4. The differences between the spectra of the physical mixture and kneaded mixtures are small and, again mainly in the region of the C=O absorption, with the spectrum of the kneaded mixture resembling that of GCD quite closely, although the band at 1703 cm^{-1} is at 1643 cm^{-1} in the spectrum of GCD. The results are similar to those found for BA and HPBCD.

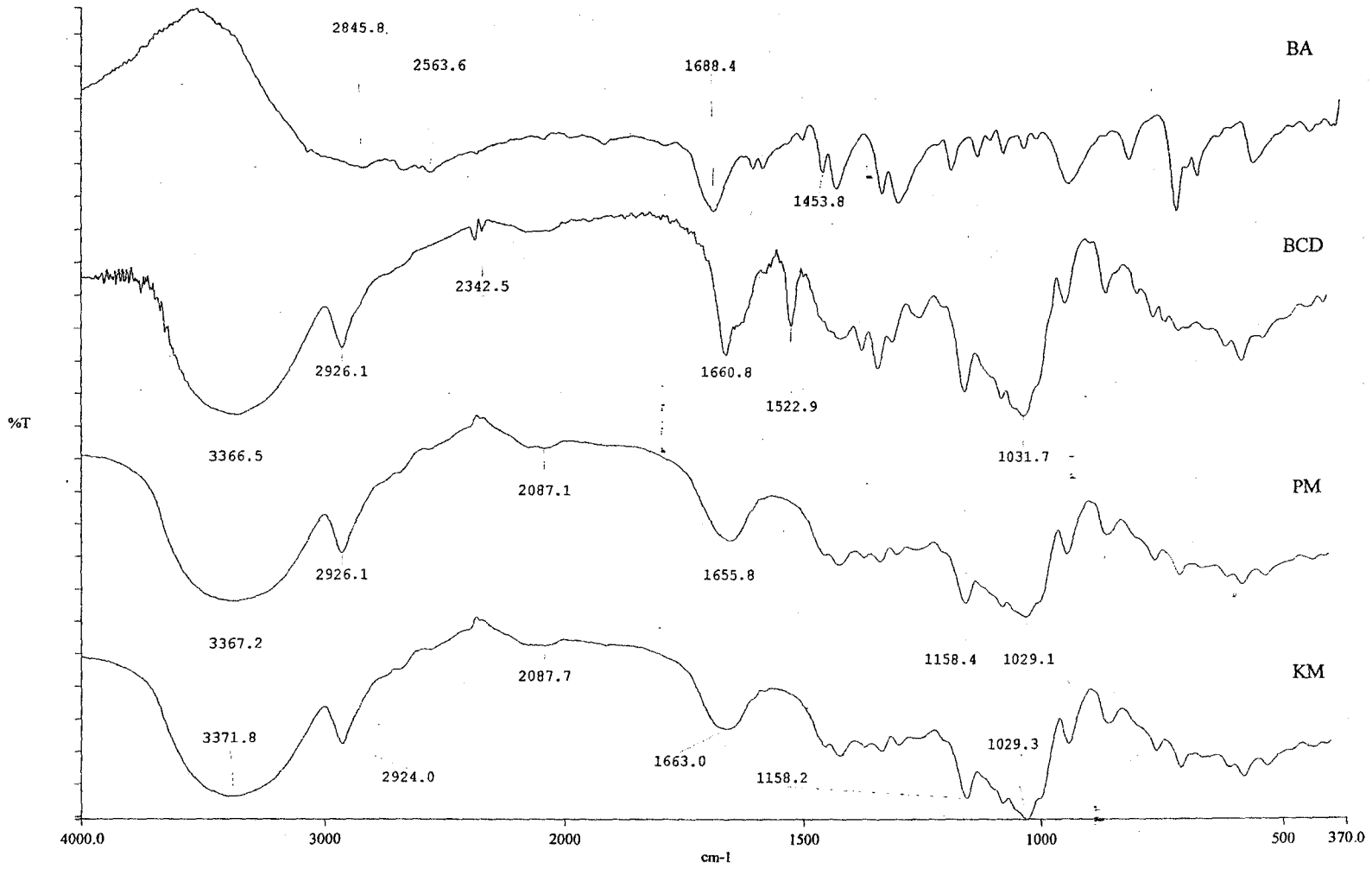

Figure 9.2: IR spectra of the pure components and of the physical and kneaded mixtures of BA with BCD.

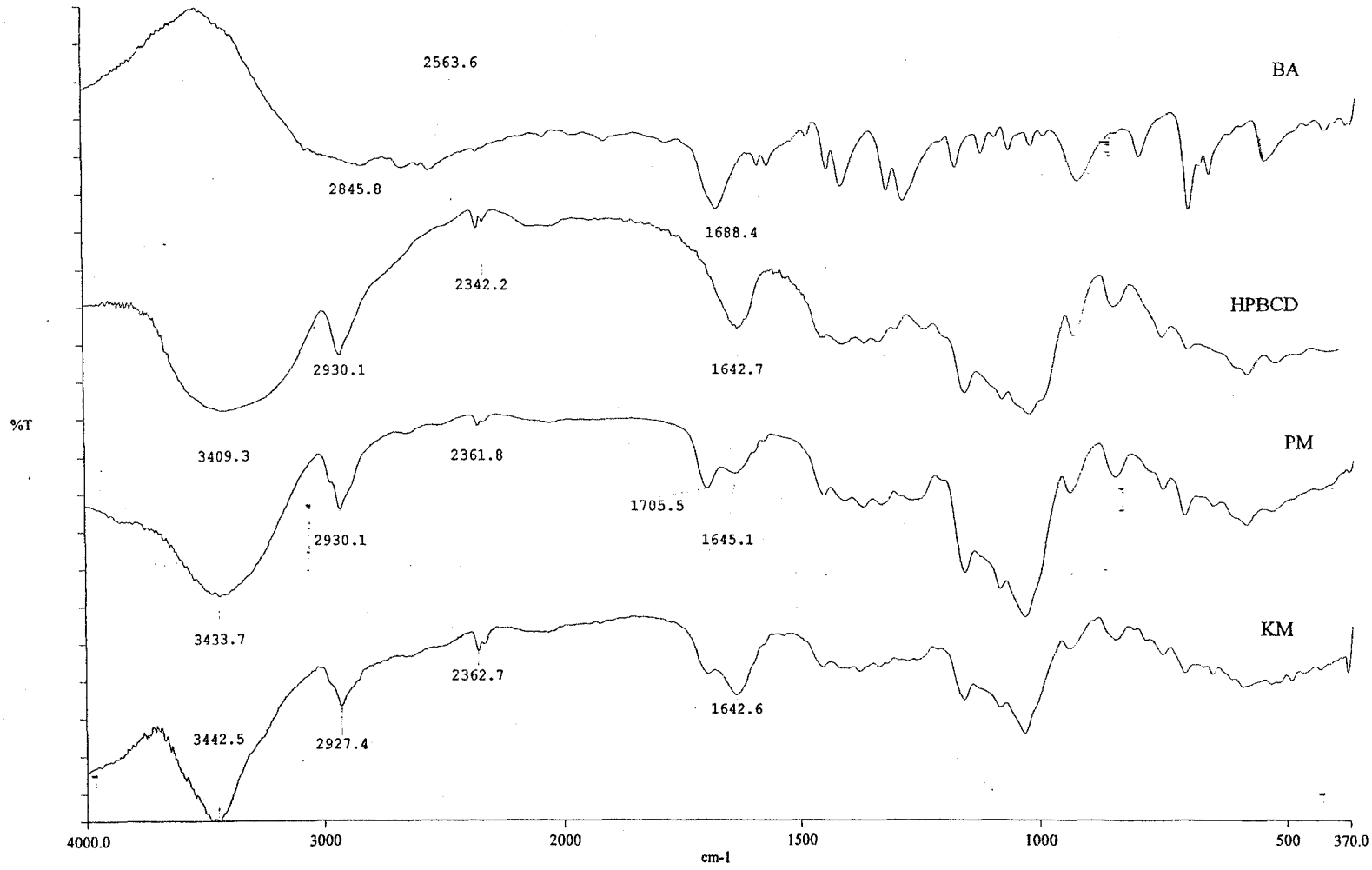

Figure 9.3: IR spectra of the pure components and of the physical and kneaded mixtures of BA with HPBCD.

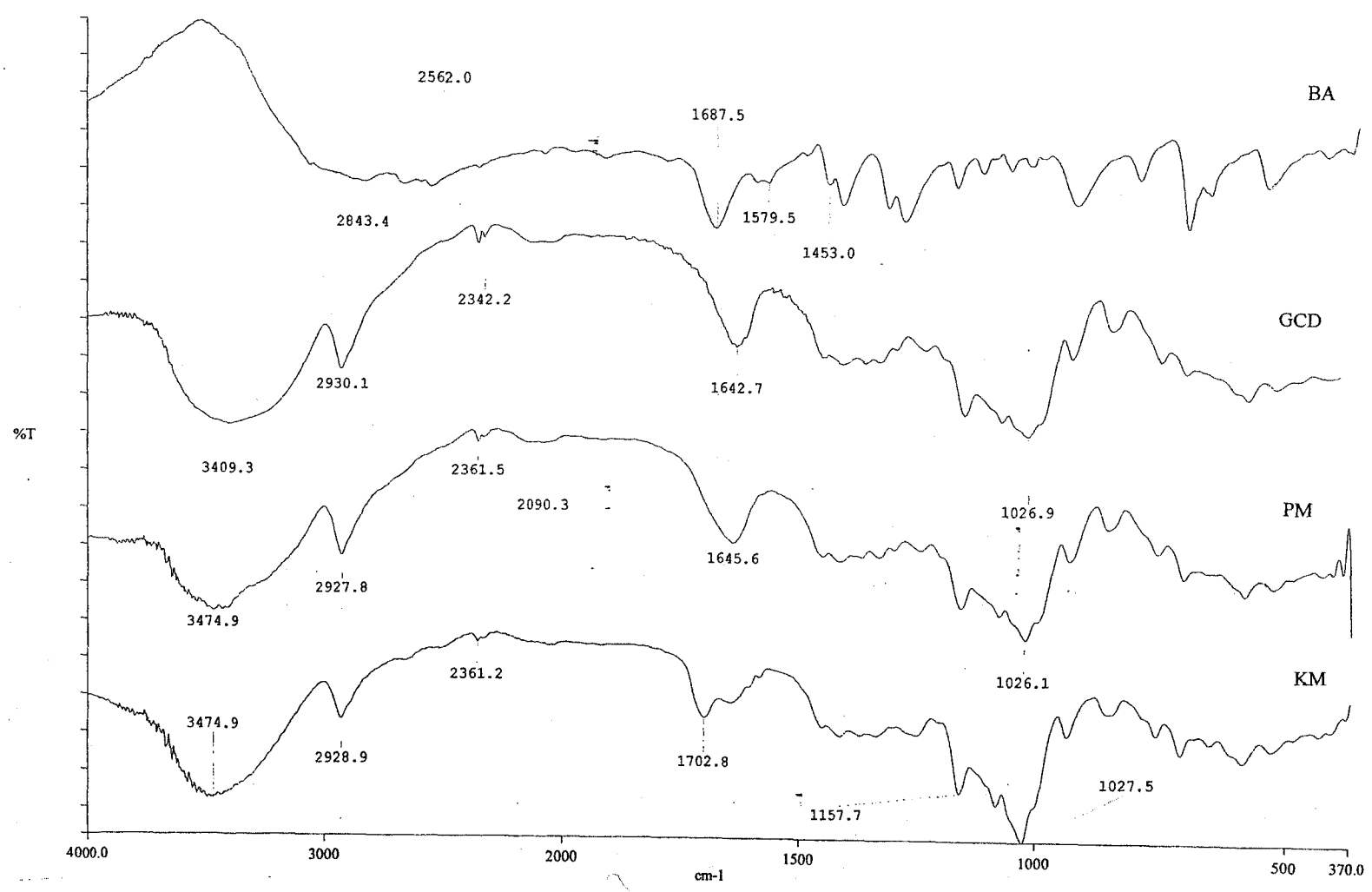

Figure 9.4: IR spectra of the pure components and of the physical and kneaded mixtures of BA with GCD.

9.4 Mixtures of salicylic acid (SA) with the cyclodextrins

The infrared spectra of BA and SA are compared in Figure 9.5. The spectra are very different especially in the useful "diagnostic" region of the C=O absorption. The spectrum of BA shows a C=O band at 1689 cm^{-1} and O-H (carboxylic acid) at 2843 cm^{-1} and 2562 cm^{-1}. The spectrum of SA shows the C=O absorption to be a doublet at 1661 cm^{-1} and 1623 cm^{-1} and O-H (phenol and carboxylic) at 3239, 2854 and 2596 cm^{-1}.

The IR spectra of SA, BCD and their physical and kneaded mixtures are compared in Figure 9.6. The spectra of the physical and the kneaded mixtures resemble each other except for the detail in the C=O absorption region. The features of the SA absorption spectrum are not really discernible in the mixtures.

The IR spectra of SA, HPBCD and their physical and the kneaded mixtures are shown in Figure 9.7. The results are similar to those found for SA and BCD.

The IR spectra of SA, GCD and their physical and kneaded mixtures are compared in Figure 9.8. The spectra of the physical and kneaded mixtures are similar. They differ significantly from the spectrum of GCD, particularly in the region of 2800 cm^{-1} to 4000 cm^{-1}. This could indicate changes in the water content of GCD caused by the mixing process.

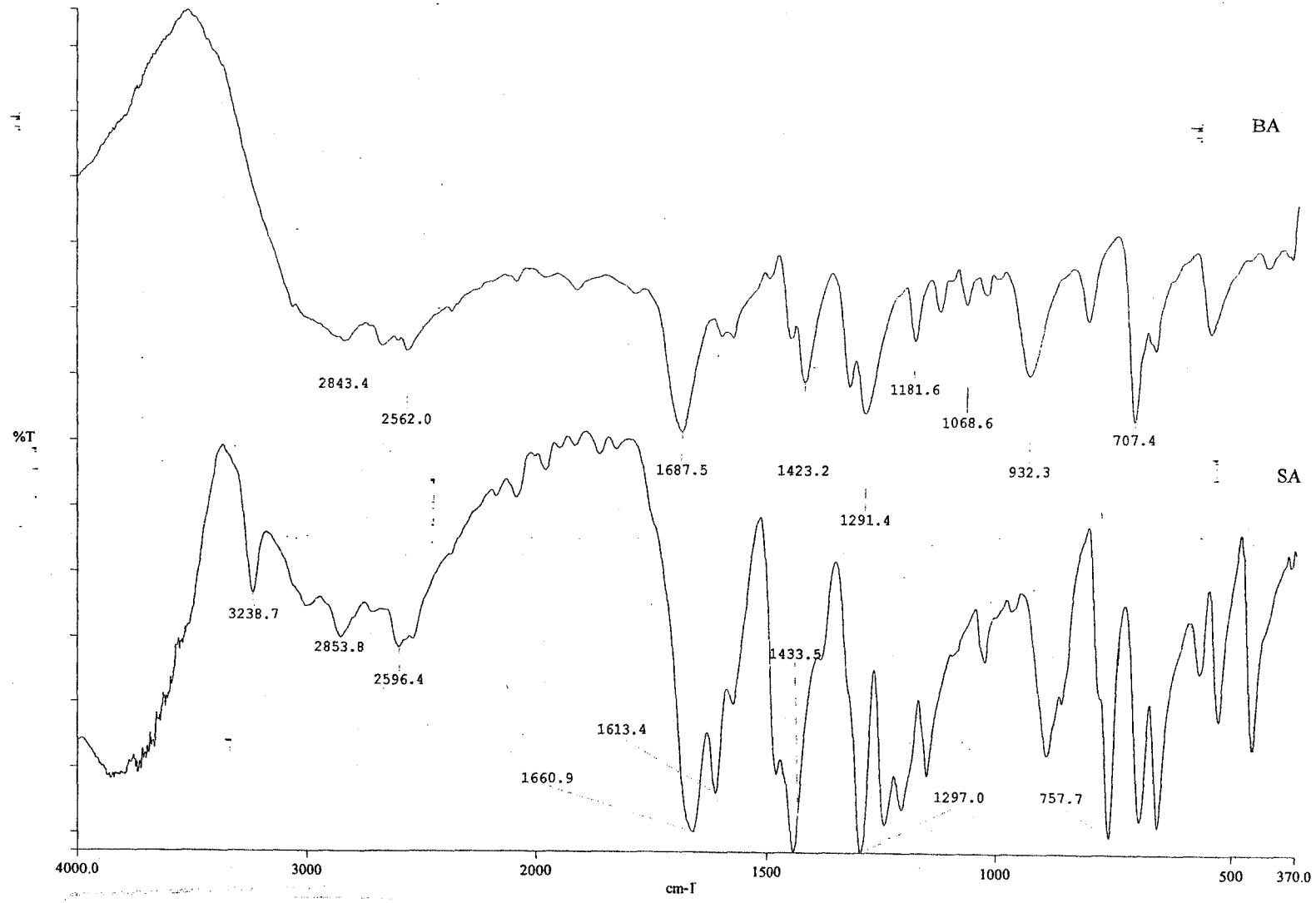

Figure 9.5: IR spectra of BA and SA.

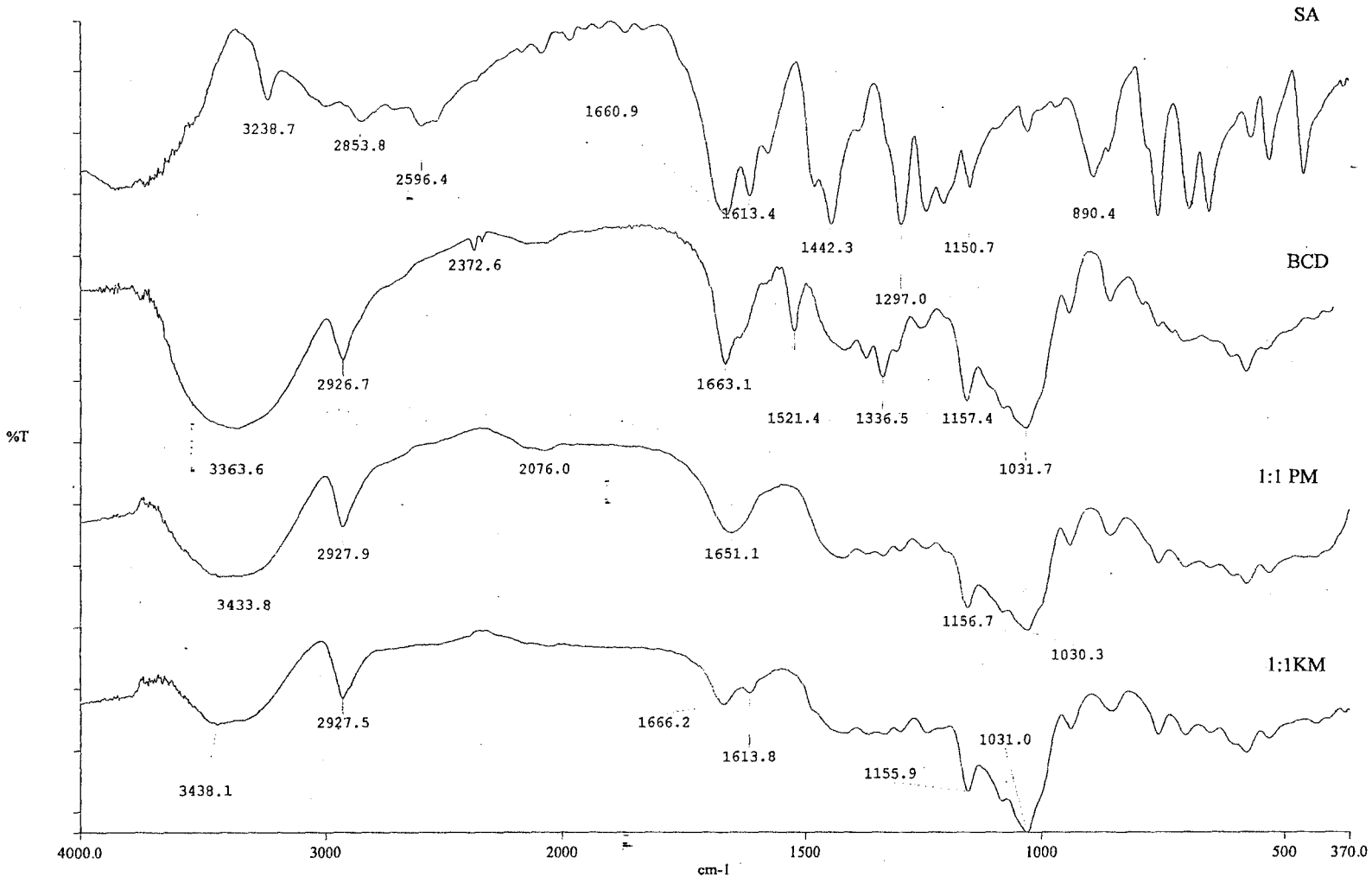

Figure 9.6: IR spectra of the pure components and of the physical and kneaded mixtures of SA with BCD.

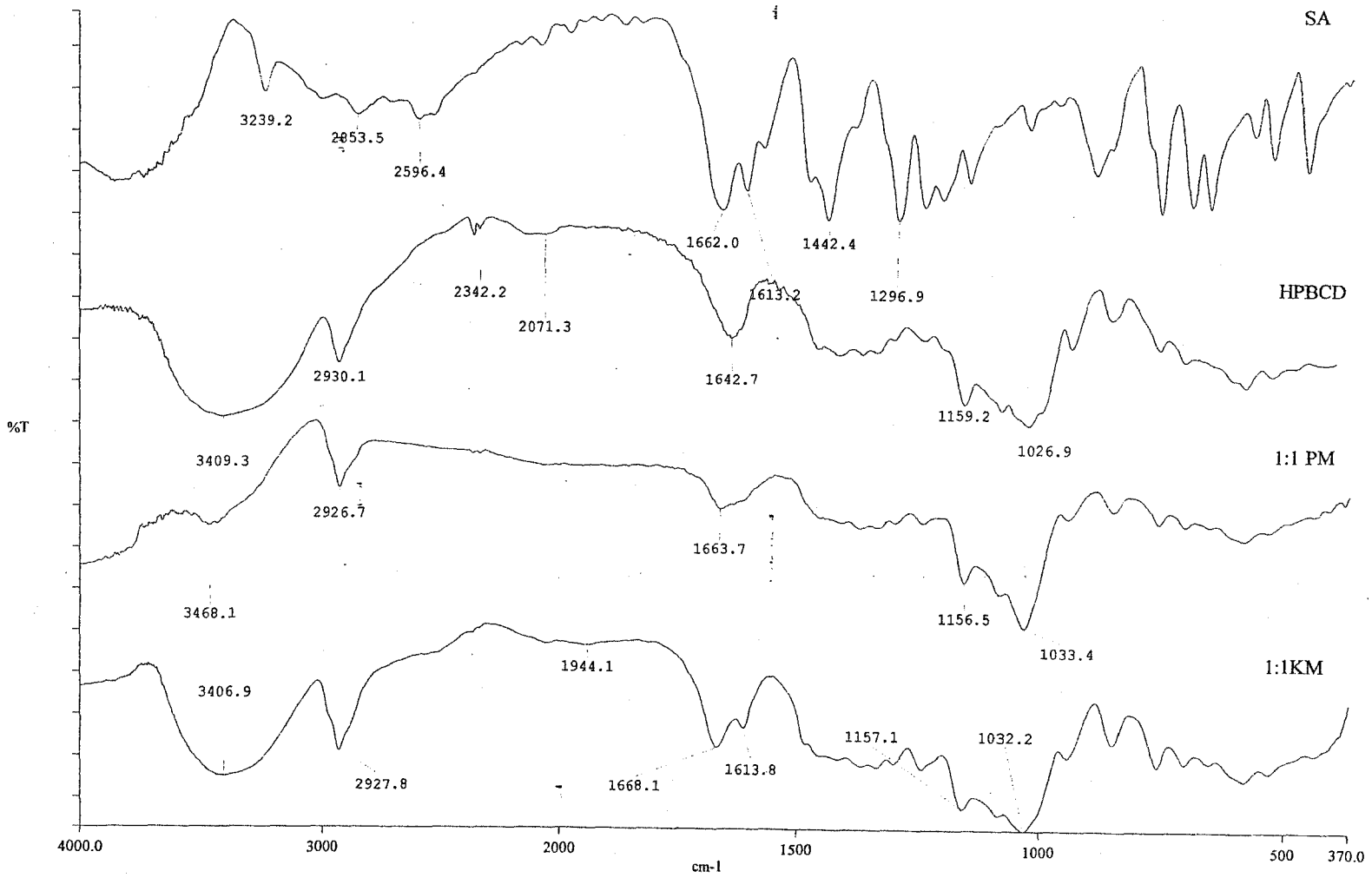

Figure 9.7: IR spectra of the pure components and of the physical and kneaded mixtures of SA with HPBCD.

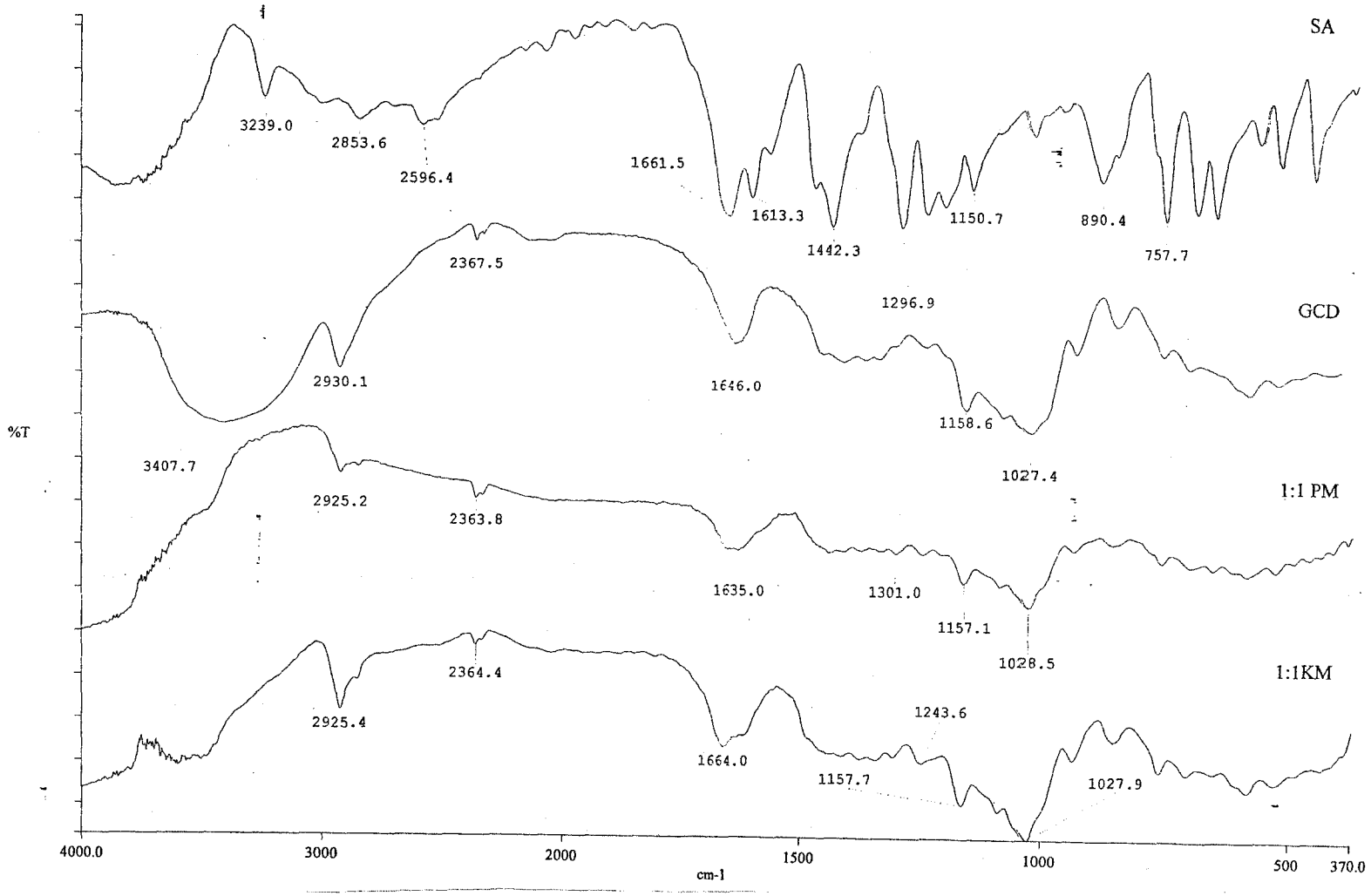

Figure 9.8: IR spectra of the pure components and of the physical and kneaded mixtures of SA with GCD.

10 INFRARED SPECTRA OF THE AMINOSALICYLIC ACIDS (ASA) AND THEIR MIXTURES WITH CYCLODEXTRINS (CD)

10.1 Introduction

The approach used was the same as described in Section 9.1. IR spectra of aminosalicylic acids (3-ASA, 4-ASA and 5-ASA) and their physical and kneaded mixtures with the cyclodextrins were recorded and compared. The IR spectra of 3-ASA, 4-ASA and 5-ASA are compared in Figure 10.1. The spectra of the three isomers are very different from each other.

An IR study on 3-ASA, 4-ASA, and 5-ASA by Gujrathi and Jose [27] showed marked differences in the nature of their molecular species in the solid state. The results revealed that 3-ASA and 5-ASA contain dipolar groups (NH_3^+ and COO^-) characteristic of zwitterionic molecules, while 4-ASA has neutral groups (NH_2 and COOH). The spectra for 3-ASA and 5-ASA show strong bands in the region of 3100-2500 cm^{-1}. The NH_2 group absorption bands which are expected at higher regions are noticeably absent in these two acids. A further study [27] on their hydrochloride salts showed the same bands in this 3100 - 2500 cm^{-1} region with broad peaks at 2850 and 2870 cm^{-1}, respectively, which are ascribed to NH_3^+ absorptions. The absence of the NH_2 absorptions and the presence of NH_3^+ absorptions indicates that 3-ASA and 5-ASA consist of dipolar molecules in the solid state. These observations were supported by the absence of absorption bands due to COOH and presence of COO^- bands (1560 and 1575 cm^{-1} for 3-ASA and 5-ASA, respectively).

The IR spectrum for 4-ASA shows NH_2 group absorptions at 3495 and 3395 cm^{-1}. The OH stretching bands of the phenolic and carboxylic acid groups are broad at about 3020 and 2870 cm^{-1}, respectively.

For comparison and identification of major spectral features, the spectra of the ABAs (3-ABA and 4-ABA) are shown in Figure 10.2. Laurence *et al.* [113] studied the effect of the substituent groups on the carbonyl stretching band in meta- and para- substituted aromatic carbonyl compounds. The absorption bands are given for benzoic acids (3-ABA) derivatives for both monomers and dimers. Meta- substituted benzoic acids had C=O bands at 1740 and 1696 cm^{-1} for the monomer and dimer, respectively. The values for the para-substituted (4-ABA) isomer are 1730 and 1685 cm^{-1}.

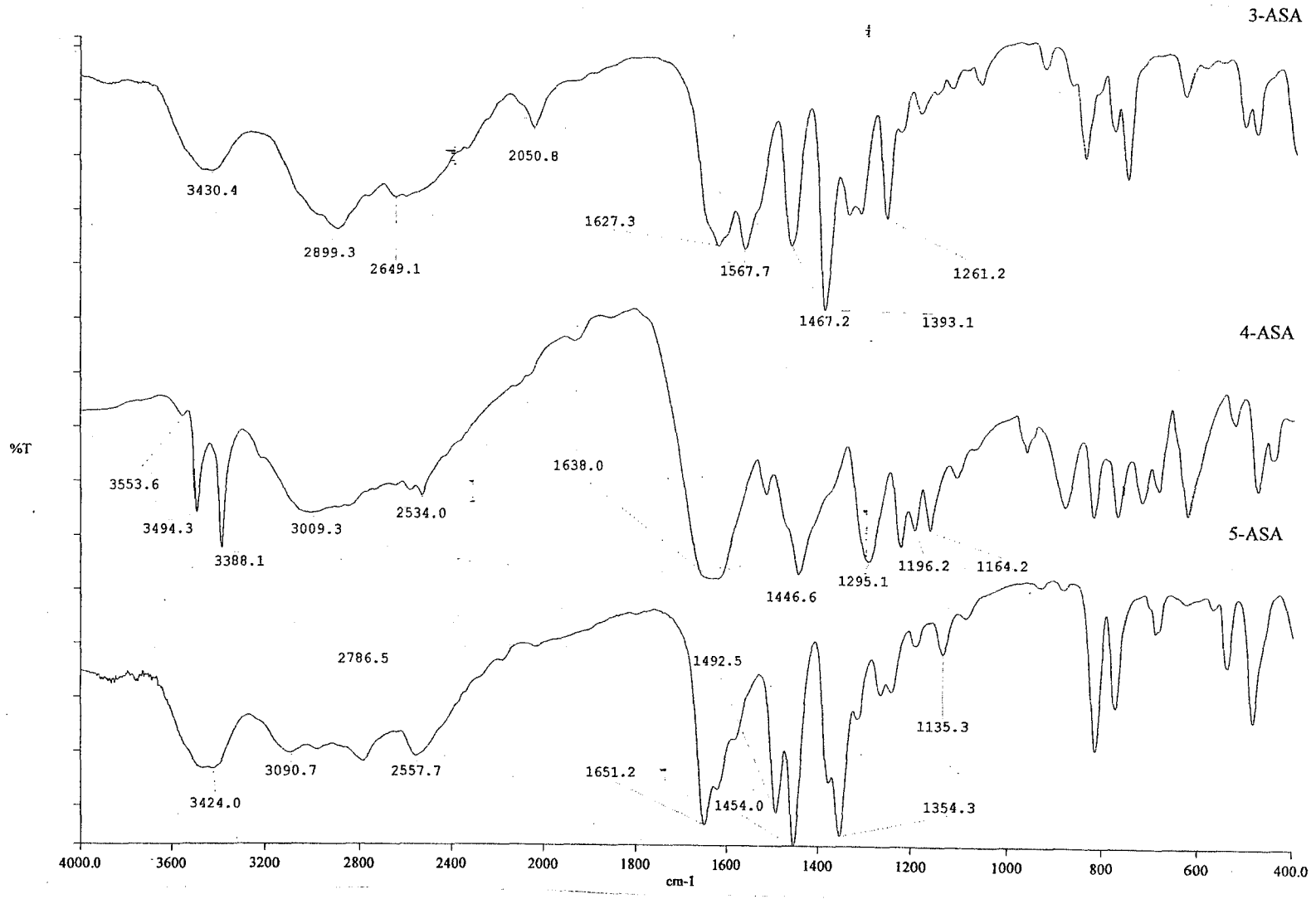

Figure 10.1: IR spectra for (a) 3-ASA, (b) 4-ASA and (c) 5-ASA.

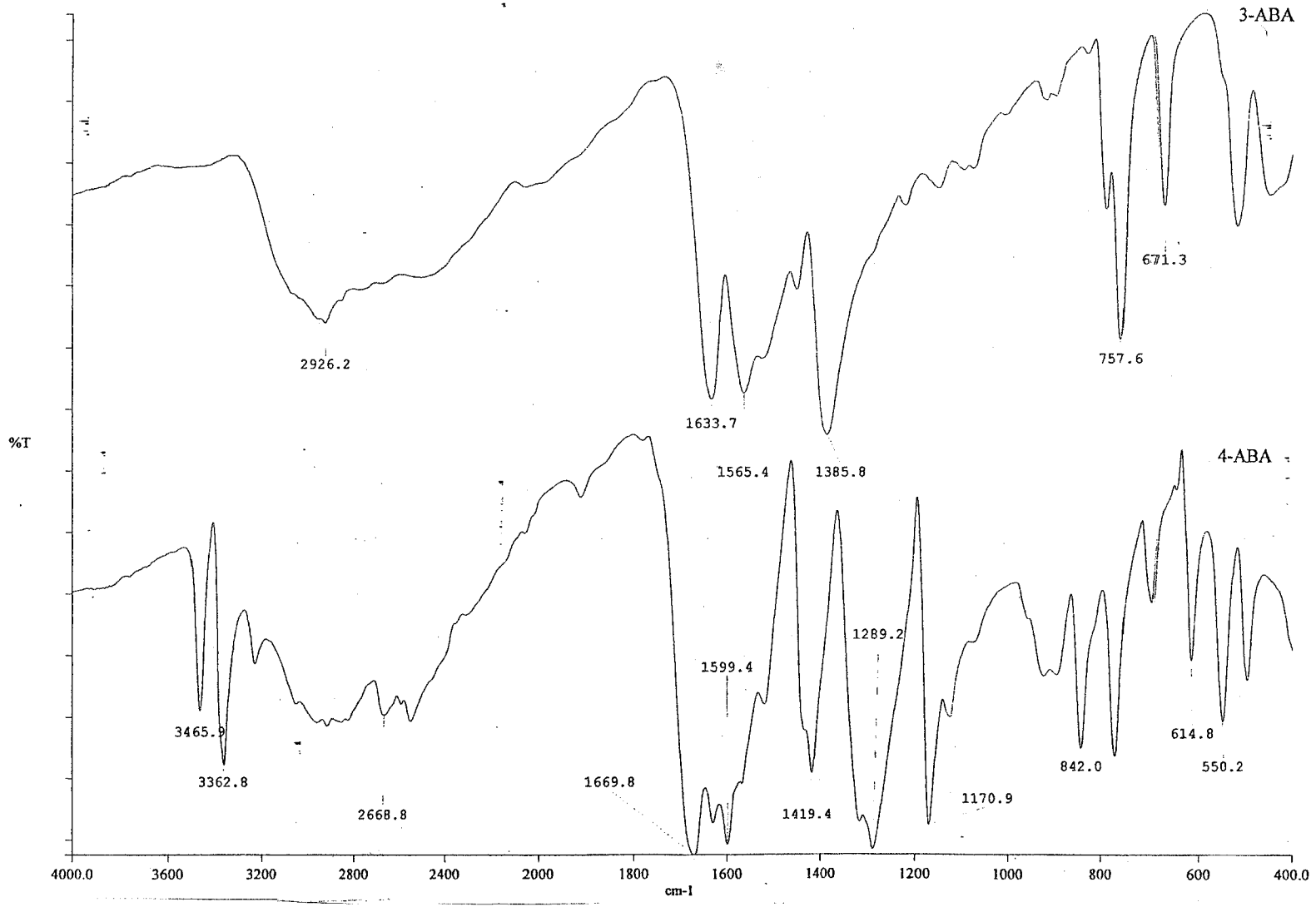

Figure 10.2: IR spectra of (a) 3-ABA and (b) 4-ABA.

Table 10.1 IR absorption maxima for the aminosalicylic and aminobenzoic acids

Compound	N-H, O-H (phenols) and OH (carboxylic acids) / cm^{-1}	C =O/ cm^{-1}
3-ASA	3458, 2893, 2046	1623
4-ASA	3496, 3389, 3200-2500 (broad)	1653
5-ASA	3420, 3100, 3400-2400 (broad), 2779, 2558	1650
3-ABA	3200-2000 (broad)	1633
4-ABA	3463, 3364, 3230, 3200-2300(broad), 2669, 2549	1670

The C=O absorption band (1670 cm^{-1}) for 4-ABA differs from the reported value (1685cm^{-1}) [113], while there is a bigger difference between the experimental value (1633cm^{-1}) for 3-ABA and that reported by Laurence (1696 cm^{-1}) [113].

10.2 Mixtures of 3-ASA with cyclodextrins

The IR spectra of 3-ASA, BCD and their physical and kneaded mixtures are shown in Figure 10.3. The spectra of the physical and the kneaded mixtures are very similar to each other, but differ from that of BCD over the region 1000 cm^{-1} to 1800 cm^{-1}.

Similar conclusions hold for the 3-ASA/HPBCD mixtures shown in Figure 10.4. Some features of the spectrum of 3-ASA are discernible in the spectra of both mixtures.

For 3-ASA and GCD mixtures, the spectra shown in Figure 10.5 suggest slightly more interaction, because of the more marked disappearance of the spectral features of 3-ASA in the kneaded mixture than in the physical mixture.

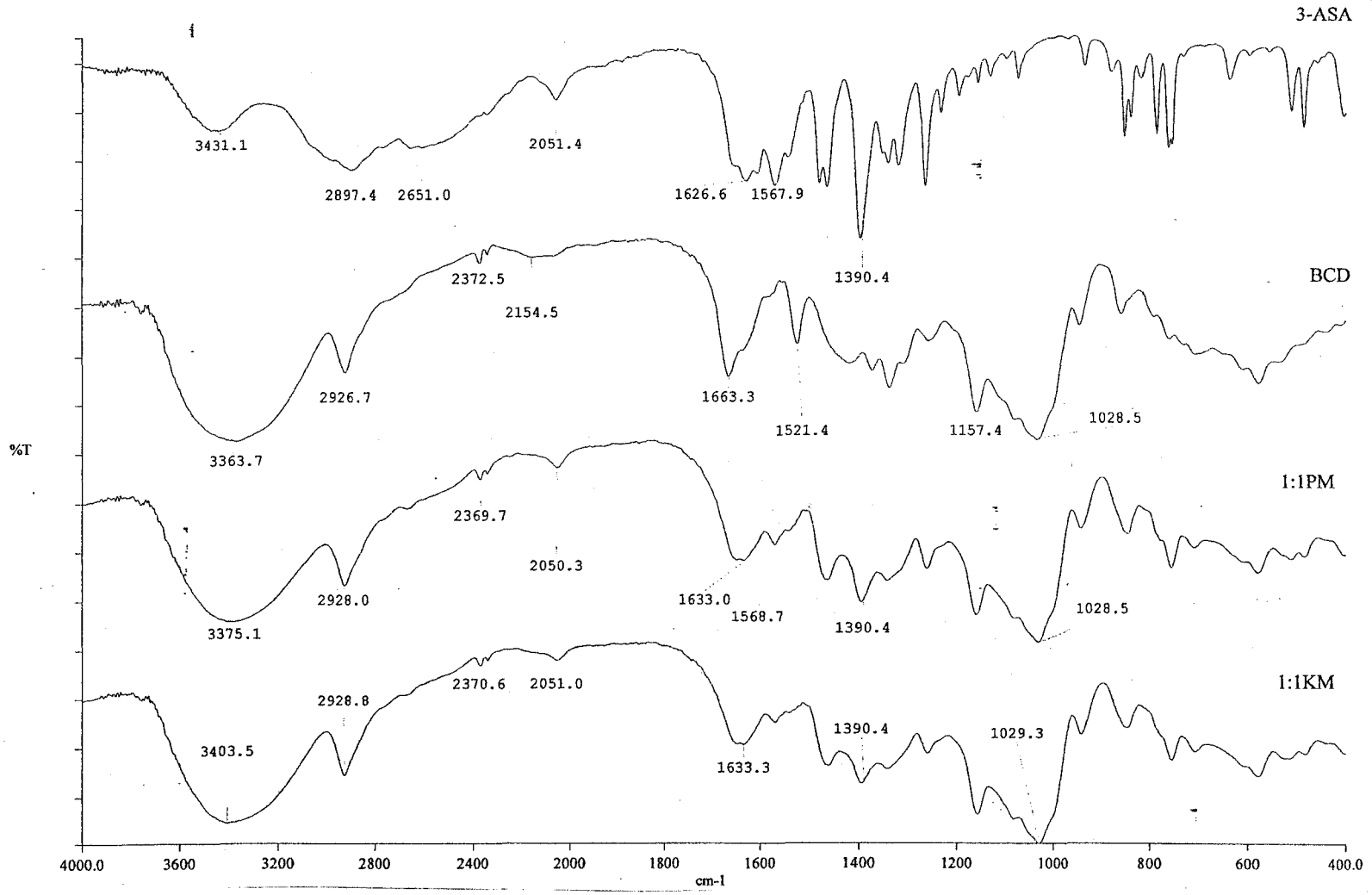

Figure 10.3: IR spectra of the pure components and of the physical and kneaded mixtures of 3-ASA with BCD.

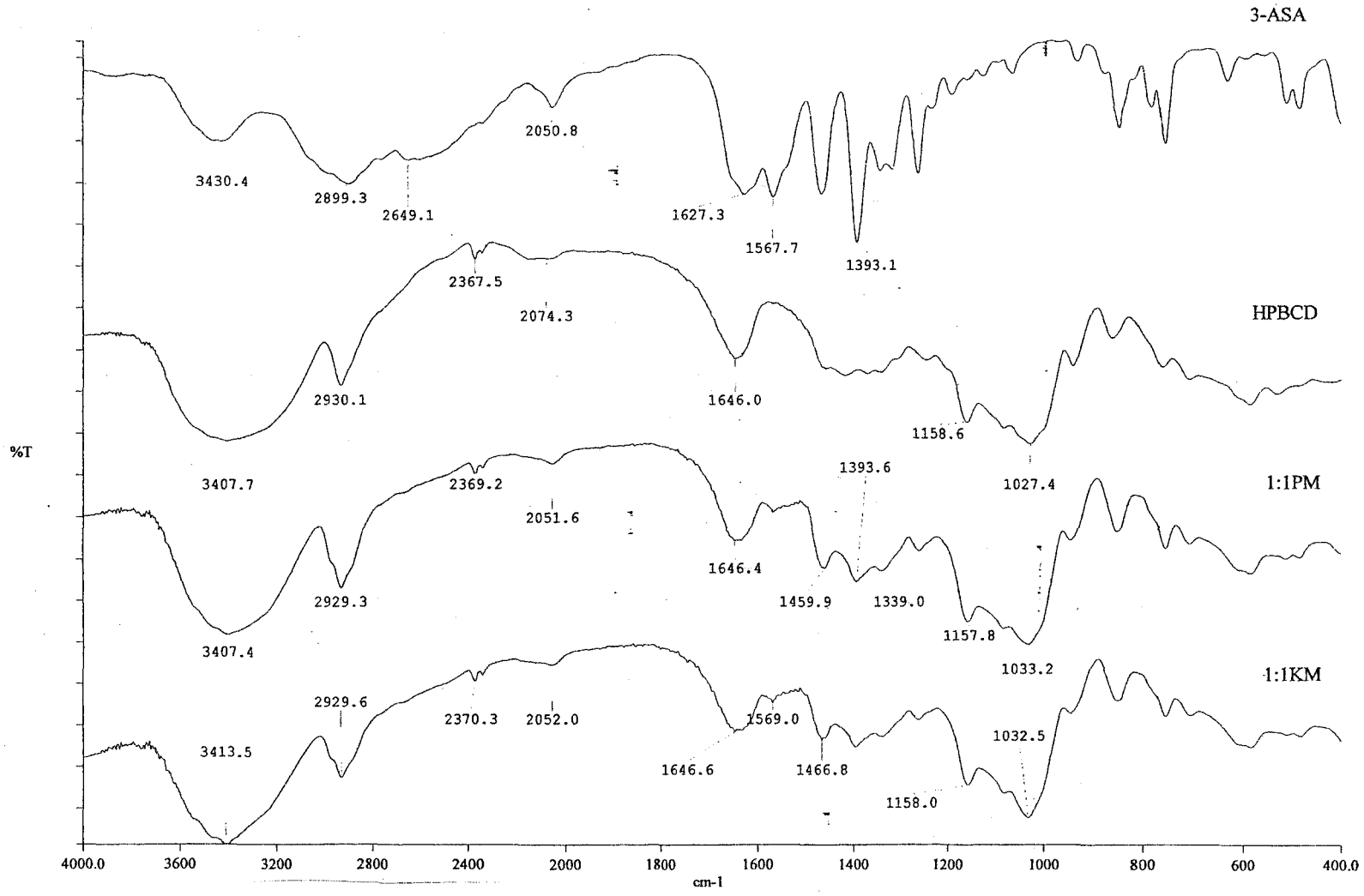

Figure 10.4: IR spectra of the pure components and of the physical and kneaded mixtures of 3-ASA with HPBCD.

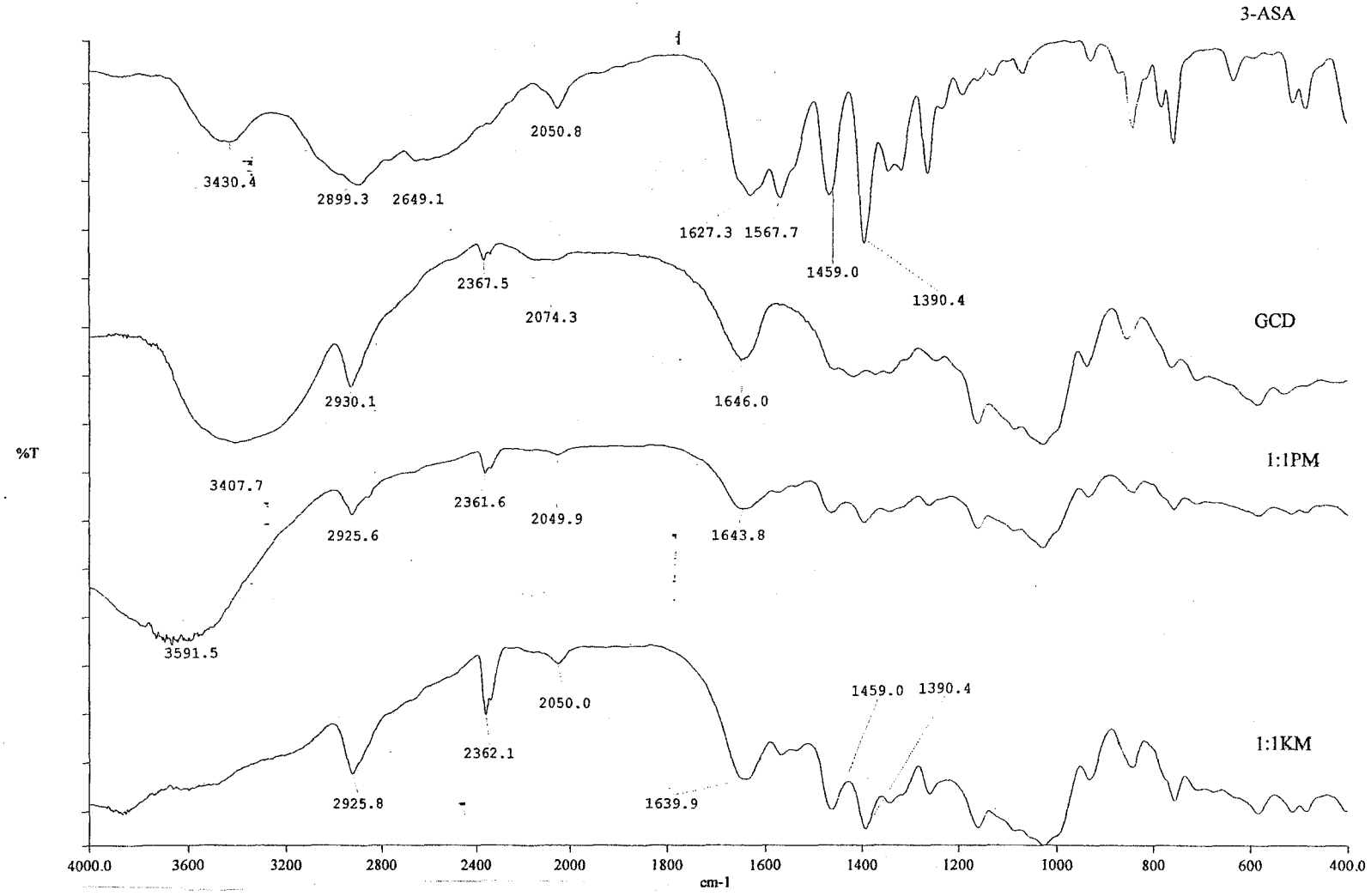

Figure 10.5: IR spectra of the pure components and of the physical and kneaded mixtures of 3-ASA with GCD.

10.3 Mixtures of 4-ASA with cyclodextrins

The IR spectra of 4-ASA, BCD and their physical and kneaded mixtures are shown in Figure 10.6. There are significant differences in the spectra of the physical and kneaded mixtures. Traces of the prominent bands (3496 cm^{-1} and 3389 cm^{-1}) of 4-ASA are apparent, superimposed on the broad band in that region associated with BCD, in the spectrum of the physical mixture. Other spectral features of 4-ASA are more noticeable in the spectrum of the kneaded mixture, particularly around 2600 cm^{-1} and below 900 cm^{-1}.

For 4-ASA/HPBCD mixtures, the spectra in Figure 10.7 show considerable similarity between the physical and the kneaded mixtures and HPBCD itself. The features of the 4-ASA spectrum do not influence the spectra of the mixtures as much as they do in Figure 10.6 for BCD as the host.

The results for 4-ASA/GCD mixtures, shown in Figure 10.8, are similar to those for 4-ASA/HPBCD shown in Figure 10.6. The spectrum of the physical mixture suggests that there is less interaction than in the kneaded mixture which is similar to that of pure GCD.

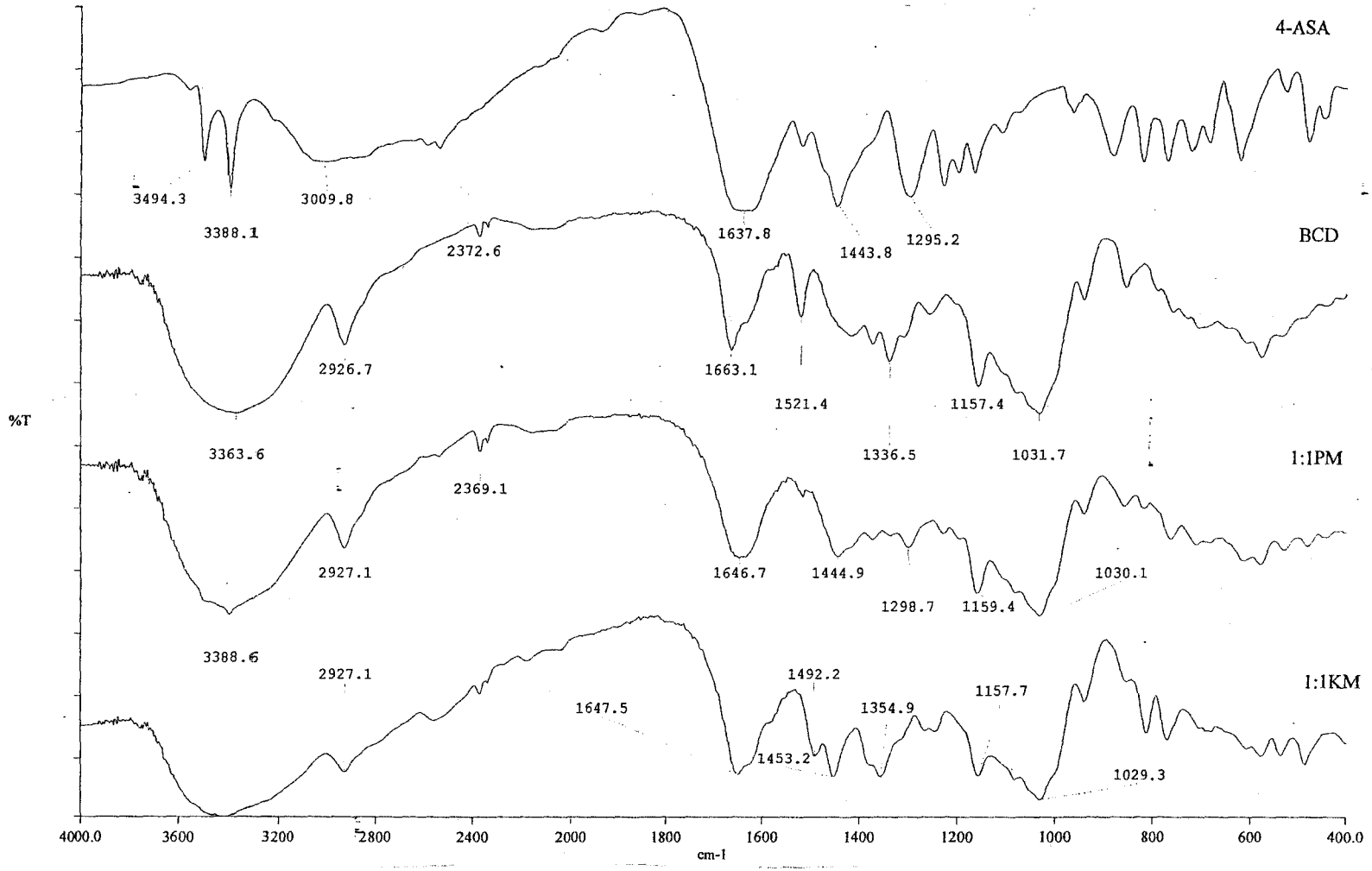

Figure 10.6: IR spectra of the pure components and of the physical and kneaded mixtures of 4-ASA with BCD.

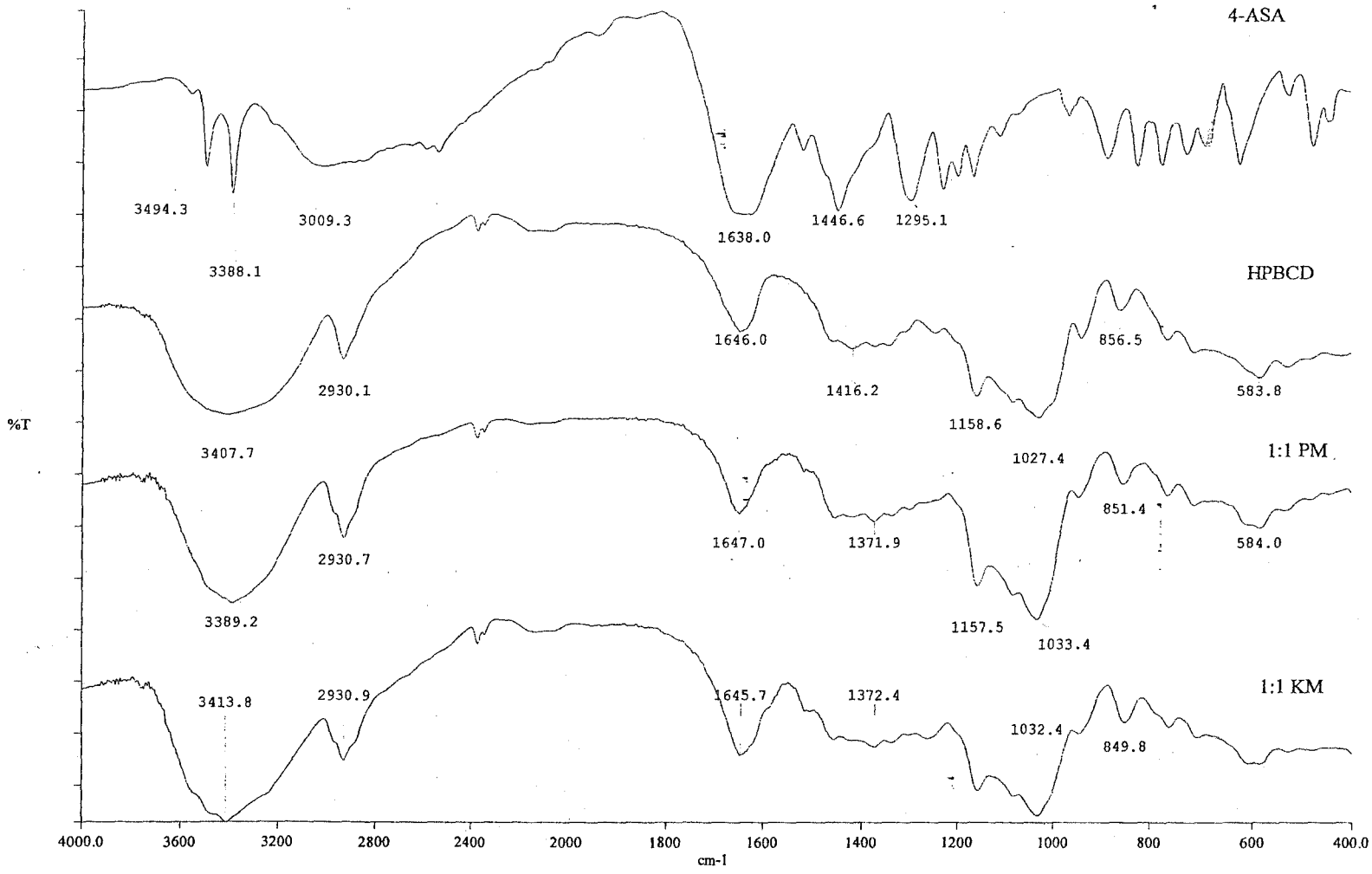

Figure 10.7: IR spectra of the pure components and of the physical and kneaded mixtures of 4-ASA with HPBCD.

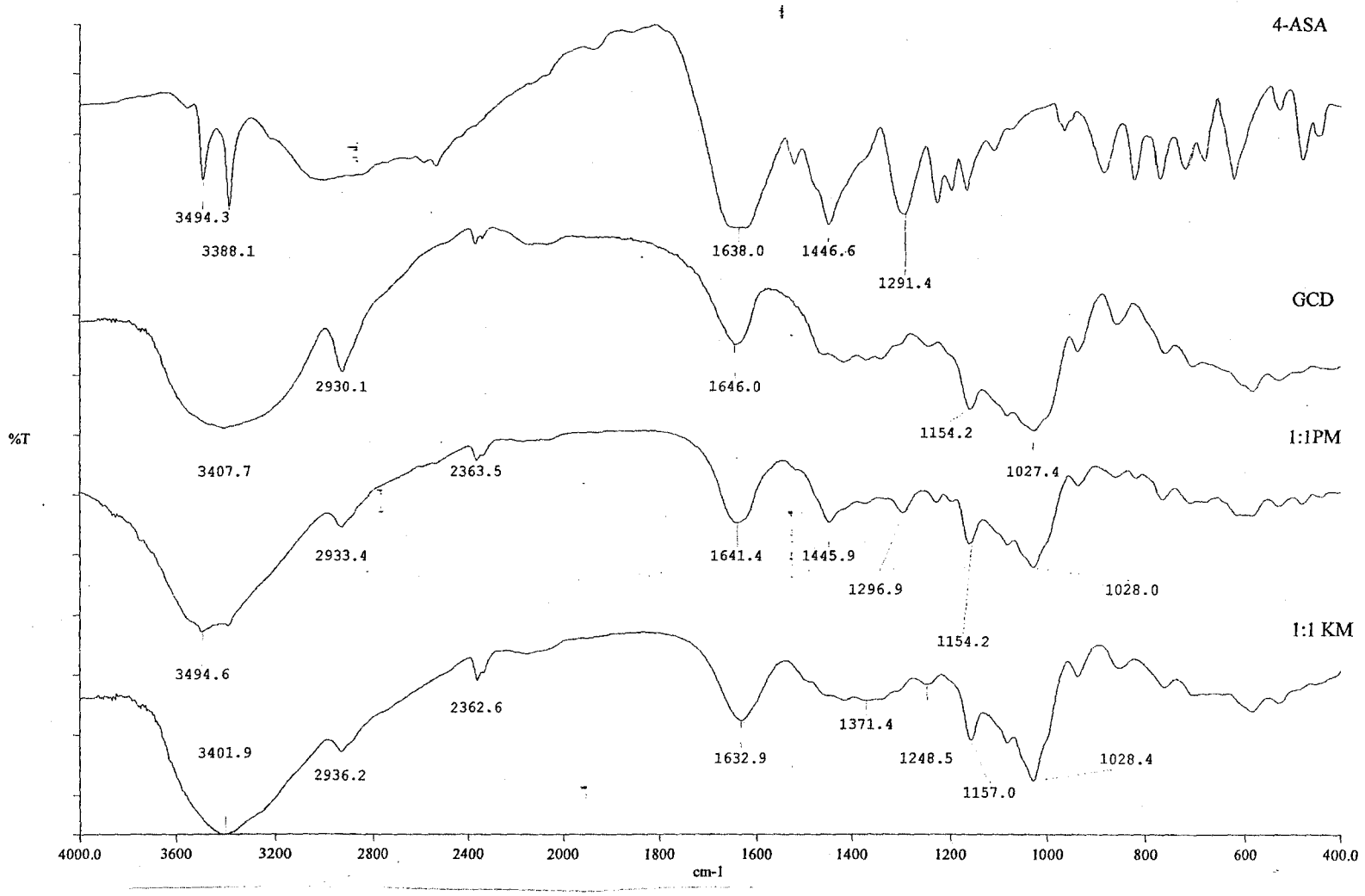

Figure 10.8: IR spectra of the pure components and of the physical and kneaded mixtures of 4-ASA with GCD.

10.4 Mixtures of 5-ASA with cyclodextrins.

The IR spectra of 5-ASA, BCD and their physical and kneaded mixtures are shown in Figure 10.9. The differences between the spectra of the physical and the kneaded mixtures are very noticeable. The spectrum of the physical mixture shows some spectral features of pure 5-ASA, suggesting that the kneading process promotes interaction between 5-ASA and BCD.

The IR spectra of the physical and kneaded mixtures of 5-ASA with HPBCD are shown in Figure 10.10. Their spectral features are very similar to each other but show differences to the spectra of the pure components.

For 5-ASA and GCD (see Figure 10.11), the spectra of the physical and the kneaded mixtures are very similar and many of the spectral features of the pure 5-ASA are evident.

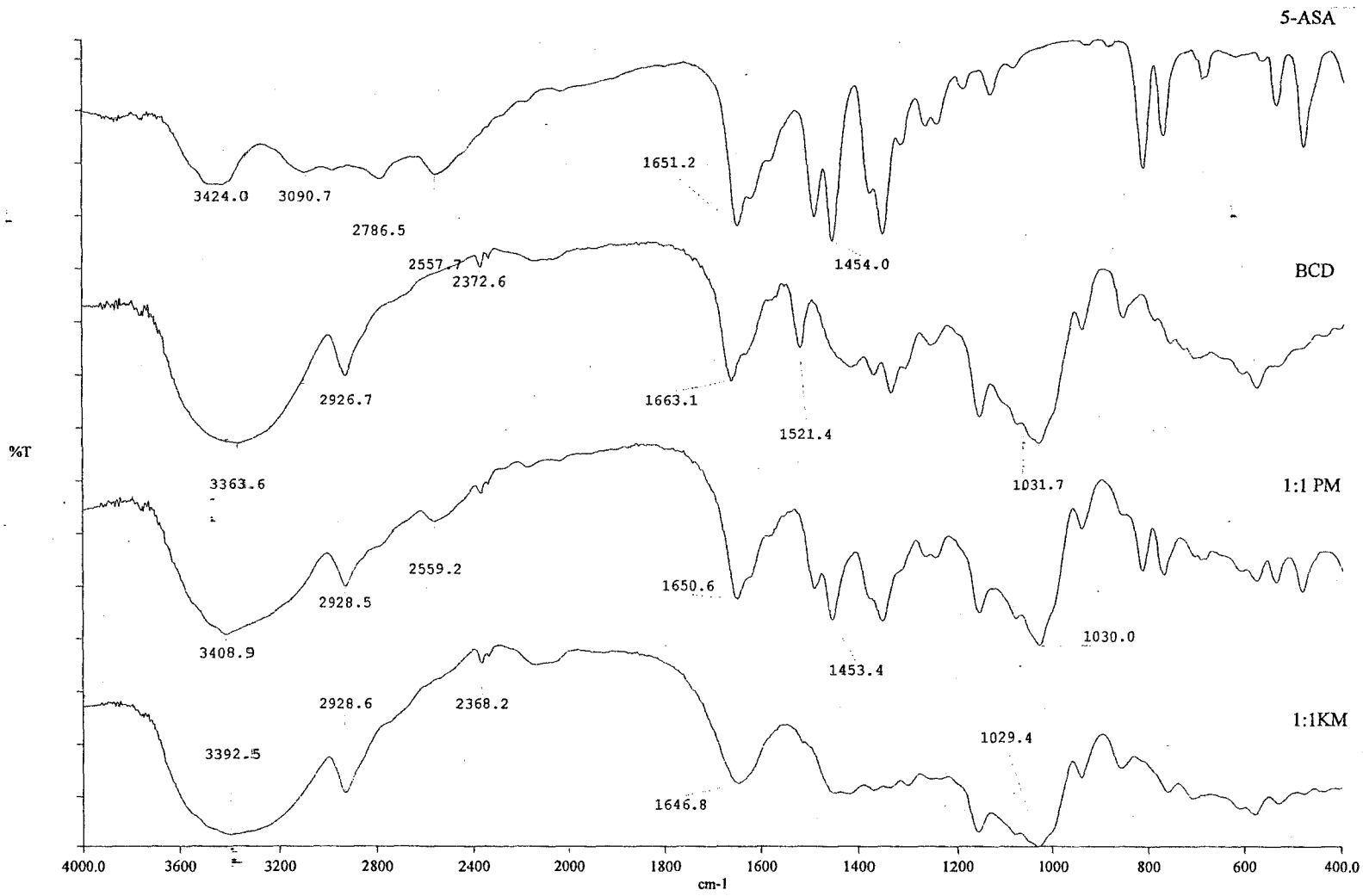

Figure 10.9: IR spectra of the pure components and of the physical and kneaded mixtures of 5-ASA with BCD.

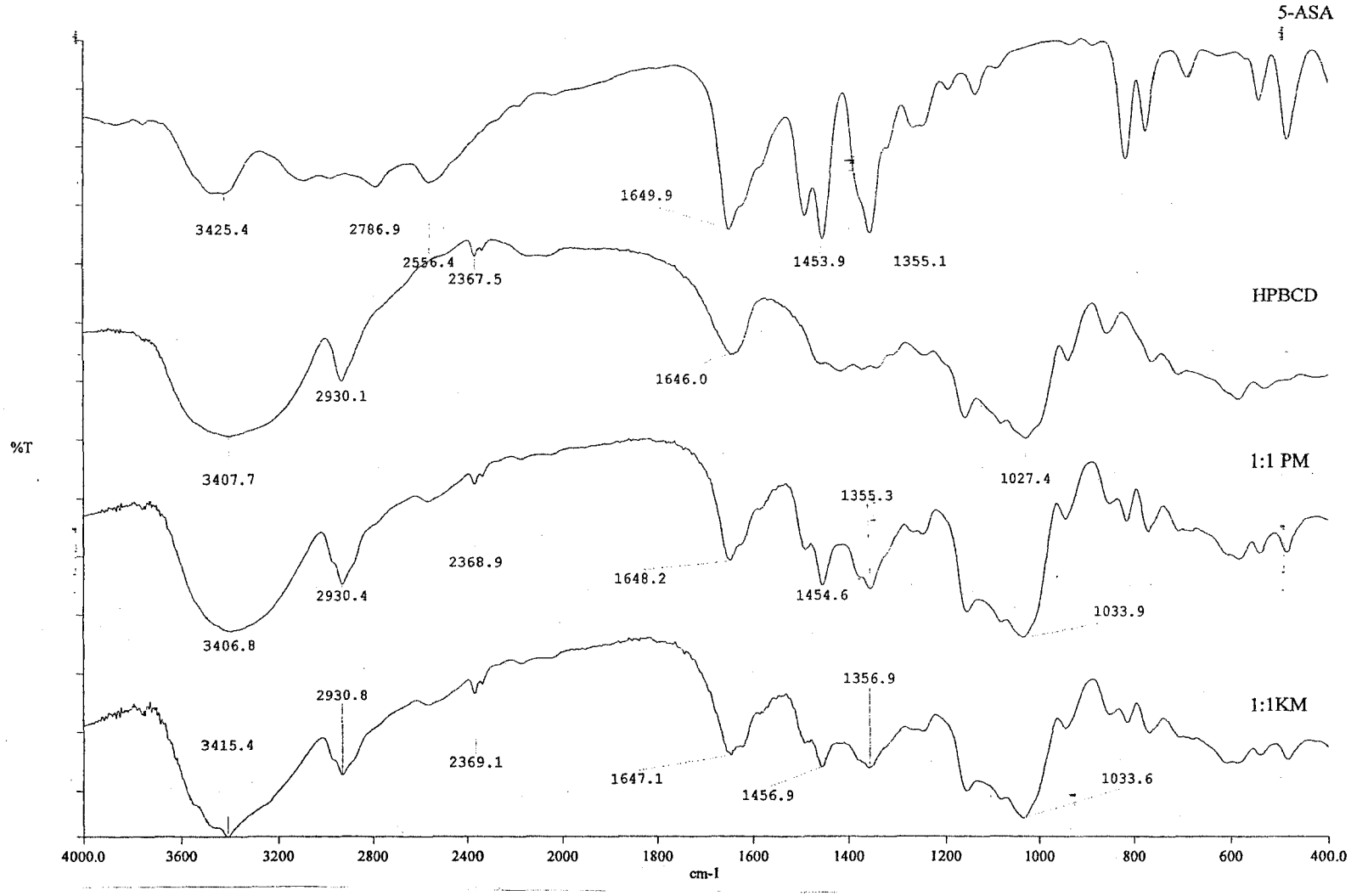

Figure 10.10: IR spectra of the pure components and of the physical and kneaded mixtures of 5-ASA with HPBCD.

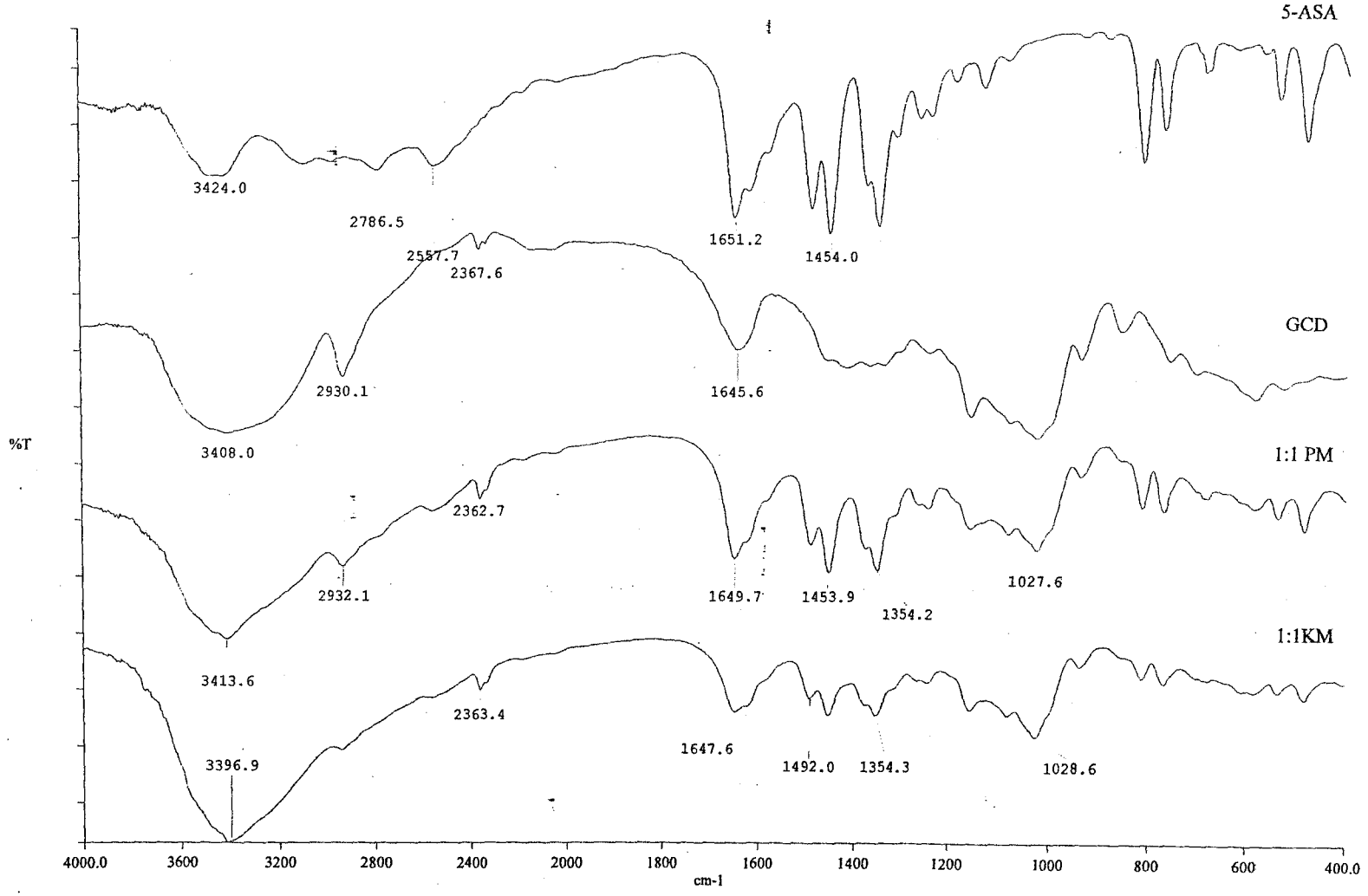

Figure 10.11: IR spectra of the pure components and of the physical and kneaded mixtures of 5-ASA with GCD.

Although the IR spectra contain a lot of information, this information is difficult to interpret even qualitatively. Little is known about the screening effects of the cyclodextrin host on the absorptions of the guest molecule.

On the assumption that the guest molecule is only partially accommodated in the CD cavity, it is possible to speculate which functional groups of the guest would be shielded (at least partially) by the CD molecule.

The scheme (Figure 10.12) was proposed after considering the IR absorptions affected by the mixing of the guest molecules and the host cyclodextrins. The N-H absorption band for all of the guest compounds was observed to have disappeared in most mixtures. This does not rule out that the KBr disc method induces complexation. Solid-state NMR studies might be able to verify this aspect further.

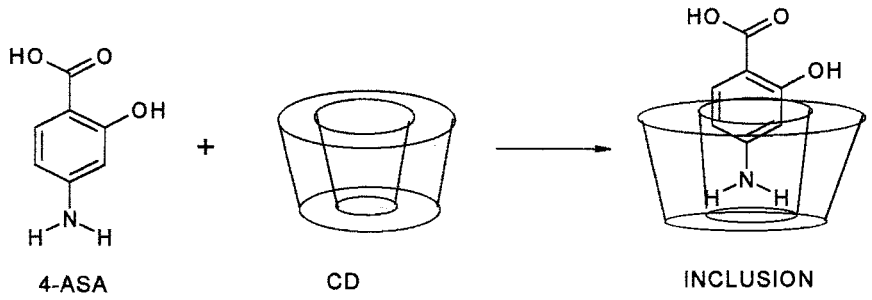

Figure 10.12: Possible mode of inclusion of 4-ASA into the cavity of a cyclodextrin.

10.5 General discussion

The conditions used in preparing the physical mixtures are very mild, yet the IR spectra of these mixtures differ considerably from those of the individual components. It was thus difficult to find examples of mixtures where little or no interaction had occurred.

The kneading procedure does, however, produce even greater changes in behaviour.

Use of thermal analysis techniques has the disadvantage that the increasing temperature programme can promote interactions that would not have occurred at ambient temperatures.

The complementary techniques used, such as IR and XRPD, do not have this disadvantage and so all results have to be considered together.

The main result of this study is thus that all of the substituted aminobenzoic acids used appear to interact with all three of the cyclodextrins used, in particular after kneading. There are striking differences in the behaviour of different isomers and also differences in the behaviour of individual cyclodextrins. HPBCD has the disadvantage, from the point-of-view of identifying its interactions, of being non-crystalline to start with. Most of the mixtures show decrease in crystallinity relative to the individual constituents.

Kneading of the cyclodextrins with the kneading solvent but without any guest present showed that HPBCD became more crystalline after kneading, while BCD became less crystalline. Not much difference was observed on the patterns of the samples of GCD before and after kneading.

A few of the mixtures, notably 3-ASA/HPBCD, 4-ASA/HPBCD (physical mixture), 4-ASA/GCD and 5-ASA/HPBCD show increased crystallinity and these would be worthy of further study using single-crystal X-ray diffraction techniques and, possibly, solid-state NMR.

11. CONCLUSIONS

11.1 **The aminobenzoic acid derivatives**

There are considerable and interesting differences between the thermal behaviours of the various sets of isomers studied. Most of the compounds began to sublime well before melting, generally with an increasing rate of mass loss beyond the melting points, which are considerably different for the different isomers.

The two aminobenzoic acid isomers (3-ABA and 4-ABA) showed differences in their thermal behaviour. Evidence was obtained from TG-FTIR for decarboxylation of 4-ABA but not of 3-ABA. DSC curves for 3-ABA showed complex endotherms that could not be resolved.

The differences in behaviour of 4-ASA and 5-ASA were the most remarkable, with 5-ASA being far more stable and apparently not decarboxylating readily. 4-ASA sublimes at temperatures below the melting point, becoming less stable and decarboxylating in the liquid form. The existence of 3- and 5-ASA as zwitterionic molecules could be the reason why they have high melting points. The presence of high percentage of polar resonance structures (40%) for the existence of molecular 4-ASA is the major contributing factor to its ease of decarboxylation compared to other the isomers [25].

The following are the competing processes when the aminosalicylic acids are subjected to a controlled temperature programme:-

3-ASA(s) → 3-ASA(l) [m.pt 240 °C]

3-ASA(s) → 3-ASA(g) (sublimation 220 °C)

3-ASA(l) → 3-ASA(g) (evaporation above 240 °C)

3-ASA(s, l, or g) → 2-AP(l) [m.pt 118 °C] + CO_2(g) (decarboxylation at about 260 °C as shown by TG-FTIR).

4-ASA(s) → 4-ASA(l) [m.pt = 131 °C]

4-ASA(s) → 4-ASA(g) (sublimation onset 110 °C)

4-ASA(l) → 4-ASA(g) (evaporation above 131 °C)

4-ASA(s, l, or g) → 3-AP(l) [m.pt 115-121 °C] + CO_2(g) (decarboxylation at about 150 °C).

Unlike the other aminosalicylic acids, decarboxylation of 4-ASA is affected by the presence of the degradation product, 3-AP, as shown by the TG-FTIR studies. The temperature at which the maximum rate of decarboxylation occurred on heating at 10 °C min^{-1} was lowered from 150 °C to 90 °C.

5-ASA(s) → 5-ASA(l) [m.pt = 278 °C]

5-ASA(s) → 5-ASA(g) (sublimation not observed)

5-ASA(l) → 5-ASA(g) (evaporation above 278 °C)

There was no evidence from the TG-FTIR for the occurrence of decarboxylation.

5-ASA(s, l, or g) → 4-AP(l) [m.pt 182 °C] + CO_2(g)

All of the sodium salts of these acids showed greater thermal stability than their corresponding acids. The DSC curve for the 3-ASA salt showed two endotherms with onsets at 91 °C and 254 °C. The salt was calculated to be the hemi-hydrate ($3\text{-}NH_2C_6H_3(OH)COONa.0.5H_2O$). The salt of 3-ASA dehydrated with onset at 91 °C and decarboxylated in three different stages: the first below 150 °C, the second between 200 °C and 300 °C and the third stage is the continuous evolution

of CO_2which was still in progress at 500°C (shown by TG-FTIR).

The DSC curve for the salt of 4-ASA showed two endotherms: with onset at 50°C and 100°C. The salt of 4-ASA lost water and carbon dioxide over a wide temperature range (250°C- 650°C). The TG results showed that the salt contained 2.4 moles of water (4-NH_2-C_6H_3(OH)COONa.2.4H_2O) and this is higher than the reported value of 2.0 moles of water [9].

The salt of 5-ASA dehydrates between 100°C and 150°C and the number of moles of water was calculated to be 1.4 (5-NH_2-C_6H_3(OH)COONa 1.4H_2O). The 5-ASA salt did not decarboxylate.

Thermal analyses of BA, SA and the ASA isomers in oxygen showed that 3-ASA and 5-ASA react with oxygen at temperatures above about 200°C, but the other compounds are volatilised completely at temperatures too low (below 200°C) for significant oxidation.

The melting point (120°C) of 3-AP is much lower than those of 2-AP (170°C) and 4-AP (183°C). Their measured enthalpies of melting are higher than the predicted value of 10 kJ mol^{-1} (see Table 3.7).

Arrhenius-type plots were used to calculate apparent activation energies for evaporation of all the compounds using the TG results. The values obtained are generally close to the predicted values (Table 3.1) for enthalpies of sublimation or vaporisation. The values of E_{vap} estimated from Arrhenius-type plots and the values predicted for the enthalpies of sublimation (Table 3.1) are in agreement for 3-ASA and 5-ASA. The E_{vap} values for 4 -ASA are different to those of the other

isomers. The experimental values of E_{vap} are closest to ΔH_{vap} for 2-AP and 3-AP, but closest to ΔH_{sublim} for 4-AP.

Use was made of the SPARTAN molecular modelling software on a Silicon Graphics computer to model the decarboxylation of the ASA isomers. The basis sets of full-geometry optimisation and semi-empirical (AMI) minimisation were applied. The pathway used is shown in Figure 11.1. The heats of formation of the isomers were calculated and are tabulated in Table 11.1.

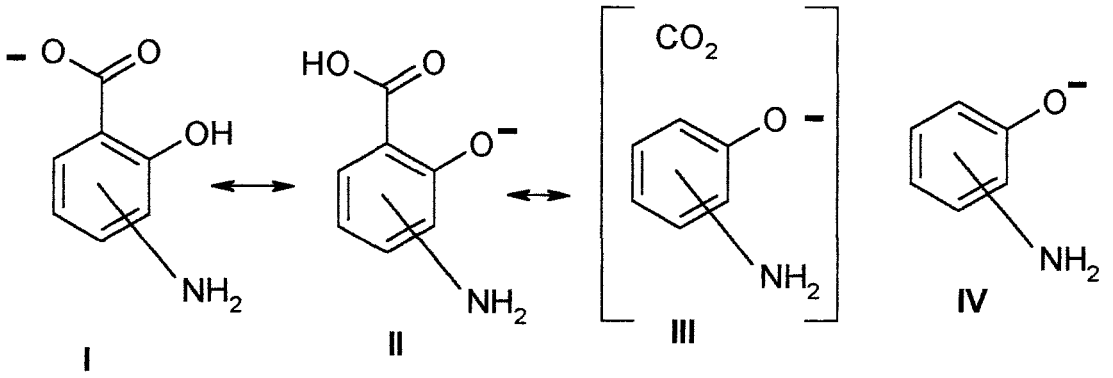

Figure 11.1: The various stages of the decarboxylation of the ASA isomers.

Table 11.1 The heats of formation of the species given in Figure 11.1

Heats of formation / kJ mol^{-1}					
Isomer	I	II	III	IV	IV +CO_2
3-ASA	-586.86	-607.80	-546.85	-185.83	-519.83
4-ASA	-522.95	-604.33	-593.31	-178.84	-512.84
5-ASA	-585.44	-595.00	-529.72	-171.62	-505.62

The minimisation of the species III in the same environment with carbon dioxide may result in the interaction of the two and hence heats of formation of the individual were calculated and added to each other.

The results show that compound II is more stable than I for all three of the isomers. The energy differences between the structure I and the total energy for structure IV plus CO_2 are 67.03, 10.00 and 79.82 kJ/mol for 3-ASA, 4-ASA and 5-ASA, respectively. The low value for the 4-ASA isomer could explain the relative ease of decarboxylation of 4-ASA. The estimated energy profiles for the decarboxylation of the isomers are given in Figures 11.2, 11.3 and 11.4.

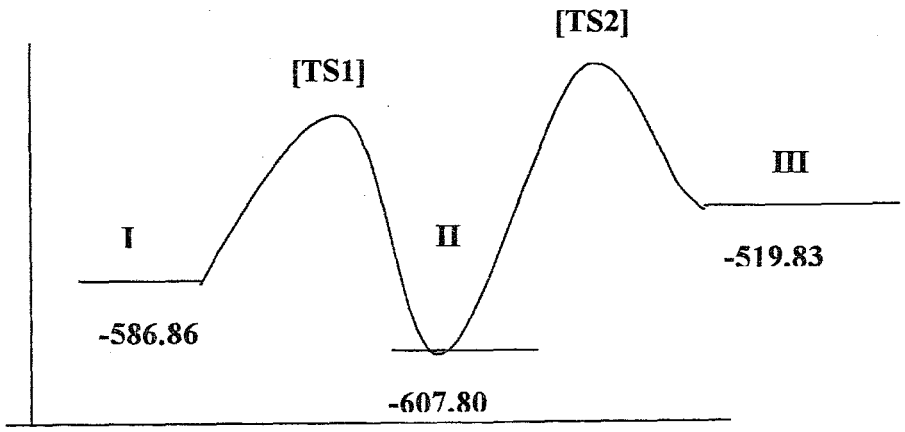

Figure 11.2: Energy profile for the decarboxylation path postulated for 3-ASA (TS1 = transition state 1 and TS2 = transition state 2).

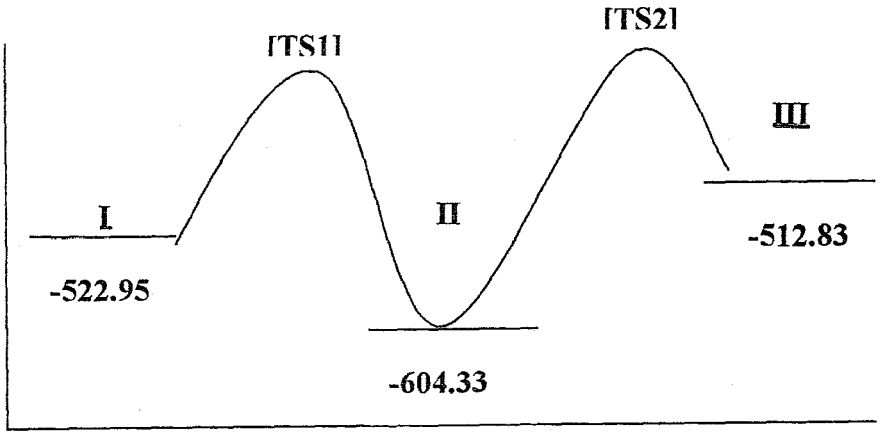

Figure 11.3: Energy profile for the decarboxylation path postulated for 4-ASA (TS1 = transition state 1 and TS2 = transition state 2).

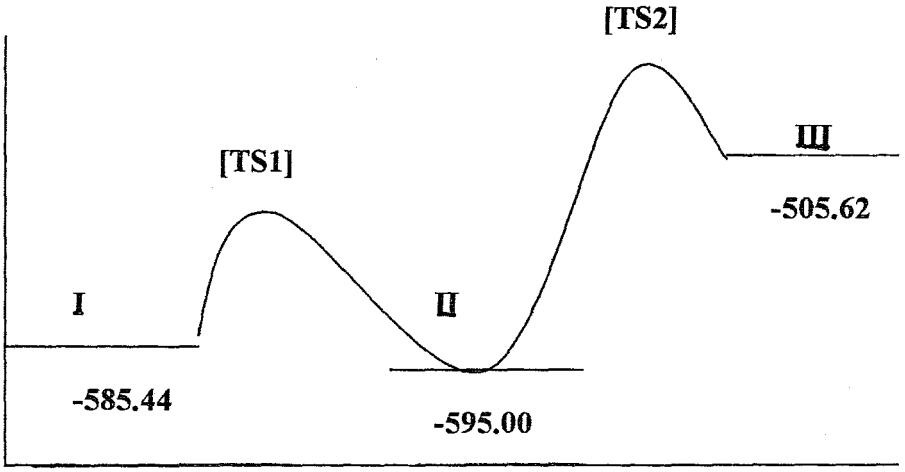

Figure 11.4: Energy profile for the decarboxylation path postulated for 5-ASA (TS1 = transition state 1 and TS2 = transition state 2).

It should be noted that the modelling applies to the gaseous state and not to the solid state where crystal structure is expected to play an important role in the process of decarboxylation.

11.2 Mixtures with cyclodextrins

11.2.1 Thermal behaviour of the reference acids with the CDs

Thermal studies of BA with the CDs showed that in both physical and kneaded mixtures of BA/BCD and BA/HPBCD there were significant interactions. Interactions in the kneaded BA/GCD mixture were the most extensive as might be expected for the CD with the largest molecular cavity.

The results for SA/BCD and SA/HPBCD mixtures were similar to those of BA/BCD and BA/HPBCD mixtures. The interactions were significant for both kneaded and physical mixtures. Again, the kneaded SA/GCD mixture showed the most interaction.

11.2.2 Thermal behaviour of the aminosalicylic acids with the CDs

The thermal behaviour of 3-ASA/HPBCD and 3-ASA/GCD mixtures indicated greater interaction than in the 3-ASA/BCD mixtures.

Interactions occurred in both kneaded and physical mixtures of 4-ASA with all three of the CDs.

Use of the melting behaviour of 5-ASA in mixtures of 5-ASA and the CDs as an indication of interaction is not practicable because the degradation temperatures of the CD and the melting temperature of 5-ASA are almost the same. Hence changes in the dehydration behaviour of the CDs are more reliable indications of interaction. All of the mixtures of 5-ASA with the three CDs showed interaction by broadening of the dehydration endotherms.

Generally, kneaded mixtures showed greater changes in thermal behaviour from that of the individual components than the physical mixtures, but changes in the physical mixtures were also significant.

Comparison of the effects of the different CDs on the thermal behaviour of individual ASA isomers showed that HPBCD has the greatest interaction with 3-ASA and 5-ASA, followed by GCD, while BCD generally showed the least interactions. For 4-ASA, the effect of GCD is more marked than for 3-ASA and 5-ASA. GCD has the largest molecular cavity.

11.2.3 X-Ray powder diffraction patterns of the reference acids with the CDs

The XRPD patterns for the CDs showed that BCD is the most crystalline of the three and HPBCD the least.

The XRPD patterns for both physical and kneaded mixtures of BA with each of the CDs differed from each other and from those of pure components, showing significant interaction between BA and CDs. The changes observed in the XRPD patterns of the mixtures of SA with CDs were similar to those observed for BA and CDs mixtures.

11.2.4 X-ray powder diffraction patterns of the aminosalicylic acids with CDs

The XRPD patterns for 3-ASA/BCD mixtures were similar, but the pattern for the kneaded mixture was less detailed than that of the physical mixture. The pattern for the kneaded mixture of 3-ASA with HPBCD differed from those of pure components, while its physical mixture showed peaks associated with 3-ASA. The XRPD pattern for the physical mixture of 3-ASA with GCD showed less interaction than in the kneaded mixture, which is more diffuse.

The XRPD pattern for the physical mixture of 4-ASA with BCD is fairly similar to that of pure BCD. The pattern for the kneaded mixture was still crystalline but differed from that of the physical mixture. The patterns for both mixtures of 4-ASA/HPBCD indicated some crystallinity. Both the physical and the kneaded mixtures of 4-ASA with GCD showed patterns which suggested extensive structural changes occurred on mixing and kneading of the components.

The XRPD patterns for both the physical and kneaded mixture of 5-ASA and BCD were similar to that of pure BCD with no contributions from pure crystalline 5-ASA. Similar results were observed for the mixtures of 5-ASA with GCD. The kneaded mixture and the physical mixture of 5-ASA with HPBCD showed patterns with marked differences indicative of significant interactions. The results were similar, but not identical, to those observed for 4-ASA/HPBCD mixtures.

In summary, the patterns for the 3-ASA/ BCD kneaded mixture indicated the least crystallinity and that for the kneaded mixture of 5-ASA with BCD the greatest crystallinity. The kneaded mixtures of the isomers with HPBCD showed more diffuse patterns. The pattern for the kneaded mixture of 3-ASA with HPBCD was the most diffuse. The patterns for the ASAs with GCD showed greatest crystallinity, while the patterns of 3-ASA and 5-ASA mixtures were much more diffuse than those of the 4-ASA mixtures.

11.2.5 Infrared spectroscopy of the reference acid with the CDs

Infrared spectroscopy was used to complement of the results of the thermal studies. The method is not always useful for the study of inclusion because of interfering absorption bands due to cyclodextrins. The C=O (carbonyl carbon) absorption region is usually interfered with subject to least interference and is thus

often used as an indicator of interaction [112].

The IR spectra of BCD, HPBCD and GCD showed a broad absorption band at 3600- 3100 cm^{-1} with a shoulder at 2920 cm^{-1}. The spectra for HPBCD and GCD are similar but different to that of BCD. These variations could be due the amount of water in the cavity of the cyclodextrins and their structural nature.

The infrared spectra of BA, BCD and their physical and kneaded mixtures were very similar to each other. The IR spectra of physical and the kneaded mixtures of BA and HPBCD differed from each other, with the band for the kneaded mixture being shifted slightly towards lower wave numbers, indicating more interaction. The differences between the spectra of the physical and kneaded mixtures of BA/GCD were small and they resembled the IR spectrum of pure GCD. These results were similar to those found for BA/HPBCD mixtures.

The spectra of the physical and the kneaded mixtures of SA and BCD resembled each other except for the detail in the C=O absorption region. The features of the SA spectrum were not really discernible in the mixtures. The results for physical and the kneaded mixtures of SA and HPBCD were similar to those found for SA and BCD. The spectra of the physical and kneaded mixtures of SA and GCD were similar, but differed significantly from the spectrum of GCD. This could indicate changes in the water content of GCD caused by the mixing process.

11.2.6 Infrared spectra of mixtures of the aminosalicylic acids with the CDs

The IR spectra for 4-ASA showed NH_2 absorption bands at 3495 and 3395 cm^{-1} and broad OH stretching band of phenolic and carboxylic acid groups at about 3020 and 2870 cm^{-1}, respectively. These absorption bands were absent in both the

3-ASA and 5-ASA isomers, hence showing the absence of the COOH group.

The spectra of the physical and the kneaded mixtures of 3-ASA and BCD were very similar to each other, but differed from that of BCD. Similar conclusions hold for the 3-ASA/HPBCD mixtures. The spectra of the 3-ASA/GCD mixtures suggested slightly more interaction.

There were significant differences in the spectra of the physical and kneaded mixtures of 4-ASA and BCD. Spectral features of 4-ASA were more noticeable in the spectrum of the kneaded mixture than in that of the physical mixture. For 4-ASA/HPBCD mixtures, the spectra showed considerable similarity between the physical and the kneaded mixtures and HPBCD itself. The features of the 4-ASA spectrum did not influence the spectra of the mixtures as much as they did in the BCD mixtures. The results for the 4-ASA/GCD mixtures were similar to those for the 4-ASA/HPBCD mixtures. The spectrum of the physical mixture suggested that there is less interaction than in the kneaded mixture which was similar to that of pure GCD

The differences between the spectra of the physical and the kneaded mixtures of 5-ASA and BCD were very noticeable. Kneading appears to promotes interaction between 5-ASA and BCD. The spectral features of the mixtures of 5-ASA/HPBCD were very similar to each other but showed differences to that of the pure components. For mixtures of 5-ASA/GCD, the spectra were also very similar and many of the spectral features of pure 5-ASA were evident.

11.3 Molecular modelling

Although quantitative molecular modelling of inclusion complexes of cyclodextrins is a specialised and demanding field (see Section 1.14), the maximum linear dimensions of optimised molecular structures (Tables 11.2 and 11.3) of the potential guest molecules (Figure 11.6) were measured and compared with those of the cavities of the hydrated cyclodextrins (Figure 11.5). The dimensions for HPBCD are not given because of its amorphous nature but are likely to be similar to those of unmodified BCD.

Table 11.2: Dimensions of the cyclodextrins [29].

CDs	Average cavity diameter / pm
BCD.11H_2O	1008
GCD.14H_2O	1175

Table 11.3: Maximum linear dimensions of the optimised potential guest molecules [26].

Guest molecule	Longest dimension / pm
BA	678
SA	651
3-ASA	683
4-ASA	691
5-ASA	671

From these dimensions it can be seen that, on geometrical grounds, inclusion of each of these compounds is possible in all three of the cyclodextrin cavities. Inclusion can be enhanced through formation of hydrogen bonds because of the presence of COOH and OH groups in all of these guest molecules.

From the IR results (see Section 10) indications are that in general the -NH_2 regions of the substituted aminobenzoic acids penetrate most deeply into the CD cavities, as illustrated for 4-ASA in Figure 10.12.

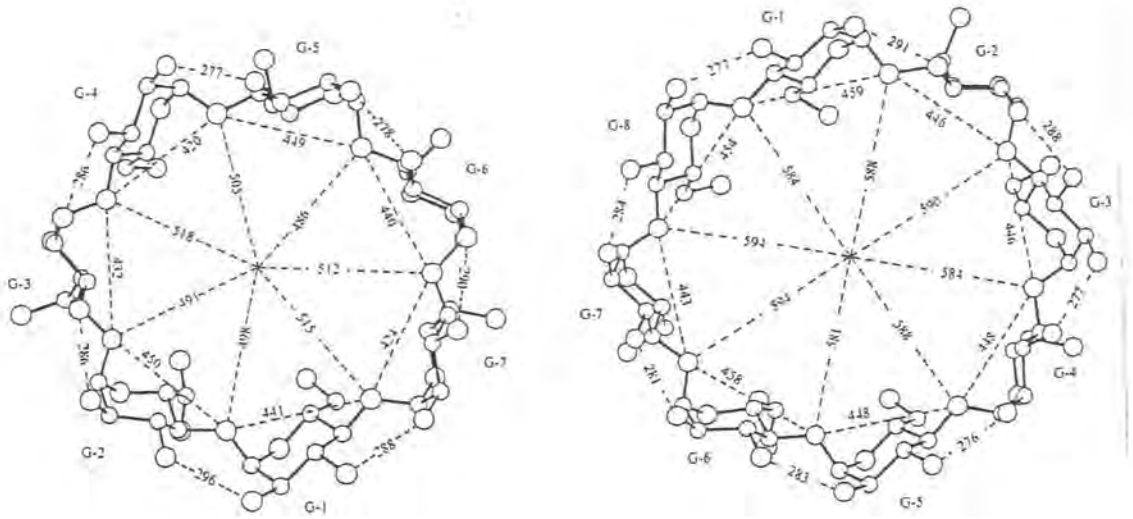

(a) (b)

Figure 11.5: X-ray crystal structures of (a) BCD.11H_2O and (b) GCD.14H_2O [29].

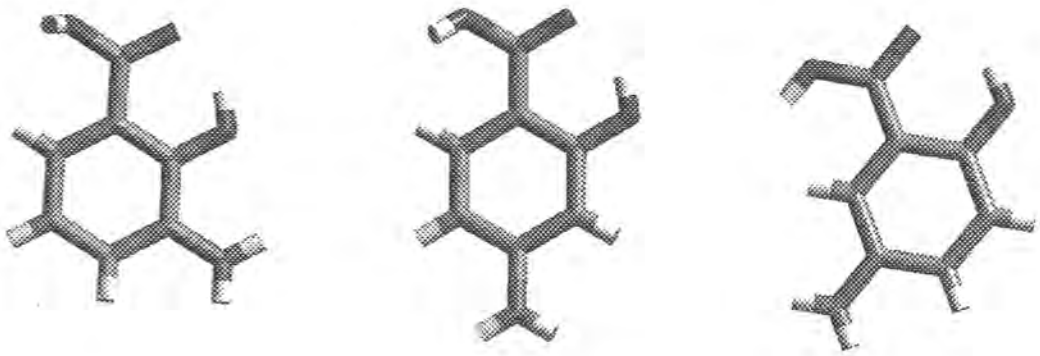

(a) (b) (c)

Figure 11.6: Optimised molecular structures of aminobenzoic acids (a) 3-ASA, (b) 4-ASA and (c) 5-ASA [26].

11.4 Suggestions for future work

It is possible that some of the complexity of the thermal behaviour observed could be resolved through use of modulated differential scanning calorimetry (MDSC). This technique is particularly useful in separating reversible and non-reversible reactions.

In this project, only 1:1 molar ratios of guest to host CD were used to enable broad comparisons of thermal behaviour to be made. Future research on detailed interactions would benefit from the use of additional ratios, and other methods of preparing mixtures, e.g, co-grinding, co-precipitation and freeze-drying as well as a more quantitative study of influence of a kneading solvent on the structures of cyclodextrins and on the inclusion process. Other techniques, such as solid-state NMR and single-crystal X-ray diffraction studies would be valuable. There is also considerable scope for molecular modelling to find the thermodynamically stable configurations resulting from interactions in these mixtures.

A more detailed study of evaporation of compounds from cyclodextrin mixtures would also be of interest.

REFERENCES

1. J.T. Carstensen, Drug Stability: Principles and Practice, Marcel Dekker Inc., New York, 2nd Edn,1990.
2. A.K. Galwey, *Drug Stability.* 1 (1995) 3.
3. A.K Galwey, *Thermochim. Acta,* 269/270 (1995) 621.
4. W.R. Young, *Drug Dev. Ind. Pharm.*, 16 (1990) 551.
5. J.H. Flynn, *J. Therm. Anal.*, 44 (1995) 499.
6. A.Wade and P.J. Welder, Handbook of Pharmaceutical Excipients, Pharmaceutical Press, London, 1994, pxi.
7. K.A. Connors, G.L. Amidon and V.J. Stella, Chemical Stability of Pharmaceuticals: A Handbook for Pharmacists, 2nd Edn, John Wiley and Sons, New York, 1986, p119.
8. C.D. Wilson, Textbook of Organic, Medicinal and Pharmaceutical Chemistry, 7th Edn, J.B. Lippincott, Co., Philadelphia, USA, (1977) p 144.
9. M. Wesolowski, *Thermochim. Acta*, 21 (1977) 243.
10. S.R. Byrn, Solid-State Chemistry of Drugs, 2nd Edn, SSCI Inc., Indiana, 1999.
11. S.E. Morsi and J.O Williams, *J. Chem. Soc. Perkin* II, (1977) 1280.
12. I. Cendrowska, M. Drewnowska, A. Grzeszkiewicz and K. Butkiewicz , *J. Chromatogr. A* , 509 (1990) 195-199.

12a. J.Jensen, C. Cornett, C.E. Olsen, J.Tjornelund and S.H. Hansen, *Int. J. Pharm.*, 88 (1992) 177.

13. G.C. De Kruif and J.G. Blok, *J. Chem. Thermodyn.*, 14 (1982) 201.
14. S.F. Wright, P. Phang, D. Dollimore and K.S. Alexander, NATAS NOTES, Vol. 3, No. 4 (2001) 4.
15. M. Wesolowski and T. Konarski, *J. Therm. Anal. Cal.*, 55 (1999) 995.
16. K. Chatterjee, D. Dollimore and K. Alexander, *J. Therm. Anal. Cal.*, 63 (2001) 629.
17. Website URL. http://www.para-aminobenzoic-acid.org

18. M. Ladd, Crystal Structures: Lattices and Solids in Stereoview, Horwood Publishing Ltd, Chichester, 1999.

19. A.C. Holler, *J. Org. Chem.*, 13 (1948) 70.

20. G.A. Sim, J. M. Robertson, and T.H. Goodwin, *Acta Cryst.*, 8 (1955) 157.

21. W.Cochran, *Acta Cryst.*,6 (1953) 260.

22. M. Sundaralingham and L.H. Jensen, *Acta Cryst.*, 18 (1965) 1053.

23. P. Pothisiri and J.T. Carstensen, *J. Pharm. Sci.*, 64 (1975) 1931.

24. T.F. Lai and R.E. Marsh, *Acta Cryst.*, 22 (1967) 885.

25. F. Bertinotti, G. Glacomello, and A.M. Liquori, *Acta Cryst.*, 7 (1954) 808

26. Cambridge Structural Database, Cambridge, Great Britain.

27. N.C. Gujrathi and C.I. Jose, *Indian J. Chem.*, 9 (1971) 822.

28. Website URL. http://www.cylodex.com.

29. K. Harata, Comprehensive Supramolecular Chemistry, Ed. J. L. Atwood, Pergamon, New York, 1996, Chapter 9.

30. M. Fodor, Cs. Novak. R. Rakosa, K. Timor, G. Pokol and S. Gal, *J. Thermal Anal.*, 48 (1997) 515.

31. Cs. Novak, M. Kata and L. Antal, *J. Thermal Anal.*, 48 (1997) 503.

32. S.P. Jones, D.J. W. Grant, J. Hadgraft and G.D. Parr, *Acta Pharm. Technol.*, 30 (1984) 213.

33. J. Szejtli, Comprehensive Supramolecular Chemistry, Ed J.L. Atwood, Vol. 3, Pergamon, New York, 1996, Chapter 5.

34. D. Duchene and W. Woussidjewe, *Drug Dev. Ind. Pharm.*, 16 (1990) 2487.

35. K. Uekama and T. Irie, Cyclodextrins and their Industrial Uses, Ed. D. Duchene, Edition de Santes, Paris, 1987, Chapter 10.

36. J. Szejtli, Comprehensive Supramolecular Chemistry, Ed. J.T. Atwood, Vol.3, Pergamon, New York, 1996, Chapter 2.

37. F. Giordano, Cs. Novak and J.R. Moyano, *Thermochim. Acta*, 380 (2001) 123.

38. H.G. Wiedemann and S. Felder-Casagrande, Handbook of Thermal Analysis and Calorimetry, Ed. M.E. Brown, Vol.1, Elsevier, Amsterdam, 1998, Chapter10.

39. A.A. van Dooren, Thermal Analysis, Proceedings of the 6th ICTA, Vol.1 (Ed. H.G. Wiedemann, Birkhäuser Verlag, Basel, 1980, p93-98.

40. System 2000 TG-IR Interface Manual, Perkin-Elmer (Ltd), Beaconsfield, Buckinghamshire, England, 1995.

41. A. Marini, V. Berbenni, D. Capsoni, R. Riccardi and T. Zerlla, *Applied Spectroscopy*, 48 (1994), 1468.

42. V. Berbenni, A. Marini, G. Bruni and T. Zerlla, *Thermochim. Acta,* 258 (1995) 125.

43. D.C. Monkhouse, *Drug Dev. Ind. Pharm.*, 10 (1984) 1175.

44. K.A. Connors, Comprehensive Supramolecular Chemistry, Ed. J. T. Atwood, Vol.3, Pergamon,1996, Chapter 6.

45. E.D. Domalski and E.D. Hearing, *J. Phys. Chem. Ref. Data,* 22 (1993) 805.

46. M.E. Brown, D. Dollimore and A.K. Galwey, Comprehensive Chemical Kinetics: Reactions in the Solid-State, Ed. C.H. Bamford and C.F.H. Tipper, Vol.22, Elsevier, Amsterdam, 1980.

47. A.K. Galwey and M.E. Brown, Thermal Decomposition of Ionic Solids, Elsevier, Amsterdam, 1999.

48. C.E.H. Bawn in " Chemistry of the Solid State", Ed. W.E. Garner, Butterworths, London, 1955, Chapter 10.

49. M.E. Brown and B.D. Glass, *Thermochim. Acta*, in press.

50. D. Dollimore, *Thermochim. Acta*, 19 (1999) 340.

51. D.M. Price, *Proc. 28th NATAS*, (2000) 216.

52. P. Phang, *Thermochim. Acta*, 340/341 (1999) 139.

53. J.T Carstensen and P. Pothisiri, *J. Pharm Sci.*, 64 (1975) 37.

54. S.S. Kornblum and B.J. Sciarrone, *J. Pharm. Sci.*, 33 (1964) 935.

55. J.T. Carstensen and M. N. Musa, *J. Pharm. Sci.*, 61 (1972) 1112.

56. E. Ben Rayana, P. Ruelle, N.T. Ito and U.W. Kesserling, Congr. Int. Technol. Pharm. 6th Assoc. Pharm. Galenique Ind., Chatenay Malabry, France, 1992, Vol.1, p 280-291.

57. T. Oguchi, E. Yonemochi, K. Yamamoto, and Y. Nakai, *Chem. Pharm. Bull.*, 37 (1989) 3088.

58. Chung-Tang Lin, Pik-Yen Siew and S.R. Byrn, *J. Chem. Soc., Perkin Trans.*, 2 (1978) 957.

59. S.G. Jivani and V.J. Stella, *J. Pharm. Sci.*, 74 (1985) 1274.

60. F. Muellar and R. Sueverkruep, *Pharm. Ind.*, 39 (1977) 1115.

61. P. Ruelle, U.W. Kesselring, N.T. Ho, E. Ben Rayana, and A. Sedas, *J. Chem. Res., Synop.*, 1988, p.90.

62. P. Ruelle, *J. Chem. Soc., Perkin Trans.*, 2 (1986)189.

63. A.V. Willi and P. Vilk, *Z. Phys. Chem.* (Frankfurt am Main), 59 (1968) 189.

64. R.K. Palsmeier, D.M. Radzik, and C.E. Lunte, *Pharm. Res.*, 9 (1992) 933.

65. R. Riesen, K. Vogel and M. Schubnell, *J. Thermal Anal. Cal.*, 64 (2001) 243.

66. S. Kohata, K. Jyodoi and A. Ohyoshi, *Thermochim. Acta*, 217 (1993) 187.

67. E.J. Sztatiz, S. Gal, J. Komives, A. Stadler-Szoke and J. Szetjli, Proc. 6th ICTA, Vol. 2, Ed. W. Hemminger, Birkhaeuser, Basel, 1980, 487.

68. A. Marini, V. Berbenni, G. Bruni, F. Giordano and M. Villa, *Thermochim. Acta*, 279 (1996) 27.

69. V. Berbenni, A. Marini and G. Bruni, *Thermochim. Acta*, 322 (1998) 137.

70. Cs. Novak. M. Fodor, G. Pokol, V. Izvekov, J. Sztatiz, M. J. Arias and J. M. Gines, *J. Thermal Anal. Cal.*, 51 (1998) 1039.

71. S.J. Tian, *J. Thermal Anal.*, 53 (1998) 825.

72. J. Cohen and J.L. Lach, *J. Pharm. Sci.*, 52 (1963) 132.

73. N. Zerrouk, J.M. Gines Dorado, P. Arnaud and C. Chemtop, *Int. J. Pharm.*,171 (1998),19.

74. V.T. Yilmaz, A. Karadag and Ichuduk, *Thermochim. Acta*, 261 (1995) 107.

75. A. Zornoza, C. Martin, M. Sanchez, I. Velaz and A. Piquer, *Int. J. Pharm.*, 169 (1998) 239.

76. J. Li, N. Zhang, X. Li, J. Wang and S. Tian, *J. Thermal Anal.*, 49 (1997) 1527.

77. M. Meier, M.T.B. Luiz, B. Szopoanicz and V. Soldi, *Thermochim. Acta*, 375 (2001) 153.

78. K.A. Connors, *Chem. Rev.*, 97 (1997) 1325.

79. M.J. Arias, J.R. Mayano, and J.M. Gines, *Int. J. Pharm.*,153 (1997) 181.

80. J.R. Mayano, M.J. Arias, J.M. Gines, J.I. Perez-Martinez, P. Munoz and F. Giordano, *J. Thermal Anal.*, 51 (1998) 1001.

81. S. Scalia, S. Villani, A. Scatturin, M.A. Vandelli and F. Forni, *Int. J. Pharm.*, 175 (1998) 2053.

82. K.B. Lipkowitz, *Chem .Rev.*, 98 (1998) 1829.

83. R. Reinhardt, M. Richter, and P.P. Mager, *Carbohydr. Res.*, 291 (1996) 1.

84. J.E.H. Koehler, W. Saenger and W.F. Gunsteren, *Eur. Biophys. Acta*, 16 (1988) 153.

85. I. Tabushi, Y. Kiyosuke, T. Sugimoto and K. Yamamura, *J. Am. Chem. Soc.*, 100 (1978) 916.

86. M. Kitagawa, H. Hoshi, M. Sakurai, Y. Inoue and R. Chujo, *Carbohydr. Res.*, 163 (1987) c1.

87. S.P. van Helden, M.J. van Drooge, A.J. Claessens, A.C.A. Jansen and L.H.M. Jansen, *Carbohydr. Res.*, 215 (1991) 251.

88. A. Entrena and C. Jaime, *J. Org. Chem.*, 62 (1997) 5923.

89. D. Salvatierra, C. Jaime, A. Virgili and F. Sanchez-Ferrando, *J. Org. Chem.*, 61 (1996) 9578.

90. M. Fathallah, F. Fotiadu and C. Jaime, *J. Org. Chem.*, 59 (1994) 1288.

91. T. Lu, D. Zhang and S. Dong, *J. Chem. Soc., Faraday Trans.* 2, 85 (1989) 1439.

92. Y. Inoue, M. Kitagawa, H. Hoshi, M. Sakurai, and R. Chujo, *Inclusion Phenom.*, 5 (1987) 55.

93. A.M.C. Myles, D.J. Barlow, G. France, and M.J. Lawrence, *Biochim. Biophys. Acta*, 1199 (1994) 27.

94. T. Furuki, F. Hosokawa, M. Sakurai Y. Inoue and R. Chujo, *J. Am. Chem. Soc.*, 115 (1993) 2903.

95. V.B. Luzkov and C.A. Venanzi, *J. Phys. Chem.*, 99 (1995) 2312.

96. A. Daubinet., Ph.D Thesis, Rhodes University, 2001.

97. S. Lerdkanchanaporn and D. Dollimore, *J. Thermal Anal.*, 49 (1997) 879.

98. S. Lerdkanchanaporn and D. Dollimore, *Thermochim. Acta*, 324 (1998) 15.

99. J.P. Elder, *J. Thermal Anal.*, 49 (1997) 897.

100. J.D.Cox and G. Pilcher, Thermochemistry of Organic and Organometallic Compounds, Academic, London, 1970, p 643.

101. D. Dollimore, *Thermochim. Acta,* 340-341 (1999) 139.

102. L. Shen and K.S. Alexander, *Thermochim. Acta*, 340/341 (1999) 271.

103. D.M. Price and M. Hawkins, *Thermochim. Acta*, 315 (1998) 19.

104. A.V. Manuel, D.S. Ribeiro and J.S.M. Manuel, *Thermochim. Acta*, 171 (1990) 169.

105. J.P. Elder, *J. Thermal Anal. Cal.*, 49 (1997) 897.

106. D. Price, S. Bashir and P.R. Derrick, *Thermochim. Acta*, 327 (1999) 167.

107. S. Murata, M. Sakiyama and S. Seki, *J. Chem. Thermodyn.*, 14 (1982) 723.

108. M.M.A Hassan, A.I. Jado and M.U. Zubair, *J. Anal. Profile Drug Substances*, 10 (1981) 1.

109. M.E. Brown, Introduction to Thermal Analysis, 1st Edn., Chapman and Hall, London,1988.

110. M. Bilal, C. de Brauer, P. Claudy, P. Germain and J.M. L_toff_, *Thermochim. Acta*, 249 (1995) 63.

111. L. Szente, Comprehensive Supramolecular Chemistry, Ed. J.L. Atwood, Pergamon, New York, 1996, Chapter 7.

112. S.M. Botella, M.A. Martin, B. del Castillo, J.C. Menendez, L. Vazquez and D.A. Lerner, *J. Pharm. Biomed. Anal.*, 14 (1996) 909.

113. C. Laurence and M. Bartholot, *J. Chem. Soc. Perkin* II, (1979) 98.